# Donor–Acceptor Systems in the Quest for Organic Semiconductors

Dissertation

zur Erlangung des Grades

„Doktor der Naturwissenschaften“

Im Promotionsfach Chemie

am Fachbereich Chemie, Pharmazie und Geowissenschaften der

Johannes Gutenberg-Universität Mainz

**Timea STELZIG** (geb. **DALLOS**)

Geboren in Tăşnad, Rumänien

Mainz

(2012)

*Dekan:*

*1. Berichterstatter:*
*2. Berichterstatter:*

*Tag der mündlichen Prüfung*: 16.04.2012

*“If we knew what we were doing, it wouldn’t be called research, would it?”*

Albert Einstein

# Table of Contents

# Index of Abbreviations

| | |
|---|---|
| 1,2-DCE | 1,2-dichloroethane |
| a.o. | air operating |
| AcOH | acidic acid |
| AFM | atomic force microscopy |
| BHJ | bulk heterojunction |
| *br* | broad (NMR signal) |
| CV | cyclic voltammetry |
| *d* | doublet (NMR signal) |
| *dd* | doublet of doublets (NMR signal) |
| DCM | dichloromethane |
| DFT | density functional theory |
| DMF | N,N-dimethylformamide |
| DSC | differential scanning calorimetry |
| Fc | ferrocene |
| FD-MS | field desorption mass spectrometry |
| FT-IR | Infrared Spectroscopy |
| GPC | gel permeation chromatography |
| h | hour |
| HOMO | highest occupied molecular orbital |
| $^{i}$Pr | iso-propyl |
| ITO | Indium tin oxide |
| LUMO | lowest unoccupied molecular orbital |
| *m* | multiplet (NMR signal) |
| MALDI-TOF | matrix-assisted laser desorption/ionization time-of flight |

| | |
|---|---|
| min | minute |
| m.p. | melting point |
| HRMS | high resolution mass spectrometry |
| *MW* | Microwave |
| NBS | *N*-bromosuccinimide |
| NIR | near-infrared |
| NMR | nuclear magnetic resonance |
| OFET | organic field-effect transistor |
| OLED | organic light emitting diode |
| OPV | organic photovoltaics |
| P3HT | poly(3-hexylthiophene) |
| $PC_{61}BM$ | phenyl-C61-methylbutyrate |
| ppm | parts per million |
| *PS* | polystyrene |
| *PPP* | poly(paraphenylene) |
| *q* | quartet (NMR signal) |
| *quin* | quintuplet (NMR signal) |
| RFID | radio frequency identification tag |
| r.t. | room temperature |
| *s* | singlet (NMR signal) |
| sec | seconds |
| *sept* | septet (NMR signal) |
| SEM | scanning electron microscopy |
| *t* | triplet (NMR signal) |
| TBAF | tetra-butyl ammonium fluoride |
| TCB | 1,2,4-Trichlorobenzene |
| TCNQ | 7,7,8,8-Tetracyanoquinodimethane |
| THF | tetrahydrofuran |
| TGA | thermo-gravimetry analysis |
| TLC | thin layer chromatography |
| TMS | tetramethylsilyl |
| TOF | time-of-flight |
| UV-Vis | ultraviolet-visible |

# 1. Introduction

Since the discovery of (semi)conductive iodine-doped polyacetylene in 1977,[1] organic semiconductors have earned great academic and industrial awareness.[2] The semiconducting nature of π-conjugated organic molecules and polymers being complemented by their unique optical properties set the scene for the advent of the fields of plastic electronics[3] and photonics.[4] In spite of the occasionally significant scientific hurdles that must be overcome during their synthesis and processing, organic semiconductors allure promising chemical versatility and low-cost fabrication, due to their mechanical flexibility and solution processability.[5]

**Figure 1.** Examples of lunched applications based on organic electronics: paper thin, flexible solar panel providing enough power to charge a mobile phone (left); Electronic paper (middle); Roll-to-Roll printed re-writable memories on flexible substrate printed radio-frequency identification tag (right).

The last few decades brought along the development of many new organic semiconductors that have been successfully incorporated into high-performance devices, such as field effect transistors (FETs),[6] organic light emitting diodes (OLEDs),[7] organic photovoltaic cells (OPVs)[8] and sensors.[9] With the technology in its development-stage some of the materials have reached the minimal requirements for commercialization[10] (Figure 1), but there is still much to be discovered, explained and understood.

The "power" of silicon technologies is still beyond reach for most of these technologies. The more than 100 years of research invested in this technology has yielded devices with lifetimes beyond 25 years, high charge carrier mobilities,[11] high power conversion efficiencies,[12] and good thermal and mechanical stability.[13] Some skeptics would say: "*Don't seriously try to make it out of anything else if it has a chance of working with silicon*" (Jerry M. Woodall, 1982).[14] However, looking at the bigger picture, one can easily see that the immediate purpose of the technologies based on organic semiconductors is not necessarily to replace their inorganic counterparts but to supplement them.[15] Their attraction lay in the cost efficient fabrication of certain optoelectronic devices doubled by the possibility of achieving new device functionalities, including impact resistance, transparency or mechanical flexibility that would be difficult to obtain with silicon.[16]

The improvement of organic electronics and photonics is marked by the principle "*Divide et impera!*". Apart from investing in the discovery of new materials, the importance of achieving much better understanding of the nature of the electronic structure and charge transport properties is of the essence. For example, the theoretical aspects of the charge transport in organic semiconductors are fundamental from the material optimization point of view.

## 1.1. Charge Transport in Organic Semiconductors

The classical theory uses the band transport model[17] to describe the charge transport in semiconductors. The charges can move by thermal excitation within an energy continuum created by the strong coupling of energy levels of single sites. While this model represents very well the charge transport in inorganic semiconductors such as silicon, it is not suitable to account for the same process in organic semiconductors characterized by weak couplings between adjacent molecules.[18] In contrast, the hopping model provides a much better description of the phenomenon for these systems. In this case the charge transport

presumably occurs through the hopping of the charges between localized states[19] with the required energy provided by lattice vibration (phonon-assisted hopping).[20]

The theory delineated in 1956 by Rudolph A. Marcus[21] had become the fundament of the theoretical description of the charge carrier processes in organic semiconductors. This theory describes the rates of electron transfer (ET) reactions, the rate at which an electron can hop from one chemical species (donor) to another (acceptor). The Marcus theory was originally formulated to address redox reactions where the chemical species change their charge without undergoing large structural changes (outer sphere electron transfer).[22] For these systems the ET rate can be calculated from the formalism:

$$k_{ET} = 2\pi/\hbar \times |H_{AD}|^2 / (4\pi\lambda_{reorg}k_bT)^{½} \exp(-(\lambda_{reorg} + \Delta G^{\#})^2 / 4\lambda_{reorg}k_bT) \quad (1)$$

where $\Delta G^{\#}$ is the activation free energy, $\lambda_{reorg}$ is the reorganization energy, $H_{AD}$ is the electronic coupling element, $k_b$ is the Boltzmann constant, and $T$ is the absolute temperature.

Later on, Noel S. Hush[23] extended this theory by taking into account the inner sphere ET contributions, consisting of distance or geometry changes in the solvation or coordination shell. The Marcus-Hush theory offers a more suitable theoretical description of ET rates and intrinsic (activation) barriers for intra- and intermolecular charge transfer processes.[24] Thus, the ET rate constant ($k_{ET}$) and activation barrier ($\Delta G^{\#}$) can be predicted within the Marcus-Hush formula as:

$$k_{ET} = \kappa\, \nu_n \exp(-\Delta G^{\#} / R\,T) \quad (2)$$

$$\Delta G^{\#} = (\lambda_{reorg} - 2H_{AD})^2 / 4\,\lambda_{reorg} \quad (3)$$

where $\kappa$ is the electronic transmission coefficient and $\nu_n$ is the nuclear vibration frequency related to the ET.

In 1967, Robin and Day[25] introduced a useful classification of the mixed-valence compounds with two (or more) redox centers into three categories: (a) the redox centers are completely localized and behave as separate entities (class I), (b) intermediate coupling between the mixed-valence centers exists (class II), and finally, (c) the coupling is so strong

that the system is completely delocalized and intermediate redox states have to be attributed to the redox centers (class III). The two key parameters (and their interplay) that determine to which class a mixed-valence compound belong are the electronic coupling ($H_{AD}$) between the two redox centers and the reorganization energy ($\lambda_{reorg}$) that characterize the electron transfer.[23b] In the extreme case $H_{AD} = 0$ (Figure 2, left) the odd electron can be in either of the two harmonic potential energy wells with an equal force constant of $2\,\lambda_{reorg}$ (class I). In this case no vertical electronic transition from one potential well to the other can be observed. For compounds belonging to class II the $\lambda_{reorg} / H_{AD} > 2$ (Figure 2, middle), whereas for those belonging to class III $\lambda_{reorg} / H_{AD} < 2$ (Figure 2, right). As a consequence, the potential-energy surface for self-exchange in class II systems consists of a pair of isergonic ground states, while only a single broad ground state characterize the class III systems.

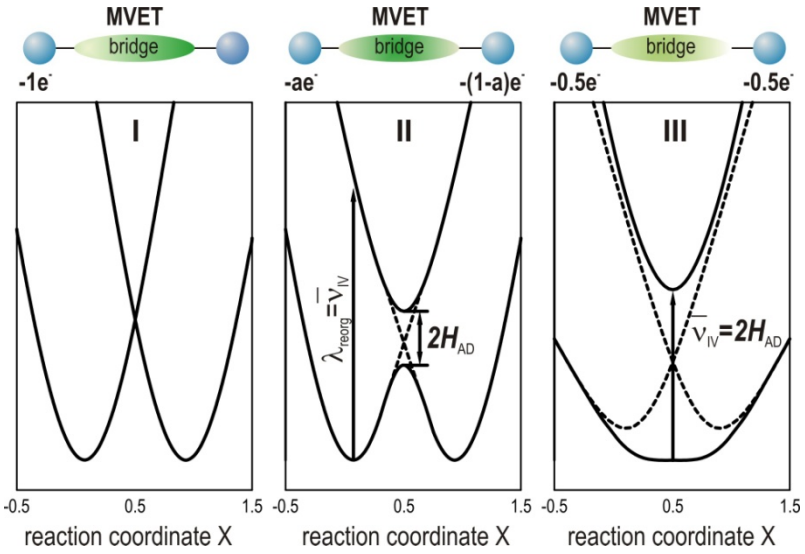


**Figure 2.** Potential ET self-exchange energy surface relative to the excited states, based on the two-state Mulliken-Hush formulation.[26]

Hence, for class II systems, the Franck-Condon transitions take place in a steeply sloping region of the higher potential well, resulting in a Gaussian distribution of energies in the ground-state. This translates into the nearly Gaussian shaped, broad, and usually structureless intervalence absorption band. The $\lambda_{max}$ of this band corresponds to the total reorganization energy. In class III systems, the limit of strong electronic coupling is reached and the resulting intervalence absorption band is relatively narrow and typically showing vibrational fine structure as it takes place to a weak sloping region of the upper potential well.[27]

The validity of the Marcus-Hush theory has been successfully tested in some direct comparison of experimentally and theoretically derived activation barriers[24b] for organic self-exchange reactions. Purely organic mixed-valence systems constitute the ideal probes for this purpose. Some of these systems simultaneously possess high reorganization energies and electronic coupling allowing the straightforward detection of the intervalence absorption band and the experimental evaluation of the ET rates by EPR spectroscopy. Hence, the extensive research in the field of organic mixed-valence materials is fed by the high interest in understanding charge transport related fundamental issues in organic semiconductors, as it is important for instance to know the size of molecular hopping stations over which an electron can be delocalized.[28] Unlike metal based mixed-valence compounds, molecules with redox sites are better suited for these studies owing to the more delocalized nature of the charge in these systems (Figure 2).[29] In the last few years significant efforts have been made to shed light on the influence of distance,[30] bridge connectivity,[31] conformation[32] and topology,[33] and multidimentionality[34] on the electron transfer processes in organic mixed-valence systems.

A simple analysis of the Marcus-Hush mathematical relations offers primary information concerning the requirements of an efficient ET process. High hopping rates (charge carrier mobilities) need efficient electronic couplings ($H_{AD}$) between the hopping sites. Within this context, the high polarizability of the π-extended systems is advantageous.[35] The reorganization energy ($\lambda_{reorg}$) should be kept at a minimum. The $\lambda_{reorg}$ is usually increasing with the distance between the hopping sites, a drawback that could be overcome by a dense packing.[36] Furthermore, a rapid hopping process is secured through maximum negative $\Delta G^{\#}$ values achievable for a perfectly uniform material. On the contrary, an inhomogeneous material would imply an increased or even positive $\Delta G^{\#}$ impeding the charge hopping from one site to the other. This phenomenon is known as “charge trapping” and it can be caused by the presence of impurities, grain boundaries, structural defects or a combination of these.[37]

The probing of the underlying theory with purely organic mixed-valence systems is not yet fully explored. The ultimate goal of a deep understanding of the nature of the electronic structure and charge transport properties in organic semiconductors is to enable the prediction of the properties of new active materials for organic electronics. At the moment, however, this goal has not yet been reached. As a result, the development of new active

materials relies on the exploration of the structure-property relationship of the existent organic semiconductors.

## 1.2. Organic Semiconductors

As the most important component of an OFET, OPV or OLED device is the organic semiconductor, the development of new materials, as well as optimization of already existent materials is crucial. There are two main classes of organic semiconductors: low molecular weight (molecular) semiconductors and high molecular weight (polymer) semiconductors. As the two types of semiconductors can be deposited from solution, both small molecules and polymers are investigated depending on the fabrication specifications.

### 1.2.1. Polymer Organic Semiconductors

There are two major structural requirements that a polymer semiconductor must fulfill for a successful application in organic electronics.[38] Firstly, the polymer must have a π-conjugated backbone that would secure extended π-orbitals along the polymer chain necessary in order to achieve proper charge transport and / or optical absorption.[39] Secondly, the polymer repeating unit(s) must be grafted with solubilizing groups, such as alkyl or alkoxy moieties. The alkyl / alkoxy chains are to ensure the solubility of the material, essential for the solution deposition method.[40] Furthermore, these groups are also known to play a positive role in improving the solid state organization through polymer interchain interactions.[41]

The most frequently employed conjugated polymer building blocks are aromatic systems, such as mono(poly)cyclic hydrocarbons or heterocycles as well as simple olefinic or acetylenic units. The degree of π-conjugation between these repeating units controls the

solution / solid state electronic structure which subsequently determines the essential characteristics of the polymer for instance optical and redox properties and energy levels.

Apart from the π-interactions within the polymer backbone, the molecular weight ($M_n$) and polydispersity index (*PDI*) are important parameters that define its photophysical and electronic characteristics. Conjugated polymers show strong molecular weight dependence with 4 to 5 orders of magnitude higher charge carrier mobility in OFET or OPV when the $M_n$ is increased with one order of magnitude.[42] By tuning these two characteristics one can influence the solubility, aggregation, thin film formation and morphology.[16b] Considering that the properties of the materials vary significantly when going from low molecular weights (oligomers) to high molecular weights, it is critical to achieve high $M_n$ and *PDI* values beyond which, the characteristics of the material do not change. Thus, a reproducibility of polymer properties from batch to batch could be accomplished.

### 1.2.2. Polymer *versus* Molecular Organic Semiconductors

The highest mobility devices demonstrated in the literature are using vapor deposited small molecule semiconductors or single crystals.[43] However, to convert these small molecule laboratory devices into dependable, large area manufacturing processes can be troublesome. Especially, since the main requirement for an economically profitable large area fabrication is the solution processability and reproducibility of the corresponding semiconductor.

The attraction of molecular semiconductors lay in their strictly monodisperse nature which promote a 2D or 3D structural organization in thin semiconducting layers. However, some of these small molecule semiconductors may also present polymorphism making their solid state organization dependent on the processing conditions (vapor *vs.* solution deposition or thermal treatment) employed.[44] Therefore, in thin layers of low molecular weight semiconductors the charge transport is strongly affected by their phase purity, meaning the size and shape of crystallites or their degree of orientation. A disadvantage of small molecule semiconductors is their typically large solubility parameter profile, which could complicate the matters when a subsequent solution deposition step is required for a particular application.[43]

One of the biggest advantages of polymers over their small molecule counterparts is the ease of their processing. The solution processed polymer films are generally characterized by smoothness and uniformity. Therefore, the structural and morphological characteristics of the polymeric films are controllable over a large scale.

The reproducibility of the device performance is ensured by the isotropic transport characteristics of the π-conjugated polymers, which is a result of the much smaller crystalline domains than the length scale of several optoelectronic devices.[16]

As mentioned above, the solution based fabrication technology requires the inertness of each deposited layer to the solvents and temperatures that is subsequently exposed during the fabrication process. Polymers are also preferred in this case, due to their narrower solubility window and large bulk viscosity. As typical device fabrication implies repeated thermal cycles, it is important to avoid interlayer diffusion, condition that is usually fulfilled by polymers owing to their negligible vapor pressure. Additionally, their robust mechanical properties could facilitate the roll-to-roll fabrication on a flexible substrate of nanometer thick semiconductor films.[43]

## 1.3. Organic Field Effect Transistors

A financially advantageous alternative technology to amorphous hydrogenated silicon transistors in the area of large arrays or low-end microelectronics (RFID tags, sensors, etc.) are organic field effect transistors (OFETs). A few of these possible applications are: backplane / driver circuits for active matrix displays, since high transistor density and switching speeds are not required or radio frequency identification tags (RFID tags) in which case, the high packaging costs of Si circuits make them unprofitable for everyday item.[45] The greatest attraction of the polymer OFET technology is the possibility to apply solution based deposition and patterning techniques like gravure, screen printing or inkjet printing.

Additionally, polymer OFET technology is compatible with plastic substrates enabling structurally robust, lightweight and flexible devices.

### 1.3.1. Operational Mode, Carrier Mobility Extraction and Classification

An OFET consists of a substrate where the dielectric layer, the organic semiconductor layer and three (gate, source and drain) electrodes are deposited (Figure 2, left). There are four different device configurations that can be fabricated as a function of the relative position of the contacts (electrodes) and the dielectric / semiconductor layers.[16b] Figure 3 shows a schematic structure of a bottom-contact bottom-gate OFET device. The advantage of such a configuration resides in the fact that the organic semiconductor layer is deposited after the growth of the dielectric layer. The modifications of its surface and patterning of the source and drain are accomplished at the end of the transistor fabrication. Hence, the structure and morphology of the semiconducting layer is not negatively influenced by the processing.

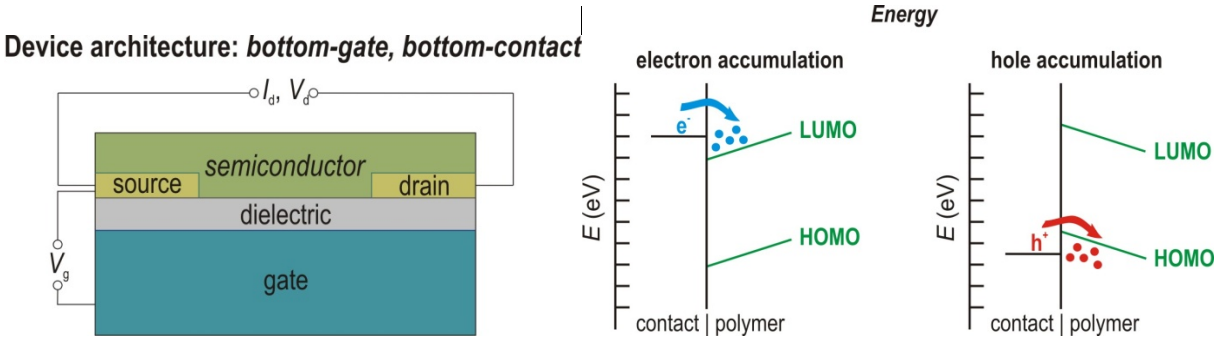


**Figure 3.** Architecture and components of the bottom-gate, bottom-contact OFET (left) and the energy levels of the contact-semiconductor materials where charge accumulation takes place (right).[16b]

Independently of the device structure, when the gate is zero ($V_G$ = 0 V) there is negligible source-drain current ($I_{SD}$ = 0 A) flow regardless of the bias applied between the source and the drain ($V_{SD}$) contacts. Under an applied gate field ($V_G \neq 0$ V) the device turns on ($I_{SD} \neq 0$ A) inducing charge carrier in the semiconductor at the interface with the dielectric layer

(Figure 3).[46] The performance of the semiconductor, as an active component of the field effect transistor, is evaluated from the field effect mobility ($\mu$), the current on / off ratio ($I_{ON}$ / $I_{OFF}$) and the threshold voltage ($V_T$). These critical parameters can be extracted from the transfer and output current-voltage plots (recording $I_{SD}$ as a function of $V_{SD}$ at a given $V_G$). Within the metal oxide-semiconductor field effect transistor (MOSFET) gradual channel model approximation, the carrier mobility in the linear and in the saturation regimes can be derived[47] from the standard MOSFET equations:

$$(I_{SD})_{lin} = (W / L)\, \mu_{lin}\, C_i\, (V_{SG} - V_T - V_{SD} / 2)\, V_{SD} \qquad (4)$$

$$(I_{SD})_{sat} = (W / 2L)\, \mu_{sat}\, C_i\, (V_{SG} - V_T)^2 \qquad (5)$$

where $V_{SD}$ is the drain voltage when the source electrode is grounded, $W$ and $L$ are the channel width and length, respectively, and $C_i$ is the capacitance of the dielectric layer per unit area.

Organic semiconductors for FET applications can be classified in three classes depending on the majority of the charge carriers: p-channel (holes), n-channel (electrons) or ambipolar (both hole and electrons) under different gate bias conditions.[16b, 48] The positively charged holes accumulate at the interface under negative gate voltage. Holes could be defined as vacant places for electrons that do not compensate the positive charge of the nucleus. By filling this empty place with an electron of a neighboring site simultaneously a new vacant position is created. Therefore, when this happens in a sequence it seems as if the hole is moving along the electric field. On the other hand, applying a positive bias induces an electron accumulation at the interface that move along the electric field. Hence, an electron rich material would be a p-type semiconductor, while an electron poor material would be an n-type semiconductor. Furthermore, the presence of a balance between electron rich and electron poor units within the same material could yield ambipolar charge transport, as a function of the gate voltage applied.[39]

## 1.3.2. Low Molecular Weight Semiconductors in OFETs

Low molecular weight semiconductors for p- and n-channel OFETs have been the focus of an extensive research in the last two decades. The n-channel semiconductors however, have only recently started to compete with their p-channel counterparts in the area of organic electronics.[49] As already mentioned, the highest charge carrier mobilities are reached for single crystals (p-channel pentacene or rubrene)[50] or vacuum deposited small molecule based p-type OFETs.

Many functionalized pentacene derivatives have been investigated in the hope of achieving solution processability while maintaining high charge carrier mobility. Recent studies have shown that the combined presence of trialkylsilylethynyl substituents at position 6 and 13 and methyl groups on the pentacene core provides the collective effect of an improved crystal structure (from "hering bone" like to 2D "brick wall")[51] and an increased solubility yielding solution cast thin layers of excellent 2.5 $cm^2V^{-1}s^{-1}$ field effect mobility[52] (**MESP**, Chart 1). Alkyl substituted dibenzothieonothiophenes (**BTBT**, Chart 1), member of the thienothiophene family, deserve special attention. For these materials very good solubility emerges with highly ordered supramolecular organization resulting in solution cast high mobility ($\mu_h$ = 2.5 $cm^2V^{-1}s^{-1}$) OFET devices operating on air.[53] Similarly, their dithienobenzodithieno analogues show solution processability combined with good electrical transport, although air-stable operation is not reported (**dTBdT**, Chart 1).[54]

There are a few low molecular weight high mobility n-channel field effect semiconductors as illustrated in Chart 1. Usually, these materials show one order of magnitude higher charge carrier mobilities when vapor deposited relative to solution processing. One of the most representative class of n-type semiconductor is functionalized perylene bisimides (**PBI**). Careful optimization of the rate of the thin layer growth by organic vapor phase deposition, dielectric surface treatment and annealing temperature, yielded high crystallinity and a remarkable 2.1 $cm^2V^{-1}s^{-1}$ electron mobility in the case of **PBI-R13**.[55]

**Chart 1.** Chemical structures of p-channel (solution processed) and n-channel (vapor deposited) low molecular weight semiconductors. (a.o.) = air operating. See text for references.

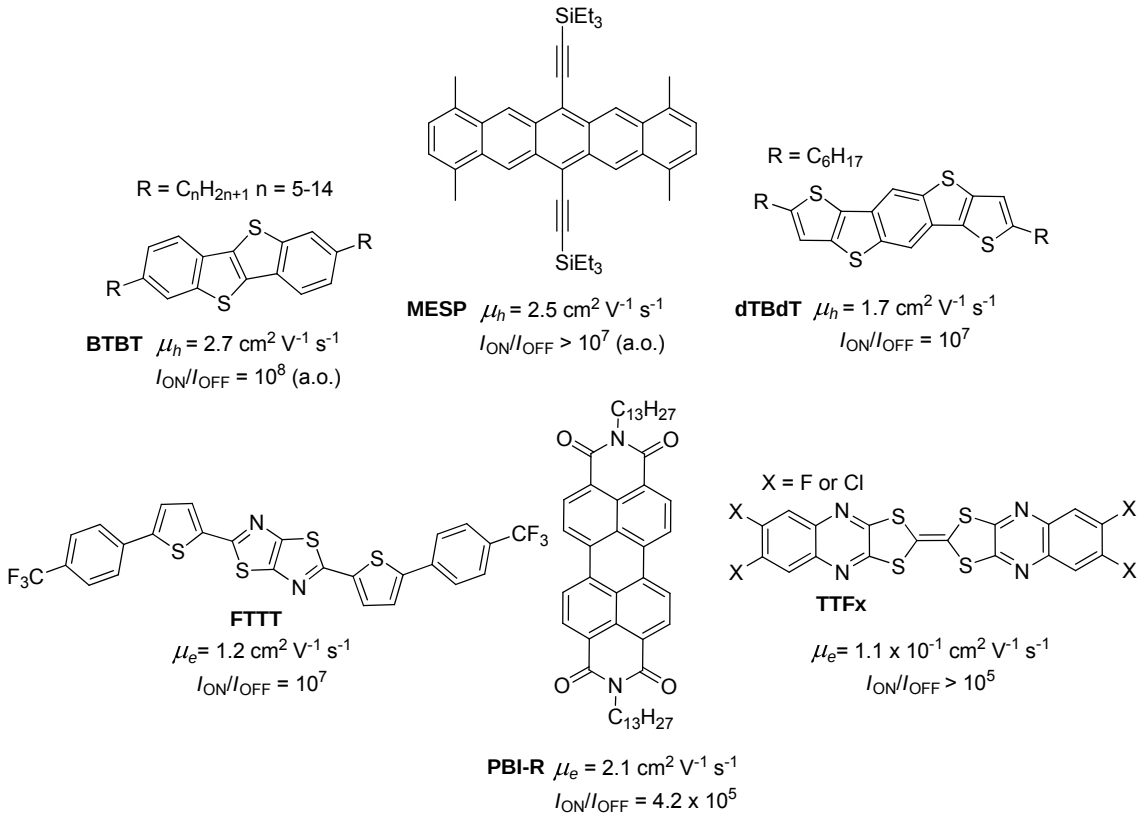


Similarly, the modification of the $SiO_2$ dielectric surface proved to be beneficial for increasing the electron charge mobility for thiophene co-oligomers with thiazolothiazole central unit. In case of **FTTT** octadecyltrichlorosilane (OTS) treatment of the $SiO_2$ enhanced the charge carrier mobility from 0.3 $cm^2V^{-1}s^{-1}$ ($I_{ON}$ / $I_{OFF}$ = $10^6$, $V_T$ = 60 V in vacuum)[56] to 1.2 $cm^2V^{-1}s^{-1}$ ($I_{ON}$ / $I_{OFF}$ = $10^7$, $V_T$ = 67 V in vacuum).[57] Quinoidal heterocyclic oligomers are another example of promising n-type semiconductors. Tetrahalogeno-tetrathiafulvalenes (**TTFx**) revealed high n-channel conductivity and ON/OFF ratios ($\mu_e$ = 0.1 $cm^2V^{-1}s^{-1}$, $I_{ON}$ / $I_{OFF}$ > $10^5$, $V_T$ ≈ 50 V in vacuum).

## 1.3.3. Polymer Semiconductors in OFETs

Up to date, the majority of the conjugated polymers, which demonstrated acceptable mobilities in OFETs, are p-channel semiconductors. Apart from the previously discussed structural requirements, p-channel charge carrier transport is enabled in a molecule with a HOMO energy level ($E_{HOMO}$) lying between -5 and -5.5 eV. A too high $E_{HOMO}$ (low ionization potential) facilitates oxidation by air and therefore considerably reduces the stability of the device and the current on-off ratio, when operated under ambient conditions. Meanwhile a $E_{HOMO}$ << -5.5 eV (high ionization potential) usually secures a large current on / off ratio and good mobility, however the devices suffer from very large threshold voltages.[16b]

**Chart 2.** Chemical structures of p- and n-channel and ambipolar high molecular weight (polymer) semiconductors. (a.o.) = air operating. See text for references.

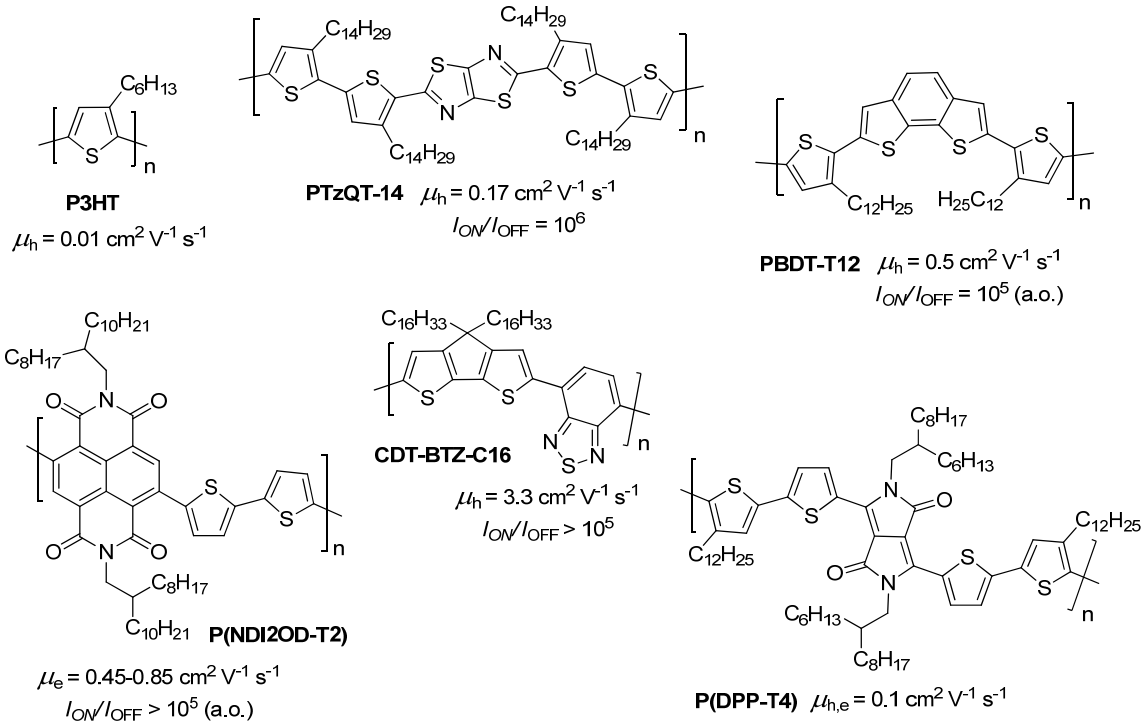

The most intensely studied p-type polymer is without a doubt poly(3-hexyl-thiophene) (**P3HT**, Chart 2). The systematic study of this polymer, as an active component in a FET device, has deepened the understanding of the charge transport properties of polymeric semiconductors.[58] During the last few years, several new structures have been developed resulting in even higher p-channel OFET performances. McCullough and co-workers have reported a copolymer incorporating a fused thiazolothiazole ring in the backbone (**PTzQT-14**) with a high hole charge carrier mobility.[59] This was surprising considering the low molecular weight ($M_n$ = 8700 g mol$^{-1}$, *PDI* = 1.8) of the material and the lack of interdigitating side chains (disordered). Müllen *et al.* developed a benzo[2,1-*b*;3,4-*b*0]dithiophene containing copolymer **PBDT-T12** (Chart 2), which showed a remarkably high hole mobility ($\mu_h$ = 0.5 cm$^2$V$^{-1}$s$^{-1}$) in an air-operating FET device on a polyethylene terephthalate (PET) substrate.[60] The same group has proven the importance of molecular weight and deposition technique optimization in case of the donor-acceptor (D-A) type polymer **CDT-BTZ-C16** (Chart 2). Hence, the initially reported[61] hole mobility of 0.17 cm$^2$V$^{-1}$s$^{-1}$ was improved by more than one order of magnitude to $\mu_h$ = 3.3 cm$^2$V$^{-1}$s$^{-1}$ and is the highest charge carrier mobility reported for a polymeric p-channel OFET, up to date.[62]

The dielectric surface passivation proved to be an efficient strategy in overcoming the efficient trapping of the electrons on a $SiO_x$, which is regularly used in OFET devices as a dielectric layer. This treatment of the $SiO_x$ dielectric could enable high n-channel transport in organic semiconductors. One of the most impressive results have been obtained with polymeric naphthalenedicarboximide-dithiophene (**P**(**NDI2OD-T2**), Chart 2). OFET devices based on this material showed electron mobilities up to 0.45-0.85 cm$^2$V$^{-1}$s$^{-1}$ with excellent ambient stability.

The understanding of the role played by traps of electrons on numerous dielectric surfaces has enabled not just the rapid development of n-channel charge carriers, but also the discovery of ambipolarity, as a general property of many polymer semiconductors. From the different polymers reported, showing clean ambipolar charge transport characteristics, those incorporating diketopyrrolopyrrole deserve special attention, since **P**(**DPP-T4**)[63] (Chart 2) constitutes the benchmark regarding the hole and electron mobilities. A solution-processed device of **P**(**DPP-T4**) using octyltrichlorosilane treated $SiO_2$ reveled nearly balanced hole

($\mu_h \approx 0.1$ $cm^2V^{-1}s^{-1}$) and electron ($\mu_e \approx 0.09$ $cm^2V^{-1}s^{-1}$) transport. Additionally, the ambipolar **P**(**DPP-T4**) transistors emit near-infrared light, under appropriate bias conditions.

## 1.4. Bulk-Heterojunction Photovoltaic Cells: Operational Mode and Characteristics

Converting solar energy into electrical power, a renewable clean energy, using organic semiconductors is still in its infancy. An important difference between organic semiconductors and their inorganic counterparts stands in the photogeneration of the charge carriers. In the case of inorganic semiconductors the absorption of light leads to free charge carriers through the bulk. Conversely, due to their low dielectric constant, light absorption in organic materials leads to coulombically bound electron-hole pair (exciton).[64] To generate charges in an organic semiconductor, the Coulomb barrier needs to be overcome. The most effective approach towards a successful charge dissociation was realized through the creation of a bulk-heterojunction (BHJ).[65]

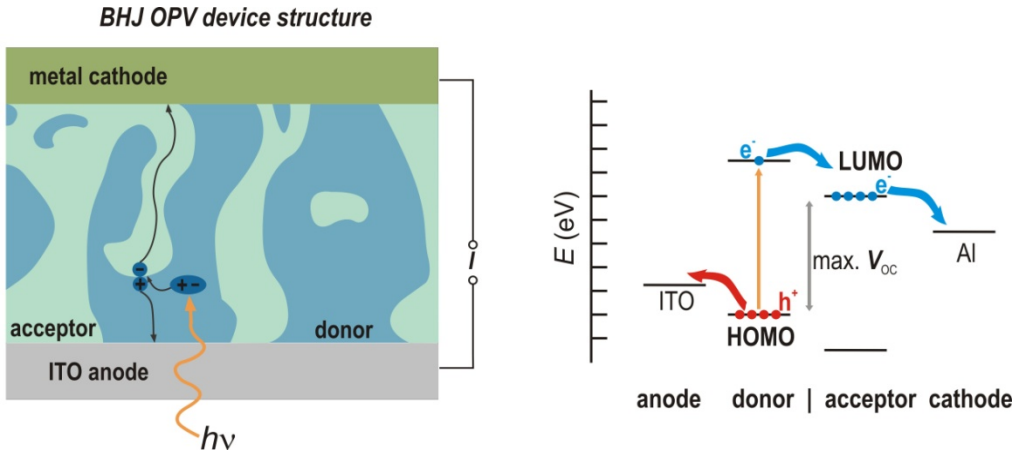


**Figure 4.** Device structure of a conventional BHJ OPV cell (left) and the energy levels of the materials where light absorption / exciton dissociation / charge collection takes place (right).[66]

The basic idea of a BHJ OPV cell is to sandwich a mixture of bicontinuous and interpenetrating donor (hole-transporting) and acceptor (electron-transporting) semiconductors between two electrodes.[66] The absorption can lead to a charge transfer and subsequent dissociation, in case of an appropriate match of the $E_{LUMO}$ and $E_{HOMO}$ of the donor and the acceptor (Figure 4). In a typical BHJ OPV cell the photoactive blend is sandwiched between an indium tin oxide (ITO) positive electrode (anode) and a metal (aluminum) negative electrode (cathode). Organic and / or inorganic interlayers are often used in order to enhance the charge collection, for example PEDOT:PSS for hole and LiF for the electron collection. In the BHJ OPV the excitons can easier access the donor-acceptor interface and dissociate into free holes and electrons, due to the intimate intermixing between the donor and the acceptor phases (Figure 4).

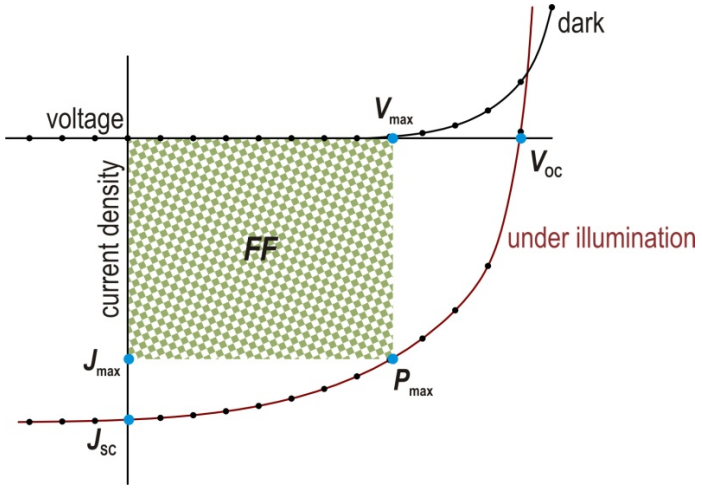


**Figure 5.** Typical current-voltage characteristics for dark and light current in a photovoltaic cell illustrating the essential parameters: $J_{max}$ and $V_{max}$ are the current and voltage at maximum power point ($P_{max}$), $J_{SC}$ is the short-circuit current density, $V_{OC}$ is the open circuit voltage and *FF* is the fill factor.[66]

The relevant performance parameters of an OPV cell can be extracted from the photocurrrent-photovoltage (*I*-*V*) curves, measured under simulated AM 1.5 solar light (Figure 5). The power conversion efficiency (*PCE* or $\eta$) can be calculated from the following equation:

$$\eta = P_{max} / P_{in} = FF\,(V_{OC}\,J_{SC}) / P_{in} \qquad (6)$$

$$FF = (V_{max} J_{max}) / (V_{OC} J_{SC}) \quad (7)$$

where $P_{max}$ is the maximum output electrical power (in W $m^{-2}$) of the device under illumination, $P_{in}$ (in W $m^{-2}$) is the light intensity incident on the device, $V_{OC}$ is the open circuit voltage, and $J_{SC}$ is the short circuit current in A $m^{-2}$.

Based on the *I-V* curve of a device the short circuit current ($J_{SC}$) and the fill factor (*FF*) can be extracted as well. $J_{SC}$ is the current produced by the device under illumination when no bias is applied ($V$ = 0 V). The *FF* is defined as where $V_{max}$ and $I_{max}$ are the voltage and current at the maximum power point in the *I-V* curve, respectively. Judging from the mathematical relation defining the overall efficiency, an ideal OPV device would have an *I-V* curve with a rectangular shape and therefore a fill factor approaching unity.

The most commonly used acceptors in BHJ OPVs are soluble fullerene derivatives, such as [6,6]-phenyl-C61-butyric acid methyl ester ($PC_{61}BM$), or its analogue $PC_{71}BM$. Its donor counterpart (polymer) in the active layer usually serves as the main light absorber and the hole transporting phase.[67] Hence, a large optical absorption, matching the solar spectrum, and a good hole (bulk) mobility are required in an efficient polymer donor for solar cell applications. In contrast to the criteria for an efficient field effect charge carrier, the charge transport of a polymer donor in an OPV has to be high in the out-of-plane direction.

Remarkable progress has been achieved in this field in last few years, resulting in *PCE*s routinely surpassing 6 %.[68, 16b] For comparison, silicon based solar cells attain efficiencies of 25 %.[69] However, it is believed that going beyond 10 % a psychological barrier for the OPV industry may be surpassed, beyond which the low production costs could compensate the efficiency gap.[70] The most extensively studied donor is **P3HT** and shows, in combination with the appropriate acceptor, a record *PCE* of 6 %.[71] Furthermore, fused coplanar thiophene based heterocycles have been also effectively incorporated in polymers and used as efficient donors in a BHJ OPV. An illustrative example is alkoxy-benzodithiophene-*alt*-thienothiophene polymer, which in combination with $PC_{71}BM$ as the acceptor, revealed an impressive *PCE* of 7.4 %.[72] The device optimization realized through the incorporation of a fluorine containing conjugated polymer as a cathode interlayer led to further improvement of the *PCE* up to 8.3 % ($V_{OC}$ = 0.75 V, $J_{SC}$ = 15.75 mA $cm^{-2}$, *FF* = 70.15 %).[73]

## 1.5. Ethynelene π-Spacers Incorporated in Organic Semiconductors

Apart from poly-arylenes, poly-arylenevinylenes (PAVs) and poly-aryleneethynylenes (PAEs) have been studied as potential semiconductors as well.[74] However, the development of triple bond based materials was shadowed by the double bond containing systems, presumably due to an incorrect understanding of their electronic properties. Certainly, if the most widely used polymers are considered, the electron delocalization and charge stabilization are better in poly-arylenes and PAV than in PAE. Larger energy gaps and narrower bandwidths are found in case of PAEs, relative to the structurally close related PAVs, which might lead to a more difficult charge separation.[75] Nonetheless, an ethynylene π-spacer could be sterically and conformationally more favorable. For example, in PAV steric interactions between the ethylene unit and the aromatic core may lead to non-planar conformations disrupting the electron delocalization. On the contrary, any direct interaction in case of ethynylenes may produce bending distortions, but due to their *quasi*-cylindrical symmetry the conjugation will be preserved.[76]

The end of 1980s beginning of 1990s brought a break-through for PAEs materials,[77] when the groups of Weder,[78] Swager[79] and Müllen[80] showed that, owing to their unique properties, these materials present great potential in explosive detection, as molecular wires in bridging nanogaps, and as polarizers for LCDs.

## 1.5.1. Synthesis of PAEs

The increasing interest in PAEs was assisted by the remarkable synthetic advances made in this area in the recent decades.[81] One of the most frequently used *C–C* bond forming processes is the palladium-catalyzed coupling reaction of an aromatic halide (bromides or iodides) to terminal alkynes. This coupling reaction, called *Heck-Cassar-Sonogashira-Hagihara*[82], but most commonly referred to as *Sonogashira-Hagihara*, is a powerful tool to form *C–C* single bonds between a $sp^2$- and a *sp*-hybridized carbon center (Scheme 1).

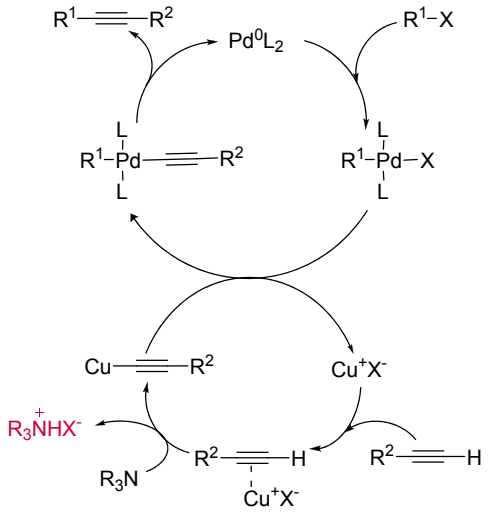


**Scheme 1.** Catalytic cycles of the copper-cocatalyzed *Sonogashira-Hagihara* cross-coupling reaction.

An often used *in situ* catalytic source of Pd(0) is $Pd(PPh_3)_2Cl_2$. It has been observed that the carbon-carbon triple bond can coordinate to the Pd(0) active complex before the oxidative addition, leading to the formation of unreactive or low reacting ($\eta$–RC≡CH)$Pd^0L_2$ complexes, through which a decelerating effect is created.[83] Although this is usually not a major problem when synthesizing low molecular weight compounds, it could be a setback in the synthesis of high molecular weight polymers, as it could limit the degree of polymerization. One possibility to overcome this difficulty is to use a small excess of the

terminal diyne to compensate for the alkyne consumed by the $Pd^{2+}$ precatalyst. Nonetheless, this approach also has a disadvantage, namely butadiyne defects might form in the polymeric backbone. To circumvent this, it is most desirable to use Pd(0) as catalyst ($Pd_2dba_3$, or $Pd(PPh_3)_4$),[84] although, as reported by Swager,[85] in order to obtain high molecular weight PAEs a small excess of diyne needs to be used even when $Pd(PPh_3)_4$ is employed.

Both, bromo- and iodo-aromatic compounds perform well as halogenated aromatic coupling partners. However, as the Pd(0) active catalyst involved in the oxidative addition step is an electron rich species, the nature of the halo-arene involved can dramatically influence the rate of this step and consequently the yield of the coupling reaction. Electron-withdrawing halogenated substrates are known to improve both the rate and the yield of the *Sonogashira-Hagihara* coupling reaction.

The choice of amine is also important. While for the coupling involving aryliodides diisopropylamine ($^{i}Pr_2NH$) or piperidine in combination with $Pd(PPh_3)_4$ work very well, for bromides, triethylamine or (isopropyl)ethylamine (Hünig's base) are more appropriate.[86] It is sometimes necessary to employ a co-solvent such as THF or toluene to ensure the solubility of the resulting polymer.

A second synthetic procedure in building up a PAE is *via* acyclic diyne methathesis (ADIMET).[87] The polymer is built up through the exchange alkylidyne units between a pair of aliphatic or aromatic acetylene derivatives. The most widely used catalysts are based on molybdenum or tungsten complexes with alkoxide or phenoxide ligands.

The first soluble and high molecular weight poly(*p*-phenylene-ethynylene)s (PPE) synthesized *via* Pd catalyzed cross-coupling was reported by Müllen in 1995.[88] It was shown that under the *Sonogashira-Hagihara* coupling conditions, high molecular weight polymers were obtainable with the iodine substituents assumed to be the end groups, although some dehalogenation under reduction or phosphonium salt formation could not be excluded (Scheme 2).[89] A few years later, the same group reported the first synthesis of PPEs *via* tungsten catalyzed alkyne methathesis.[90] The research of the following years has been oriented towards the development of a new catalyst meant to secure the synthesis of high purity PPEs in quantitative yields. The *in situ* generated *Mortreux-Mori-Bunz* (Scheme 2)

catalyst, from the commercially available $Mo(CO)_6$ and phenol reagents, fulfilled this requirement.[91]

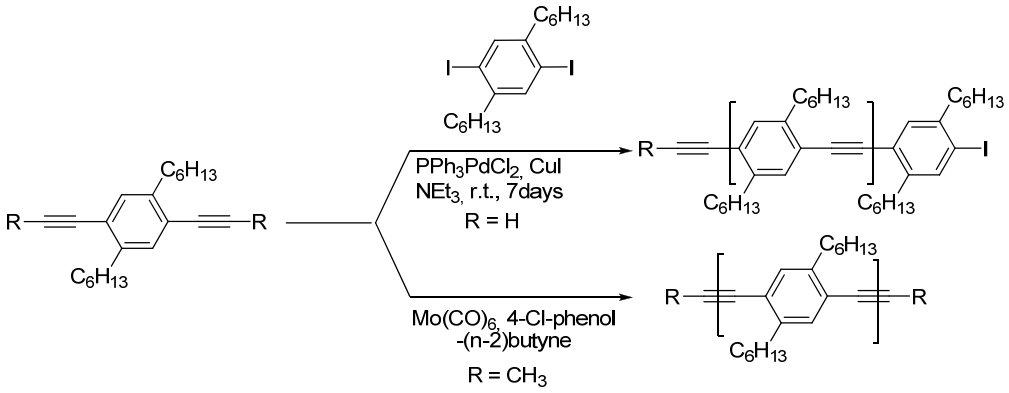


**Scheme 2.** Synthesis of dihexyl substituted poly-(*p*-phenylenes) *via* palladium catalyzed *Sonogashira-Hagihara* cross-coupling and acyclic diyne methathesis by the *Mortreux-Mori-Bunz* catalyst.

However, the applicability of the ADIMET is limited. In the case of D-A type PAEs, the synthesis of the required monomer would be in most cases a tedious multi-step reaction sequence. Therefore, the majority of the acetylene based materials reported as promising semiconductor candidates were typically obtained under *Sonogashira-Hagihara* cross-coupling conditions.

## 1.5.2. OFET and OPV Applications of PAEs

The triple bond containing low molecular weight materials proved to be propitious competitors in the quest of finding high charge transport materials suitable for OFET or OPV applications. For example, Roy *et al*. have shown that vapor-deposited oligomeric arylacetylenes (**TPA**) could show field effect hole mobilities as high as 0.3 $cm^2V^{-1}s^{-1}$ ($I_{ON}$ / $I_{OFF}$ = $10^5$) (Chart 3).[92] The work of Meng *et al.* revealed that solution–processed thiophene-ethynyl-phenylenes[93] (**DTEP**) exhibit hole mobilities approaching 0.1 $cm^2V^{-1}s^{-1}$ ($I_{ON}$ / $I_{OFF}$ = $10^5$). Vacuum-deposited diethynyl–naphthalenes[94] (**BH202**, Chart 3) proved to perform well in high performance OFETs with hole mobilities over 0.1 $cm^2V^{-1}s^{-1}$

($I_{ON}$ / $I_{OFF}$ ≈ $10^5$). Silvestri *et al.* have very recently reported on the promising performance of solution-processed anthracene-ethynyl-phenylenes (**A-P6t** and **PA-P6t**, Chart 3) as active components of OFETs and OPVs.[95b] Although **A-P6t** showed satisfactory power conversion efficiency, as the donor in combination with $PC_{61}BM$ in bulk heterojunction solar cells, its field effect hole mobility was modest.[95] By introducing an additional ethynylene-phenyl repeating units at both 9 and 10 positions of anthracene (**PA-P6t**), the hole mobility of the resulting oligomer was increased by 2 orders of magnitude (measured in vacuum). Additionally, **PA-P6t** exhibited similar solar cell efficiency (*PCE* = 1.2 %) reflecting high $V_{OC}$ ≈ 0.9 V and good $J_{SC}$ ≈ 3 mA $cm^{-2}$ values.

**Chart 3.** Representative low molecular weight semiconductors with incorporated ethynylene π-spacers.

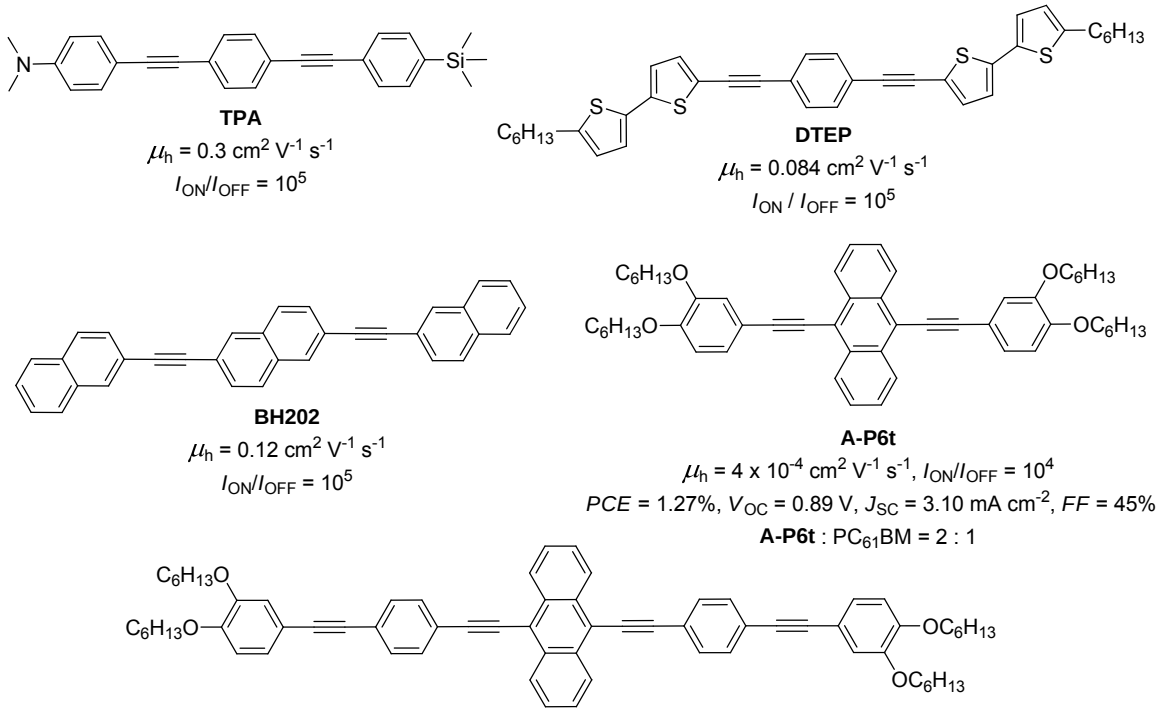


A variety of PAEs were synthesized and proved to be promising candidates for mostly optoelectronic applications. Chart 4 contains some of the representative polymers of this class. The group of René Janssen[96] synthesized a poly(ethynylene-bithienylene) (**P3HTE**) tested as a donor in OPV cell and the results were compared to the device based on the

structurally similar **P3HT**. The results emphasize the beneficial effect of the ethynylene linker on the $V_{OC}$. The PCBM / **P3HTE** device showed a $V_{OC}$ of 1.03 V, significantly higher than the one measured for PCBM / **P3HT** cell ($V_{OC} \approx 0.62$ V).[97] However, the lack of aggregation of **P3HTE** in blend with PCBM limited the photon absorption and the mobility of the photogenarated holes. The low fill factor and $J_{SC}$ reduced the efficiency to 1.13%. Ashraf *et al.*[98] synthesized a thienopyrazine based low band gap poly(heteroarylethynylene) polymer (**PT12TP**). Owing to the efficient D-A interaction through the ethynylene π-spacers within the polymer backbone, the resulting material revealed absorption between 300 - 800 nm. Applied in a OPV device fabricated on a polyester foil as a counterpart to PCBM, the cell exhibited a $J_{SC}$ = 10.72 mA cm$^{-2}$ and modest fill factor and $V_{OC}$ values and therefore a PCE of 2.37%. Recently the group of Baek[99] developed a series of Pt-based D (thienothiophene) – A (benzothiadiazole) type polymers (**PTTBTZ-Pt**) that showed the great potential of ethynylene containing polymers as field effect charge carriers ($\mu_h$ = 0.01 cm$^2$V$^{-1}$s$^{-1}$, $I_{ON}$ / $I_{OFF}$ = 10$^6$) and donors in an BHJ OPV cell (average power conversion efficiency of 3.73%).

**Chart 4.** Representative high molecular weight semiconductors with incorporated ethynylene π-spacers.

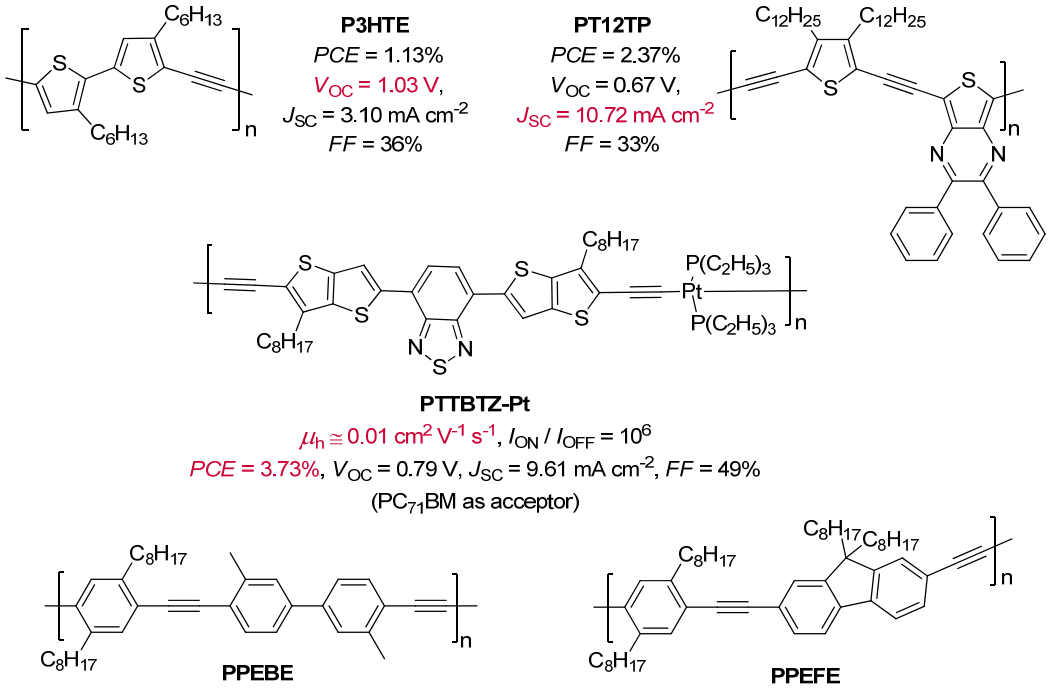

Notably, there are no reports on clean ambipolar charge transport behavior for triple bond containing polymers or small molecules when applied in OFETs. However, the group of Jung-Il Jin[100] reported on blue-light emitting PAEs (**PPEBE** and **PPEFE**) and correlated their performance as active components in OLED devices with the mobilities determined by time of flight (TOF) measurements (Chart 4). The measured charge carrier mobilities for **PPEBE** were $\mu_h = 2 \times 10^{-4}$ $cm^2V^{-1}s^{-1}$ and $\mu_e = 7 \times 10^{-5}$ $cm^2V^{-1}s^{-1}$ (at an electric field of $1.9 \times 10^5$ V $cm^{-1}$). In contrast **PPEFE** showed lower mobilities for both carriers, with the $\mu_h = 8 \times 10^{-6}$ $cm^2V^{-1}s^{-1}$ (at an electric field of $1.7 \times 10^6$ V $cm^{-1}$) a 120 times its $\mu_e = 6.5 \times 10^{-8}$ $cm^2V^{-1}s^{-1}$ (at an electric field of $8.6 \times 10^5$ V $cm^{-1}$).

## 1.6. Aims and Scope of the Research: The Playground is Set, the Tools Were Handed Out

The research described in this work aims to design, synthesize and characterize new semiconducting polymers with tuned optoelectronic properties that would enable efficient ambipolar or n-type charge carriers transport for OFETs or OPVs applications. The main goal is achieved by following rational design principles meant to exploit the beneficial properties of the thiadiazolo[3,4-*g*]quinoxaline (TQ)[101] building block as a planar, electron deficient heterocycle and those of ethynylene π-spacers,[74] connecting the donor and the acceptor unit in a D-A copolymer. The donor strength variation of the electron rich building block aims to tune the position and separation of the energy levels. Within this frame of work, synthetic issues as well as detailed optoelectronic studies of the conjugated polymers and their corresponding model compounds are covered. The charge carrier properties of the obtained polymer semiconductors are investigated as active components of OFET devices. It shall be shown that incorporating ethynylene π-spacers in π-conjugated systems is an effective strategy for tuning charge transport characteristics. The performance of these semiconducting polymers is then correlated with their solid state organization as investigated by X-ray

scattering and atomic force microscopy. Additionally, the possibility of incorporating this type of polymers, as a substitute for PCBM, in an efficient OPV cell is addressed as well. Therefore, the results of this research shall constitute a useful template that might lead to advances in the design of new materials for efficient charge carrier transport applications.

For the design of functional materials with predefined molecular properties, it is desirable to understand electron transfer (ET) processes.[102] The study of the ET processes is one of the most fundamental tools for the investigation of electron flow over large distances, as it is most likely to occur by hopping mechanism.[103] For instance, it would be essential to know the extent of the molecular hopping positions over which an electron can be delocalized. The molecules with purely organic redox centers are most suitable to investigate the basic aspects of the ET theories,[104] as their intervalence absorption band typically tends to show high extinction coefficients. Hence, it is possible to check the applicability of the Markus ET theory and its extension, the Hush theory, for interpreting the intervalence charge transfer band.[105] Within this context, the last part of this work aims to explore mixed-valence phenothiazines (**Ptz**) and their electron transfer processes, when connected *via* an electron deficient π-bridge, such as benzo[*c*][2,1,3]thiadiazole. Additionally, the high reorganization energy typical for phenothiazine derivatives could open the possibility to directly measure the ET rates by electron paramagnetic resonance (EPR) spectroscopy.

### 1.6.1. Enabling Electron Charge Transport in a Thiadiazolo[3,4-*g*]quinoxaline-based Polymer Semiconductor: Design Considerations

The design strategy for the synthesis of polymers showing electron charge transport was based on the idea that semiconducting polymers should intrinsically be able to effectively transport both holes and electrons. The number of different n-channel and ambipolar polymers reported up to date, hold the common feature of being low energy gap materials (< 2 eV). This is usually obtained for alternating donor-acceptor-like (D-A) structures, realized

through the copolymerization of an electron-rich (donor) and an electron-poor (acceptor) heteroaromatic unit. The presence of strong acceptor cores in the polymer backbone should promote an efficient electron charge transport. Hence, thiadiazolo[3,4-*g*]quinoxaline (TQ), as an acceptor core, is the focus of this research owing to its high electron affinity and available functionalizable positions. By accessing these positions the solubility of the resulting polymer could be enhanced and the optoelectronic properties tuned. TQs have been incorporated in D-A type copolymers that were mostly studied as donors in combination with PCBM derivatives for photovoltaic applications. Notably, all of these polymers possessed at least two D segments per repeating unit and none of them revealed ambipolar and / or electron charge transport characteristics.

Therefore, the structural design pursued in this research work was guided by the following points:

- To enable electron charge transport in the TQ-based systems the electron rich character of the resulting polymer must be reduced by decreasing the number of D segments per repeating unit to one;
- The introduction of alkyl chains at the TQ and / or D is mandatory for the solution processability of the semiconducting polymer;
- To ensure good π-orbital overlap along the polymer backbone, essential for an efficient charge transport, any possible steric hindrance between the TQ core and the donor segment must be minimized;
- Introduction of a π-spacer (ethylene or ethynylene) between the TQ and the D core is accommodating for a minimal steric constrains;

The nature of the π-spacer can be further explored in the fine tuning of the optoelectronic properties of the resulting semiconducting material. It is well known that the properties of the polymers could be correlated to characteristics of their corresponding model compounds.[106] Within this context, model compounds were synthesized and investigated. The role played by the nature of the:

- π-spacer (ethylene or ethynylene) inserted between the TQ and the D unit;
- donor attached directly, and through a π-spacer to the TQ core

on the fine tuning of the electronic (energy levels) and photophysical (absorption and emission) properties. The scrutinized experimental findings serve as an additional starting

point for structural design leading towards an efficient electron charge transport in a TQ-based polymer.

## 1.6.2. Mixed-Valence Phenothiazines: Design Considerations

The inter- and intramolecular self-exchange between **Ptz** redox centers has been investigated in the recent years but almost exclusively in systems in which the **Ptz** redox centers were connected via their N atom to the phenyl bridge and thereby the effective ET distance (separation parameter) was rather low (< 8.6 Å).

This research explores the theoretical and experimental repercussions of an increased effective ET distance between the two **Ptz** redox centers coupled through an electron deficient bridge, such as benzo[*c*][2,1,3]thiadiazole. Upon connecting the π-bridge to the **Ptz** segment at position 3, the separation parameter is increased. The ET process could be analyzed within the Markus-Hush formalism[107] based on the transient appearance of the diagnostic intervalence absorption band. Furthermore, the theoretical evaluation of the electronic coupling element, the effective activation barrier, and the rate constant of the ET is also possible. Apart from being able to investigate the molecular model of such a system, the synthesis of the corresponding polymer and the study of the ET in this system would offer additional mechanistic insight into the ET processes.

# 1.7. References

*1.* Shirakawa, H.; Louis, E. J.; MacDiarmid, A. G.; Chiang, C. K.; Heeger, A. J. *J. Chem. Soc. Chem. Commun*. **1977**, *16*, 578.

*2.* (a) Kertész, M.; Choi, C. H.; Yang, S. *Chem. Rev.* **2005**, *105*, 3448. (b) Roncali, J. Leriche, P. Cravino A. *Adv. Mater.* **2007**, *19*, 2045.

*3*. (a) Farchioni, R.; Grosso, G. *"Organic Electronic Materials: Conjugated Polymers and Low Molecular Weight Organic Solids"* Springer: Berlin, **2001**.(b) Miller, L. S.; Mullin, J. B. *"Electronic Materials: From Silicon to Organics"* Plenum Press: New York, **1991**.

*4*. Küppe, A.; Bossart, O.; Calzaferri, G.; Sariciftci, N. S. *Sol. Energ. Mater. Sol. Cell.* **2007**, *91*, 986. (b) Chen, C. P.; Chan, S. H.; Chao, T. C.; Ting, C.; Ko, B. T. *J. Am. Chem. Soc.* **2008**, *130*, 12828. (c) Bagnis, D.; Beverina, L.; Huang, H.; Silvestri, F.; Yao, Y.; Yan, H.; Pagani, G. A.; Marks, T. J.; Facchetti, A. *J. Am. Chem. Soc*. **2010**, *132*, 4074.

*5*. (a) Luo, J.; Zhou, Y.; Niu, Z. Q.; Zhou, Q. F.; Ma, Y.; Pei, J. *J. Am. Chem. Soc.* **2007**, *129*, 11314. (b) Ooi, Z. E.; Tam, T. L.; Shin, R. Y. C.; Chen, Z. K.; Kietzke, T.; Sellinger, A.; Baumgarten, M.; Müllen, K.; deMello, J. *J. Mater. Chem.* **2008**, *18*, 4619. (c) Allard, S.; Forster, M.; Souharce, B.; Thiem, H.; Sherf, U. *Angew. Chem. Int. Ed.* **2008**, *47*, 4070. (d) Tang, M. L.; Mannsfeld, S. C. B.; Sun, Y. -S.; Becerril, H. A.; Bao, Z. *J. Am. Chem. Soc.* **2009**, *131*, 882. (e) Wei, S. K. H.; Chen, S. H.; Dolgaleva, K.; Lukishova, S.; Boyd, R. W. *Appl. Phys. Lett.* **2009**, *94*, 041111/1.

*6*. (a) Sirringhaus, H.; Ando, M. *MRS Bull.* **2008**, *33*, 676. (b) Facchetti, A. *Mater. Today* **2007**, *10*, 28. (c) Arias, A. C.; MacKenzie, J. D.; McCulloch, I.; Rivnay, J.; Salleo, A. *Chem. Rev.* **2010**, *110*, 3.

*7.* Sirringhaus, H.; Tessler, N.; Friend, R. H. *Science* **1998,** *280*, 1741. (b) Friend, R. H.; Gymer, R. W.; Holmes, A. B.; Burroughes, J. H.; Marks, R. N.; Taliani, C.; Bradley, D. D. C.; Dos Santos, D. A.; Bredas, J. L.; Logdlund, M.; Salaneck, W. R. *Nature* **1999**, *397*, 121.

*8.* (a) Thompson, B. C.; Frechet, J. M. J. *Angew. Chem. Int. Ed.* **2008**, *47*, 58. (b) Shrotriya, V. *Nature Photon.* **2009**, *3*, 447. (c) Beaujuge, P. R.; Reynolds, J. R. *Chem. Rev.* **2010**, *110*, 268

*9*. Someya, T.; Pal, B.; Huang, J.; Katz, H. E. *MRS Bull.* **2008**, *33*, 690.

*10.* Arias, A. C.; MacKenzie, J. D.; McCulloch, I.; Rivnay, J.; Salleo, A. *Chem. Rev.* **2010**, *110*, 3.

*11*. (a) Norton, P.; Braggins, T.; Levinstein H. *Phys. Rev.* **1973**, *B8*, 5632. (b) Morin, F. J.; Maita, J. P. *Phys. Rev.* **1954**, *96*, 28.

*12*. Ginley, D.; Green, M. A.; Collins, R. *MRS Bull.* **2008**, *33*, 355.

*13*. Dargys, A.; Kundrotas, J. *„Handbook on Physical Properties of Ge, Si, GaAs and InP“*, Vilnius, Science and Encyclopedia Publishers, **1994**.

*14*. Woodall, J. M.; IBM T.J. Watson Research Center, private communication, "*Don't seriously try to make it out of anything else if it has a chance of working with silicon*" [paraphrased], **1982**.

*15*. (a) Pingel, P.; Zhu, L.; Park, K. S.; Vogel, J. -O.; Janietz, S.; Kim, E.-G.; Rabe, J. P.; Bredas, J. -L.; Koch, N. *J. Phys. Chem. Lett.* **2010**, *1*, 2037. (b) Bredas, J.-L.; Norton, J. E.; Cornil, J.; Coropceanu, V. *Acc. Chem. Res.* **2009**, *42*, 1691.

*16.*(a) Choi, S. H.; Risko, C.; Ruiz Delgado, M. C.; Kim, B. S.; Bredas, J. -L.; Frisbie, C. D. *J. Am. Chem. Soc.* **2010**, *132*, 4358. (b) Facchetti, A. *Chem. Mater*. **2011**, *23*, 733.

*17*. Bonilla, L. L. *J. Phys.-Condes. Matter* **2002**, *14*, R341.

*18*. Coropceanu, V.; Cornil, J.; da Silva, D. A.; Olivier, Y.; Silbey, R.; Bredas, J. L. *Chem. Rev.* **2007**, *107*, 2165.

*19.* Jaiswal, M.; Menon, R. *Polym. Int.* **2006***, 55,* 1371*.*

*20.* Emin, D. *Adv. Phys.* **1975**, *24,* 305.

*21*. (a) Marcus, R. A. *Angew. Chem., Int. Ed. Engl*. **1993**, *32*, 1111. (b) Marcus, R. A. *Discuss. Faraday Soc.* **1960**, *29*, 21. (c) Marcus, R. A. *J. Chem. Phys.* **1965**, *43*, 679. (d) Marcus, R. A.; Sutin, N. *Biochim. Biophys. Acta* **1985**, *811*, 265.

*22*. (a) Newton, M. D. *"Electron Transfer in Chemistry"* Balzani, V., Ed.; Wiley-VCH: New York, **2001**; *pp 3*. (b) Astruc, D. *"Electron Transfer and Radical Processes in Transition-Metal Chemistry"*; Wiley-VCH: New York, **1995**. (c) Cannon, R. D. *"Electron-Transfer Reactions"*; Butterworth: London, **1980**.

*23*. Hush, N. S. *Trans. Faraday Soc.* **1961**, *57*, 557. (b) Hush, N. S. *Prog. Inorg. Chem.* **1967**, *8*, 391. (c) Hush, N. S. *Electrochim. Acta* **1968**, *13*, 1005.

*24*. (a) Eberson, L. *"Electron-Transfer Reactions in Organic Chemistry"* Springer-Verlag: New York, **1987**. (b) Nelsen, S.; Pladziewicz, J. *Acc. Chem. Res.* **2002**, *35*, 247.

*25*. Robin, M. B.; Day, P. *Adv. Inorg. Chem. Radiochem.* **1967**, *10*, 247.

*26*. Rosokha, S. V.; Kochi, J. K. *J. Am. Chem. Soc.* **2007**, *129*, 3683.

*27*. Baumgarten, M.; Huber, W.; Müllen, K. *Advances in Physical Organic Chemistry* Academic Press: London, **1993**, 28, *p.* 1.

*28.* (a) Hankache, J.; Wenger, O. S. *Chem. Rev.* **2011**, *111*, 5138. (b) D'Alessandro, D. M.; Keene, F. R. *Chem. Soc. Rev.* **2006**, *35*, 424.

*29*. (a) Pettersson, K.; Wiberg, J.; Ljungdahl, T.; Mårtensson, J.; Albinsson, B. *J. Phys. Chem. A* **2006**, *110*, 319. (b) Nelsen, S. F.; Ismagilov, R. F.; Powell, D. R. *J. Am. Chem. Soc.* **1997**, *119*, 10213. (c) Nelsen, S. F.; Newton, M. D. *J. Phys. Chem. A* **2000**, *104*, 10023.

*30*. (a) Zhou, G.; Baumgarten, M.; Müllen, K. J. *Am. Chem. Soc.* **2007**, *129*, 12211. (b) Knorr, A.; Daub, J. *Angew. Chem., Int. Ed.* **1997,** *36*, 2817.

*31.* (a) Jones, S. C.; Coropceanu, V.; Barlow, S.; Kinnibrugh, T.; Timofeeva, T.; Brédas, J. L.; Marder, S. R. *J. Am. Chem. Soc.* **2004**, *126*, 11782. (b) Schull, T. L.; Kushmerick, J. G.; Patterson, C. H.; George, C.; Moore, M. H.; Pollack, S. K.; Shashidhar, R. *J. Am. Chem. Soc.* **2003,** *125*, 3202.

*32.* (a) Amthor, S.; Lambert, C. *J. Phys. Chem. A* **2006**, *110*, 1177. (b) Kattnig, D. R.; Mladenova, B.; Grampp, G.; Kaiser, C.; Heckmann, A.; Lambert, C. *J. Phys. Chem. C* **2009**, *113*, 2983.

*33.* (a) Nelsen, S. F.; Ismagilov, R. F.; Powell, D. R. *J. Am. Chem. Soc.* **1997**, *119*, 10213. (b) Rosokha, S. V.; Sun, D. -L.; Kochi, J. K. *J. Phys. Chem. A* **2002**, *106*, 2283.

*34.* (a) Sun, D.; Rosokha, S. V.; Kochi, J. K. *Angew. Chem., Int. Ed.* **2005**, *44*, 5133. (b) Yan, X. Z.; Pawlas, J.; Goodson, T.; Hartwig, J. F. *J. Am. Chem. Soc*. **2005**, *127*, 9105.

*35*. Heeger, A. J. *Rev. Mod. Phys.* **2001**, *73*, 681.

*36*. Heeger, A. J. *Faraday Discuss. Chem. Soc.* **1989**, *88*, 203.

*37.* (a) Sharma, A.; Mathijssen, S.; Smits, E.; Kemerink, M.; de Leeuw, D.; Bobbert, P. *Phys. Rev. B* **2010**, *82*, 075322. (b) Häusermann, R.; Batlogg, B. *Appl. Phys. Lett.* **2011**, *99*, 083303.

*38.* Malliaras, G. *"Organic Semiconductors and Devices"* Ed.; JohnWiley & Sons: Hoboken, **2003**.

*39*. (a) Sirringhaus, H. *Nat. Mater.* **2003**, *2*, 641. (b) Kowalsky, W.; Becker, E; Benstem, T.; Johannes, H. -H.; Metzdorf, D.; Neuner, H.; Schobel, J. *Adv. Solid State Phys*. **2000**, *40*, 795. (c) Horowitz, G. *Adv. Mater.* **1990**, *2*, 287.

*40*. (a) Katz, H. E. *Chem. Mater.* **2004**, *16*, 4748. (b) Allard, S.; Forster, M.; Souharce, B.; Thiem, H.; Scherf, U. *Angew. Chem., Int. Ed.* **2008**, *47*, 4070.

*41.* (a) Li, Y. N.; Wu, Y. L.; Liu, P.; Birau, M.; Pan H. L.; Ong, B. S. *Adv. Mater.* **2006**, *18*, 3029. (b) Chabinyc, M. L.; Toney, M. F.; Kline, R. J.; McCulloch, I.; Heeney, M. *J. Am. Chem. Soc.* **2007**, *129*, 3226.

*42*. (a) Kline, R. J.; McGehee, M. D.; Kadnikova, E. N.; Liu J.; Frechet, J. M. J. *Adv. Mater.* **2003**, *15*, 1519; (b) Kline, R. J.; McGehee, M .D.; Kadnikova, E. N.; Liu, J.; Frechet, J. M. J.; Toney, M. F. *Macromolecules* **2005**, *38*, 3312. (c) Schilinsky, P.; Asawapirom, U.; Scherf, U.; Biele, M.; Brabec, C. J. *Chem. Mater*. **2005**, *17*, 2175.

*43*. Pron, A.; Gawrys, P.; Zagorska, M.; Djurado, D.; Demadrille, R. *Chem. Soc. Rev.* **2010**, *39*, 2577.

*44*. Gawrys, P.; Boudinet, D.; Zagorska, M.; Djurado, D.; Verilhac, J.-M.; Horowitz, G.; Pecaud, J.; Pouget, S.; Pron, A. *Synth. Met.* **2009**, *159*, 1478.

*45*. (a) Klauk, H. *"Organic Electronics: Materials, Manufacturing, and Applications"* Ed.; Wiley-VCH: Weinheim, Germany, **2006**. (b) Crawford, G. P. *"Flexible flat panel display"* Ed.; Wiley: New York, **2005**.

*46*. (a) Allard, S.; Forster, M.; Souharce, B.; Thiem H.; Scherf, U. *Angew. Chem., Int. Ed.* **2008**, *47*, 4070. (b) Murphy A. R.; Frechet, J. M. J. *Chem. Rev*. **2007**, *107*, 1066. (c) Newman, C. R.; Frisbie, C. D.; da Silva Filho, D. A.; Bredas, J. -L.; Ewbank P. C.; Mann, K. R. *Chem. Mater.* **2004**, *16*, 4436.

*47*. Katz, H. E.; Huang, J. *Annu. Rev. Mater. Res.* **2009**, *39*, 71.

*48.* Cornil, J.; Bredas, J. L.; Zaumseil, J.; Sirringhaus, H. *Adv. Mater.* **2007**, *19*, 1791.

*49*. Facchetti, A.; Letizia, J.; Yoon, M. -H.; Mushrush, M.; Katz, H. E.; Marks, T. J. *Chem. Mater.* **2004**, *16*, 4715.

*50.* (a) Sundar, V. C.; Zaumseil, J.; Podzorov, V.; Menard, E.; Willett, R. L.; Someya, T.; Gershenson, M. E.; Rogers, J. A. *Science* **2004**, *303*, 1644. (b) Jurchescu, O. D.; Popinciuc, M.; van Wees, B. J.; Palstra, T. T. M. *Adv. Mater.* **2007**, *19*, 688.

*51*. Anthony, J. E. *Chem. Rev.* **2006**, *106*, 5028.

*52*. Llorente, G. R.; Dufourg-Madec, M. B.; Crouch, D. J.; Pritchard, R. G.; Ogier S.; Yeates, S. G. *Chem. Commun.* **2009**, 3059.

*53*. Ebata, H.; Izawa, T.; Miyazaki, E.; Takimiya, K.; Ikeda, M.; Kuwabara, H.; Yui, T. *J. Am. Chem. Soc.* **2007**, *129*, 15732.

*54*. Gao, P.; Beckmann, D.; Tsao, H. N.; Feng, X.; Enkelmann, V.; Baumgarten, M.; Pisula, W.; Müllen, K. *Adv. Mater.* **2009**, *21*, 213.

*55*. Tatemichi, S.; Ichikawa, M.; Koyama, T.; Taniguchi, Y. *Appl. Phys. Lett.* **2006**, *89*, 112108.

*56.* Ando, S.; Nishida, J.; Tada, H.; Inoue, Y.; Tokito, S.; Yamashita, Y. *J. Am. Chem. Soc.* **2005**, *127*, 5336.

*57*. Kumaki, D.; Ando, S.; Shimono, S.; Yamashita, Y.; Umeda, T.; Tokito, S. *Appl. Phys. Lett*. **2007**, *90*, 053506.

*58*. (a) Zhang, R.; Li, B.; Iovu, M. C.; Jeffries, L. M.; Sauve, G.; Cooper, J.; Jia, S.; Tristram-Nagle, S.; Smilgies, D. M.; Lambeth, D. N.; McCullough, R. D.; Kowalewski, T. *J. Am. Chem.* Soc. **2006**, *128*, 3480. (b) Chang, J. -F.; Sun, B.; Breiby, D. W.; Nielsen, M. M.; Soelling, T. I.; Giles, M.; McCulloch, I.;

Sirringhaus, H. *Chem. Mater.* **2004**, *16*, 4772. (c) Kim, D. H.; Jang, Y.; Park, Y. D.; Cho, K. *J. Phys. Chem. B* **2006**, *110*, 15763. (d) Surin, M.; Leclere, Ph.; Lazzaroni, R.; Yuen, J. D.; Wang, G.; Moses, D.; Heeger, A. J.; Cho, S.; Lee, K. *J. Appl. Phys.* **2006**, *100*, 033712.

*59.* Osaka, I.; Zhang, R.; Sauve, G.; Smilgies, D; Kowalewski, T.; McCullough, R. D. *J. Am. Chem. Soc.* **2009**, *131*, 2521.

*60*. Rieger, R.; Beckmann, D.; Pisula, W.; Steffen, W.; Kastler, M.; Müllen, K. *Adv. Mater.* **2010**, *22*, 83.

*61*. Zhang, M.; Tsao, H. N.; Pisula, W.; Yang, C.; Mishra, A. K.; Müllen, K. *J. Am. Chem. Soc.* **2007**, *129*, 3472.

*62*. Tsao, H. N.; Cho, D. M.; Park, I.; Hansen, M.; Mavrinskiy, A.; Yoon, D. Y.; Graf, R.; Pisula, W.; Spiess, H. W.; Müllen, K. *J. Am. Chem. Soc.* **2011**, *133*, 2605.

*63*. Burgi, L.; Turbiez, M.; Pfeiffer, R.; Bienewald, F.; Kirner, H.; Winnewisser, C. *Adv. Mater.* **2009**, *20*, 2217.

*64.* (a) Arkhipov, V. I.; Bässler, H. *Phys. Status Solidi A* **2004**, *201*, 1152. (b) Gregg, B. A.; Hanna, M. C. *J. Appl. Phys.* **2003**, *93*, 3605. (c) Hoppe, H.; Sariciftci, N. S. *J. Mater. Res.* **2004**, *19*, 1924.

*65.* Tang, C. W. *Appl. Phys. Lett.* **1986**, *48*, 183.

*66*. Li, C.; Liu, M.; Pschirer, N. G.; Baumgarten, M.; Müllen, K. *Chem. Rev.* **2010**, *110*, 6817.

*67*. Li, Y.; Zou, Y. *Adv. Mater.* **2008**, *20*, 2952.

*68.* Boudreault, P. -L. T.; Najari, A.; Leclerc, M. *Chem. Mater.* **2011**, *23*, 456.

*69*. Green, M. A.; Emery, K.; Hishikawa, Y.; Warta, W. *Prog. Photovolt. Res. Appl.* **2009**, *17*, 85.

*70*. (a) Brabec, C. J.; Scherf, U.; Dyankonov, V. *"Organic Photovoltaics: Materials, Device Physics, and Manufacturing Technologies"*, 1st Ed.; Wiley-VCH, **2008**. (b) http://www.solardaily.com/reports/Solarmer_Energy_Breaks_Psychological_Barrier_999.html

*71*. He, Y.; Chen, H. -Y.; Hou, J.; Li, Y. *J. Am. Chem. Soc.* **2010**, *132*, 1377.

*72*. Liang, Y.; Xu, Z.; Xia, J.; Tsai, S. -T.; Wu, Y.; Li, G.; Ray, C.; Yu, L. *Adv. Mater.* **2010**, *22*, E135.

*73*. He, Z.; Zhong, C.; Huang, X.; Wong, W. -Y.; Wu, H.; Chen, L.; Su, S.; Cao, Y. *Adv. Mater.* **2011**, *23*, 4636.

*74.* Silvestri, F.; Marrocchi, A. *Int. J. Mol. Sci.* **2010**, *11*, 1471.

*75.* Bredas, J. L.; Chance, R. R.; Baughman, R. H.; Silbey, R. *J. Chem. Phys.* **1982**, *76*, 3673.

*76.* (a) Young, J. K.; Moore, J. S. *"Modern Acetylene Chemistry"*; Stang, P.J.; Diederich, F. Eds.; CH: Weinheim, Germany, **1995**, *p.* 415. (b) Bunz, U. H. F. *Chem. Rev.* **2000**, *100*, 1605.

*77.* (a) Rutherford, D. R.; Stille, J. K. *Macromolecules* **1988**, *21*, 3530. (b) Neenan, T. X.; Callstrom, M. R.; Scarmoutzos, L. M.; Stewart, K. R.; Whitesides, G. M.; Howes, V. R. *Macromolecules* **1988**, *21*, 3525. (c) Grubbs, R. H.; Kratz, D. *Chem. Ber.* **1993**, *126*, 149. (d) Schumm, J. S.; Pearson, D. L.; Tour, J. M. *Angew. Chem.* **1994**, *33*, 1360. (e) Prest, P. J.; Prince, R. B.; Moore, J. S. *J. Am. Chem. Soc.* **1999**, *121*, 5933.

*78.* (a) Weder, C.; Sarwa, C.; Montali, A.; Bastiaansen, G.; Smith, P. *Science* **1998**, *279*, 835. (b) Montali, A.; Bastiaansen, G.; Smith, P.; Weder, C. *Nature* **1998**, *392*, 261.

*79.* Yang, J. S.; Swager, T. M. *J. Am. Chem. Soc.* **1998**, *120*, 11864.

*80.* Mangel, T.; Eberhardt, A.; Scherf, U.; Bunz, U. H. F.; Müllen, K. *Macromol. Rapid Commun.* **1995**, *16*, 571.

*81.* (a) Nielsen, M. B.; Diederich, F. *Chem. Rev.* **2005**, *105*, 1837. (b) Li, C.; Li, Y. *Macromol. Chem. Phys.* **2008**, *209*, 1541. (c) Kivala, M.; Diederich, F. *Acc. Chem. Res.* **2009**, *42*, 235. (d) Liu, J.; Lam, J. W. Y.; Tang, B. Z. *Chem. Rev.* **2009**, *109*, 5799.

*82.*(a) Dieck, H. A.; Heck, R. F. *J. Organomet. Chem.* **1975**, *93*, 259. (b) Cassar, I. J. Organomet. Chem. **1975**, 93, 253. (c) Sonogashira, K.; Tohda, Y.; Hagihara, N. *Tetrahedron Lett.* **1975**, *16*, 4467.

*83.* (a) Jutand, A. *Pure Appl. Chem.* **2004**, *76*, 565. (b) Amatore, C.; Bensalem, S.; Ghalem, S.; Jutand, A.; Medjour, Y. *Eur. J. Org. Chem.* **2004**, 366.

*84.* (a) Häger, H.; Heitz, W. *Macromol. Chem. Phys.* **1998**, *199*, 1821. (b) Moore, J. S.; Zhang J. S. *Angew. Chem.* **1992**, *31*, 922. (c) Ofer, D.; Swager, T. M.; Wrighton, M. S. *Chem. Mater*. **1995**, *7*, 418.

*85.* Zhou, Q.; Swager, T. M. *J. Am. Chem. Soc.* **1995**, *117*, 12593.

*86.* Alami, M.; Ferri, F.; Linstrumelle, G. *Tetrahedron Lett.* **1993**, *34*, 6403.

*87.* (a) Brizius, G.; Pschirer, N. G.; Steffen, W.; Stitzer, K.; zur Loye, H. C.; Bunz, U. H. F. *J. Am. Chem. Soc.* **2000**, *122*, 12435. (b) Schrock, R. R.; Czekelius, C. *Adv. Synth. Catal.* **2007**, *349*, 55. (c) Fürstner, A.; Davies, P. W. *Chem. Commun.* **2005**, *18*, 2307.

*88.* Francke, V.; Mangel, T.; Müllen, K. *Macromolecules* **1998**, *31*, 2447.

*89.* Goodson, F. E.; Wallow, T. I.; Novak, B. M. *J. Am. Chem. Soc.* **1997**, *110*, 12441.

*90.* Weiss, K.; Michel, A.; Auth, E. M.; Bunz, U. H. F.; Mangel, T.; Müllen, K. *Angew. Chem.* **1997**, *36*, 506.

*91.* Bunz, U. H. F. *Acc. Chem. Res.* **2001**, *34*, 998.

*92*. Roy, V. A. L.; Zhi, Y. -G.; Xu, Z. -X.; Yu, S. -C.; Chan, P. W. H.; Che, C. -M. *Adv. Mater.* **2005**, *17*, 1258.

*93*. Meng, Q.; Gao, J.; Li, R.; Jiang, L.; Wang, C.; Zhao, H.; Liu, C.; Li, H.; Hu, W. *J.Mater. Chem.* **2009**, *19*, 1477.

*94*. Yasuda, T.; Kashiwagi, K.; Morizawa, Y.; Tsutsui, T. *J. Phys. D: Appl. Phys.* **2007**, *40*, 4471.

*95.* (a) Marrocchi, A.; Seri, M.; Kim, C.; Facchetti, A.; Taticchi, A.; Marks, T. J. *Chem. Mater.* **2009**, *21*, 2592. (b) Silvestri, F.; Marrocchi, A.; Seri, M.; Kim, C.; Marks, T. J. Facchetti, A.; Taticchi, A. *J. Am. Chem. Soc*. **2010**, *132*, 6108.

*96*. Cremer, J.; Bauerle, P.; Wienk, M. M.; Janssen, R. A. J. *Chem. Mater.* **2006**, *18*, 5832.

*97*. (a) Kim, Y.; Cook, S.; Tuladhar, S. M.; Choulis, S. A.; Nelson, J.; Durrant, J. R.; Bradley, D. D. C.; Giles, M.; Mcculloch, I.; Ha, C. S.; Ree, M. *Nat. Mater.* **2006**, *5*, 197. (b) Ma, W.; Yang, C.; Gong, X.; Lee, K.; Heeger, A. J. *Adv. Funct. Mater.* **2005**, *15*, 1617.

*98*. Ashraf, R.S.; Shahid, M.; Klemm, E.; Al-Ibrahim, M.; Sensfuss, S. *Macromol. Rapid Commun*. **2006**, *27*, 1454.

*99*. Baek, N. S.; Hau, S. K.; Yip, H. L.; Acton, O.; Chen, K.S.; Jen, A. K. Y. *Chem. Mater.* **2008**, *20*, 5734.

*100*. Joo, S. -H.; Jeong, M. -Y.; Ko, D. H.; Park, J. -H.; Kim, K. Y.; Bae, S. J.; Chung, I. J.; Jin, J. -I. *J. Appl. Polym. Sci.* **2006**, *100*, 299.

*101*. Kitamura, C.; Tanaka, S.; Yamashita, Y. *Chem. Mater.* **1996**, *8*, 570.

*102*. (a) Tolbert, L. M.; Zhao, X.; Ding, Y.; Bottomley, L. A. *J. Am. Chem. Soc.* **1995**, *117*, 12891. (b) Davies, W. B.; Svec, W. A.; Ratner, M. A.; Wasielewski, M. R. *Nature* **1998**, *396*, 60. (c) Creager, S.; Yu, C. J.; Bamdad, C.; O'Connor, S.; MacLean, T.; Lam, E.; Chong, Y.; Olsen, G. T.; Luo, J.; Gozin, M.; Kayyem, J. F. *J. Am. Chem. Soc.* **1999**, *121*, 1059

*103*. (a) Cordes, M.; Giese, B. *Chem. Soc. Rev.* **2009**, *38*, 892. (b) Gray, H. B.; Winkler, J. R. *Proc. Natl. Acad. Sci. U. S. A.* **2005**, *102*, 3534.

*104*. (a) Creutz, C. *Prog. Inorg. Chem.* **1983**, *30*, 1. (b) Richardson, D. E.; Taube, H. *Coord. Chem. Rev.* **1984**, *60*, 107.

*105*. Hush, N. S. *Coord. Chem. Rev.* **1985**, *64*, 135.

*106.* (a) Martin, R. E.; Diederich, F. *Angew. Chem. Int. Ed.* **1999**, *38*, 1350. (b) van Hutten, P. F.; Krasnikov, V. V.; Hadziioannou, G *Acc. Chem. Res.* **1999**, *32*, 257.

*107*. Sutin, N. *Prog. Inorg. Chem*. **1983**, *30*, 441.

# 2. Thiadiazolo[3,4-*g*]quinoxaline Derivatives

## 2.1. Introduction

Thiadiazolo[3,4-*g*]quinoxaline (TQ) derivatives became attractive building blocks for the construction of narrow band-gap polymers, being established in the pioneering work of Yamashita *et al.* in the mid 1990s.[1] Several *o*-quinoid acceptors were developed and incorporated in D-A systems that were later on electropolymerized, leading to the lowest energy-gap materials up to that date (Chart 5).

**Chart 5.** Narrow energy-gap systems consisting of thiophene as donor (D) and heterocyclic *o*-quinoid acceptor (A) units.

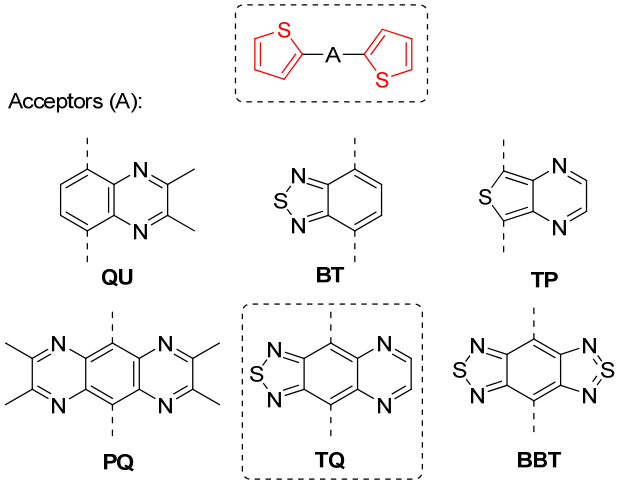


It was demonstrated that by introducing strong electron accepting moieties, such as pyrazino[2,3-*g*]quinoxaline (PQ), TQ or benzobis(thiadiazole) (BBT) in a D-A system, the energy-gap can be reduced to as low as 0.5 eV (Table 1). However, the lack of solubilizing groups along the polymer backbone rendered these materials insoluble in any common

organic solvents, which hindered their full characterization and applicability in organic electronics.

In the following years several other acceptor units were explored within the D-A approach aiming for the tuning of the energy levels to better fit the desired application. One of the major challenges was to enable the solubility of the polymer without hampering its π-conjugation and / or the solid state packing.

**Table 1.** Absorption maxima and energy-gaps of the *o*-quinoid acceptor-based monomers in combination with thiophene as donor and their corresponding polymer listed in Chart 5.

| Compd. | $\lambda_{max}$ (nm)[a] D-A | $E_{op}$ (eV) | |
|---|---|---|---|
| | | D-A[b] | Poly(D-A)[c] |
| **QU** | 405 | 2.66 | 1.4 |
| **BT** | 466 | 2.45 | 1.2 |
| **TP** | 529 | 2.02 | 1.0 |
| **PQ** | 491 | 2.19 | 0.9 |
| **TQ** | 604 | 1.80 | 0.7 |
| **BBT** | 702 | 1.48 | 0.5 |

[a] In $CHCl_3$ solution; [b] Based on CV measurements (0.1 mol $dm^{-3}$ *n*-$Bu_4NClO_4$ in PhCN, Pt electrode, scan rate 100 mV $s^{-1}$); [c] On ITO electrode.

An illustrative example of an acceptor unit with high electron affinity and therefore, attractive for the construction of n-type polymers, is BBT (Chart 5, Table 1). However, the introduction of alkyl chains as solubilizing groups at the BBT core is not possible, since this unit possesses only two available positions for functionalization. Unlike BBT, TQ has 4 functionalizable positions as illustrated in Chart 6. Solubilizing groups can be attached to this core at positions 6 and 7, while having positions 4 and 9 free for further structural modifications or even polymerization.

**Chart 6.** Functionalizable positions at the TQ core.

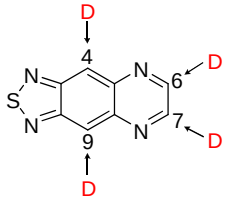

**Chart 7.** Chemical structure of low energy-gap polymers: APFO-Green 1, APFO-Green 3 and APFO-Green 4.

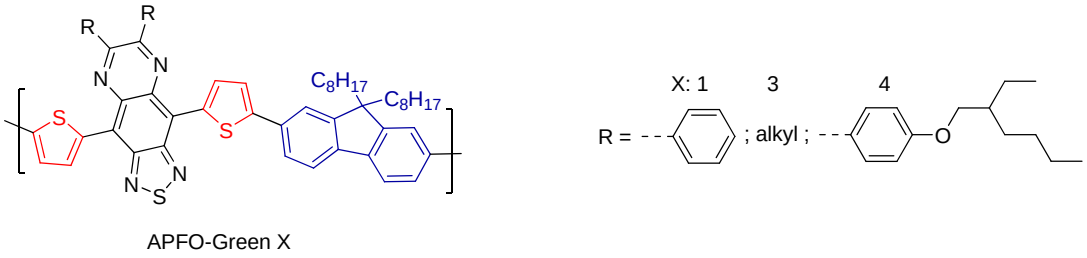


Nonetheless, it was not until 2004 that the group of Mats R. Andersson has obtained the first soluble polymer based on TQ as acceptor unit, the APFO-Green X polymers (Chart 7).[2] The solubility of the polymer however, was still an issue that impeded the synthesis of high molecular weight materials. Besides the two thiophene units anchoring the TQ core, alkylated fluorene was integrated in the polymer backbone as well, in order to increase its solubility and stability. Despite their low molecular weight (for example APFO-Green 1: $M_n$ < 4 kg mol$^{-1}$), these materials were successfully incorporated in OLEDs[3], OFETs (hole mobilities up to $10^{-2}$ cm$^2$ V$^{-1}$ s$^{-1}$)[4] and extensively explored as donors in BHJ OPVs (blended with $PC_{70}BM$, *PCE* = 0.7%).[5]

In the years to come, a variety of donors were chosen to be polymerized with the thiophene anchored TQ units (Chart 8). The great majority of these systems were designed for OPV applications, as they hold the attraction of being light absorbers up to 1200 nm.[6] For instance, the copolymerization with dialkoxy-phenylene yielded a material with p-type charge carrier mobilities up to 5 x $10^{-3}$ cm$^2$ V$^{-1}$ s$^{-1}$ and photovoltaic response up to 1200 nm.[7] However, their low laying LUMO energy levels (3.8-4.0 eV)[8] generally caused an energy mismatch with the n-type material (usually $PC_{60}BM$) resulting in low driving force for the photoinduced charge separation and thereby limiting the performance of the OPV.[9]

**Chart 8.** Chemical structures of representative TQ containing low energy-gap polymers.

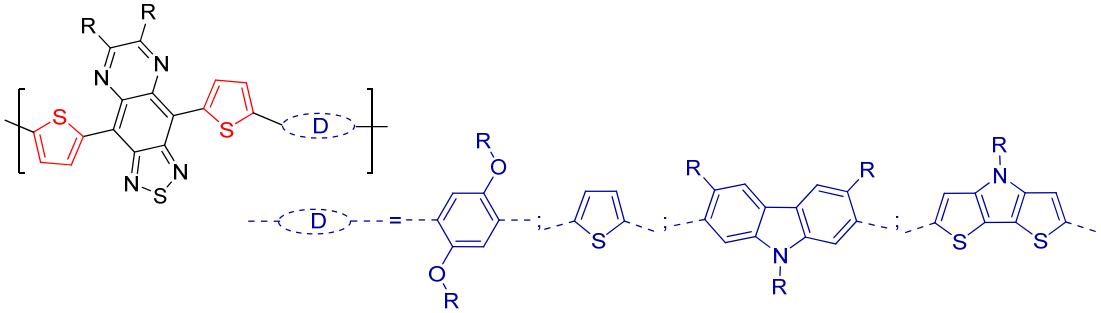

Surprisingly, none of these materials showed electron charge transport, despite the characteristic high electron affinity of the TQ building block. This could be attributed to the typically applied design concept. The repeating units of the up to date reported TQ containing polymers were always consisting of thiophenes (D) flanking the TQ core and one additional donor. This concept diminished the electron deficient nature of the resulting material. By decreasing the number of donor segments per repeating unit, one could increase the electron affinity of the polymer, leading to electron charge transport within the system. Within this context, the introduction of π-spacers, such as ethynylene or ethylene becomes an attractive option.[10] The presence of triple bond linkers within the polymer backbone could offer several advantages such as enhanced π-conjugation due to reduced steric hindrance and tunable molecular orbital energetics *via* skeletal functionalization.[11] On the account of these considerations new $[D\text{-}TQ]_n$ type, low energy-gap polymers were designed in this work, as possible n-type charge carriers. Bearing in mind that the properties of the polymers are closely related to those of structurally defined monomers (D-A-D) the research presented herein starts with the synthesis and characterization of such monomers as model compounds for $[D\text{-}TQ]_n$ polymers.

# 2.2. Thiadiazolo[3,4-*g*]quinoxaline Containing Donor-Acceptor type Small Molecules Connected *via* π-Spacers

## 2.2.1. Functionalized Thiadiazolo[3,4-*g*]quinoxaline Monomers

The investigation of model systems allows the gain of valuable information regarding the presence and nature of the π-spacers at positions 4 and 9, influencing the photophysical and electrochemical properties. Within this framework, the role played by the nature of substituents directly attached to the TQ core at positions 6 and 7 (Chart 6), has been scrutinized as well.

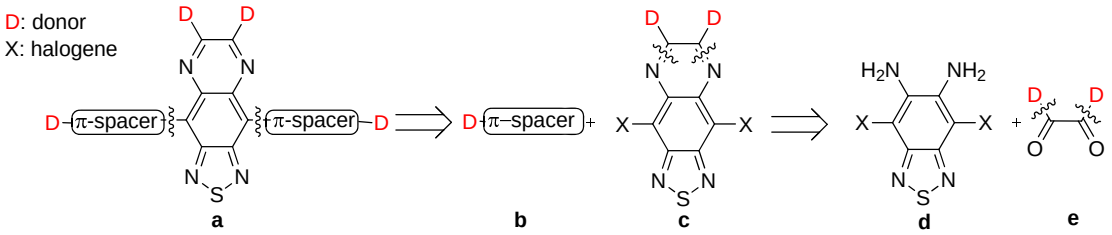


**Scheme 3.** Retrosynthetic analysis of the targeted monomers and model compounds.

As illustrated in the retrosynthetic analysis depicted in Scheme 3, different donors bearing a π-spacer (**b**) could be introduced at the TQ core by taking advantage of one of the transition metal catalyzed *C–C* cross-coupling reactions. The aromatic terminal acetylene could be coupled *via Sonogashira-Hagihara*[12] palladium catalyzed coupling reaction, while an aromatic vinyl derivative, *via Mizoroki-Heck*[13] coupling reaction. Both types of couplings require the presence of halogen atoms on the TQ segment at positions 6 and 7 (**c**). The central TQ could be built up through the condensation of the already halogenated benzo[*c*][2,1,3]thiadiazole-5,6-diamine (**d**) with a suitably functionalized α-diketone **e**.

Bromine was chosen as the halogen functionality to be attached to the starting material benzo[*c*][2,1,3]thiadiazole (**1**, **BT**), following the well documented dibromination reaction of the **BT**,[14] as depicted in Scheme 4. The obtained dibromobenzo[*c*][2,1,3]thiadiazolo (**2**) was then reacted with a mixture of $H_2SO_4$ and $HNO_3$, affording the dinitro derivative **3** in over 60 % yield. Although several reagents were tested for the reduction of compound **3**, such as tin(II) chloride ($SnCl_2$),[15] indium[16] or dicobalt octacarbonyl [$Co_2(CO)_8$],[17] the highest conversion into diamine **4** was obtained using iron powder[1] (89 %) in acetic acid (AcOH). Notably, special attention needs to be paid to the removal of the reducing agent during the purification of diamine **4** as traces of Fe could significantly decrease the yield of the subsequent condensation step.

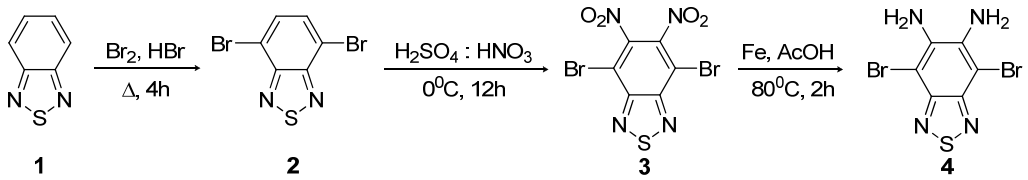


**Scheme 4.** Synthesis of 4,7-dibromobenzo[*c*][2,1,3]thiadiazole-5,6-diamine (**4**).

The directly connected substituents at positions 6 and 7 were introduced through the corresponding α-diketone derivatives (Scheme 3, **e**). Substituents with different donor strengths (alkyl, phenyl and thienyl) were chosen to be attached at the above mentioned positions, in order to evaluate their role on the tuning of the energy levels.

The alkylated diketone[18] was isolated in 48 % yield as a product of the reaction between ethylhexyl-magnesium bromide (**6**) and oxalyl chloride (**7**), in the presence of CuBr (I) and LiBr (Scheme 5).

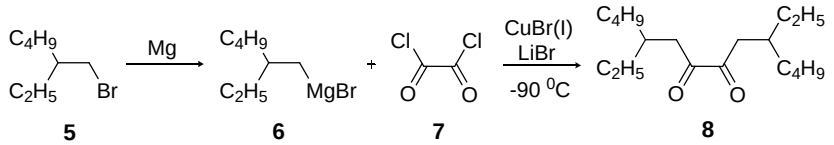


**Scheme 5.** Synthesis of 5,10-diethyltetradecane-7,8-dione (**8**).

A widely explored route towards alkylated phenyl-diketones is the oxidation of the alkylated diphenylacetylene derivative (Scheme 6).[19] This synthetic procedure implies long reaction times and rather harsh reaction conditions typical providing a 70 % overall

conversion of **9** into **12**. However, it was found that compound **12** can be easily synthesized in one step *via* classic *Friedel-Crafts* acylation[20] of dodecylbenzene (**13**) in only 30 minutes (Scheme 6). 1,2-Bis(5-octylthiophen-2-yl)ethane-1,2-dione (**15**) was isolated in high yields (65 %) following the same reaction procedure[21] (Scheme 7).

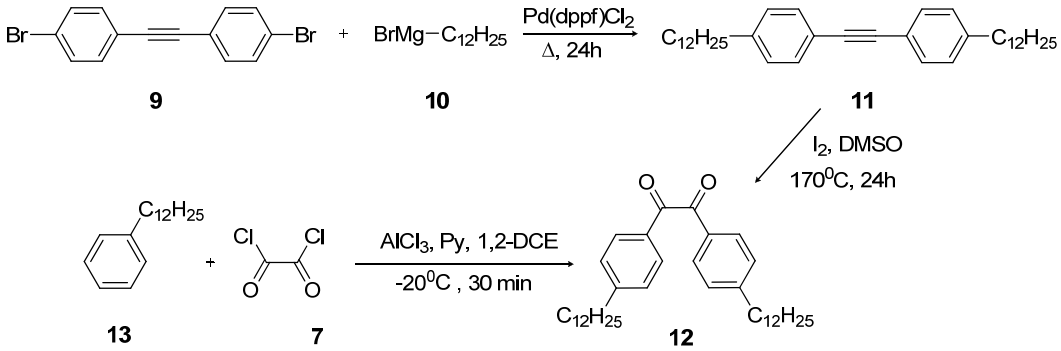


**Scheme 6.** Synthesis of 1,2-bis(4-dodecylphenyl)ethane-1,2-dione (**12**).

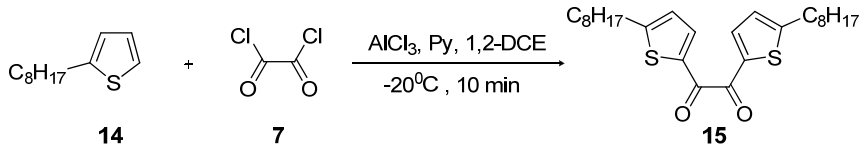


**Scheme 7.** Synthesis of 1,2-bis(5-octylthiophen-2-yl)ethane-1,2-dione (**15**).

With the key derivatives in hand, the condensation reactions were completed under acidic condition in AcOH.[22] The alkyl functionalized TQ derivative (**RTQ**, Scheme 8) proved to be air and heat sensitive and therefore its synthesis was carried out under inert atmosphere, at room temperature. To avoid decomposition occurring upon prolonged exposure to air, **RTQ** was stored, if necessary, at 5$^0$C under inert atmosphere.

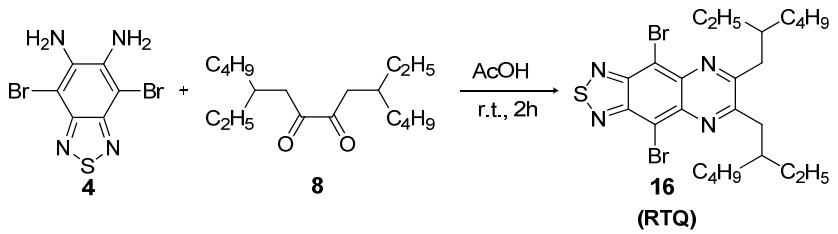


**Scheme 8.** Synthesis of alkyl substituted 4,9-dibromo TQ derivative (**16**, **RTQ**).

As the presence of aromatic substituents on the TQ core proved to have a stabilizing effect on the target molecules, their synthesis and purification did not call for any special

handling. Both **PTQ** (72 %) and **TTQ** (46 %) were obtained in moderate to high yields under microwave (*MW*) assisted synthesis (Scheme 9). Certainly, one of the major advantages of the *MW* promoted reactions over those performed under conventional conductive heating, is the typically shorter reaction time. Additionally, the formation of undesired side reactions is usually reduced to minimum.[23] Furthermore, the reaction set up under *MW* irradiation enables the reactions to be carried out at elevated temperatures avoiding local overheat while maintaining full control over the pressure, temperature and *MW* input power.[23] The synthesis of both **PTQ** and **TTQ** under conventional conductive heating (reflux conditions, 12 h) was characterized by significantly lower reaction yields (< 30 %), due to a significant debromination. The presence of monobrominated TQ derivative made the purification procedure rather tedious. On the contrary, 2 hours *MW* irradiation at 140$^0$C of the corresponding starting materials enabled the synthesis of the desired TQ derivatives without the formation of undesired side products.

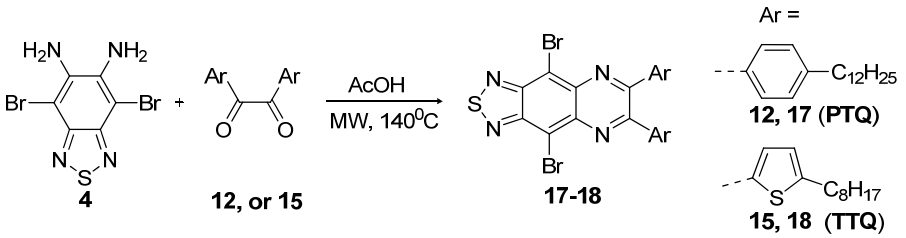


**Scheme 9.** Synthesis of thiadiazoloquinoxaline derivatives **PTQ** (**17**) and **TTQ** (**18**).

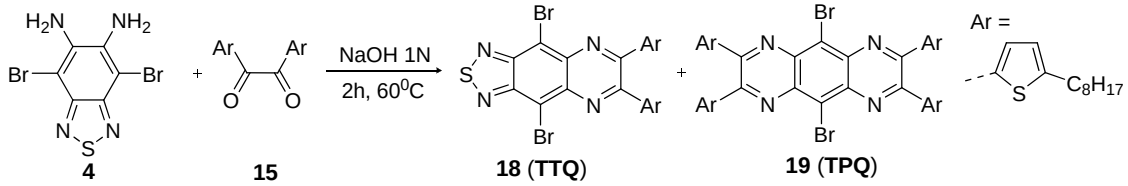


**Scheme 10.** Synthesis of **TTQ** (**18**)and 2,3,7,8-tetrathienyl-pyrazino[2,3-*g*]quinoxaline derivative (**TPQ**, **19**) under strong basic conditions.

Alternative synthetic routes that would provide higher yields were sought for the condensation reaction of **4** and **15.** Performing the reaction in a basic medium, such as ethanol, resulted in the formation of the monobrominated **TTQ**, that hindered the isolation of the target compound. A stronger basic medium, such as NaOH 1 N aqueous solution, secured the formation of **TTQ** as major product (25 %). However, the susceptibility of the **BT**

core to undergo reductive sulfur extrusion under strong basic conditions[24] led to the formation of pyrazino[2,3-*g*]quinoxaline derivative **19** (**TPQ**) as side product (15 %) (Scheme 10).

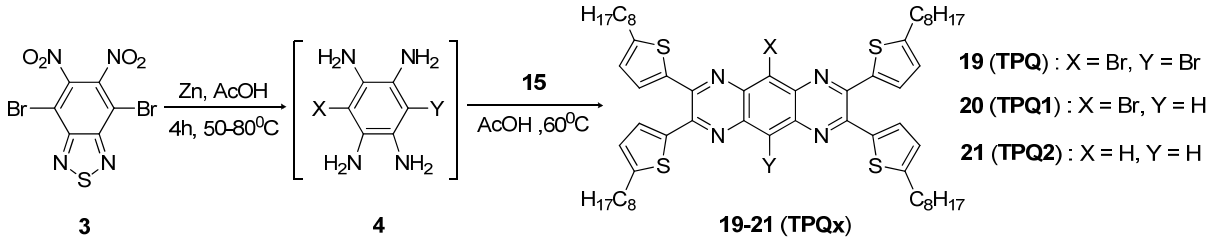


**Scheme 11.** Synthesis of 2,3,7,8-tetrathienyl-pyrazino[2,3-*g*]quinoxaline derivatives **TPQx** (**19**-**21**).

Alternative reaction procedures that would improve the isolation yields of **TPQ** were pursued, since a direct comparison of the photophysical and electrochemical properties of **TPQ** *vs.* **TTQ** would offer an initial validation of the design concept followed in this work. Consequently, **TPQ** was prepared following the reaction conditions depicted in Scheme 11. A reaction temperature below 50$^0$C ensured the isolation of **TPQ** as major product (76 %). When desired, **TPQ2** could be obtained (41 %) by taking advantage of the high temperature (80$^0$C) induced debromination.

## 2.2.2. Optical and Electrochemical Characterization of the Functionalized TQ Monomers: RTQ, PTQ and TTQ

The investigation of the photophysical and electrochemical profile of the monomers (Chart 9) offers valuable information regarding their electronic structure. Knowing the energy levels of the monomers is of aid in the design of further structural modifications of the TQ derivatives.

**Chart 9.** Synthesized TQ monomers bearing substituents with different electron donating strength at positions 6 and 7.

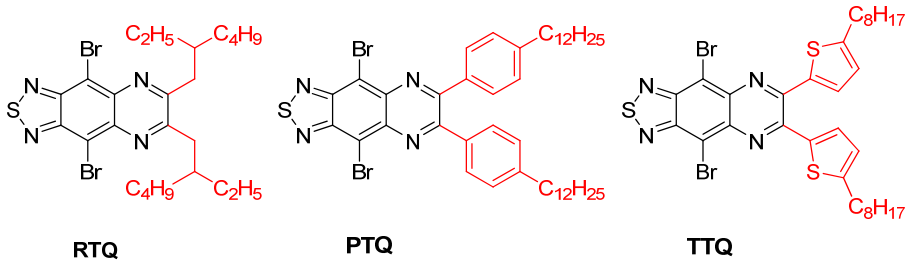


**RTQ** **PTQ** **TTQ**

A straightforward technique to indicate charge transfer (CT) interactions is by means of UV-Vis spectroscopy. When partial electron density transfer occurs from the D to the A, transitions from HOMO-1 to the partially depopulated HOMO could take place in the D, or transitions from partially occupied LUMO to the LUMO+1 could arise in the acceptor. These low energy transitions are responsible for the absorption at longer wavelengths.[25] Nonetheless, when examining intermolecular CT one should keep in mind that linear (polyenes) and cyclic (aromatic) conjugated systems are characterized by lower energy absorptions, as a function of the degree of π-conjugation. By efficiently extending the π-electron system, the low lying π-π* transition is decreased and therefore the wavelength of the corresponding absorption band increased.[26] However, as the electron transfer in solution is closely related to solvent polarization effects, relaxation processes can contribute

to or even control the electron transfer.[27] One of the consequences is the solvent dependence of the absorption and / or emission of D-A type molecules with favored intramolecular CT.

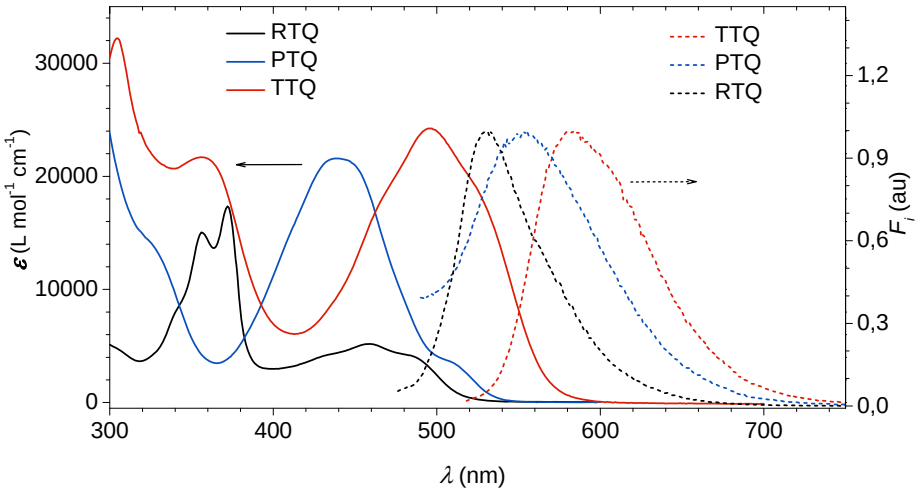


**Figure 6.** Absorption (solid line) and emission (dashed line) of **RTQ**, **PTQ** and **TTQ** in chloroform solution ($c = 10^{-5}$ mol $L^{-1}$).

Therefore, the absorption and emission spectra were recorded in chloroform for monomers **RTQ**, **PTQ** and **TTQ**, respectively (Figure 6), at low concentrations ($10^{-5}$ mol $L^{-1}$). Comparing the absorption profiles of these compounds, the influence of the substituents attached to the TQ core at positions 6 and 7 is apparent. **RTQ** showed a strong absorption band between 325-380 nm and a weaker band from 380 nm to 520 nm with an optical energy-gap ($E_{op}$) of 2.39 eV. By replacing the ethylhexyl substituents with aromatic phenyl ones (**PTQ**), the π-conjugation was enhanced, which is reflected in the 0.09 eV lower $E_{op}$ (Table 2). Additionally, a hyperchromic effect was observed with a fourfold higher maximum molar absorption coefficient ($\varepsilon = 21600$ L $mol^{-1}$ $cm^{-1}$) at $\lambda_{max}$ when compared to **RTQ** ($\varepsilon = 5200$ L $mol^{-1}$ $cm^{-1}$). The presence of the stronger electron donating thienyl substituents, in conjugation with the TQ core in case of **TTQ**, yielded a 50 nm bathochromic shift of $\lambda_{max} = 497$ nm accompanied by a decreased $E_{op}$ (Table 2). A similar trend could also be observed in the emission (Figure 6). Systematically increasing the donor character of the substituents, while simultaneously extending the π-conjugation (**PTQ** and **TTQ**), the emission

maximum ($\lambda_{em}$) was red shifted from 530 nm (**RTQ**), to 553 nm (**PTQ**) and to 584 nm (**TTQ**), respectively.

The solvent dependent absorption and emission were studied in case of **TTQ** (Figure 7). For clarity, the spectra registered in three aprotic solvents are shown in Figure 7, going from the non-polar hexane through chloroform to the polar acetone. Both the absorption and emission profiles in hexane are characterized by the presence of vibrational bands. In more polar solvents, the bands became structureless with a slightly bathochromically shifted long wavelength absorption $\lambda_{max}$. Considering that the absorption bandwidth, defined as the spread of wavelength at half-height, increased with solvent polarity, it is most likely that the spectral broadening originates from inhomogeneous broadening of the electronic bands, a solvent effect which results from the variations of the local environment of solute molecules.[28] However, bearing in mind that **TTQ** is not a totally rigid molecule, the homogenous broadening of the absorption spectra due to the increased number of rotational and vibrational sublevels can not be excluded.

**Table 2.** Summary of the optical and electrochemical data of the series **RTQ**, **PTQ** and **TTQ**.

| Compd. | $\lambda_{max}$ (nm)[a] | $E_{op}$ (eV)[a] | $\lambda_{em}$ (nm)[a] | $E_{pc}$ (V)[b] | $E_{LUMO}$ (eV)[b] | $E_{HOMO}$ (eV)[c] |
|---|---|---|---|---|---|---|
| **RTQ** | 356, 372, 459, 485 (sh) | 2.39 | 530 | -0.43 | -3.63 | -6.02 |
| **PTQ** | 440 | 2.30 | 553 | -0.36 | -3.79 | -6.09 |
| **TTQ** | 305, 355, 497 | 2.17 | 584 | -0.35 | -3.80 | -5.97 |

[a]Chloroform solution ($10^{-5}$ mol $L^{-1}$); [b]0.1 mol $dm^{-3}$ of *n*-$Bu_4NPF_6$, in THF, Pt electrode, scan rate 50 mV $s^{-1}$, calculated from $E_{LUMO} = -(E_{Red}^{onset} - E^{(½)}_{Fc^+/Fc} + 4.8)$ eV; [c] Calculated from $E_{HOMO} = E_{op} - E_{LUMO}$.

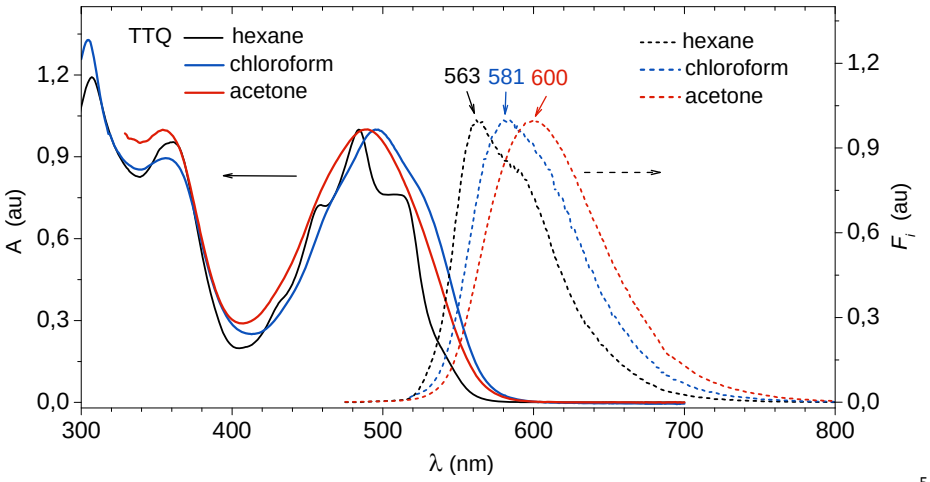


**Figure 7.** Solvent dependent absorption (solid line) and emission (dashed line) of **TTQ** ($c = 10^{-5}$ mol $L^{-1}$).

The emission of **TTQ** was also affected by the polarity of the solvent. Complete loss of vibrational structure was observed upon placing **TTQ** in a polar medium, such as acetone (Figure 7). However, special care needs to be taken when evaluating the shift of the emission maximum in case of brominated systems. Generally, for aromatic halogenated compounds the solvatochromic shifts of the emission spectra, if any, are very small.[29] Furthermore, these shifts are not necessarily the result of an actual charge transfer contribution, but they may be related to the change in polarizability and the subsequent alteration of the induced dipole moment. It has to be noted that $E_{op}$ decreased from 2.23 eV in non-polar medium (hexane) to 2.18 eV calculated for the more polar solvent chloroform. A more pronounced bathochromic shift of the emission maximum ($\Delta\lambda_{em}$ = 27 nm) was observed when going from hexane to acetone, suggesting a more polar molecular structure in the excited state relative to the ground state.

The electrochemical reduction of these materials, investigated by means of cyclic voltammetry (Figure 8), offered additional information as to the impact of the functionalization on the energy levels ($E_{LUMO}$). The measurements were carried out using a 0.1 mol $L^{-1}$ THF solution of *n*-$Bu_4NPF_6$ as electrolyte, while the analyte was dissolved in a concentration of $10^{-3}$ mol $L^{-1}$. To be able to estimate the $E_{LUMO}$, ferrocene (Fc) was employed as an internal standard ($10^{-3}$ mol $L^{-1}$), due to its reversible and well defined one-electron oxidation to a ferrocenium ion ($Fc^+$).[30] Moreover, the oxidation potential of Fc can be reliably approximated to its half-wave potential ($E^{1/2}_{Fc/Fc^+}$) given by the midpoint between the values of the potentials corresponding to the anodic and the cathodic peak in its cyclic voltammogram.[31] All the spectra were normalized to the standard $E^{1/2}_{Fc/Fc^+}$, corresponding to the measurement conditions.[32] The $E_{LUMO}$ levels were estimated based on the equation: $E_{LUMO}$ = -($E^{onset}_{Red}$ - $E^{1/2}_{Fc/Fc^+}$ + 4.8) eV and listed in Table 2, along with the first reduction peak potentials ($E_{pc}$). The cyclic voltammetry investigations suggested that the introduction of aromatic substituents (**PTQ** or **TTQ**) *vs.* alkyl (**RTQ**) at the TQ core eased the reducibility of the materials. The electron accepting ability was enhanced, probably as a result of the π-conjugation extension, as sustained by the very similar $E_{pc}$ values measured for both **PTQ** and **TTQ**. Considering the typically fairly good agreement between the optically and electrochemically determined energy-gap,[33] using the simple formula: $E_{HOMO} = E_{op} - E_{LUMO}$,

the HOMO energy levels ($E_{HOMO}$) were derived and listed in Table 2. The calculated values corroborate the initial expectation that the functionalization of the TQ core with a stronger donor, such as thiophene, should increase the $E_{HOMO}$. The tuning of the HOMO energy level was accomplished without significantly affecting the LUMO energy level of the material.

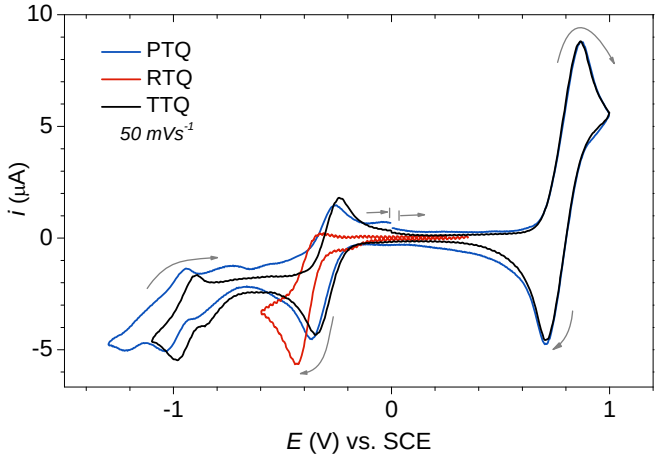


**Figure 8.** Electrochemical reduction of **RTQ**, **PTQ** and **TTQ**, respectively, in THF at 50 mV $s^{-1}$, with ferrocene as internal standard.

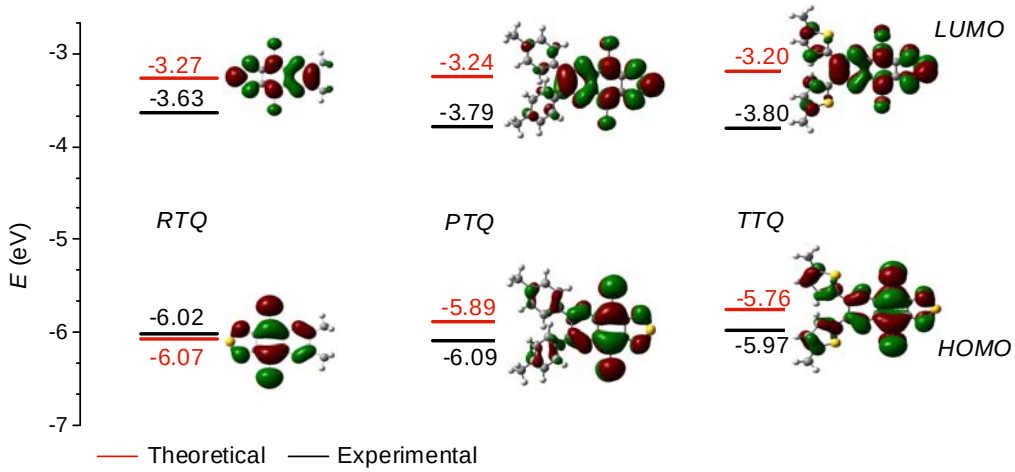


**Figure 9.** Orbital energies based on theoretical calculations (red) and experimental findings (black), and corresponding frontier molecular orbital electronic density contours of **RTQ**, **PTQ** and **TTQ**, respectively.

Quantum mechanical calculations by density functional theory (DFT), using B3LYP functional with 6-31G* basis set, were employed to establish the geometry and electronic

structure of the presented molecules. The calculated energy levels were then correlated with the experimentally estimated $E_{LUMO}$ and $E_{HOMO}$ and summarized in Figure 9, together with the electronic density contours calculated for the frontier molecular orbitals. When directly comparing the theoretical and experimental data, it has to be kept in mind that, the experimentally determined energy levels were based on measurements carried out in solution. In the quantum mechanical calculations performed, solvochromic effects were neglected and thus, the energy level values obtained are related to molecules in the gas phase.[34] Additionally, to minimize the calculation time and power, only methyl groups were considered instead of the long alkyl chain substituents. The theoretical electron density contour of **TTQ** supported the experimental findings according to which the thienyl substituents have a stronger contribution to the HOMO orbital surface distribution than the phenyl moieties (**TPQ**). At the same time, both substituents indicate similar weak contributions to the LUMO orbital.

## 2.2.3. 2,3,7,8-Tetrathienyl-pyrazino[2,3-*g*]quinoxalines (TPQx) *vs.* 6,7-dithienyl-thiadiazolo[3,4-*g*]quinoxaline (TTQ)

To have a frame of reference, the photophysical and electrochemical properties of **TTQ** were compared with those of the pyrazinoquinoxaline derivative **TPQ** and its corresponding unhalogenated analogue **TPQ2** (Chart 8).

**Chart 8.** Chemical structures of the compared acceptors **TPQ2**, **TPQ** and **TTQ**.

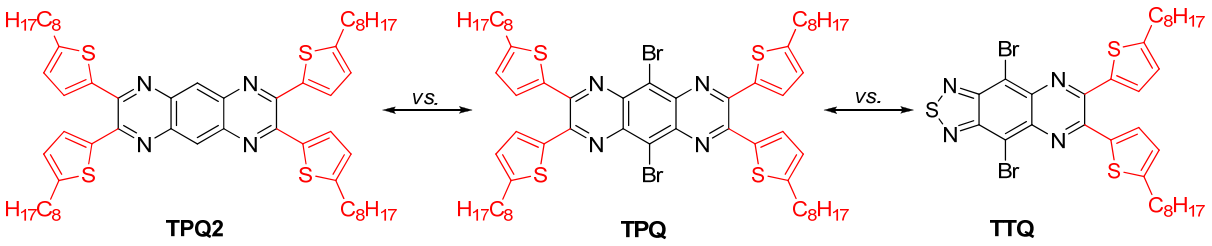


**TPQ2** possesses no halogen atoms attached to its pyrazinoquinoxaline (**PQ**) core and therefore, the solvatochromic effects in its absorption and / or emission spectra would be most likely due to a charge transfer interaction between the thienyl functionalities and the acceptor **PQ** center. A series of aprotic solvents with different polarities were tested, going from hexane to acetone and isopropyl alcohol ($^{i}$PrOH) as a protic solvent (Figure 10). The absorption profile of **TPQ2** typically revealed two main absorption bands. A first between 300 and 400 nm and a second band, most likely originating from the extended π-conjugation, between 400 and 550 nm. Due to the relatively high $D_{2h}$ symmetry of **TPQ2**, the low energy absorption band in the non-polar hexane was characterized by the presence of vibronic bands. As the environment became more polar (see acetone), the absorption band lost its fine structure. Furthermore, very weak positive solvatochromic shifts ($\Delta\lambda_{max}$) were registered upon increasing solvent polarity, suggesting a weak charge transfer interaction between the electron donating thienyl substituents and the PQ core. Going from

hexane to chloroform, $\Delta\lambda_{max}$ reached 10 nm, polarity beyond which $\Delta\lambda_{max}$ slightly decreased. It is rather difficult to interpret this weak negative solvatochromic shift ($-\Delta\lambda_{max}$ = 4 nm), since it is within the limits of the measurement error. Nevertheless, $E_{op}$ values between 2.34 and 2.27 eV were extracted for the two extremes. Additionally, when **TPQ2** is placed in a protic medium ($^{i}$PrOH), the absorption profile was very similar to that ascertained in acetone, suggesting the lack of any solvent specific interactions, such as hydrogen bonding.

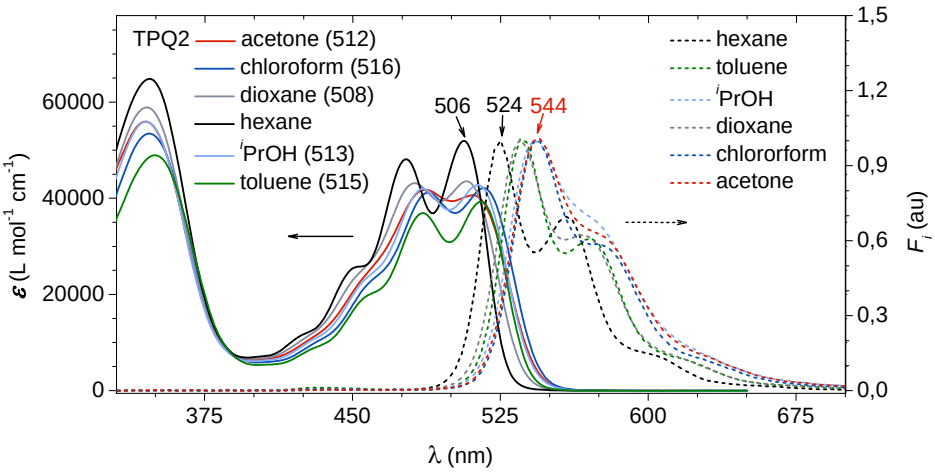


**Figure 10.** Solvent dependent absorption (solid line) and emission (dashed line) of **TPQ2** ($c$ = $10^{-5}$ mol $L^{-1}$).

Similarly, the emission of **TPQ2** was characterized by spectral broadening with increasing solvent polarity (Figure 10). However, a more pronounced solvatochromic effect was observed in the emission relative to the absorption. A $\Delta\lambda_{em}$ of 40 nm was derived going from hexane to acetone, demonstrating a stronger D-A interaction in the excited state than in the ground state. Certainly, the presence of electron withdrawing bromines at the PQ core had an impact on the electronic profile and such a meaningful comparison with **TTQ** can only be done with the structurally similar **TPQ**. The long wavelength absorption band and emission of **TPQ** presented vibronic structure, due to the fact that the attachment of bromine atoms did not disturb the symmetry (Figure 11). However, the absorption maximum in chloroform was shifted to 554 nm and the $E_{op}$ decreased to 2.14 eV, values that are very close to those registered for **TTQ**. Setting the photophysical properties of **TPQ** against those of **TTQ**, it has to be noted that the former posses two additional thienyl groups in π-conjugation with the PQ core.

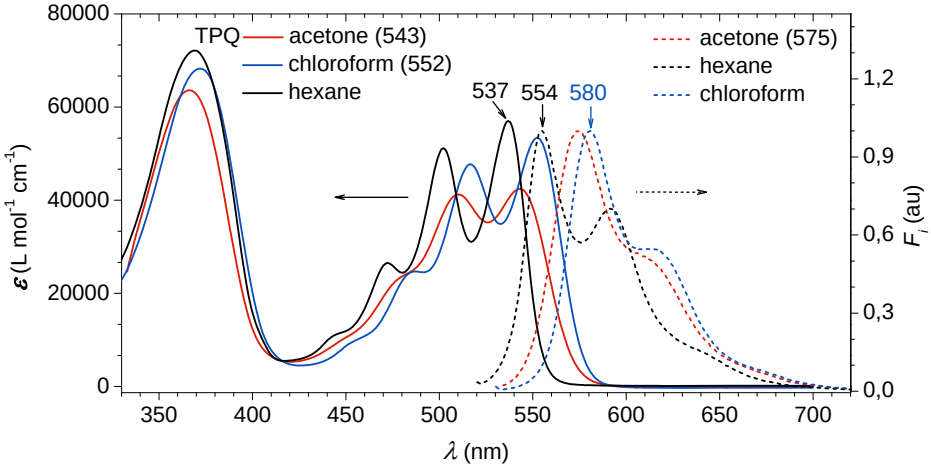


**Figure 11.** Solvent dependent absorption (solid line) and emission (dashed line) of **TPQ** ($c$ = $10^{-5}$ mol $L^{-1}$).

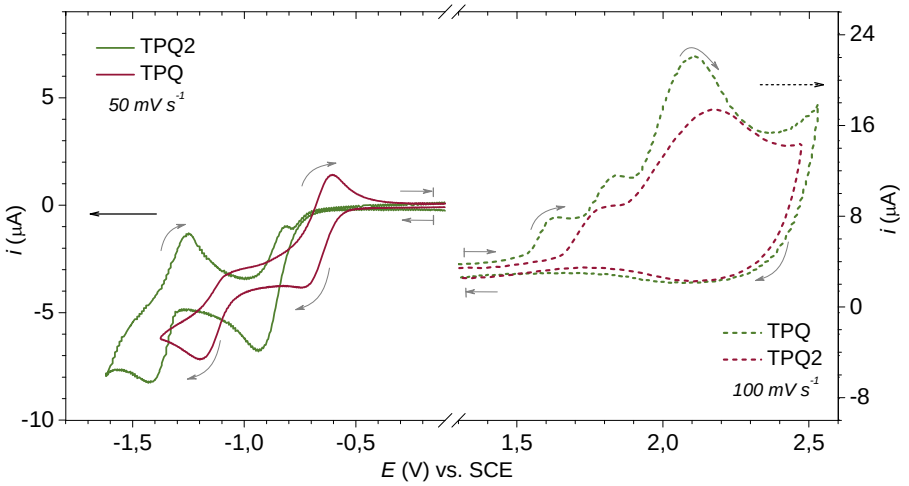


**Figure 12.** Cyclic voltammograms of **TPQ** and **TPQ2** in DCM at 50 mV $s^{-1}$ (reduction) and 100 mV $s^{-1}$ (oxidation) scan rate, measured with ferrocene as internal standard.

Despite their similar optical energy-gaps, the significant difference between **TPQ** and **TTQ** may lay in the position of their energy level. In order to investigate their p- and n-dopability, both **TPQ** and **TPQ2** were subjected to cyclic voltammetry measurements. The oxidation and the reduction of the PQ derivatives were evaluated in DCM following the procedure described for **TTQ**. Ferrocene was used as internal standard, but for clarity this region (between -0.1 and 1.3 V) is not shown in Figure 12. The presence of brom substituents on the PQ (**TPQ2**) core resulted in a more electron poor molecule that was more difficult to reduce relative to its unhalogenated homologue **TPQ**. The energy levels, as

estimated from the onset of the first oxidation and reduction waves respectively, are illustrated in Figure 13, including the values corresponding to **TTQ** for comparison.

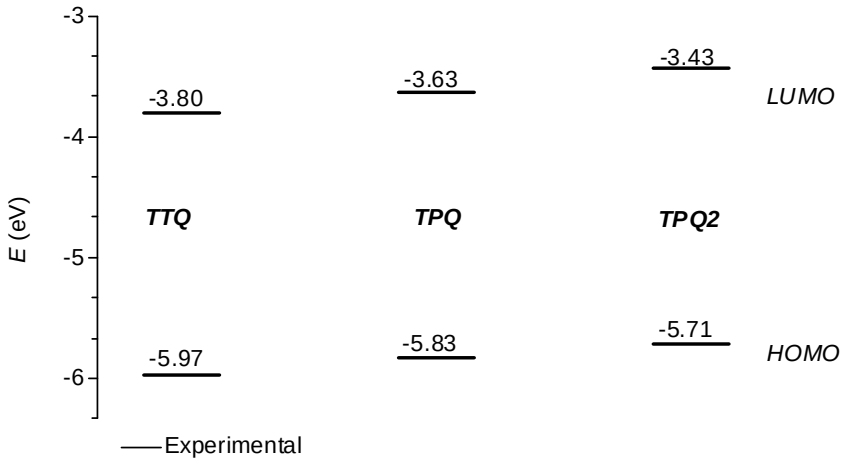


**Figure 13.** Orbital energies based cyclic voltammetry measurements of **TTQ**, **TPQ** and **TPQ2**, respectively. The $E_{HOMO}$ of **TTQ** was derived from equation $E_{HOMO} = E_{op} - E_{LUMO}$.

It is not surprising that the presence of electron deficient bromine atoms in **TPQ** led to decreased $E_{LUMO}$ (from -3.43 eV to -3.63 eV) and $E_{HOMO}$ (from -5.71 eV to -5.83 eV) relative to **TPQ2**. The energy-gap derived electrochemically ($E_g^{CV}$) was in very good agreement with $E_{op}$ (for **TPQ2**, $E_g^{CV}$ = 2.28 eV, while $E_{op}$ = 2.27 eV in chloroform and for **TPQ** $E_g^{CV}$ = 2.20 eV, while $E_{op}$ = 2.14 eV). Although, **TPQ** and **TTQ** showed almost identical optical energy gaps, significant differences were found in their energy levels. The higher $E_{HOMO}$ of **TPQ** could be rationalized through the two additional thienyl substituents connected at the PQ core. Notably, the essential difference between the two compounds is the 0.14 eV lower $E_{LUMO}$ of **TTQ**, confirming the stronger electron accepting nature of the functionalized TQ derivative relative to PQs.

## 2.2.4. Conclusion

The introduction of substituents at positions 6 and 7 of the TQ core was successfully accomplished, while holding positions 4 and 9 free for further functionalization.

Additionally, the comprehensive photochemical, electrochemical and theoretical studies presented above showed that the π-conjugation could be tuned through the incorporation of aromatic donor substituents, leading to monomers that show absorption up to 575 nm (**TTQ**). Hence, it has been shown that the optical properties as well as energy-gap could be effectively tuned through the nature of the donor attached to the TQ core. More importantly, the energy-gap modulation was achieved through increasing the HOMO level while keeping the LUMO level and thus the high n-dopability unaffected.

The direct comparison of the photophysical and electrochemical properties of **TTQ** with **TPQ** showed that although two compounds might posses almost identical optical energy-gaps, their energy levels could be very different. Furthermore, the lower laying $E_{LUMO}$ of **TTQ** relative to **TPQ** comes to support the design concept of this research work that is based on the high electron affinity of the TQ core.

## 2.2.5. References

*1*. Kitamura, C.; Tanaka, S.; Yamashita, Y. *Chem. Mater.* **1996**, *8*, 570.

*2.* (a) Wang, X.; Perzon, E.; Mammo, W.; Oswald, F.; Admassie, S.; Persson, N-. K.; Langa, F.; Anderson, M.; Inganäs, O. *Thin Solid Films* **2006**, *511*, 576. (b) Wang, X.; Perzon, E.; Delgado, J. L.; de la Cruz, P.; Zhang, F.; Langa, F.; Anderson, M. R.; Inganäs, O. *Appl. Phys. Lett.* **2004**, *85*, 5081**.**

*3.* Chen, M. X.; Perzon, E.; Robisson, N.; Jönsson, S. K. M.; Andersson, M. R.; Fahlman, M.; Berggren, M. *Synthetic Metals* **2004**, *146*, 233.

*4.* (a) Andersson, L. M.; Inganäs, O. *Appl. Phys. Lett.* **2006**, *88*, 082103. (b) Chen, M.; Crispin, X.; Perzon, E.; Andersson, M. R.; Pullerits, T.; Andersson, M.; Inganäs, O.; Berggren, M. *Appl. Phys. Lett.* **2005**, *87*, 252105.

*5.* Wang, X.; Perzon, E.; Mammo, W.; Oswald, F.; Admassie, S.; Persson, N-. K.; Langa, F.; Anderson, M.; Inganäs, O. *Thin Solid Films* **2006**, *511-512*, 576.

*6.* Andersson, L. M.; Inganäs, O. *Appl. Phys. Lett*. **2006**, 082103.

*7.* Perzon, E.; Zhang, F.; Andersson, M.; Mammo, W.; Inganäs, O.; Andersson, M. R. *Adv. Mater.* **2007**, *19*, 3308.

*8.* Admassie, S.; Inganäs, O.; Mammo, W.; Perzon, E.; Andersson, M. R. *Synthetic Metals*, **2006**, *156*, 614.

*9*. Wang, X.; Perzon, E.; Oswald, F.; Langa, F.; Admassie, S.; Anderson, M. R.; Inganäs, O. *Adv.Funct.* **2006**, *511-512*, 576.

*10.* (a) Kraft, A.; Grimsdale, A. C.; Holmes, A. B. *Angew. Chem., Int. Ed.* **1998**, *37*, 402. (b) Yasuda, T.; Kashiwagi, K.; Morizawa, Y.; Tsutsui, T.; *J. Phys. D: Appl. Phys.* **2007**, *40*, 4471. (c) Meng, Q.; Gao, J.; Li. R.; Jiang, L.; Wang, C.; Zhao, H.; Liu, C.; Li, H.; Hu, W. *J. Mater. Chem.* **2009**, *19*, 1477.

*11.* (a) Bunz, U. H. F.; Rubin, Y.; Tobe, Y. *Chem. Soc. Rev.* **1999**, *28*, 107. (b) Li, C.; Li, Y. *Macromol. Chem. Phys.* **2008**, *209*, 1541.

*12*. Tohda, Y.; Sonogashira, K.; Hagihara, N. *Tetrahedron Lett.* **1975**, *16*, 4467.

*13*. Heck, R. F.; Nolley, Jr., J. P. *J. Org. Chem.* **1972**, *37*, 2320.

*14.* Tsubata, Y.; Suzuki, T.; Yamashita, Y.; Mukai, T.; Miyashi, T. *Heterocycles* **1992**, *33*, 337.

*15.* Gamble, A. B.; Garner, J.; Gordon, C. P.; O'Conner, S. M. J.; Keller, P. A. *Synthetic Communications* **2007**, *37*, 2777.

*16.* Pitts, M. R.; Harrison, J. R.; Moody, C. J. *J. Chem. Soc., Perkin Trans. 1*, **2001**, 955.

*17.* Lee, H-. Y.; An, M. *Bull. Korean Chem. Soc.* **2004**, *25*, 1717.

*18.* (a) Karsten, B. P.; Janssen, R. A. J. *Org. Lett.* **2008**, *10*, 3513. (b) Karsten, B. P.; Viani, L.; Gierschner, J.; Cornil, J.; Janssen, R. A. J. *J. Phys. Chem. A* **2008**, *112*, 10764.

*19.* Bernhardt, S.; Kastler, M.; Enkelmann, V.; Baumgarten, M.; Müllen, K. *Chem. Eur. J.* **2006**, *12*, 6117.

*20.* (a) Friedel, C.; Crafts, J. M. *Compt. Rend.* **1877**, *84*, 1392.

*21.* (a) Belen'kii, L. I.; *Chem. Heterocycl. Comp.* **1981**, *16*, 1195. (b) Belen'kii, L. I.; Shirinyan, V. Z.; Gromova, G. P.; Kolotaev, A. V.; Strelenko, Y. A.; Tandura, S. N.; Shumskii, A. N.; Krayushkin, M. M. *Chem. Heterocycl. Comp.* **2003**, *39*, 1570.

*22.* Perzon, E.; Wang, X.; Zhang, F.; Mammo, W.; Delgado, J. L.; Cruz, P.; Inganäs, O.; Langa, F.; Andersson, M. R. *Synthetic Metals* **2005***, 154*, 53.

*23*. Loupy, A. "*Microwaves in Organic Synthesis"*, 2nd Ed. Wiley-VCH: Weinheim, **2006**.

*24.* Neto B. A. D.; Lopes, A. S.; Wüst, M.; Costa, V. E. U.; Ebeling, G.; Dupont, J. *Tetrahedron Letters* **2005**, *46*, 6843.

*25*. Newton, M. D. *"Electron Transfer in Chemistry"*, Chapter 1, Wiley-VCH: New York, **2001**.

*26.* Valeur, B. *"Molecular Fluorescence: Principles and Applications"*, Chapter 2, Wiley-VCH: Weinheim, **2001**.

*27.* Barbara, P. F.; Meyer, T. J.; Ratner, M. A. *J. Phys. Chem.* **1996**, *100*, 13148.

*28.* Suppan, P.; Ghoneim, N. *"Solvatochromism"* The Royal Society of Chemistry, Cambridge, **1997**, *p.*14.

*29.* Lakowicz, J. R. *"Principles of Fluorescence Spectroscopy"*, Plenum Publishers, New York, **1999**.

*30*. Gritzner, G. *Pure Appl. Chem.* **1990**, *62*, 1839.

*31.* (a) Tsierkezos, N. G. *J. Solution Chem.* **2007**, *36*, 289. (b) Bond, A. M.; McLennan, E. A.; Stojanovic, R. S.; Thomas, F. G. *Anal. Chem.* **1987**, *59*, 2853.

*32.* Bao, D.; Millare, B.; Xia, W.; Steyer, B. G.; Gerasimenko, A. A.; Ferreira, A.; Contreras, A.; Vullev, V. I. *J. Phys. Chem. A* **2009**, *113,* 1259.

*33.* Sariciftci, N. S. *"Primary Photoexcitations in Conjugated Polymers: Molecular Excitons vs Semiconductor Band Model"*; World Scientific: Singapore, **1997**.

*34.* Langhals, H. *New J. Chem.* **1981**, *5*, 97.

# 2.3. Thiadiazolo[3,4-*g*]quinoxaline Model Compound: Ethynylene *vs.* Ethylene π-Spacers

## 2.3.1. Synthesis

It is well accepted that the properties of polymers could be straightforwardly correlated to the characteristics of their structurally defined monomers. Therefore, useful details could be gained by studying the fundamental phenomena of interest in these model systems.[1] Properties of polymers could be predicted by extrapolating the characteristics of a series of corresponding oligomers when such in depth study is feasible.[2] The characterization of a simple model system of a [D-A-D] type could already offer valuable primary data for a later polymer. For example, if within such a model system the π-conjugation is perturbed due to steric interactions, it is most likely that the π-conjugation in its corresponding polymer will be also disturbed. Therefore, it is important to examine the properties of such small systems in detail. Accordingly, the influence of triple bond as π-spacer introduced between the TQ unit and different donor molecules could be evaluated on model compounds of the [D-TQ-D] type. In the view of their similar LUMO energy levels (see Section 2.2.2.), **PTQ** and **TTQ** were chosen for the synthesis of such model systems. Hence, the role played by the π-spacer in the tuning of the energy levels can be directly assessed.

Firstly, under the conditions of the well established *Sonogashira-Hagihara* cross-coupling reaction,[3] **PTQ** was reacted with excess of phenylacetylene in a 1 : 1 mixture of THF : $^{i}Pr_2NH$ and catalytic amounts of CuI (I) and $Pd(PPh_3)_4$ (Scheme 12). After stirring the reaction mixture over night at room temperature, a primarily analysis of the reaction mixture by mass spectrometry did not show the presence of the target compound **25** (**PTQEP**), but a mixture of two compounds with 2 and 4 units higher molecular weight. Separation of this mixture resulted in the isolation of compounds **23** (**PTQV2P**) and **24** (**PTQVP**), respectively. A closely monitored reaction by FD-MS and thin layer chromatography (TLC), set up under the

conditions detailed above revealed that after only 15 min **PTQ** was fully converted into **PTQEP**, as it was also indicated by the strong color change from orange-red to dark candy apple red. If the reaction was not stopped, **PTQEP** underwent an *in situ* reduction yielding **PTQV2P** (η = 11 %) and **PTQVP** (η = 6 %), respectively.

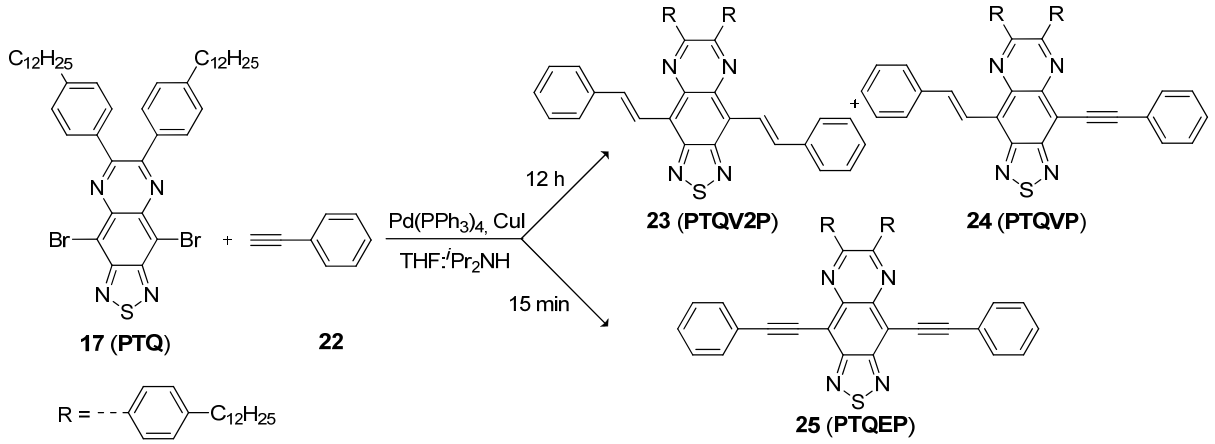


**Scheme 12.** Cross-coupling reaction of **PTQ** and phenylacetylene (**22**) under *Sonogashira-Hagihara* reaction conditions.

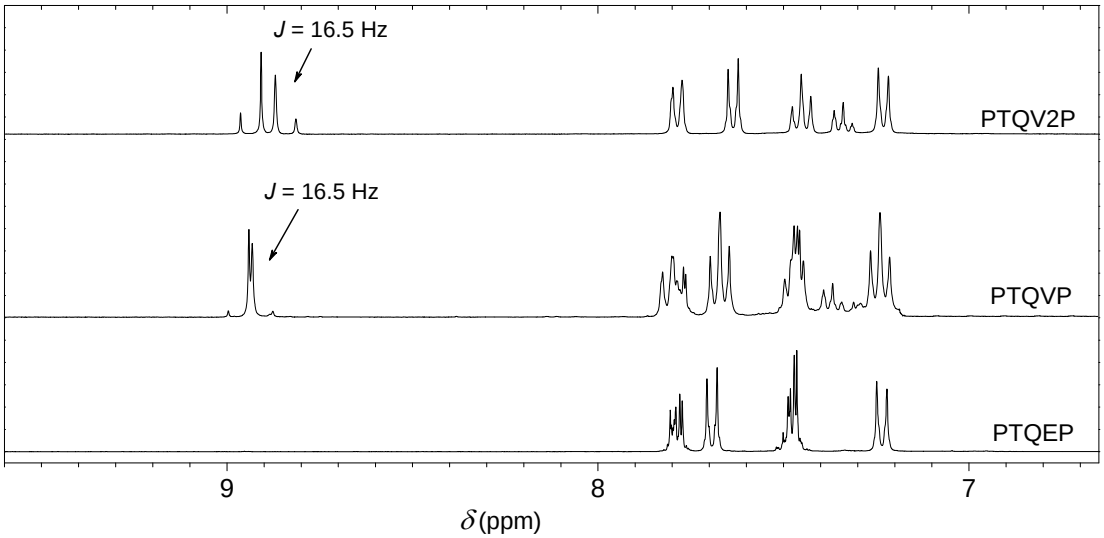


**Figure 14**. $^{1}$H-NMR of **PTQV2P**, **PTQVP** and **PTQEP** in $CD_2Cl_2$ at r.t. not necessarily recorded at the same spectrum amplitude. For a better visualization only the aromatic region between 6.6 and 9.6 ppm is shown.

NMR investigations confirmed the exclusively *E* (trans) stereochemistry of the double bonds formed for both **PTQV2P** and **PTQVP** (Figure 14). As the vinyl group was placed between the highly electron deficient TQ core and phenyl, the electron density around the

corresponding protons was decreased and as a consequence the signals corresponding to these protons appeared downfield at around 8.9 ppm. The *E* configuration of the olefinic protons, for both **PTQVP** and **PTQV2P**, was validated by their characteristic 16.5 Hz vicinal-coupling constant.[4]

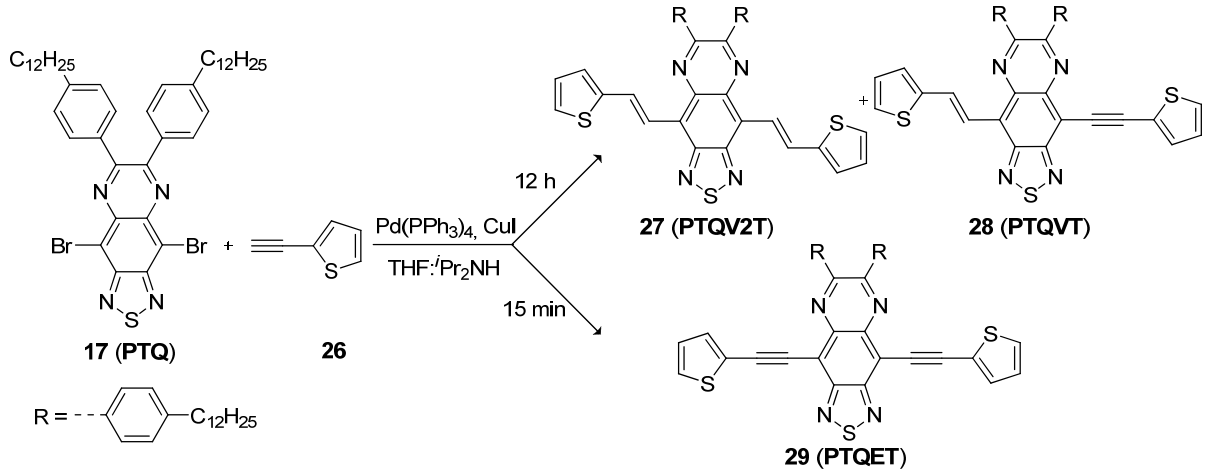


**Scheme 13.** Cross-coupling reaction of **PTQ** and ethynylthiophene (**26**) under *Sonogashira-Hagihara* reaction conditions.

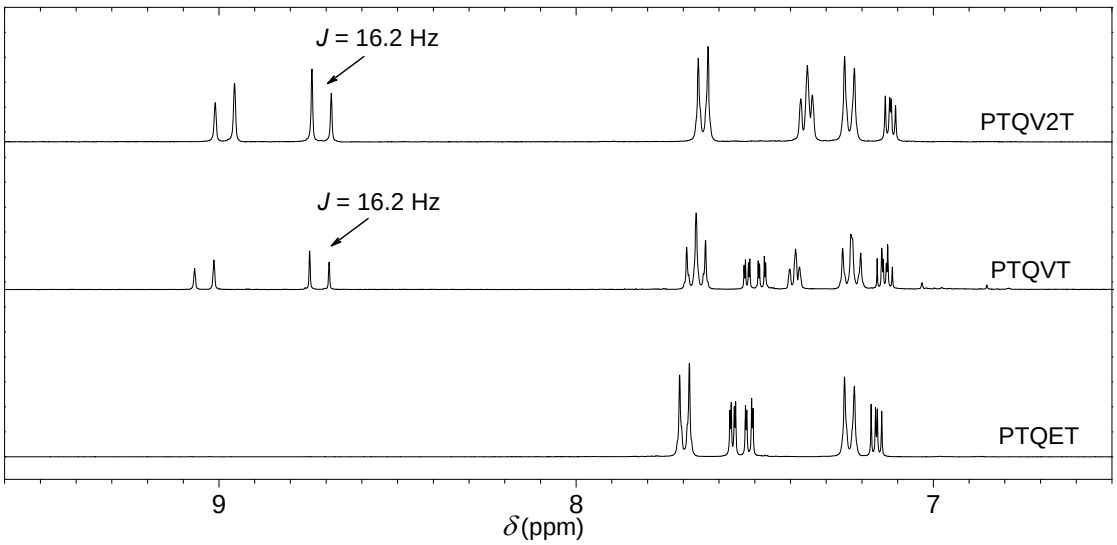


**Figure 15.** $^{1}$H-NMR of **PTQV2T**, **PTQVT** and **PTQET** in $CD_2Cl_2$ at r.t. not necessarily recorded at the same spectrum amplitude. For a better visualization only the aromatic region between 6.5 and 9.6 ppm is shown.

Secondly, the reaction between ethynylthiophene (**26**) and **PTQ** was examined. Similarly to the previously presented case using an excess of **26** (3 equiv.), different reaction times yielded distinct products (Scheme 13). After approx. 15 min an intense colour change from

red-orange to dark violet was observed, indicating the formation of compound **29** (η = 85 %). Letting the reaction to proceed for 12 h resulted in the formation of compounds **27** (**PTQVT**, η = 16 %) and **28** (**PTQV2T**, η = 12 %). The configuration of the double bonds for both **27** and **28** was undoubtedly clarified by $^{1}$H-NMR. As expected, the vinyl proton doublets appeared downfield at 8.7 ppm and approx. 9.0 ppm (Figure 15). In both cases, the characteristic 16.2 Hz vicinal coupling constant confirmed the *E* configuration of the vinyl π-spacers.

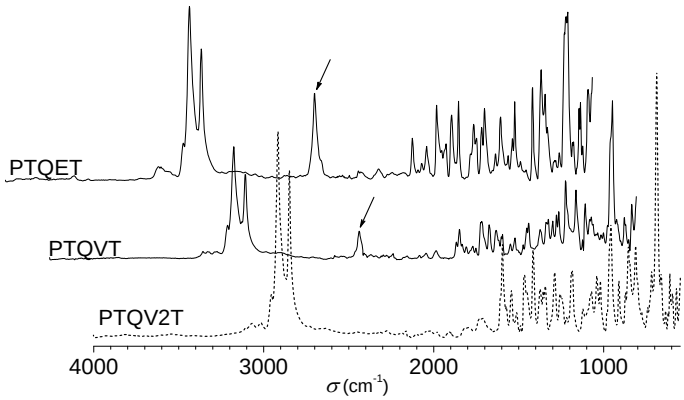


**Figure 16.** FT-IR spectrum of **PTQV2T**, **PTQVT** and **PTQET**. The arrows are indicating the characteristic infrared band for the *C*≡*C* stretch.

Apart from the $^{13}$C-NMR studies, which revealed the characteristic quaternary carbon signals at 90.06 ppm and 99.02 ppm (**PTQET**) and 90.60 ppm and 97.60 ppm (**PTQVT**), additional conformation as to the presence of triple bond(s) in **PTQET** and **PTQVT** was obtained from IR measurements (Figure 16). Both compounds exhibited the typical *C*≡*C* triple bond stretch[5] near 2180 cm$^{-1}$, while in the case of **PTQV2T** this signal was absent.

The isolation of these derivatives gave the opportunity of direct comparison of the physical properties that are related to the influence of π-spacer in the given [D-A-D] series, for example compounds **PTQV2T**, **PTQVT** and **PTQET**, respectively. As the main goal was to synthesize polymeric systems containing triple bond π-spacers, it was essential to elucidate the triggering parameter responsible for the in situ reduction of the *Sonogashira-Hagihara* coupling products and if possible to eliminate it.

Within this frame there were two questions raised:

1. What are the parameter(s) that lead to the in situ formation of the ethylene bond*?*

*2.* How can this "side reaction" be avoided (in the view of the fact that copolymerization is intended and a strict control of the structure is imperative)*?*

To be able to answer these questions, several control reactions were carried out according to Scheme 14, changing one of the parameters at the time.

The following parameters were changed and their influence determined:

*Reaction time:* –The *in situ* formation of the double bonds occurred subsequent to the *Sonogashira-Hagihara* coupling.

*Solvent:* –The nature of the solvent (THF or toluene) did not significantly influence the *in situ* reduction.

*Base:* –The use of slightly weaker base (triethylamine - $Et_3N$) did not prevent the formation of neither **PTQV2T** nor **PTQVT**.

*Catalyst:* –The use of different Pd(0) sources, such as $Pd(PPh_3)_4$, $PdCl_2(PPh_3)_2$ or PdOAc and $PPh_3$ did not impede the "side reactions" from taking place.

*Molar ratio of terminal alkyn:* –Using exactly 2 equiv. of terminal alkyne yielded **PTQET** ($\eta > 80$ %) after 30 min;

–No traces of either **PTQV2T** or **PTQVT** were found even after 24 h, when 2 equiv. of terminal alkyne were employed.

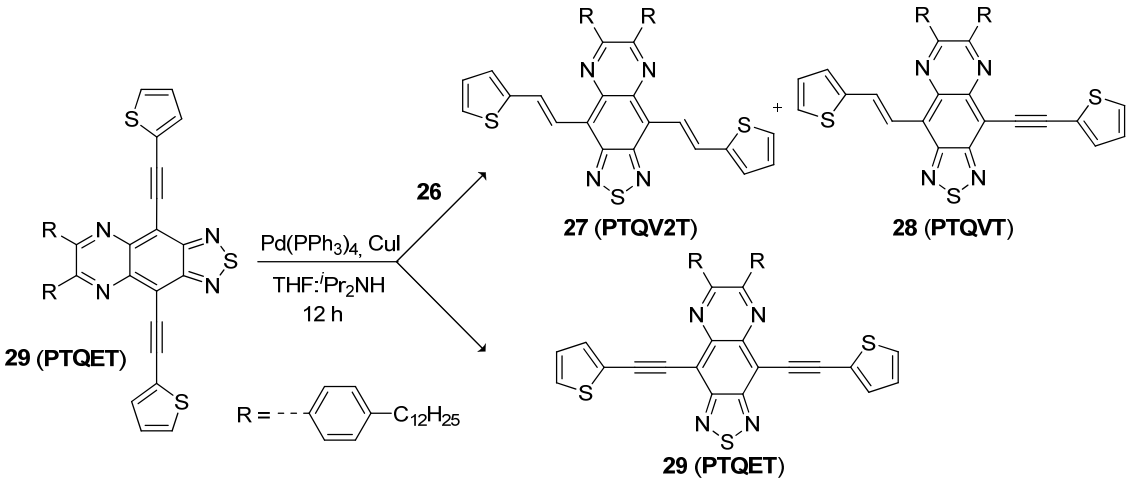


**Scheme 14.** Influence of the terminal acetylene on the reduction of the ethynyl bond under *Sonogashira-Hagihara* reaction conditions.

With a strong indication that one of the key elements in the *in situ* reduction of the triple bonds is played by the excess of terminal acetylene, two additional parallel experiments were

undertaken (Scheme 14). In two different flasks equal amounts of **PTQET** were placed, together with catalytic amounts of $Pd(PPh_3)_4$ and CuI, in a mixture of THF and $^{i}Pr_2NH$. More than 4 equiv. of ethynylthiophene were added in only one of the flasks. After several days of stirring at room temperature the flask with the added terminal acetylene contained both **PTQV2T** and **PTQVT** with no traces of **PTQET**. Meanwhile, the second flask, where no terminal acetylene was added contained only **PTQET**.

Although, through the rigorous control of the amount of terminal acetylene used the *in situ* reduction of the *Sonogashira-Hagihara* cross-coupling product could be overcome, it was suspected that the strong electron deficient nature of the TQ core played an important role as well. Therefore, a simple experiment was carried out to verify this idea. A weaker acceptor, such as benzothiadiazole (**BT**) was subjected to coupling conditions that led to the *in situ* reduction of **PTQET** or **PTQEP** (Scheme 15). Even though the terminal alkyne was used in a great excess (> 4 equiv.), compound **30** suffered no further *in situ* reactions, regardless of the reaction time (> 24 hours). Therefore, it is reasonable to assume that the strong electron deficient nature of the TQ core does facilitate the *in situ* reduction of the ethynylene π-spacers, probably by promoting the creation of dipoles on the *C*≡*C* bond.

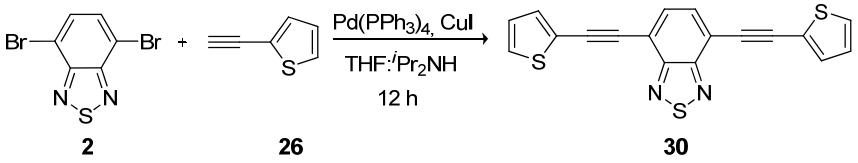


**2** **26** **30**

**Scheme 15.** Cross-coupling reaction of **BT** (**2**) and ethynylthiophene (**26**) under *Sonogashira-Hagihara* conditions. Synthesis of 4,7-bis(thiophene-2-ylethynyl)-benzo[*c*][2,1,3]thiadiazole (**30**).

There are hardly any examples in the literature of related accounts observed under *Sonogashira-Hagihara* coupling conditions. The group of Philippe Meunier[6] repeatedly observed similar "side reactions" taking place, when the coupling reaction was carried out in an ionic liquid ([BMIM][$BF_4$]), in the presence of pyrrolidine as base. The hydrogenation of the ethynylene bond occurred in case of certain electron deficient substrates in long term reactions. It has been suggested that subsequent to the *Sonogashira-Hagihara* coupling reaction, the palladium might act as a hydrogen-transfer catalyst. Furthermore, the acidic hydrogenopyrrolidinium salt resulting from the terminal acetylene deprotonation step of the *C–C* coupling was proposed as a proton source[7] (see the *Sonogashira-Hagihara* catalytic cycle[8]

in Scheme 1, Chapter 1.). This scenario however, could not account for the fact that the hydrogenation in this case, occurred not as a concurrent reaction, but as a consecutive one and most importantly could be totally avoided by not using excess of terminal alkyne.

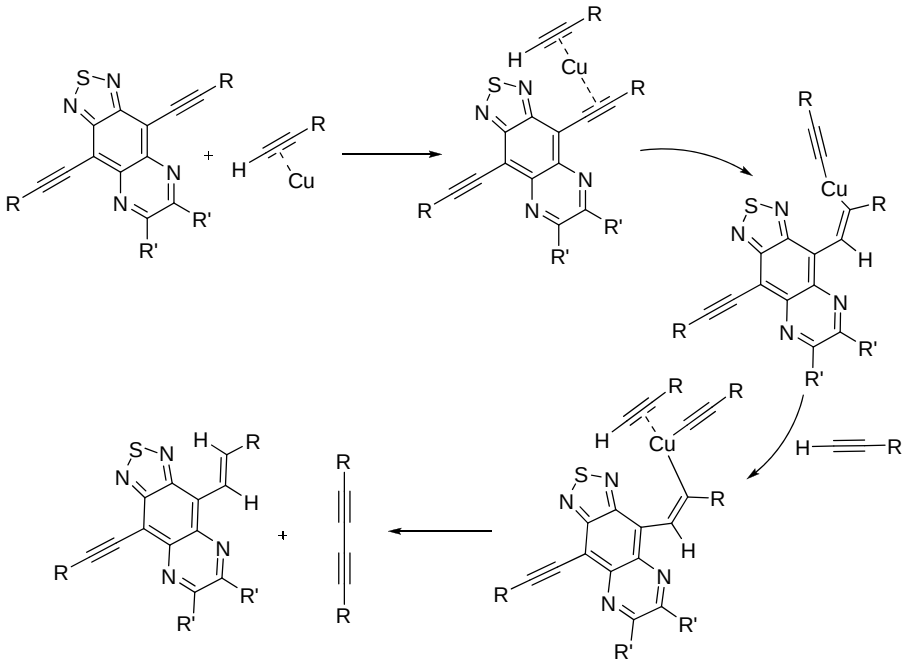

**Scheme 16.** Proposed mechanism for the *in situ* hydrogenation of the triple bond under *Sonogashira-Hagihara* reaction conditions.

Although a more detailed study would be required in order to fully elucidate the mechanism, based on the collected data it is reasonable to assume that the hydrogenation directly involves the π-alkyne-Cu complex,[9] formed in the Cu-cycle, as illustrated in Scheme 16.

The importance of the isolation of the vinyl π-spacer containing derivatives is further augmented by the fact that *via* the *Heck coupling* of **PTQ** with phenylethene, neither **PTQV2P**, nor **PTQV2T** could be synthesized. Under mild reaction conditions [$Pd_2(dba)_3$, P($^t$Bu)$_3$, CyNMe, 1,4-dioxane, r.t.][10] prolonged reaction times (over 48 hours) yielded only traces of the *Heck coupling* product. Significant amount of debrominated TQ derivative was recovered, suggesting that although the insertion of the palladium took place, the coupling failed. The ligand-free catalytic conditions were explored ($Pd(OAc)_2$, $K_3PO_4$, DMA, 140$^0$C) as well.[11] The rather strong base, usually required in excess, caused the decomposition of the TQ core presumably through reductive sulfur extrusion. There are other alternatives in building up a

double bond, such as the *Horner-Wadsworth-Emmons* reaction[12] or the *Knoevenagel* condensation.[13] Both of these procedures would involve the presence of aldehyde or nitrile groups on the TQ core. The introduction of these substituents might be possible only through elaborate synthetic procedures which did not fall into the intended aim of this work.

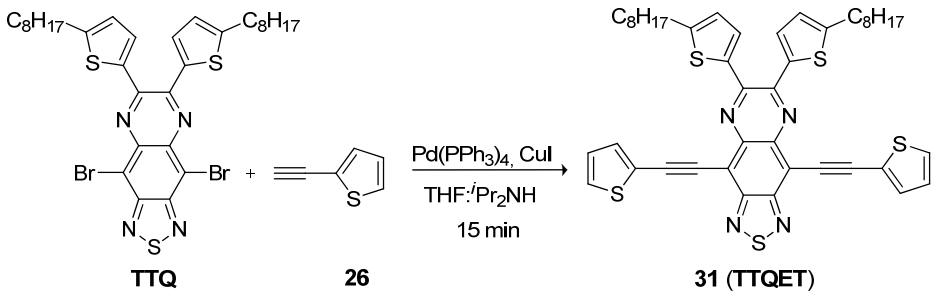


**Scheme 17.** Synthesis of **TTQET** (**31**).

Finally, to complete the series of the model compounds containing ethylene linkers, **TTQ** was reacted with 2 equiv. of ethynylthiophene leading to the formation of compound **31** (**TTQET**) in 81 % yield (Scheme 17).

## 2.3.2. Optical and Electrochemical Characterization of the TQ Model Compounds Containing Ethynylene π-Spacers

The influence of the substituents connected to the TQ core directly at the positions 6 and 7 or *via* ethynyl π-spacers at positions 4 and 9 on the electronic properties was investigated in details. Chart 8 contains the model compounds that are compared in this section. In order to put the results into prospective a literature known compound was considered as well.[14] Although several TQ monomers were synthesized with thiophene units directly connected at positions 4 and 9 to the electron deficient segment, these materials were polymerized without further characterization (see Subchapter 2.1. for relevant references). The structurally closest thiophene functionalized, literature known TQ derivative

having partially reported photophysical and electrochemical properties, is compound **32**[14] (Chart 8).

**Chart 8.** Compared model compounds within the series containing solely ethynylene π-spacers (literature known compound **32** is listed for comparison).

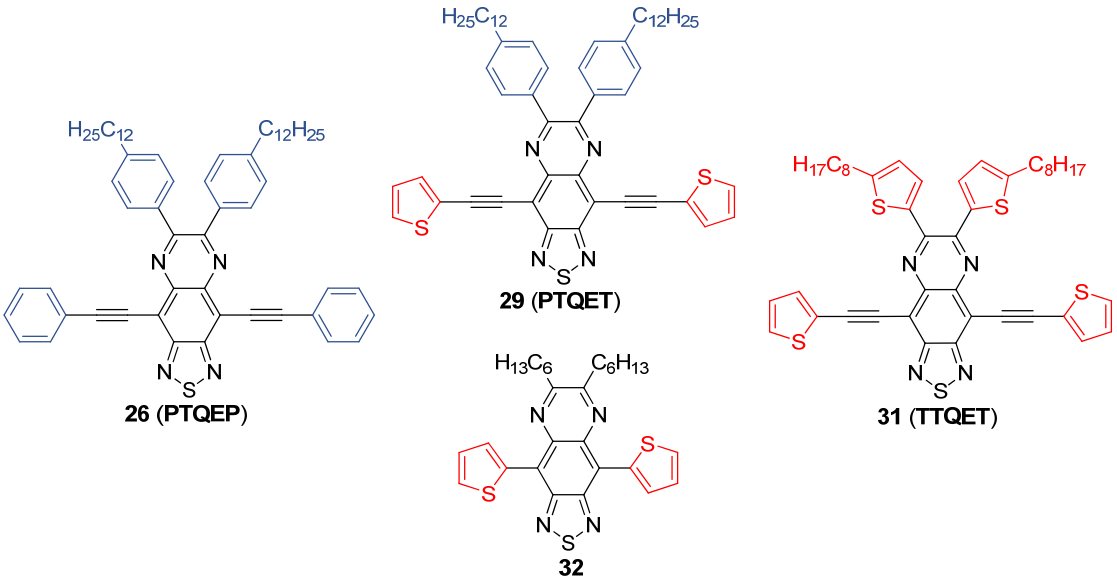


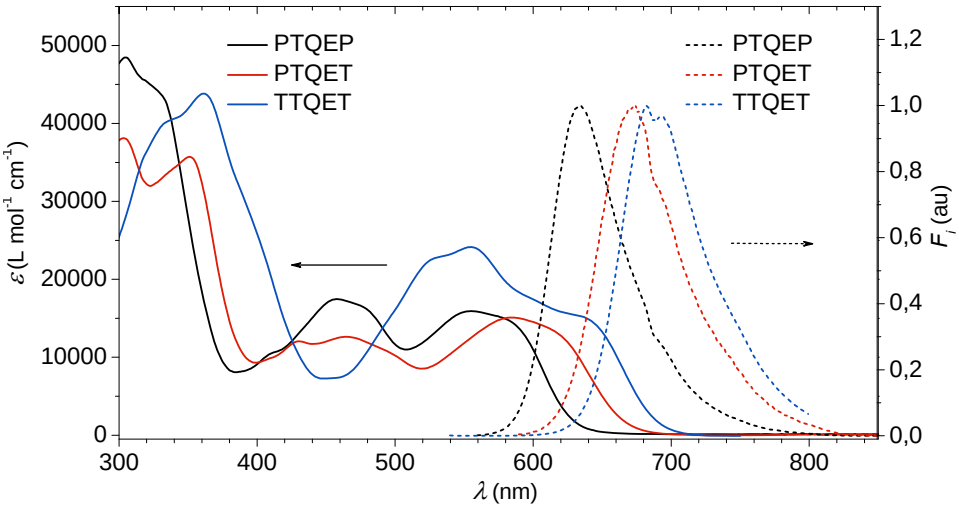


**Figure 17.** Absorption (solid lines) and emission (dashed lines) of **PTQEP**, **PTQET** and **TTQET** in chloroform solution ($c = 10^{-5}$ mol $L^{-1}$). Excited at the maximum of the long wavelength absorption band characteristic for each compound.

As pointed out earlier (see Section 2.2.2.), the simplest way to evaluate π-conjugation extension or D-A interactions is by photophysical means. The characteristic optical cross-section in solution of the three new model compounds is depicted in Figure 17 and the

relevant data are listed in Table 3. At a first glance it is apparent that the introduction of aromatic functionalities connected *via* ethynylene π-spacers at the TQ segment resulted in the extension of the absorption up to 700 nm (**TTQET**). While **PTQEP** and **PTQET** presented three main absorption bands, **TTQET** showed two broad bands. It can not be excluded that the absorption band between 375-525 nm is the retained absorption of the parent TQ derivative (see Figure 6, Section 2.2.2.). The long wavelength absorption band at 525-630 nm for **PTQEP** and 525-675 nm for **PTQET** respectively, originated from the extension of the π-conjugation through the ethynyl π-spacers. In case of **PTQET**, with thiophene units connected *via* triple bonds to the acceptor core, revealed a 30 nm red shift of the long wavelength absorption band relative to **PTQEP**. The reduced energy-gap of **PTQET** ($E_{op}$ = 1.85 eV) could be attributed to the improved D–A interaction. In case of **TTQET**, having only thiophene substituents, the long wavelength absorption band was further red shifted and the derived $E_{op}$ was 1.78 eV. If the optical parameters of **PTQET** or **TTQET** are juxtaposed with those reported for compounds **32**, it was found that they are at least comparable (Table 3).

**Table 3.** Summary of the photophysical data for the series **PTQEP**, **PTQET** and **TTQET**, respectively.

| Compd. | $\lambda_{abs}$ (nm) / log $\varepsilon$[a] | $\lambda_{em}$ (nm)[a] / $\Phi_F$ (%)[b] | $\lambda_{abs}$ (nm) / $\lambda_{em}$ (nm) - film[c] | $E_{op}$ (eV)[a] |
|---|---|---|---|---|
| **PTQEP** | 304 / 4.68; 460 / 4.24; 556 / 4.20 | 634 / 79 | 311, 466, 564, 607 / 645 | 1.96 |
| **PTQET** | 352 / 4.55; 464 / 4.10;586 / 4.17 | 673 / 30 | 312, 595 / 695 | 1.85 |
| **TTQET** | 361 / 4.64; 556 / 4.38; 640 / 4.18 | 682 / 13 | 355, 555, 646 / 701 | 1.78 |
| **32**[d] | 593 / - | - / - | - / - | 1.86 |

[a]in chloroform solution ($c = 10^{-5}$ mol $L^{-1}$); [b]in toluene, estimated using the comparative method with cresyl violet as standard fluorophore ($\Phi_F$ = 67 % in methanol); [c]spin-coated on a glass substrate from a 10 mg $mL^{-1}$ toluene solution (thickness 120 nm); [d]literature data.[14]

Similarly, the emission spectra of the three TQ model compounds revealed red-shifts of different magnitude as a function of the donor strength of the substituent attached to the TQ segment *via* the π-spacers. **PTQEP** displayed $\lambda_{em}$ at 634 nm, significantly higher than the corresponding starting **PTQ**, proving the successful extension of the conjugation *via* the triple bond π-spacers. **PTQET** proved to have an emission maximum 40 nm shifted to higher wavelengths relative to **PTQEP**. This red-shift supports the fact that introducing stronger donor units through ethynyl π-spacers at the TQ core improved the π-conjugation. The highest $\lambda_{em}$ = 682 nm was registered for **TTQET** that contained solely thiophene units as donors. This confirms the observation according to which, the attachment of stronger donor substituents

at the TQ core improved the π-conjugation in the system. Additionally, it also showed that the substituents attached in positions 6 and 7 at the TQ core do play an important role in the tuning of the photophysical properties of the model compounds.

To investigate the existence of intramolecular donor-acceptor interactions, the model compounds were subjected to solvent dependent absorption and emission studies. Additionally, their photophysical properties in thin film prepared by spin-coating on a glass substrate from a 10 mg $mL^{-1}$ toluene solution were analyzed. In most of the examined solvents the absorption of **PTQEP** was characterized by unstructured bands (Figure 18). In non-polar solvents, like hexane, the fine structure of the vibrational bands was more pronounced. Since different vibrational band become prominent as a function of solvent polarity it is rather difficult to define the longest wavelength $\lambda_{max}$ for each solvent. Notably, the differences in $E_{op}$ were more suggestive. As it turned out, the maximum $E_{op}$ was detected in the polar acetone (2.00 eV), while the lowest value was derived in chloroform solution (1.96 eV). In the solid state, as a result of an improved organization the absorption was extended up to 650 nm lowering the $E_{op}$ to 1.88 eV. Moreover, the long wavelength absorption band was reduced, while the second absorption band was increased in its intensity.

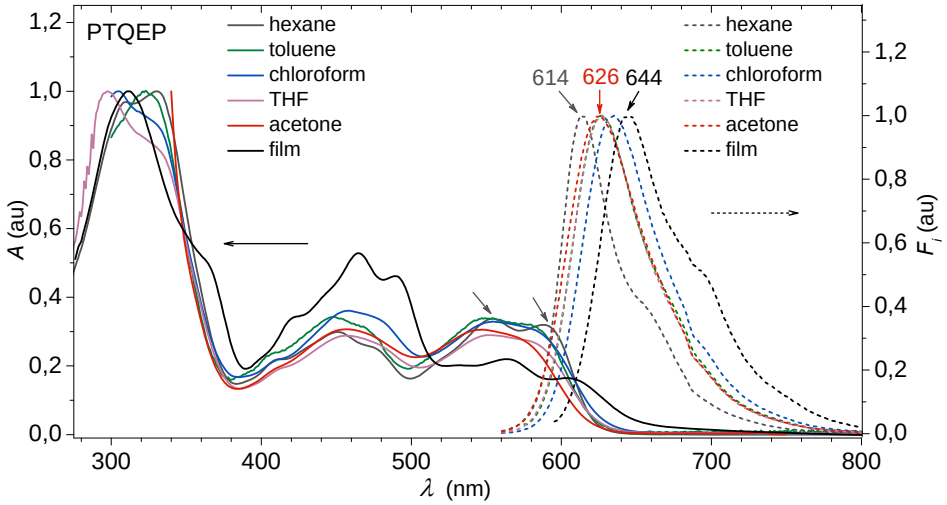


**Figure 18.** Solvent dependence of the absorption (solid lines) and emission (dashed lines, $\lambda_{ex}$ = 530 nm) of **PTQEP** (**26**, $c = 10^{-5}$ mol $L^{-1}$).

A better defined fingerprint of the solvent polarity was observed in the emission spectra. Going from hexane to chloroform an 18 nm bathochromic shift of $\lambda_{em}$ was ascertained. A more polar medium, such as acetone led to an 8 nm hypsochromic shift relative to chloroform, with almost identical emission profile to the one registered in toluene or THF. Although these shifts were moderate, they suggest a more polar molecular structure in the excited state than in the ground state, hence an efficient charge transfer from the donor to the electron deficient TQ core. Comparing the solution and solid state emission, the 10 nm red-shift of the $\lambda_{em}$ of the thin film *vs.* chloroform was caused by an effective π-π stacking in the solid state.

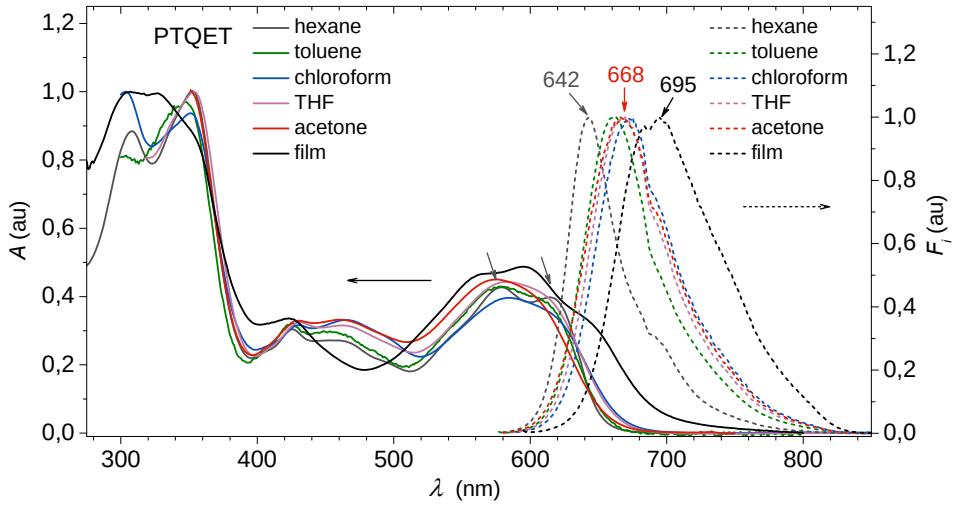


**Figure 19.** Solvent dependence of the absorption (solid lines) and emission (dashed lines, $\lambda_{ex}$ = 570 nm) of **PTQET** (**29**, $c = 10^{-5}$ mol $L^{-1}$).

Very similar solvent dependence was found for **PTQET** in which the phenylacetylene substituents were replaced with thienylacetylene (Figure 19). As a function of polarity, the optical energy-gap, determined from the onset of the absorption, varied between 1.90 eV (hexane) and 1.84 eV (chloroform). The influence of the solvent polarity being more pronounced for **PTQET** relative to **PTQEP**, demonstrated the better D-A-D interaction. Furthermore, in the solid state the absorption was extended up to 700 nm ($E_{op}$ = 1.77 eV). Unlike in case of **PTQEP**, the long wavelength absorption band of **PTQET** in the solid state gained in intensity relative to the band between 375 and 520 nm. Similarly, stronger dependence on the solvent's polarity was discerned in the emission. A bathochromic shift of

31 nm could be observed going from hexane to chloroform. Additionally, due to an effective π-π stacking in the solid state the $\lambda_{em}$ was bathochromically shifted to 695 nm.

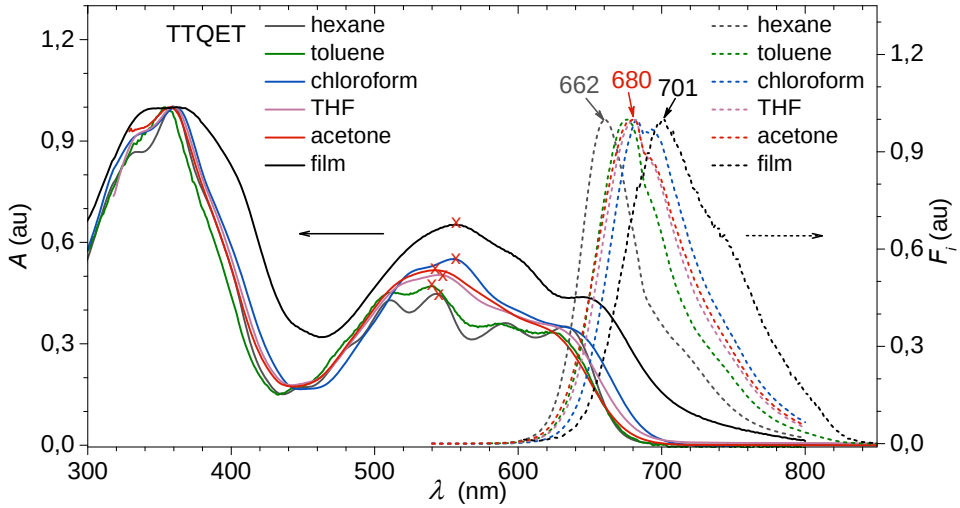


**Figure 20.** Solvent dependence of the absorption (solid lines) and emission (dashed lines, $\lambda_{ex}$ = 540 nm) of **TTQET** (**31**, $c = 10^{-5}$ mol $L^{-1}$).

The photophysical properties of **TTQET**, having only thienyl substituents connected to the TQ core, revealed a much pronounced solvent dependence. While in hexane the local absorption maxima of the absorption band at longer wavelength was detectable, a more polar environment left this band structureless. Nonetheless, it was possible to identify a $\lambda_{max}$ in each solvent as it is indicated in Figure 19. A positive bathochromism ($\Delta\lambda_{max}$ = 13 nm) going from hexane to chloroform was identified, suggesting the presence of an efficient intramolecular charge transfer. Further increasing the solvent polarity yielded hypsochromic shifts up to $\Delta\lambda_{max}$ = -15 nm (acetone *vs.* chloroform). Solvents with a high dielectric constant, such as acetone (37.5) appear to favor excessive charge transfer within the molecule, leading to back electron transfer which in turn is the source of the negative $\Delta\lambda_{max}$ values.[15] The more polar structure in the excited state was again indicated by the $\Delta\lambda_{em}$ = 23 nm derived for hexane *vs.* chloroform. Finally, both the absorption and the emission in the solid state presented bathochromic shifts relative to their corresponding spectra recorded in solution. The calculated energy was $E_{op}$ = 1.72 eV and the $\lambda_{em}$ was red-shifted to 700 nm.

Hence, the induced structural modifications led to model compounds that revealed emissions covering the red region (630-720 nm) of the visible spectrum.[16] The fluorescence

emission of these model compounds was quantified by measuring their fluorescence quantum yield ($\Phi_F$) with the comparative[17] method and the data are listed in Table 3. Figures 21*a-b* illustrate the plots corresponding to **PTQEP** and **TTQET** respectively, based on which the calculations were made. The corresponding experimental procedure is detailed in Chapter 5. Cresyl violet was chosen as a fluorescence standard having a well documented $\Phi_F$ of 67 % in methanol.[18]

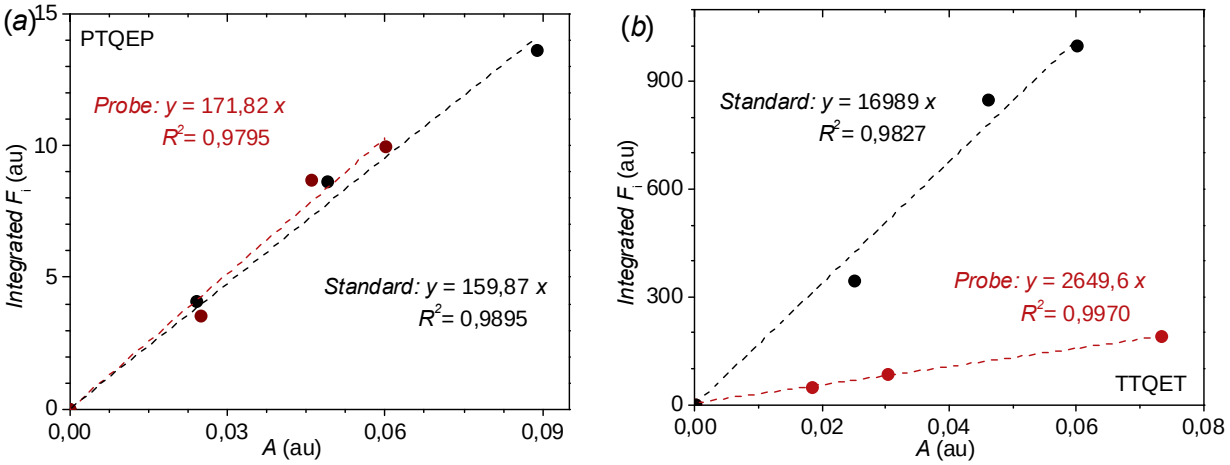


**Figure 21.** Linear plots of the standard (cresyl violet) and **PTQEP** (*a*), and **TTQET** (*b*). The data obtained based on these representations were converted into the specific $\Phi_F$ listed in Table 3.

The highest $\Phi_F$ was found for **PTQEP** ($\Phi_F$ = 79 %). As the phenyl rings were substituted with thiophene, $\Phi_F$ decreased dramatically down to 13 % in case of **TTQET**. Considering that the quantum yield is affected by any given excited state process, it is difficult to judge whether the fluorescence quenching (the lower $\Phi_F$ value) of **PTQET** and **TTQET** is due to intramolecular processes, such as intramolecular charge transfer[19] or heavy atom effect, induced by the presence of sulfur atoms.[20] It is beyond the scope of this work to study in details the cause of the fluorescence quenching in these model compounds.

Having analyzed the photophysical repercussion of π-conjugation extension *via* ethynyl π-spacers, the n-dopability was evaluated by cyclic voltammetry measurements. By registering the characteristic reduction processes of these materials, the $E_{LUMO}$ levels could be estimated from the onset of the first reduction peaks. For accuracy, ferrocene was used as an internal standard and the registered spectra were corrected to the $Fc^+$ / Fc half wave potential ($E^{1/2}_{Fc/Fc^+}$), as documented in the literature (Figure 17).[21]

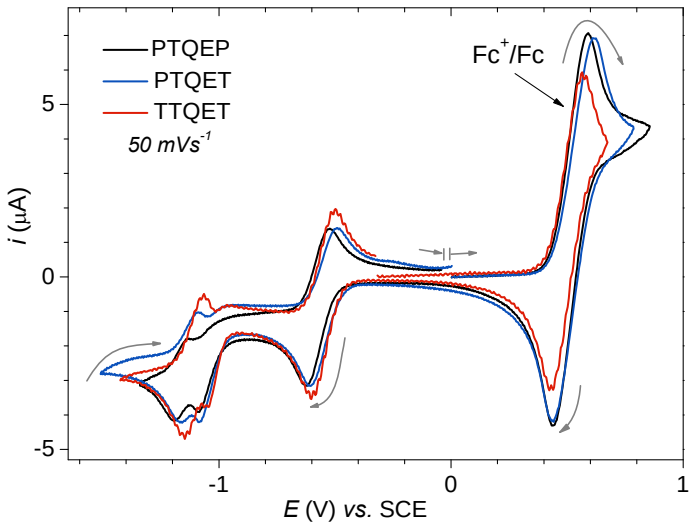


**Figure 22.** Cyclic voltammograms of the model compounds **PTQEP** (**26**), **PTQET** (**29**) and **TTQET** (**31**), respectively as measured in THF with ferrocene as internal standard.

**Table 4.** Summary of the electrochemical data and energy levels of the series **PTQEP**, **PTQET** and **TTQET**, respectively.

| Compd. | $E_{op}$ (eV)[a] | $E_{pc}$ (V)[b] | $E^{1/2}_{pc}$ (V)[b] | $E_{LUMO}$ (eV)[c] | $E_{HOMO}$ (eV)[d] | $E_{calc}$ (eV)[e] |
|---|---|---|---|---|---|---|
| **PTQEP** | 1.98 | -0.62 | -0.568 | -3.79 | -5.77 | 2.02 |
| **PTQET** | 1.86 | -0.61 | -0.553 | -3.80 | -5.66 | 1.89 |
| **TTQET** | 1.78 | -0.59 | -0.532 | -3.83 | -5.62 | 1.86 |
| **32**[f] | 1.86[f] | -0.81[f] | - | - | - | - |

[a]in chloroform solution ($10^{-5}$ mol $L^{-1}$); [b]0.1 mol $dm^{-3}$ of *n*-$Bu_4NPF_6$, in THF, Pt electrode, scan rate 50 mV $s^{-1}$; [c]calculated $E_{LUMO}$ = -( $E^{onset}_{Red}$ - $E^{1/2}_{Fc/Fc^+}$ + 4.8) eV; [d]calculated from $E_{LUMO} = E_{opt} - E_{LUMO}$; [e]DFT quantum mechanical calculations (B3LYP/6-31G*); [f]literature data.[14]

All three compounds showed similar reduction reactions, out of which the first is a typical Nernstian process, followed by two quasi–reversible reduction processes. While the reduction peak potential ($E_{pc}$) of a reversible process could vary depending on the measurement conditions, the corresponding half wave potential ($E^{1/2}_{pc}$) is independent from the scan rate. The electrochemical properties of the model compounds and the estimated energy levels are listed in Table 4. Compared to the literature known **32**, **PTQEP**, **PTQET** and **TTQET** undergo much easier reduction. The onset of the first reduction peak was used to estimate the LUMO energy levels. The insertion of ethynyl π-spacers between the donor units and the TQ segment slightly lowered the $E_{LUMO}$ of the corresponding compound, relative to their parent TQ derivatives (**PTQ**, **TTQ** see Section 2.2.2.). Additionally, with increasing donor strength, the $E_{LUMO}$ was slightly decreased. The $E_{HOMO}$ were derived based on the formula $E_{HOMO} = E_{op} - E_{LUMO}$ (Table 4).

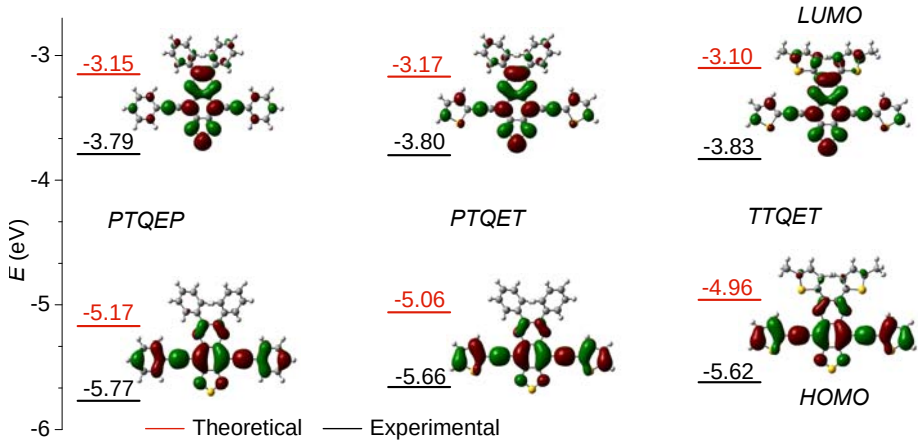


**Figure 23.** Orbital energies based on DFT calculations (red) and experimental findings (black), and corresponding frontier molecular orbital electronic density contours of **PTQEP**, **PTQET** and **TTQET**, respectively.

DFT quantum mechanical calculations (B3LYP/6-31G*) were performed and the obtained results compared with the experimental findings. Although the absolute values do not coincide as illustrated in Figure 23, a similar trend was found for both experimentally and theoretically calculate energy levels. The electronic density contours corresponding to the frontier molecular orbitals showed that for all compounds the LUMO orbital is localized on the TQ segment, while the HOMO orbital resides along the conjugated backbone. Furthermore, the calculated energy-gaps ($E_{calc}$) listed in Table 4 were in very good agreement with the optically determined $E_{op}$.

## 2.3.4. Optical and Electrochemical Characterization of the Model Compounds: Ethylene *vs.* Ethynylene π-Spacers

Generally, in conjugated molecules that contain double bond π-spacers, the electron delocalization and charge stabilization are better than in the case of the structurally related arylethynylenes.[22] However, steric interactions between the aromatic nuclei and the alkene unit may result in non-planar conformation, disrupting the π-conjugation.[23] As far as ethynyl π-spacers are concerned, direct interactions may result in bending distortion having little

affect on the conjugation, due to the cylindrical electronic symmetry of the triple bond.[24] Consequently, replacing the triple bond spacer by a double bond might have a significant influence on the properties of the given system. The synthesis of **PTQEP**, **PTQV2P**, **PTQET**, **PTQVT** and **PTQV2T** enabled the study of the role of the π-spacer in the photophysical and electrochemical behavior of the TQ-based D-A-D type of model compounds (Chart 9).

**Chart 9.** Compared TQ model compounds: ethylene *vs.* ethynylene π-spacers.

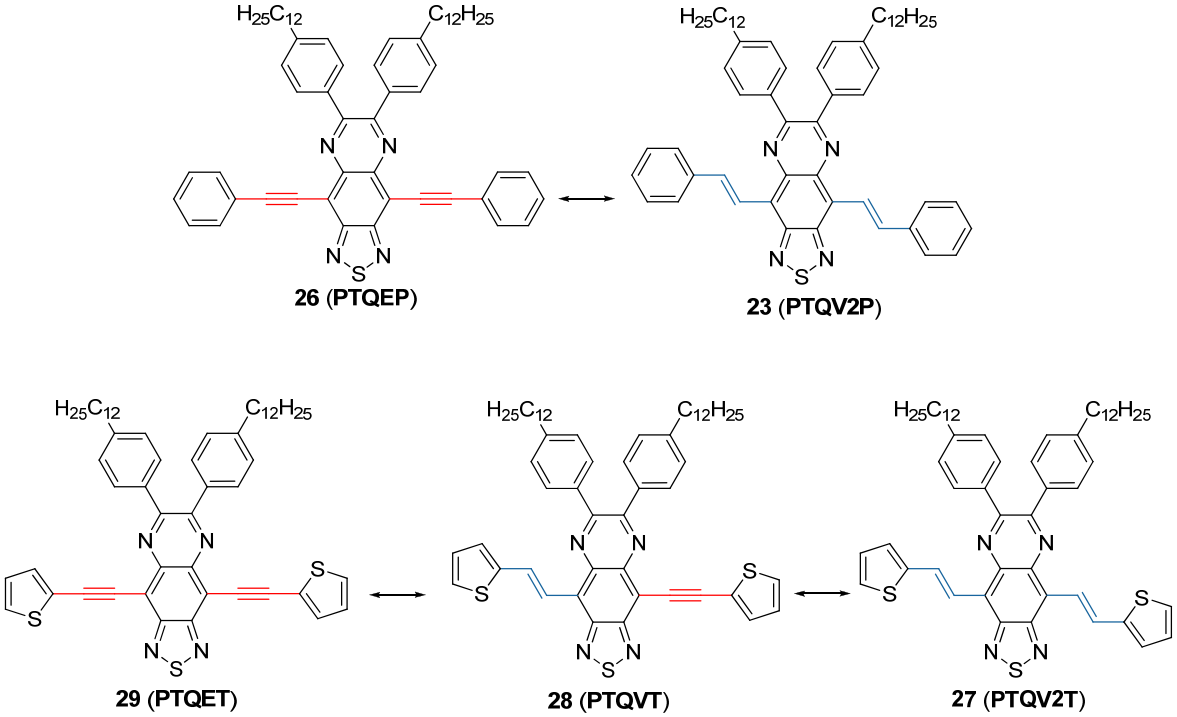


Firstly, the absorption patterns of **PTQEP** (**26**) and **PTQV2P** (**23**) were compared (Figure 24). **PTQV2P** showed two main absorption bands, out of which the low energy absorption band (500-700 nm) was very broad with $\lambda_{max} \approx 625$ nm. The energy-gap derived for **PTQV2P** ($E_{op}$ = 1.75 eV) was significantly lower than in case of the structurally close related **PTQEP**. The narrower optical energy-gap implies a much improved π-electron delocalization within the molecule. Additionally, it also indicates the lack of steric hindrance. The better delocalization in arylvinylene *vs*. arylacetylenes could be rationalized in terms of bond length. For instance, as a consequence of the electron delocalization, the average *C–C* bond length in the aromatic benzene (approx. 1.4 Å) is slightly greater than the typical bond length of the *C=C* bond (approx. 1.34 Å).[25] In contrast, the *C≡C* bond, with a considerably shorter bond

length of approx. 1.21 Å, might influence the extent of the π-electron delocalization by disrupting the uniformity of the bond lengths along the conjugation back-bone when incorporated in a D-A-D system.

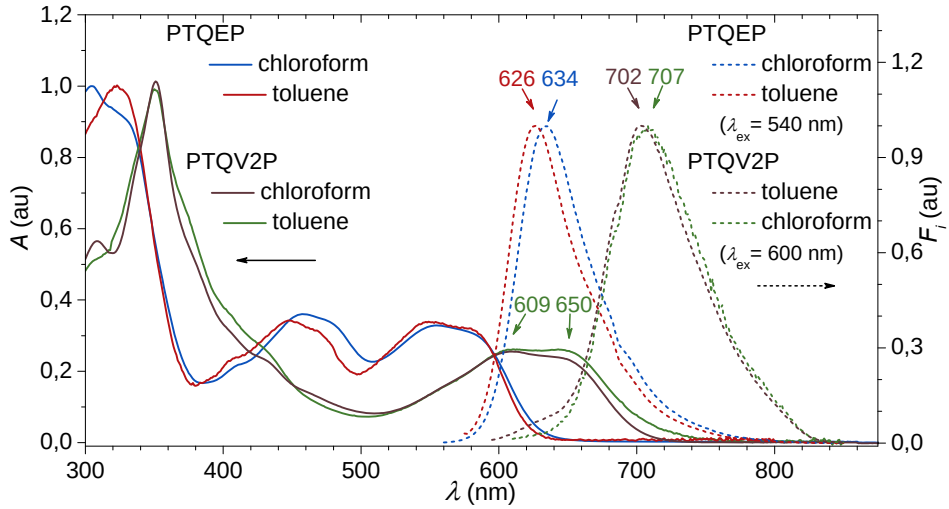


**Figure 24.** Absorption (solid lines) and emission (dashed lines) of the model compounds **PTQV2P** (**23**) and **PTQEP** (**26**) ($c = 10^{-5}$ mol $L^{-1}$).

The enhanced π-conjugation was also reflected in the emission spectrum of **PTQV2P** (Figure 24). In the absence of steric repulsions, the presence of vinyl spacers shifted the $\lambda_{em}$ in chloroform to approx. 700 nm. The fluorescence quantum efficiency ($\Phi_F$ = 8 %) estimated for **PTQV2P** based on the comparative method,[26] was considerably lower when compared to the structurally similar **PTQEP** ($\Phi_F$ = 79 %). Considering that processes such as intramolecular charge transfer and / or conformational changes are playing a decisive role in the possible de-excitation pathways that compete with fluorescence emission,[19] the low $\Phi_F$ is not surprising. While triple bond containing molecules tend to be rod-like structures the rotation about a *C=C* bond is less restricted favoring de-excitation through internal conversion. Moreover, it is known that the smaller the energy-gap between the initial and final electronic states, the larger the efficiency of internal conversion.[19]

Turning to the series **PTQET**, **PTQVT** and **PTQV2T**, the impact of replacing the triple bond π-spacers with double bond π-spacers on the photophysical properties was similar to that described above. The absorption and emission spectra in solution are illustrated in Figure 25. It is apparent that only by substituting one of the ethynylene π-spacer with ethylene (**PTQVT**)

an approx. 40 nm red-shift of the $\lambda_{max}$ (594 nm → **PTQET** *vs*. 634 nm → **PTQVT**) was induced, resulting in a compound with an $E_{op}$ = 1.73 eV. In case of **PTQV2T**, possessing solely double bond π-spacers, $\lambda_{max}$ reached 665 nm and the $E_{op}$ derived was 1.64 eV. The systematic replacement of acetylene linkers with vinylene, within a [D-TQ-D] system, led to compounds emitting in the NIR region, with $\lambda_{em}$ as high as 742 nm (**PTQV2T**).

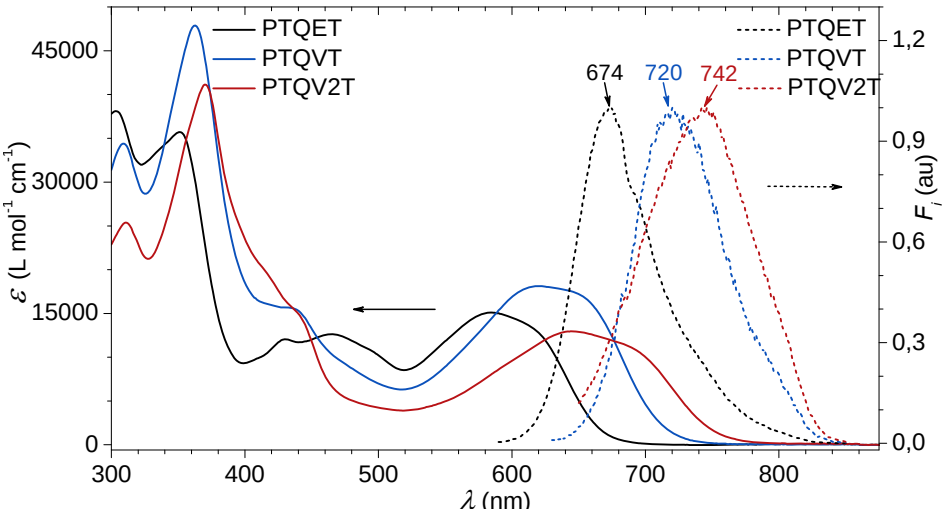


**Figure 25.** Absorption (solid lines) and emission (dashed lines) in chloroform of the model compounds **PTQET** (**29**), **PTQVT** (**28**) and **PTQV2T** (**27**) ($c$ = $10^{-5}$ mol $L^{-1}$).

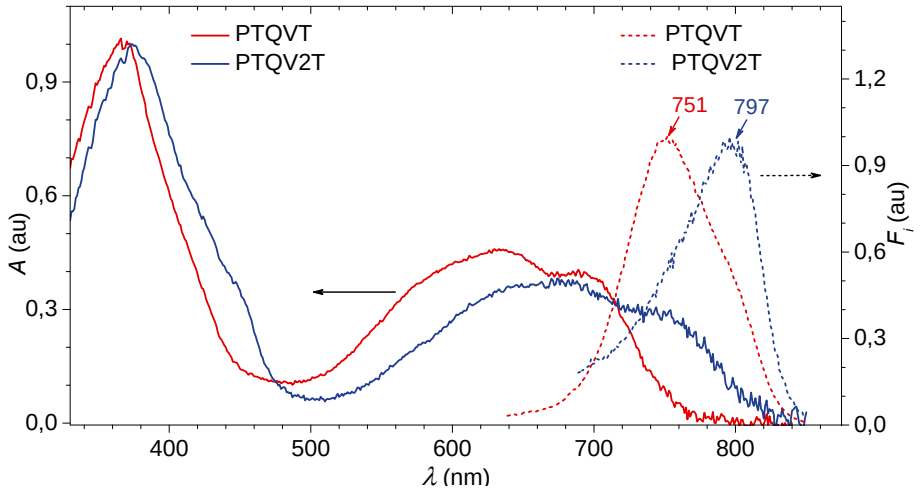


**Figure 26.** Absorption (solid lines) and emission (dashed lines) spectra of the model compounds **PTQVT** (**28**) and **PTQV2T** (**27**) spin-coated on a glass substrate from a 1 mg $mL^{-1}$ toluene solution.

Figure 26 shows the absorption and emission of both **PTQVT** and **PTQV2T** measured in solid state. Although, the long wavelength absorption maximum was not significantly red-shifted,

the presence of a shoulder around 700 nm in case of **PTQVT** and 750 nm for **PTQV2T** suggested an enhanced π-π interaction in the solid state. Similarly, the emission maximum was bathochromically shifted with more than 30 nm in the solid state, relative to the one in solution (751 nm → **PTQVT**; 797 nm → **PTQV2T**). It has to be mentioned here, that the somewhat "cut-off" emission spectrum of **PTQV2T**, around 840 nm is caused by the drop in sensitivity of the spectrofluorometer used for the measurements.

As far as low energy-gap is concerned, the general trend within [D-TQ-D] model systems is certainly in favor of ethylene π-spacers. Nonetheless, it has to be kept in mind that one of the limiting parameters for most of the applications involving organic materials is their energy levels.[27] Thus, it is equally important to look at the electronic structure and the energy levels of the materials. The impact of the nature of the π-spacer on the electron affinity of the structurally related model compounds could be evaluated *via* cyclic voltammetry measurements. Figures 27*a* and 27*b* illustrate the registered reduction curves for all the model compounds compared in this section.

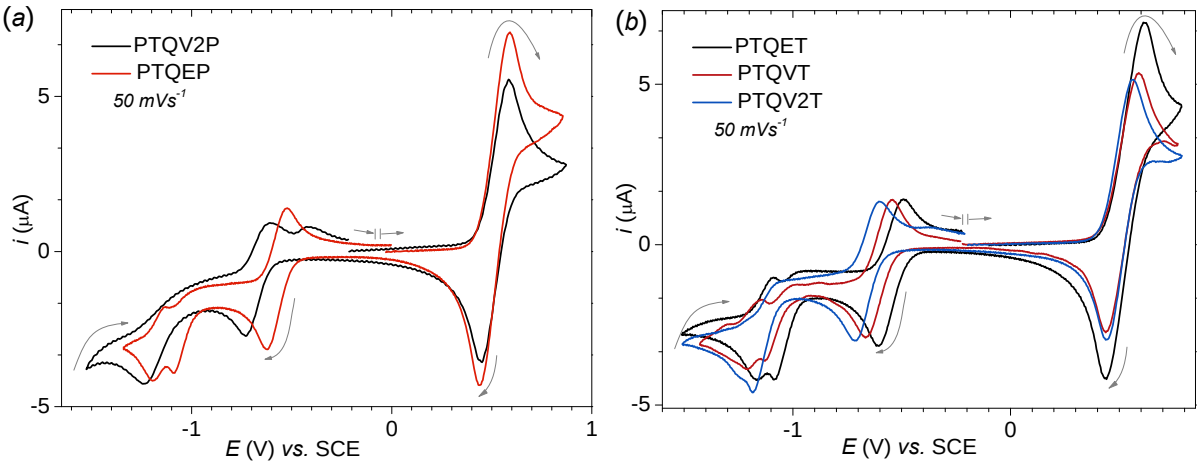


**Figure 27.** Cyclic voltammograms of the model compounds **PTQEP** and **PTQV2P** (*a*) and of the model compounds **PTQET**, **PTQVT** and **PTQV2T** (*b*), respectively. All the measurements were carried out in THF with ferrocene as internal standard.

As it is shown in Figure 27*a*, by replacing the ethynyl π-spacers with vinyl ones (**PTQV2P**) the reduction became more difficult. The corresponding first reduction peak potential ($E_{pc}$ = -0.73 eV) was more than 0.2 eV lower compared to **PTQEP**. The reversibility of the first reduction made it possible to determine the characteristic first half wave potential

($E^{½}$ = -0.670 eV) being 0.1 eV lower than in the case of **PTQEP**. Consequently, the estimated LUMO energy level was increased to -3.69 eV (Table 5).

**Table 5.** Summary of the electrochemical data and energy levels for **PTQV2P**, **PTQVT** and **PTQV2T,** respectively.

| Compd. | $E_{op}$ (eV)[a] | $E_{pc}$ (V)[b] | $E^{½}$ (V)[b] | $E_{LUMO}$ (eV)[c] | $E_{HOMO}$ (eV)[d] | $E^{calc}_{LUMO}$ (eV)[e] | $E_{calc}$ (eV)[e] |
|---|---|---|---|---|---|---|---|
| **PTQV2P** | 1.75 | -0.73 | -0.670 | -3.69 | -5.44 | -3.10 | 1.83 |
| **PTQVT** | 1.73 | -0.66 | -0.606 | -3.75 | -5.48 | -3.13 | 1.79 |
| **PTQV2T** | 1.64 | -0.72 | -0.656 | -3.70 | -5.34 | -3.09 | 1.69 |

[a]in chloroform solution ($10^{-5}$ mol $L^{-1}$); [b]0.1 mol $dm^{-3}$ of *n*-$Bu_4NPF_6$, in THF, Pt electrode, scan rate 50 mV $s^{-1}$; [c]calculated from $E_{LUMO}$ = -( $E^{onset}_{Red}$ - $E^{½}_{Fc/Fc^+}$ + 4.8) eV; [d]calculated from $E_{HOMO} = E_{op} - E_{LUMO}$; [e]DFT quantum mechanical calculations (B3LYP/6-31G*).

The **PTQET**, **PTQVT** and **PTQV2T** series showed a similar trend in the n-dopability (Figure 27*b*). As the triple bonds are replaced by double bond π-spacers, the corresponding model compounds became more difficult to reduce. The first $E^{½}_{pc}$ was decreased with approx. 0.05 eV per incorporated vinyl π-spacer. The derived $E_{LUMO}$ values (Table 5) reflect the same tendency. As the $E_{op}$ is calculated assuming that the long wavelength transitions in the absorption spectrum are primarily defined by the HOMO – LUMO transition, this value can be used to estimate the $E_{HOMO}$. These values (Table 5) indicate that although the $E_{op}$ was systematically decreased through the introduction of vinyl π-spacers, in detriment of ethynyl ones, both $E_{HOMO}$ (with over 0.3 eV) and $E_{LUMO}$ were increased as a result of the structural changes. The observed trend could be rationalized considering the difference in electronegativity of the two π-spacers. Typically, the electronegativities of the carbon atoms decrease as their hybridization takes on more p-character.[28] Thus an ethynyl π-spacer can be regarded as more electron deficient than a vinyl π-spacer. Consequently, by incorporating the less electron deficient vinyl π-spacer in these molecules their electron affinity is decreased.

In order to gain a better insight into the electronic structure of these model compounds, theoretical calculations were performed as well. The ground state geometries, the frontier orbital, and their respective energies were calculated with the B3LYP functional using a 6-31G* basis set (Figure 28). Typically, the HOMOs are delocalized in the direction of the extended π-conjugation, with only limited contribution on the thidiazole subunit. On the contrary, the LUMOs are delocalized over the entire molecule. This difference in the HOMO / LUMO delocalization is in agreement with the strong electronegativity of the central

TQ core. Although not identical in their absolute value, the calculated energy levels resemble the same trend observed in the experimentally (CV and UV-Vis) determined values. Additionally, the computed HOMO – LUMO energy differences ($E_{calc}$) were in very good agreement with those estimated from the UV-Vis absorption spectra (Table 5).

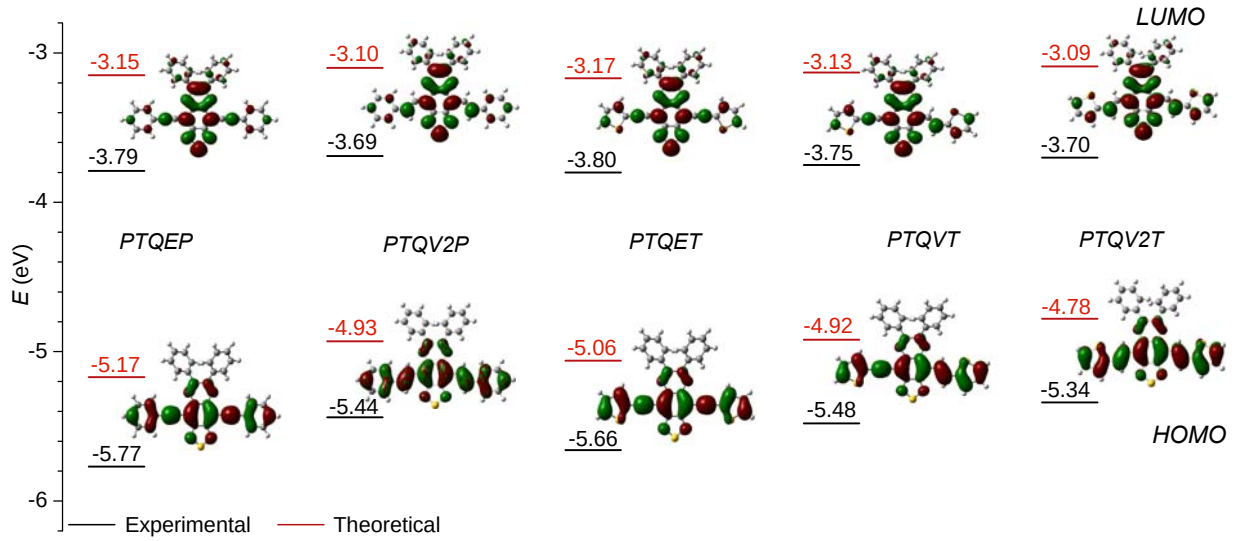


**Figure 28.** Orbital energies based on theoretical calculations (red) and experimental findings (black) and corresponding frontier molecular orbital electronic density contours of **PTQV2P**, **PTQVT** and **PTQV2T**, respectively. For an easier assessment, **PTQEP** and **PTQET** were also included.

## 2.3.5. Solid-State Studies

In recent years, the attention was focused not just on the development of new materials for electronic applications, but also towards the improvement of device performance through new fabrication techniques.[29] The importance of these new techniques lies not merely in reducing the fabrication complexity and costs, but also in obtaining a better control of the morphology of the active layer.[30] This is important as it has been shown that solid state morphology of conjugated materials plays a significant role in the performance characteristics of organic electronic devices.[31] Therefore, it is equally significant to carefully study the solid-state order of the molecules. Certainly, when available X-ray measurements performed on

single crystals would give valuable information regarding the packing mode. Nonetheless, it has to be kept in mind that most of the applications require solvent processing which could result in a very different organization relative to that present in crystals.

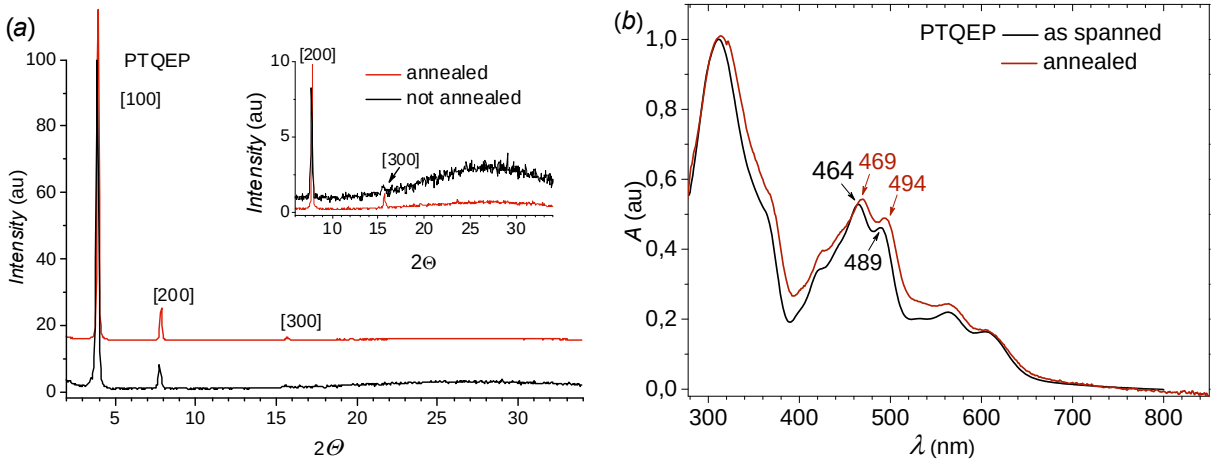


**Figure 29.** ***PTQEP***: X-ray scattering in reflection of film deposited on a glass substrate, before and after annealing at 100$^0$C (the representation contains an offset of X scale of 3 2Θ degrees) (a). Absorption of the thin film before and after annealing (*b*).

As the industrially most feasible deposition technique is via solvent processing, the microstructure (X-ray diffraction analysis) and morphology (AFM) of the films deposited *via* solvent processing were investigated. Consequently, films were prepared by spin-coating onto a glass substrate from a 15 mg mL$^{-1}$ toluene solution and subjected to UV-Vis, X-ray diffraction, AFM and SEM studies. Additionally, the effects of thermal treatment on the surface morphology and microstructure were investigated as well. The XRD pattern of the as spanned **PTQEP** thin film exhibits two reflections (Figure 29*a*). The first order, very strong peak at 2*Θ* = 3.9° corresponds to a higher order reflection, suggesting a lamellar arrangement in the solid-state.[32] The AFM (Figure 30*a*) and SEM (Figure 30*d*) analysis supported this view. Step heights ranging between 3.7 and 4 nm could be measured. The absorption profile of the film after being thermally treated at 100$^0$C for 30 min (Figure 29*b*), revealed a somewhat improved organization as suggested by the small shifts of the local absorption maxima (Figure 29*b*). Similarly, a third order peak could be identified in the corresponding X-ray pattern corroborating an annealing induced enhancement of the long range order. Notably, there were no peaks suggesting π-π stacking. Furthermore, the AFM images of the thermally

processed material (Figure 30*b*) showed the presence of well defined lamellae. The derived step heights were reduced to 1.6-1.7 nm (Figure 30*c*).

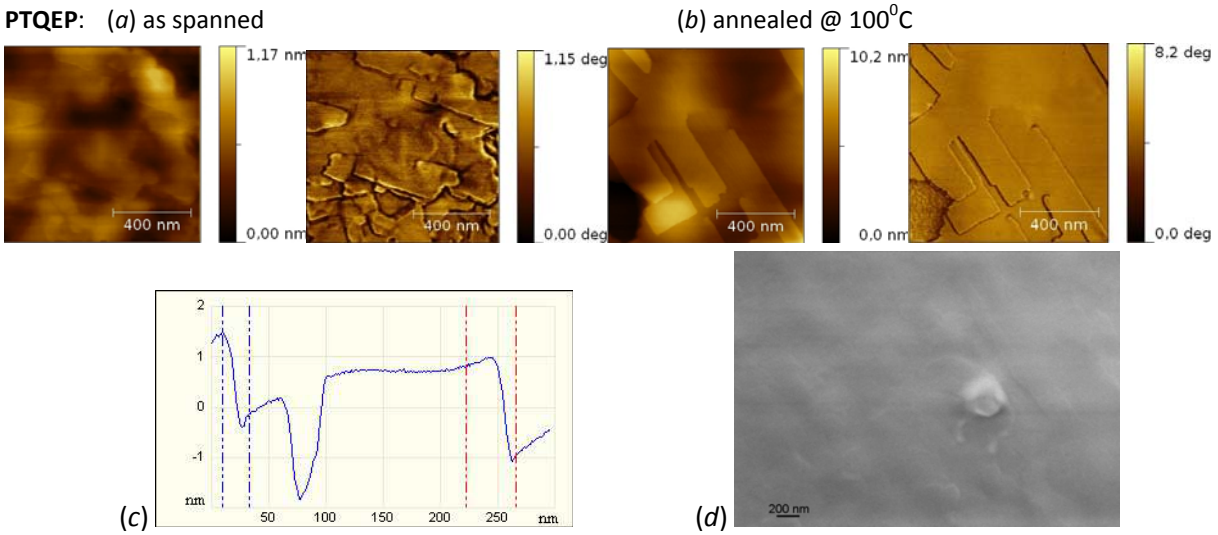


**Figure 30.** ***PTQEP***: AFM topography and phase contrast images of the as spanned (*a*) and the annealed (at 100$^0$C for 30 min) (*b*) thin film deposited from a 15 mg mL$^{-1}$ toluene solution. (*c*) Section analysis of the annealed thin film. (*d*) SEM image of the as spanned film.

It has to be mentioned here that none of the discussed model compounds presented obvious thermal transitions between 20$^0$C and 300$^0$C based on the differential scanning calorimetry (DSC) studies. Additionally, all three compounds are stable up to 400$^0$C according to the thermogravimetric analysis (TGA) performed in nitrogen atmosphere.

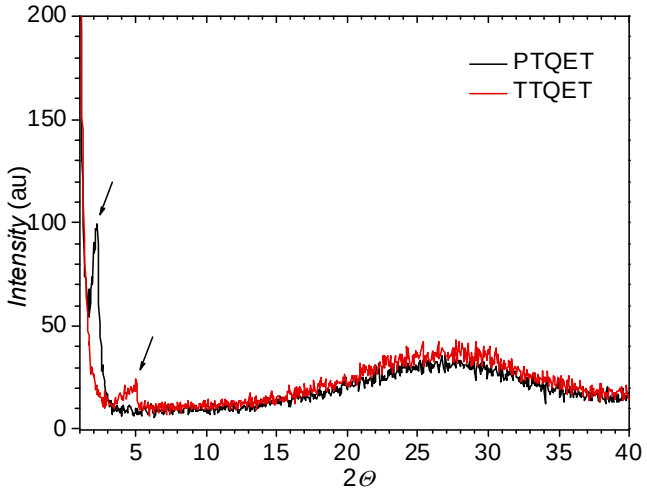


**Figure 31.** X-ray scattering in reflection of **PTQET** and **TTQET** films spin-coated on a glass substrate from a 15 mg mL$^{-1}$ toluene solution.

**PTQET**, having thiophene units connected *via* ethynyl π-spacer to the TQ segment, presented a different morphology when processed under identical condition. The XRD pattern of its thin film (Figure 31) showed only one first order reflection ($2\Theta$ = 2.0°), but there were no higher order peaks present. In the AFM images can be clearly seen that by introducing thiophene units instead of phenyl ones, the morphology was changed from lamellar to fibrillar (Figure 32*a*). The randomly oriented approx. 500 nm long fibers became more dens upon annealing (Figure 32*b*).

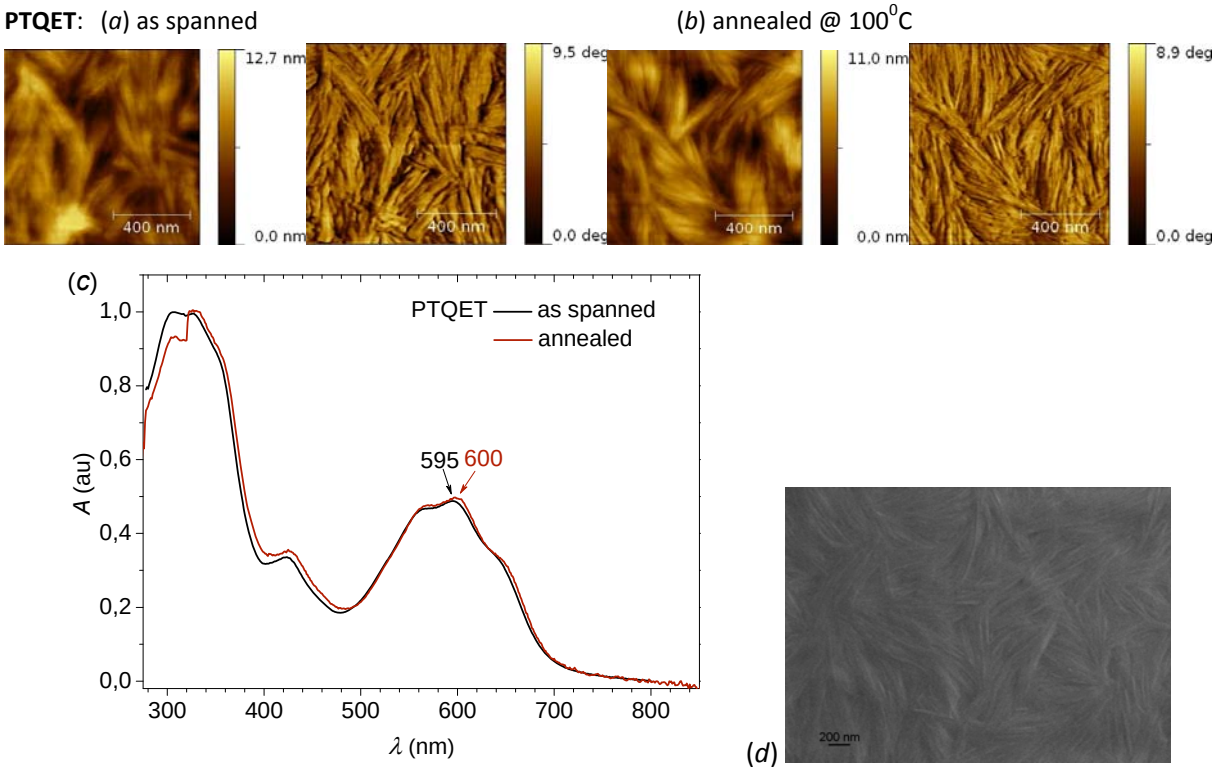


**Figure 32.** ***PTQET***: AFM topography and phase contrast images of the as spanned (*a*) and the annealed (at 100$^0$C for 30 min) (*b*) thin film deposited from a 15 mg mL$^{-1}$ toluene solution. Absorption of the thin film before and after annealing (*c*).SEM image of the as spanned film (*d*).

Exchanging the phenyl substituents directly connected to the TQ core to thiophene ones (**TTQET**) proved to have a great impact on the microstructure and morphology. As revealed by the AFM (Figure 33*a*-*b*) and SEM (Figure 33*d*) images, the compound showed bad film forming properties. Islands built up around long fibrils could be identified with the fibrils in some places reaching several tens of micrometers. However, it is not excluded that through a

different deposition technique, such as drop-casting or dip-coating the film quality could be improved.

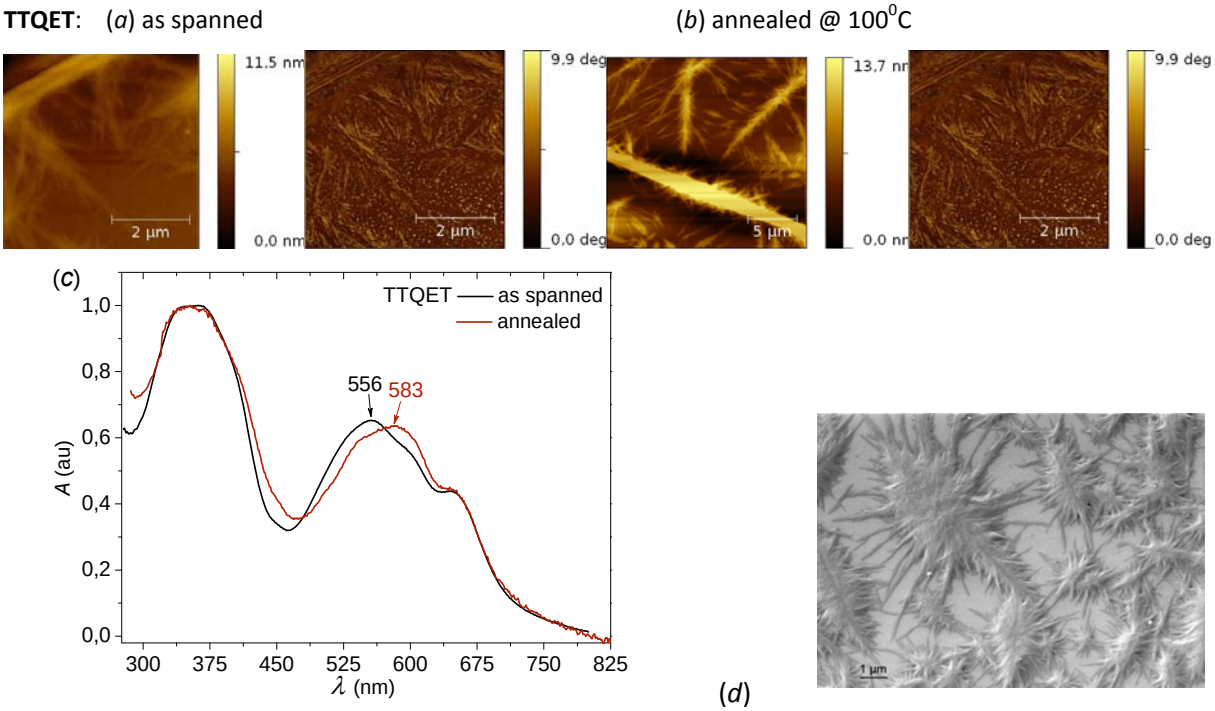


**Figure 33.** ***TTQET***: AFM topography and phase contrast images of the as spanned (*a*) and the annealed (at 100$^0$C for 30 min) (*b*) thin film deposited from a 15 mg mL$^{-1}$ toluene solution. Absorption of the thin film before and after annealing (*c*).TEM image of the as spanned film (*d*).

## 2.3.6. Conclusion

In the pursuit of developing new semiconductor polymers, two series of novel TQ based model compounds containing different π-spacers, were prepared. While the ethynylene π-spacers were introduced *via* a *Sonogashira-Hagihara* cross-coupling reaction (**PTQEP**, **PTQET** and **TTQET**), the ethylene π-spacer containing model compounds were obtained through *in situ* hydrogenation of the triple bond (**PTQVP**, **PTQV2P**, **PTQVT** and **PTQV2T**). This could be achieved by employing excess of terminal acetylene in the *Sonogashira-Hagihara* coupling reaction. The reaction could be easily controlled through the amount of terminal alkyne used. Although, in the former case the reaction yields were rather low, the importance of this procedure is amplified by the inefficiency of other cross-coupling procedures, such as *Heck* coupling available for the synthesis of these materials.

Through the presented functionalization of the TQ core, valuable insight into the photophysical and electrochemical repercussions of the nature of the donor connected to the TQ core, as well as the role played by different π-spacers connecting them, were obtained.

It has been demonstrated that by connecting donor units *via* ethynylene π-spacers to a functionalized TQ core, the π-conjugation can be extended through the efficient D-A interaction materializing in a lower HOMO – LUMO energy-gap (**PTQEP**, **PTQET** and **TTQET**). As a consequence, the obtained materials were emitting in the red region with fluorescence quantum efficiency as high as 79 % (**PTQEP**). Notably, the efficient charge transfer between the TQ acceptor segment and the thiophene donor units, through the ethynylene π-spacers (**TTQET**) was proven by solvent dependent absorption measurements. As a result of the electron deficient nature of the ethynylene π-spacer, the engineering of the energy-gap is accomplished, while preserving the high electron affinity of the resulting compounds. The structural modification has a major impact only on the HOMO energy level, while the LUMO is kept at a low value, making these materials promising candidates for n-type semiconductors.

Owing to the performed systematic study, additional valuable knowledge was gained regarding the influence of the nature of the π-spacer incorporated in a D-A system (**PTQET**, **PTQVT** and **PTQV2T**). Due to the lack of steric hindrance between the vinylic protons and the neighboring aromatic units the double bonds seems to promote π-conjugation more efficiently when compared with triple bond spacers. This is not surprising when one considers the length of the vinylic bond and the $sp^2$ character of the carbon atoms involved which is more similar to the bonds of an aromatic π-system. The "small" structural modification led to materials absorbing up to 825 nm in the solid-state. The cyclic voltammetry studies, supported by theoretical calculation, undoubtedly showed that the lower energy-gap in these molecules is achieved by increasing the $E_{LUMO}$.

In the view of these results, the attention was turned towards the synthesis of alternating TQ-D copolymers connected *via* ethynylene π-spacers, due to the more favorable LUMO energy levels for an electron transport, presented by the studied model compounds.

## 2.3.6. References

*1.* (a) Martin, R. E.; Diederich, F. *Angew. Chem. Int. Ed.* **1999**, *38*, 1350. (b) van Hutten, P. F.; Krasnikov, V. V.; Hadziioannou, G. *Acc. Chem. Res.* **1999**, *32*, 257.

*2.* (a) Gierschner, J.; Cornil, J.; Egelhaaf, H. J. *Adv. Mater.* **2007**, *19*, 173. (b) de Mello, J. S.; Silva, L. M.; Becker, R. S. *J. Chem. Phys.* **1999**, *111*, 5427. (c) Otto, P.; Gu, F. L.; Ladik, J. *J. Chem. Phys.* **1999**, *110*, 2717.

*3.* For representative references, see: (a) K. Sonogashira, in *Handbook of Organopalladium Chemistry for Organic Synthesis*, ed. E.-I. Negishi, John Wiley, **2002**, *p.* 493; (b) K. Sonogashira, in *"Metal-catalyzed Cross-coupling Reactions"*, Ed. F. Diederich and P. J. Stang, Wiley-VCH, **1998**, *p.* 203; (c) D. Chinchilla, R.; Najera, C. *Chem. Rev.* **2007**, *107*, 874. For a monograph on various palladium-catalyzed cross-coupling reactions see: J. Tsuji, *"Palladium Reagents and Catalysts"*, Wiley, Chichester, UK, 2nd Ed, **2004**.

*4.* (a) Jackman, L. M. *"Applications of Nuclear Magnetic Resonance Spectroscopy to Organic Chemistry"*, Perganon Press. London, **1959**, *p.* 57. (b) Roberts, J. D. *"Nuclear Magnetic Resonance"*, McGraw-Hill Book Co., New York, **1959**, *p.* 54.

*5.* Silverstein, R. M.; Bassler, G. C.; Morrill, T. C. *"Spectrometric Identification of Organic Compounds*" 4th Ed. New York: John Wiley and Sons, **1981**.

*6.* Hierso, J. C.; Picquet, M.; Cattey, H.; Meunier, P. *Synlett* **2006**, *18*, 3005.

*7.* Raebiger, J. W.; Miedaner, A.; Curtis, C. J.; Miller, S. M.; Anderson, O. P.; DuBois, D. L. *J. Am. Chem. Soc.* **2004**, *126*, 5502.

*8.* Chinchilla, R.; Nájera, C. *Chem. Rev.* **2007,** *107*, 874.

*9.* Bertus, P.; Fécourt, F.; Bauder, C.; Pale, P. *New J. Chem.* **2004**, *28*, 12.

*10.* Littke, A. F.; Fu, G. C. *J. Am. Chem. Soc.* **2001**, *123*, 6989.

*11.* de Vries, A. H. M.; Mulders, J. M. C. A.; Mommers, J. H. M.; Henderickx, H. J. W.; de Vries, J. G. *Org. Lett.* 2**003**, *5*, 3285.

*12.* (a) Wadsworth, W. *Org. React*. **1977**, *25*, 73. (b) Horner, L.; Hoffmann, H. M. R.; Wippel, H. G. *Ber.* **1958**, *91*, 61. (c) Horner, L.; Hoffmann, H. M. R.; Wippel, H. G.; Klahre, G. *Ber.* **1959**, *92*, 2499.

*13.* Kürti, L.; Czakó, B. *"Strategic applications of named reactions in organic synthesis"* Elsevier Academic Press, **2005**, *p.* 242.

*14*. Kitamura, C.; Tanaka, S.; Yamashita, Y. *Chem. Mater.* **1996**, *8*, 570.

*15.* Davies, J. A.; Elangovan, A.; Sullivan, P. A.; Olbricht, B. C.; Bale, D. H.; Ewy, T. R.; Isborn, C. M.; Eichinger, B. E.; Robinson, B. H.; Reid, P. J.; Li, X.; Dalton, L. R. *J. Am. Chem. Soc.*, **2008**, *130*, 10565.

*16*. Bohren C. F. *"Fundamentals of Atmospheric Radiation: An Introduction with 400 Problems"* Wiley-VCH. **2006**, *p*. 214.

*17.* (a) Williams, A. T. R.; Winefield, S. A.; Miller, J. N. *Analyst* **1983**, *108*, 1067. (b) Birks, J. B. *"Photophysics of Aromatic Molecules"* Wiley, New York, **1970**.

*18.* Isak, S. J.; Eyring**.** E. M. *J. Photochem. Photobiol. A: Chem.* **1992**, *64*, 343.

*19.* Valeur, B. *"Molecular Fluorescence: Principles and Applications"* Wiley-VCH, **2001.**

*20.* de Melo, J. S.; Burrows, H. D.; Svensson, M.; Andersson, M. R.; Monkman, A. P. *J. Chem. Phys.* **2003**, *118*, 1550.

*21.* Bao, D.; Millare, B.; Xia, W.; Steyer, B. G.; Gerasimenko, A. A.; Ferreira, A.; Contreras, A.; Vullev, V. I. *J. Phys. Chem. A* **2009**, *113,* 1259.

*22.* Silvestri, F.; Marrochi, A. *Int. J. Mol. Sci.* **2010**, *11*, 1471.

*23*. (a) Silvestri, F.; Assunta Marrocchi, A.; Seri, M.; Kim, C.; Marks, T. J.; Facchetti, A.; Taticchi, A. *J. Am. Chem. Soc.* **2010***, 132,* 6108. (b) Bredas, J. L.; Chance, R. R.; Baughman, R. H.; Silbey, R. *J. Chem. Phys.* **1982**, *76*, 3673.

*24.* Young, J. K.; Moore, J. S. *„Modern Acetylene Chemistry*" Stang, P. J., Diederich, F., Eds.; VCH: Weinheim, Germany, **1995**; *p.* 415.

*25*. Moran, D.; Simmonett, A. C.; Leach, F. E.; Allen, W. D.; Schleyer, P. v. R.; Schaefer, H. F. *J. Am. Chem. Soc.* **2006,** *128*, 9342.

*26*. (a) Isak, S. J.; Eyring, E., M. *J. Phys. Chem.* **1992**, *96*, 1738. (b) Williams, A.; Winfield, S. A.; Miller, J. N. *Analyst* **1983**, *108*, 1067.

*27.* (a) Hutchison, G. R.; Ratner, M. A.; Marks, T. J. *J. Am. Chem. Soc.* **2005**, *127*, 16866. (b) Lang, N. D.; Kohn, W. *Physical Review B.* **1971**, *3*, 1215.

*28.* Bruice, P. Y. *"Organic Chemistry"* Pearson/Prentice Hall; *International 4$^{th}$ Ed.* **2005**.

*29*. (a) Huang, C.; West, J. E.; Katz, H. E. *Adv. Funct. Mater.* **2007**, *17*, 142. (b) Takimiya, K.; Kunugi, Y.; Toyoshima, Y.; Otsubo, T. *J. Am. Chem. Soc.* **2005**, *127*, 3605. (c) Kastler, M.; Pisula, W.; Wasserfallen, D.; Pakula, T.; Müllen, K. *J. Am. Chem. Soc.* **2005**, *127*, 4286. (d) Pal, B. N.; Trottman, P.; Sun, J.; Katz, H. E. *Adv. Funct. Mater.* **2008**, *18*, 1832.

*30*. Pisula, W.; Menon, A.; Stepputat, M.; Lieberwirth, I.; Kolb, U.; Tracz, A.; Sirringhaus, H.; Pakula, T.; Müllen, K. *Adv. Mater.* **2005**, *17*, 684.

*31.* (a) Anthony, J. E. *Chem. Rev.* **2006**, *106*, 5028; (b) Anthony, J. E. *Angew. Chem.* **2008**, *120*, 460; (c) Anthony, J. E. *Angew. Chem. Int. Ed.* **2008**, *47*, 452.

*32.* Lanquindanum, J. G.; Katz, H. E.; Lovinger, A. J. *J. Am. Chem. Soc.* **1998**, *120*, 664.

# 2.4. Acetylene-based Thiadiazolo[3,4-*g*]quinoxaline Copolymers in Organic Electronics

## 2.4.1. Thiadiazolo[3,4-*g*]quinoxalines: Ethynylene-Phenylene Copolymers

### 2.4.1.1. Polymer Synthesis

The synthesis of π-conjugated polymers of a D-A architecture connected *via* ethynylene π-spacers was achieved by palladium catalyzed *Sonogashira-Hagihara*[1] step-growth polymerization reaction conditions. Alkyl chains were grafted on the phenylene co-monomer, in order to ensure the maximum solubility of the resulting polymer and to promote lamellar packing.[2] If the phenylene unit is functionalized with only one alkyl substituent the synthetic procedure would yield a regioirregular polymer. Therefore, two dodecyl solubilising side chains were introduced to this core in order to overcome irregularity and solubility issues.

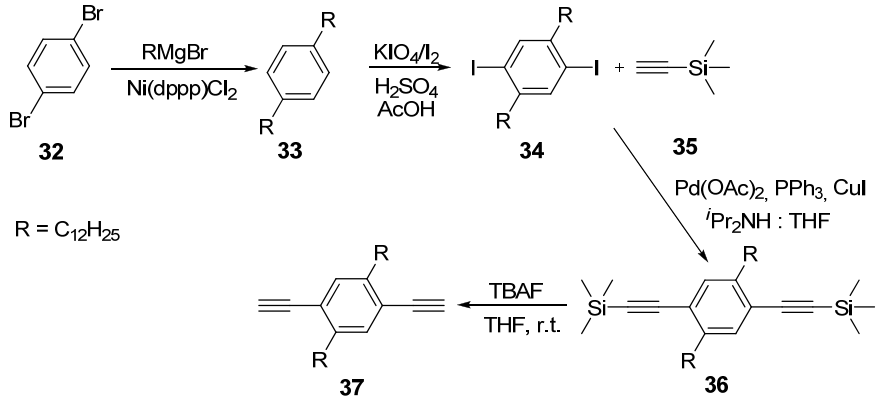


**Scheme 18.** Synthesis of alkyl substituted *p*-phenylene monomer **37**.

The *p*-diethynyl-phenylene derivative **37** was obtained following the slightly modified reaction procedure reported by Francke *et al.*,[3] as depicted in Scheme 18. The alkyl substituents were introduced on the phenyl ring (**33**) under *Kumada coupling*[4] conditions. 1,4-Diethynyl-2,5-dialkylbenzene (**37**) was prepared by the halogenation[5] of **33** leading to 1,4-diiodo-2,5-dialkylbenzene (**34**). Treatment of **34** with 2.1 equiv. of (trimethylsilyl)acetylene, under $Pd(OAc)_2/PPh_3$/CuI catalysis,[6] gave the protected ethynylene functionalized phenylene derivative **36** in only 30 minutes. Note that the isolation of this compound is not mandatory. After removing the catalyst via filtration through Celite 545 followed by removal of the solvent under high vacuum, the reaction mixture was redissolved in THF. The trimethylsilyl protecting groups were effectively detached using tetra-*n*-butylammonium fluoride (TBAF).[7] Purification by column chromatography, followed by recrystallization from hexane led to the desired co-monomer **37**.

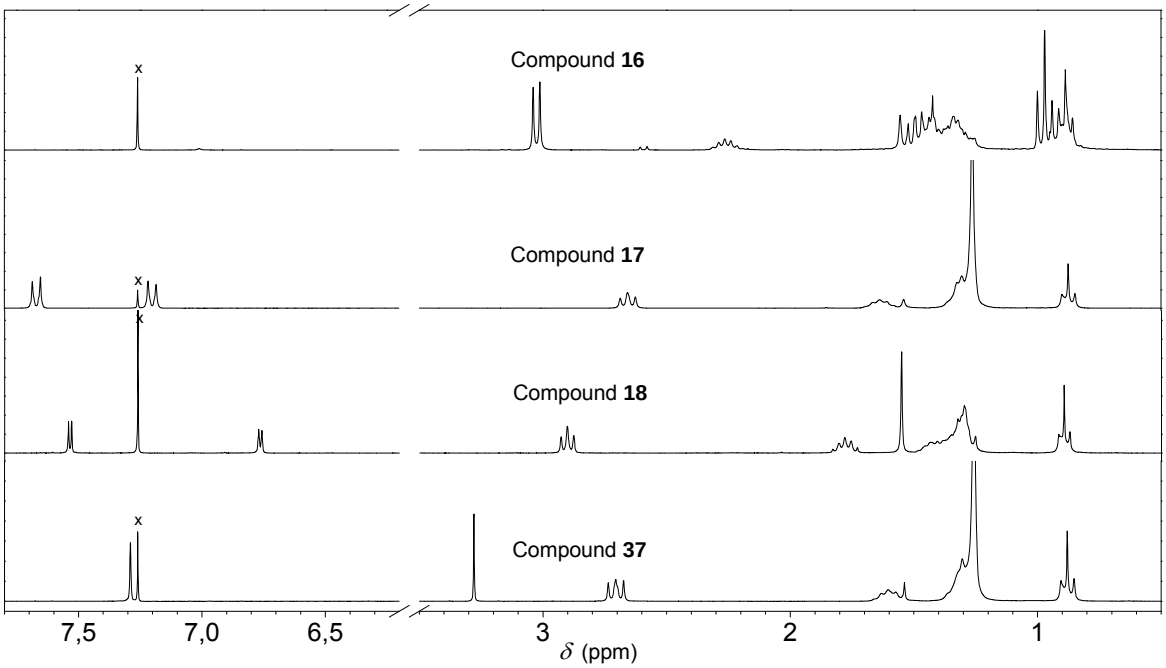


**Figure 34.** $^1$H-NMR of compounds **16** (**RTQ**), **17** (**PTQ**), **18** (**TTQ**) and **37** in $CDCl_3$ (marked with "x") at r.t., not necessarily recorded at the same spectrum amplitude (@ 250 MHz). For a better visualization the region between 3.5 and 6.2 ppm is not shown.

Similarly to other metal mediated cross-coupling polymerization methodologies, such as *Suzuki* or *Stille*, the *Sonogashira-Hagihara* polymerization proceeds by a step-growth mechanism. This translates into the sensitivity of the molecular weight and polydispersity

index (*PDI*) of the polymer to the purity and stoichiometry of the monomers.[8] Therefore, the required high purity of the co-monomers was confirmed by high resolution mass spectrometry (HRMS) and NMR spectroscopy. Figure 34 illustrates the $^1$H-NMR of the monomers. The characteristic signals corresponding to the alkyl side chains grafted on each of the monomers could be clearly identified between 0.75 and 3.10 ppm. Furthermore, the $^1$H-NMR of compound **37** contained a singlet at 3.27 ppm corresponding to the two terminal acetylenic protons. Except compound **16** (**RTQ**), having no aromatic protons, all the other monomers (**PTQ** and **TTQ**) showed the corresponding characteristic aromatic proton signals between 6.7 and 7.8 ppm.

The $Pd(PPh_3)_4$ / CuI / $^iPr_2NH$ as catalyst / co-catalyst / base system was preferred for the *Sonogashira-Hagihara* polycondensation reaction (Scheme 19) due to its high efficiency displayed during the model compound synthesis (see Section 2.2.1.). Furthermore, to avoid cross-linking that might occur when the reaction is conducted at temperatures higher than $70^0$C,[9, 10] THF was chosen as co-solvent due to its low boiling point. The vast majority of poly(arylethynyle)s necessitate extended reaction times (24-48 h)[9] in order to ensure the consumption of the monomers and to obtain polymers of high molecular weight. To significantly reduce the reaction time the polymerization reactions were carried out under microwave (*MW*) irradiation. The polymerization procedure was screened on the reaction between **PTQ** (**17**) and **37** (Scheme 19). It was found that high molecular weight $\mathbf{P_2}$ (**PPTQP**) could be achieved in only 1 h 20 min at $50^0$C under *MW* irradiation. Upon prolonged reaction times the polymer started to precipitate from the reaction mixture. To evaluate the reproducibility all the following polymerization reactions were performed under identical conditions.

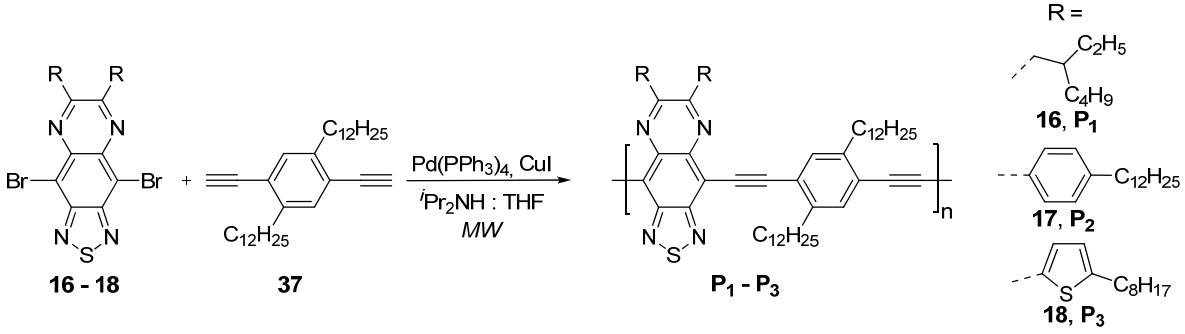


**Scheme 19.** Synthesis of acetylene-based thiadiazolo[3,4-*g*]quinoxaline-phenylene polymers $\mathbf{P_1}$, $\mathbf{P_2}$ and $\mathbf{P_3}$.

While the polymerization of **TTQ** (**18**) and **37** resulting in polymer $\mathbf{P_3}$ (**PTTQP**) (Chart 10), proceeded very similar to the above mentioned case, the synthesis of polymer $\mathbf{P_1}$ (**PRTQP**) revealed some peculiarities. The 80 min of polymerization time yielded a dark green solid which precipitated from the reaction mixture. The precipitate formed could not be redissolved in common organic solvent such as toluene, DCM or chlorinated benzene derivatives. This irreversible aggregation was somewhat unexpected considering the presence of branched alkyl chains at the TQ segment, which should assist the solubility of the material. Such behavior of poly(arylethynylene)s is not well documented in the literature, probably due to the fact that most of the studies was conducted on poly(phenylene-ethynylene)s, polymers that do not contain extended planar π-systems. Nonetheless, the Bunz group experienced irreversible aggregation of high molecular weight poly(*p*-phenylene-ethynylene)s bearing various styryl-like side groups.[11] Additionally, the same group encountered similar solubility issues during the synthesis of poly(fluorenylene-ethynylene)s.[12]

**Chart 10.** Chemical structure of the synthesized thiadiazolo[3,4-g]quinoxaline *alt* *p*-phenyleneethynylene polymers $\mathbf{P_1}$, $\mathbf{P_2}$ and $\mathbf{P_3}$.

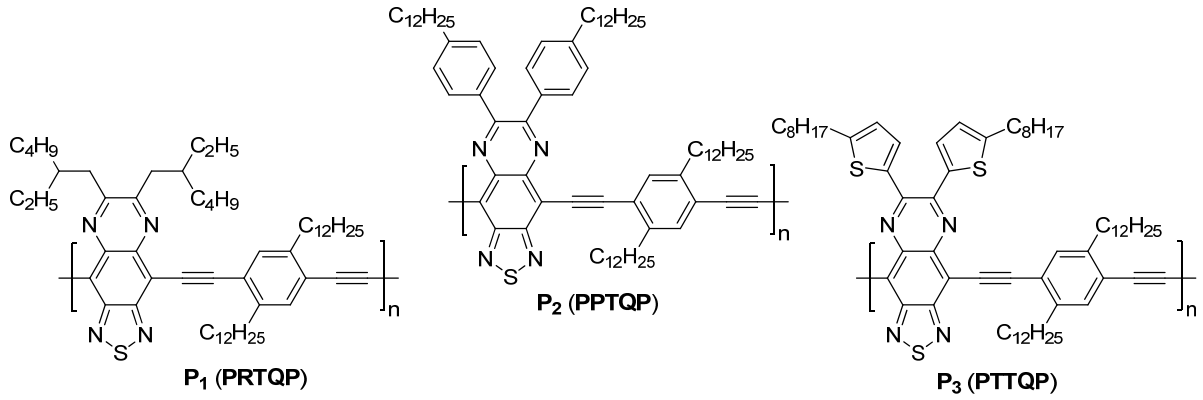


$\mathbf{P_2}$ and $\mathbf{P_3}$ (Chart 10) were subjected to repeated precipitations in methanol and acetone. The removal of the low molecular weight fractions from the polymeric mixture, for both $\mathbf{P_2}$ and $\mathbf{P_3}$, was achieved through fractionation *via* Soxhlet extraction with methanol, acetone and chloroform. The chloroform soluble fraction was then further characterized. The isolated polymers $\mathbf{P_2}$ and $\mathbf{P_3}$ were soluble in a variety of common organic solvents such as THF, chloroform, toluene or chlorinated benzene derivatives. Both $\mathbf{P_2}$ and $\mathbf{P_3}$ were characterized by

NMR and IR spectroscopy, gel permeation chromatography (GPC) and were studied by thermal analysis (DSC and TGA).

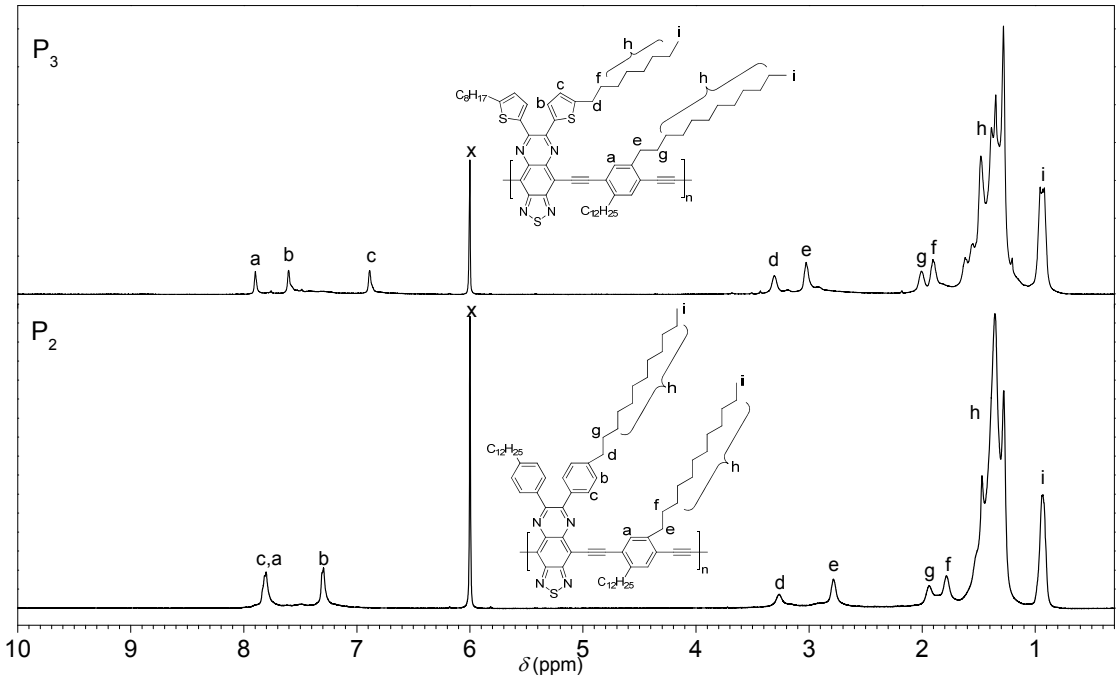


**Figure 34.** $^{1}$H-NMR of **$P_2$** and **$P_3$** in $C_2D_2Cl_4$ (marked with "x") at 100$^{0}$C (@ 500 MHz), not necessarily recorded at the same spectrum amplitude.

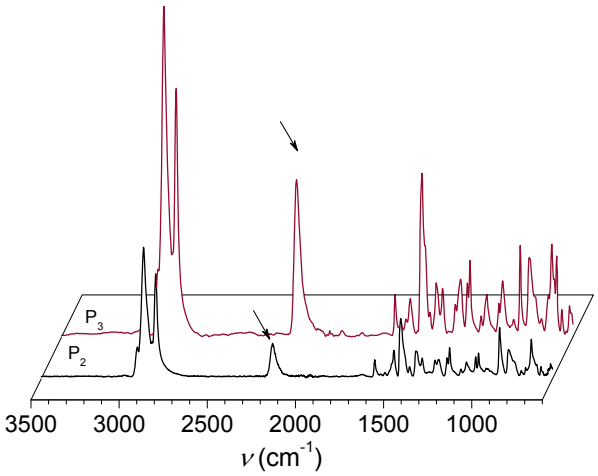


**Figure 35.** IR spectra of polymers **$P_2$** and **$P_3$**. The arrows are indicating the characteristic infrared band for the internal *C*≡*C* bond stretch (≈ 2135 cm$^{-1}$).

Figure 34 illustrates the $^{1}$H-NMR of **$P_2$** and **$P_3$** registered at elevated temperature in deuterated tetrachlorethane ($C_2D_2Cl_4$). The presence of alkyl side-chains grafting the polymer

backbone could be clearly identified for both **$P_2$** and **$P_3$** in the characteristic region from 0.8 to 3.5 ppm. Furthermore, the aromatic protons **a**, **b** and **c**, as defined in the inlet of Figure 34 for **$P_2$**, appeared as two broad singlets between 7 and 8 ppm in a 2 : 3 ratio (**c**, **a** : **b**) in agreement with the proposed polymer structure. Similarly, for polymer **$P_3$** three singlets could be identified between 6.5 and 8 ppm as in a 1 : 1 : 1 ratio (**c** : **b** : **a**). No diacetylene defects could be detected in the $^{13}$C-NMR spectra, which otherwise should appear between 80 ppm and 100 ppm.

Confirmation of the successful insertion of the ethynylene π-spacers in the polymer backbone was given by FT-IR spectroscopy (Figure 35). The characteristic signal corresponding to the internal *–C≡C–* stretch[13] could be identified at approx. 2130 cm$^{-1}$ for both polymers. Moreover, there was no strong narrow band present between 3260 and 3330 cm$^{-1}$ suggesting the absence of acetylene end groups, since this region is characteristic for *–C≡C–H* stretching.

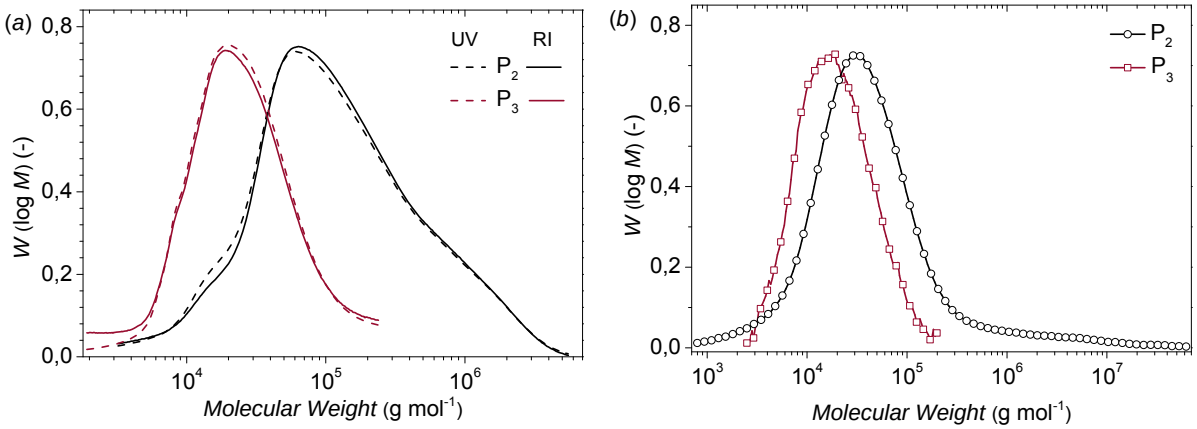


**Figure 36.** Molecular weight distribution of **$P_2$** and **$P_3$** as measured by GPC in THF at 30$^0$C (*a*) and in TCB at 135$^0$C (*b*).

The molecular weights of the polymers **$P_2$** and **$P_3$** were determined by gel permeation chromatography (GPC). As shown in Figure 36*a* and 36*b*, the molecular weight obtained by GPC measurements of the two polymers is at least temperature dependent. Both **$P_2$** and **$P_3$** presented broad molecular weight distributions in THF, at 30$^0$C (Figure 36*a*). The corresponding number average molecular weights ($M_n$), the weight average molecular weights ($M_w$), and the polydispersity indexes (*PDI*), *vs.* polystyrene (*PS*) or poly(*p*-phenylene) (*PPP*) as standards, are listed in Table 6.

**Table 6.** Summary of molecular weights as determined by GPC measurements for $\mathbf{P_2}$ and $\mathbf{P_3}$.

| Compd. | THF, 30$^0$C *vs. PPP* | | | THF, 30$^0$C *vs. PS* | | | TCB, 135$^0$C *vs. PS* | | | |
|---|---|---|---|---|---|---|---|---|---|---|
| | $M_n$ x $10^3$ (g mol$^{-1}$) | $M_w$ x $10^3$ (g mol$^{-1}$) | *PDI* | $M_n$ x $10^3$ (g mol$^{-1}$) | $M_w$ x $10^3$ (g mol$^{-1}$) | *PDI* | $M_n$ x $10^3$ (g mol$^{-1}$) | $M_w$ x $10^3$ (g mol$^{-1}$) | *PDI* | *PD* |
| $\mathbf{P_2}$ | 33.8 | 127.3 | 3.77 | 53.4 | 298.2 | 5.60 | *17.4* | 53.6 | 3.08 | 15-45 |
| $\mathbf{P_3}$ | 10.1 | 21.4 | 2.11 | 17.5 | 36.7 | 2.09 | *13.8* | 26.9 | 1.95 | 14-25 |

It is apparent that the data of the molecular weights were also dependent on the GPC standard employed (*PS* or *PPP*), with higher values obtained using *PS* as standard. Similar discrepancies between the molecular weight as determined using the two standards were observed during the early investigations of the structurally similar poly(*p*-phenylene-ethynylene)s (PPEs).[9] It was found that the molecular weight of these rigid rod-type polymers obtained using *PS*, a flexible coiled polymer as standard, results in overestimation by a factor of 2-3.[14] GPC with a *PPP* standard reduced this overestimation to 1.2-1.5.[15] Nonetheless, it has to be noted that while low molecular weight PPEs are indeed rigid rods, above a polymerization degree (*PD*) of approx. 20, PPEs behave as worm-like chains and should not be considered as rigid rods anymore.[16] The broad shape of the molecular weight distribution curves, as measured at 30$^0$C in THF, led to rather high *PDI* values (see $\mathbf{P_2}$) suggesting the presence of aggregates. To verify this assumption, the GPC measurements were repeated at elevated temperature (135$^0$C) in trichlorbenzene (TCB) and the molecular weights derived relative to *PS* (Table 6). The resulting molecular weight distribution curves (Figure 36*b*) were much sharper when compared to those recorded at 30$^0$C in THF. Nonetheless, even at 135$^0$C in TCB ($\mathbf{P_2}$), a tail in the molecular weight distribution curve could be observed indicating the presence of residual aggregates. When comparing the molecular weight of both $\mathbf{P_2}$ and $\mathbf{P_3}$ with other D-A type heterocyclic poly(arylene-ethynylene)s (PAEs) obtained *via Sonogashira-Hagihara* polymerization reported in the literature, the here presented procedure yielded polymers with the highest molecular weights reported up to date.[17]

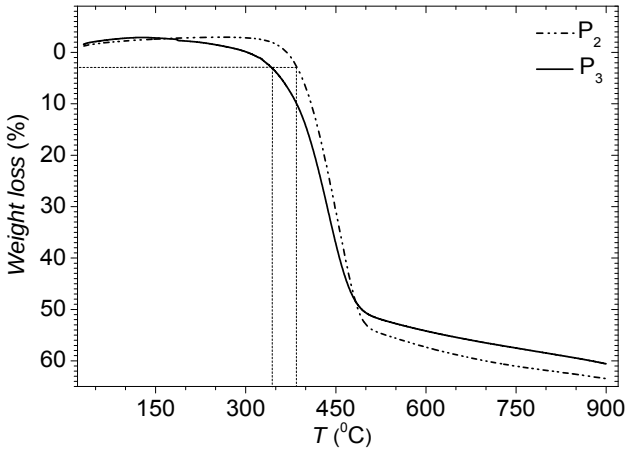


**Figure 37.** Thermogravimetric analysis of **$P_2$** and **$P_3$** at a heating rate of 10 K $min^{-1}$, under a $N_2$ atmosphere.

The thermal stability of both **$P_2$** and **$P_3$** was investigated by thermogravimetric analysis (TGA) under an inert atmosphere. The temperature of 5 % weight loss based on the initial weight ($T_{d5}$) occurred for both polymers over $340^0$C (Figure 37). Additionally, neither **$P_2$** nor **$P_3$** showed any obvious thermal transition between 20 and $300^0$C according to the DSC analysis.

## 2.4.1.2. Optical and Electrochemical Characterization of $P_2$ and $P_3$

Owing to the good solubility of both **$P_2$** and **$P_3$** their photophysical investigation was feasible. Their UV-Vis absorption was examined in dilute chloroform, THF and toluene solutions (Figure 38). **$P_2$** showed two main absorption bands extended up to approx. 815 nm in dilute chloroform solution (Figure 38*a*). The origin of this extended absorption is evident if one compares the absorptions of **$P_2$** with its corresponding model compound **PTQEP** (Section 2.3.1). As **PTQEP** absorbed only up to 625 nm, the successful extension of the conjugation and the efficient D-A interaction through the ethynylene π-spacer along the polymer backbone translates in the widened absorption of **$P_2$**. At a closer look, this long wavelength absorption band of **$P_2$** in dilute chloroform was composed of two local maxima, one at 686 nm and a second one at 736 nm. In all the other examined solvents (toluene and

THF) the local absorption maximum at 686 nm was reduced to a shoulder. Such behavior could be explained through the presence of aggregates. This is not very surprising, given the temperature dependence of the GPC measurements that strongly suggested the presence of aggregates in dilute solution at $30^0$C. Therefore, the calculation of $E_{op}$ in solution would be inappropriate. Going from solution to thin film, the long wavelength absorption band became sharper and the $\lambda_{max}$ was bathochromically shifted to 757 nm. The red-shift of the absorption of the solid state absorption spectrum relative to the one in dilute solution of a conjugated polymer, such as poly(thiophene)s or poly(diacetylene)s, is well understood.[18] The enhanced π-π interactions in the solid state gave rise to the characteristic red-shift of the $\lambda_{max}$.[19] The $E_{op}$, as calculated from the onset of the long wavelength absorption maximum ($\lambda_{onset}$ = 814 nm), was 1.52 eV. Note that identical $E_{op}$ can be found when calculated form the spectra recorded in toluene or THF solution, solvents in which the aggregation is more prominent (Table 7).

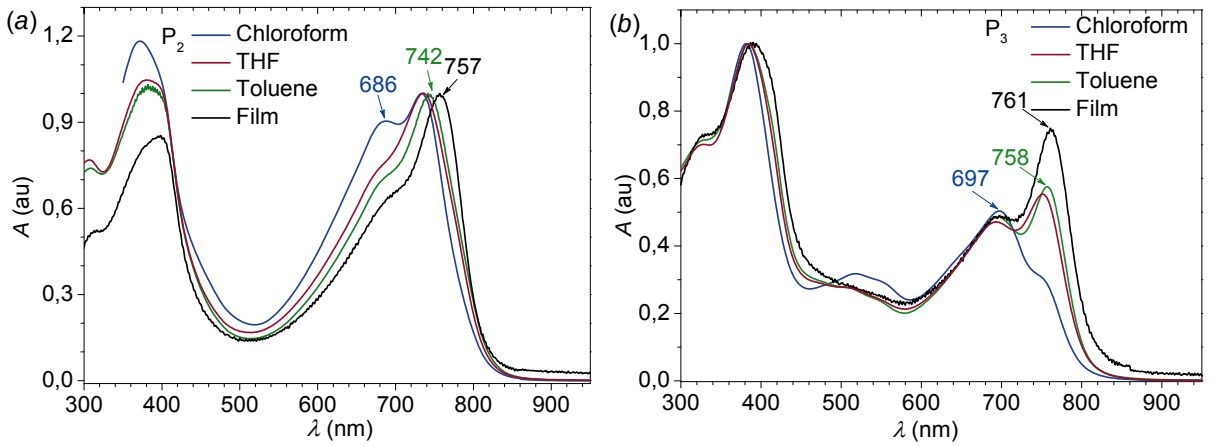


**Figure 38.** UV-Vis absorption profile of **$P_2$** (*a*) and **$P_3$** (*b*) in dilute solution ($c = 10^{-6}$ mol $L^{-1}$) and thin film, prepared by spin-coating on a glass substrate from a 5 mg $mL^{-1}$ toluene solution.

**$P_3$** presented a similar absorption profile (Figure 38*b*). The successful extension of the π-conjugation *via* ethynylene π-spacers translated in absorption up to 800 nm with $\lambda_{max}$ = 697 nm in dilute chloroform solution. The solvent dependent absorption profile of **$P_3$** revealed some similarities to that of **$P_2$**. While in chloroform the long wavelength absorption showed only a small shoulder around 745 nm, in THF or toluene the intensities of the local maxima were reversed and $\lambda_{max} \approx 750$ nm became the predominant local maximum. Consequently, this strongly suggests the presence of aggregates, similarly to **$P_2$**. In the solid

state $\lambda_{max}$ = 761 nm was over 60 nm bathochromically shifted relative to one registered in chloroform solution, but only a few nanometers *vs.* toluene or THF solution. The $E_{op}$, as calculated from the solid state absorption onset is 1.52 eV, identical to **$P_2$**. Hence, the presence of octyl-thienyl substituents at the TQ segment does not hinder the π-conjugation within the polymer backbone (Table 7).

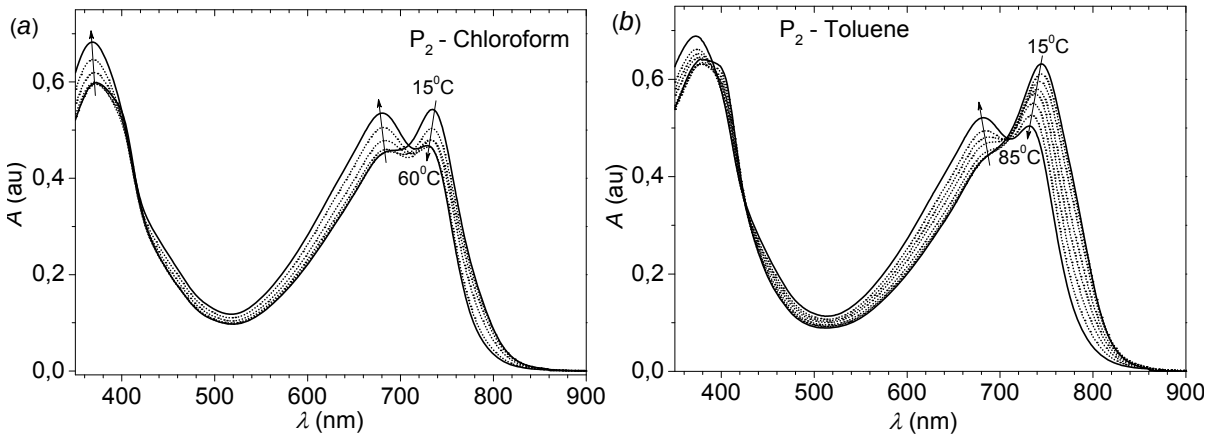


**Figure 39.** Temperature dependent UV-Vis absorption profile of **$P_2$** in chloroform (*a*) and toluene (*b*) ($c = 10^{-6}$ mol $L^{-1}$).

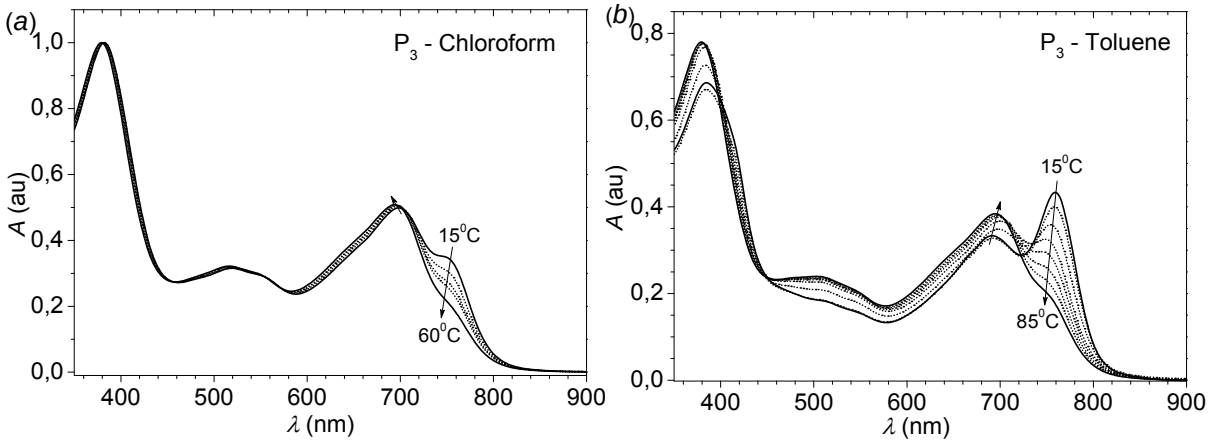


**Figure 40.** Temperature dependent UV-Vis absorption profile of **$P_3$** in chloroform (*a*) and toluene (*b*) ($c = 10^{-6}$ mol $L^{-1}$).

The existence of aggregates in dilute solution can be verified by performing temperature dependent UV-Vis measurements. Typically, these measurements were carried out in two different solvents, chloroform and toluene. The procedure involves the recording of the absorption spectrum at increasing temperatures ($10^0$C / measurement), starting from

$15^0$C up to a temperature close to the boiling point of the solvent (Figure 39*a-b* and Figure 40*a-b*). The spectral changes induced by the temperature variations are very illustrative for both polymers. While at $15^0$C the long wavelength absorption maximum of **$P_2$** was around 740 nm in both solvents, at temperatures close to the boiling point of the solvent this band was reduced to a shoulder, leaving $\lambda_{max}$ at 680 nm (Figure 39*a-b*). **$P_3$** showed a similar behavior (Figure 40*a-b*). Increasing the temperature from $15^0$C to $85^0$C in toluene the band with a $\lambda_{max}$ at 759 nm was steadily reduced in intensity and the band having $\lambda_{max}$ at 696 nm became the long wavelength absorption maximum. Note that the long wavelength shoulder in the absorption spectra remained in both cases, suggesting the presence of residual aggregates. A similar, but weaker effect was observed for other heterocyclic poly(aryl-ethynylene)s, for example in the case of thiophene (D) and benzo[*c*][2,1,3]thiadiazole (A) based polymers.[20]

**Table 7.** Summary of the optical and electrochemical properties of **$P_2$** and **$P_3$**.

| Compd. | $\lambda_{max}$ (nm)[a] | $\lambda_{max}$ (nm)film[b] | $\lambda_{em}$ (nm)[c] | $E_{op}$ (eV)[b] | $E_{LUMO}$ (eV)[d] | $E_{HOMO}$ (eV)[d] | $E_{CV}$ (eV)[e] |
|---|---|---|---|---|---|---|---|
| **$P_2$** | 680 | 757 | 711 | 1.52 | -4.05 | -5.82 | 1.77 |
| **$P_3$** | 696 | 761 | 731 | 1.52 | -4.09 | -5.76 | 1.67 |

[a]in chloroform @ $60^0$C; [b]spin-coated on a glass substrate from a 5 mg mL$^{-1}$ solution; [c]in chloroform, $25^0$C; [d]calculated $E_{LUMO} = -(E_{Red}^{onset} - E_{Fc/Fc^+}^{1/2} + 4.8)$ eV; [e]calculated from $E_{CV} = |E_{HOMO}| - |E_{LUMO}|$

The aggregates of conjugated polymers are usually classified as H- and J-type based on the angle between the transition moments and the stacking direction. H-aggregates ($< 54^0$) show a hypsochromic absorption shift with respect to the polymer's absorption, while the J-aggregates ($> 54^0$) absorb at longer wavelengths[21] as observed for **$P_2$** and **$P_3$**. In other words, the polymer chains line up in a way that the transition moment of the single chains are oriented parallel. The spectral alterations caused by π-π stacking of conjugated polymers were explained by this phenomenon.[22] Hence, it is reasonable to assume that at lower temperatures **$P_2$** and **$P_3$** have the tendency to adopt a more planar conformation that improves the π-π stacking and therefore facilitates the formation of aggregates.

The assessment of the energy levels ($E_{LUMO}$ and $E_{HOMO}$) and implicitly the energy-gap ($E_{CV}$) is of major importance from an application point of view.[23] As already mentioned, cyclic

voltammetry is one of the methods available to estimate these values. It has to be kept in mind though, that typically the measurements performed in solution provide values for $E_{CV}$ far lower than those calculated optically, which may lead to misinterpretations.[24] Measuring the redox properties in the solid state provides more reliable information, since the movement of charges is more comparable to the one found in organic materials based devices for example OPVs.[25, 54]

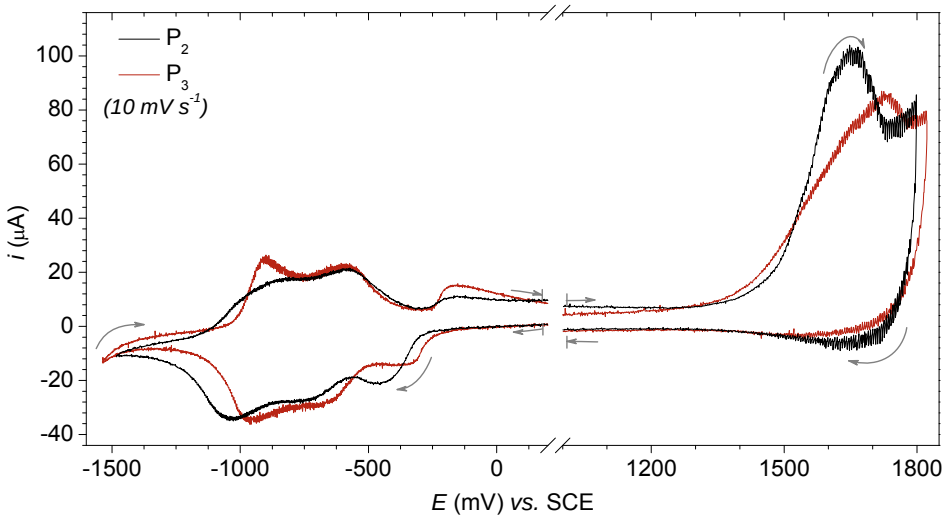


**Figure 41.** Cyclic voltammograms of **$P_2$** and **$P_3$** as thin films deposited on a Pt electrode in acetonitrile.

The electrochemical properties of **$P_2$** and **$P_3$** were evaluated in thin film by cyclic voltammetry. Both polymers showed reversible reduction and irreversible oxidation waves, characteristic for TQ derivatives as illustrated in Figure 41. The $E_{LUMO}$ and $E_{HOMO}$, estimated from onset of the first reduction and oxidation steps, respectively, are listed in Table 7. As expected, due to the stronger electron donating properties of the thienyl substituents relative to phenyl ones on the TQ core, a 0.1 eV higher $E_{HOMO}$ was derived for **$P_3$**. On the other hand, the nature of the substituents on the TQ segment had little influence on the $E_{LUMO}$. The ~4.0 eV $E_{LUMO}$ estimated for both **$P_2$** and **$P_3$** illustrates the potential of these materials as n-type semiconductors. The approx. 0.2 eV difference between the optically and electrochemically determined energy gaps might be attributed to the exciton binding energy of the polymers, which is believed to be in the range of 0.1-0.4 eV.[26]

The photophysical and electrochemical properties of both **$P_2$** and **$P_3$**, especially their low $E_{LUMO}$, recommend their application as n-type materials in an organic photovoltaic device.

### 2.4.1.3. All-Polymer Solar Cells

The most efficient bulk heterojunction (BHJ) organic photovoltaic (OPV) devices are composed of a conjugated polymer as the donor p-type material[27] and a $C_{60}$ or $C_{70}$ fullerene derivative as the acceptor n-type material.[28] These fullerene derivatives hold the advantage of good electron mobility[29] due to their semicrystalline nature[30] and good solubility in a variety of organic solvents. Their disadvantage lies in their reduced optical absorption. Although $PC_{70}BM$ shows enhanced absorption relative to $PC_{60}BM$, it peaks in the blue region and it is not useful in extending the response of BHJ cells into the red and / or near infrared (NIR) regions.[31] Additionally, fullerenes offer limited chemical modification possibilities to tune their absorption properties.[32] Hence, to be able to challenge fullerene derivatives the substitute n-type material should possess a band gap below 1.8 eV. PDIs,[33] malononitriles[34] and dicyanoimidazoles[35] have been recently explored as n-type molecular replacements for fullerene derivatives. Additionally, polymers bearing cyano groups to induce n-type behavior where also investigated as PCBM surrogates,[36] reaching a power conversion efficiency up to 1.7 %. A polymer / polymer approach offers the advantage of versatile processability, forming high quality thin films.[31] Furthermore, due to the possibility of fine-tuning the energy offset at the heterojunction, promoting minimized energy losses in the charge transfer step, all-polymer devices have already shown good open-circuit voltages.[37] The major requirement for an efficient photovoltaic device operation is the efficient charge separation and collection at the device electrodes. In the case of organic molecules and polymers charge separation is a multistep process. Photoexcitation does not lead directly to charge generation, since the photoexcited exciton state has a higher binding energy of approx. 0.4 eV. Therefore, to ensure the electron / hole transfer process, a greater energy offset than 0.4 eV is required between the LUMOs and HOMOs of the polymers.[31, 38]

The all-polymer solar cells were prepared in collaboration with the group of Prof. Serdar N. Sariciftci in Linzer Institut für Organische Solarzellen (LIOS) Linz, Austria. Poly(3-hexylthiophene) (**P3HT**) was considered as p-type material, being one of the most studied donor counter parts in OPV applications. **P3HT** has an $E_{LUMO}$ of -3.20 eV and $E_{HOMO}$ of -5.10 eV.[39] Accordingly, the complementary n-type material for **P3HT** would ideally have its $E_{LUMO}$ < -3.50 eV and $E_{HOMO}$ < -5.40 eV.

Due to the applied synthetic design, $\mathbf{P_2}$ and $\mathbf{P_3}$ fulfill the initial requirements of a promising counterpart for **P3HT** in an OPV device. As both materials showed equally low LUMOs (~4.00 eV) and $E_{op}$ (1.52 eV), $\mathbf{P_2}$ was chosen to be tested based on its broader and more intense absorption at longer wavelengths.

On the basis of the $E_{HOMO}$ (D) of the p-type material and $E_{LUMO}$ (A) of the n-type counterpart it is possible to estimate the open circuit voltage ($V_{OC}$) for the corresponding solar cell using the empirical relation $V_{OC} = |E_{HOMO}(D) - E_{LUMO}(A)| - 0.18$ V.[39] Applying the formula lead, in this case, to an expected value of 0.95 V.

Figure 42 shows the normalized UV-Vis absorption of the **P3HT**:$\mathbf{P_2}$ (1 : 1) blend. For comparison the solid state spectrum of **P3HT** is added as well. The thin film of the blend revealed absorption up to 820 nm, although with a somewhat reduced intensity relative to the band between 400 and 600 nm corresponding to **P3HT**.

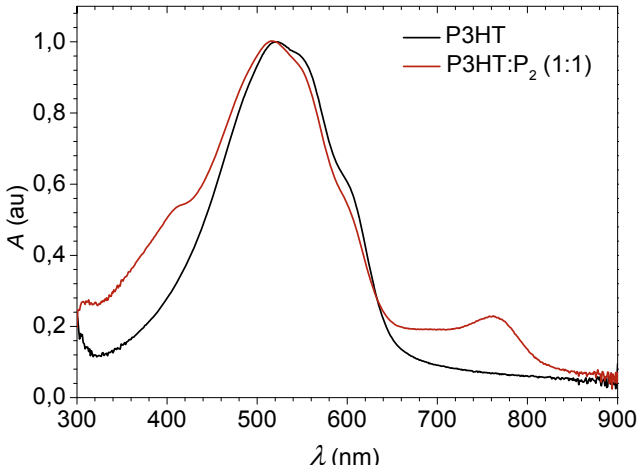


**Figure 42.** Normalized UV-Vis absorption of **P3HT** and **P3HT**:$\mathbf{P_2}$ blend at a ratio used for solar cell fabrication.

Photovoltaic cells were fabricated by spin-coating from an aqueous solution a 40 nm thick layer of PEDOT-PSS onto an ITO covered glass substrate. On top an *o*-dichlorobenzene solution containing **P3HT** and **$P_2$** in a 1 : 1 weight ratio was spin casted. Finally, a 100 nm thick aluminum layer was deposited from the gas phase as top electrode. The cell was illuminated with 100 mW $cm^{-1}$ of AM1.5G light, resembling the solar spectrum.[40] As cast, the cells reached a power conversion efficiency of $\eta$ = 0.04 %, with a short-circuit current density of $J_{SC}$ = 0.18 mA $cm^{-1}$, an open-circuit voltage of $V_{OC}$ = 0.60 V and a fill factor *FF* = 0.40. A standard cell composed of **P3HT**:$PC_{60}BM$ (2 : 1) was also prepared for comparison, showing the following parameters: $J_{SC}$ = 1.10 mA $cm^{-1}$, $V_{OC}$ = 0.60 V, *FF* = 0.50 and a power conversion efficiency of $\eta$ = 3.30 %.

For the all polymer cell the extracted open-circuit voltage was identical to the standard cell, but did not reach the expected value of 0.90 V. The *FF* was in the range of most all-polymer solar cells, but nevertheless low. This is often associated with trap limited electron transport,[41] but can also be caused by a slow separation and the resulting recombination of the geminate photogenerated electron-hole pair.[42] Additionally, the short circuit current was very low, being one of the major limiting parameters. A low photocurrent could have several causes,[38] such as inefficient photoinduced electron transfer, or absence of long-living charges in the active layer, or an unsuitable morphology for charge separation and / or transport.

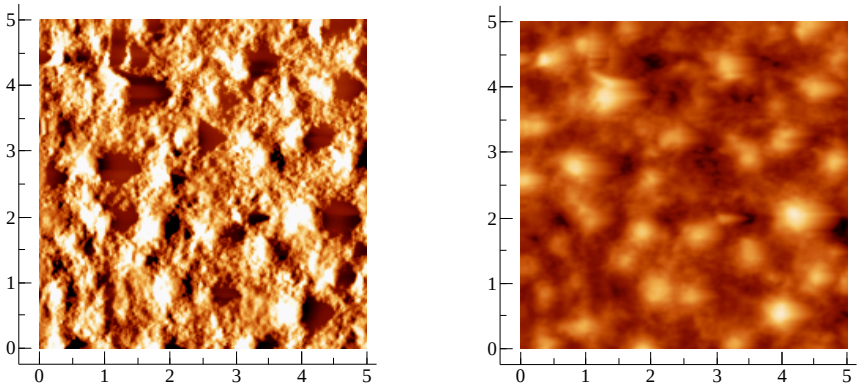


**Figure 43.** Phase (left) and height (right) AFM images of the surface of the **P3HT**:**$P_2$** blend all-polymer OPV device (5 µm x 5 µm).

A crucial factor in obtaining high power conversion efficiencies is the morphology of the blend, as exciton dissociation requires donor-acceptor domains smaller than 10 nm; an efficient charge separation occurs in case of separated domains and clean interfaces;[43] and charge collection entails separated domains and interconnected pathways.[31] Hence, the morphology of the **P3HT**:**$P_2$** (1 : 1) blend was investigated by AFM. The height image revealed a very rough surface, as illustrated in Figure 43. The corresponding phase image showed contrast that could be related to two phase segregated materials at the surface. Nonetheless, this does not necessarily imply pure donor and pure acceptor phases. The sizes of these domains were typically larger than 10 nm. Hence, the inadequate morphology of the blend might be responsible (in part) for the limited short-circuit current.

The following section deals with the charge carrier mobility of both **$P_2$** and **$P_3$** since this process is another performance limiting factor of any material applied in organic electronics.

### 2.4.1.4. Mobility Measurements

The charge carrier mobility is dependent not only on the material, but also on the experimental condition. There are many measurement techniques available to determine charge carrier mobilities, such as time-of-flight (TOF), analysis of space-charge limited current (SCLC), or field effect transistors (FET) just to mention a few.[44] In TOF the sample is sandwiched between two electrodes and the conduction of the charges is perpendicular to the substrate plane, therefore the measurement conditions are more similar to OPV. Contrary, in FETs the charge mobility is characterized within the plane of the substrate.[45] While in some cases the results measured by these two different methods were comparable,[46] there are reports of FET mobilities of two orders of magnitude smaller or higher than those determined by TOF.[46, 47] Despite these differences, field effect mobility is more often used as an indicator of relative film electron / hole mobility.[48] For example PCBM (60 or 70) has reported electron mobility of around $10^{-2}$ $cm^2V^{-1}s^{-1}$ measured in FET prepared under similar conditions as an OPV device.[49]

Hence, for a "quick" assessment of the charge carrier mobilities, both **$P_2$** and **$P_3$** were tested as the active component of a FET bottom contact device. Heavily n-doped silicon was used as gate electrode with a 200 nm thick hexamethyldisilazane (HMDS) treated silicon dioxide layer as dielectric.[50] The source and drain electrodes were patterned by photolithography (50 nm). The polymer was than drop-casted from a 5 mg $mL^{-1}$ toluene solution. These measurements were carried out by Dirk Beckmann, Max Planck Institute for Polymer Research, Mainz.

While **$P_2$** showed no detectable field effect mobility, for **$P_3$** a saturation electron mobility of $\mu_{e,sat} = 1.7 \times 10^{-6}$ $cm^2V^{-1}s^{-1}$ with an on / off current ratio under 100 could be measured. It should be noted that the processing conditions were not optimized, but kept identical to those used during the preparation of the solar cell reported in Subsection 2.4.1.3. A "small" modification of the substituents attached to the TQ core phenyl *vs.* thienyl, induced electron transport when applied in a field effect transistor. The fact that **$P_2$** showed no detectable field effect electron charge carrier mobility adds to the possible reasons for the low $J_{SC}$ measured in the solar cell. Despite the fact that the measured electron mobility of **$P_3$** was low, it is a promising result. It shows that the incorporation of triple bond π-spacers into the polymer backbone of a TQ copolymer is advantageous for enabling electron charge transport.

Certainly, TOF measurements would offer a more eloquent mobility evaluation, since this technique measures the photo-generated charge carriers. Additional information could be obtained by measuring the charge carrier mobilities of the blends. Further testing and / or optimizations of both **$P_2$** and **$P_3$** as acceptors in all polymer cells are on going.

### 2.4.1.5. Conclusion

This chapter presents the synthesis and characterization of thiadiazolo[3,4-*g*]quinoxaline-phenylene copolymers containing ethynylene π-spacers. A microwave mediated *Sonogashira-Hagihara* synthetic procedure was developed to enable the synthesis of high molecular weight materials with high reproducibility. Following this synthetic procedure three polymers were synthesized with identical polymeric backbones, bearing different substituents on the TQ core, ranging from alkyl (**$P_1$**) through phenyl (**$P_2$**) to thienyl (**P3**) moieties.

As it turned out, ethyl-hexyl alkyl side chains grafted on the TQ segment were not sufficient to ensure the solubility of the corresponding high molecular weight polymer **$P_1$**. On the other hand, alkylated phenyl or thienyl functionalities offered good solubility for the corresponding high molecular weight polymers **$P_2$** and **$P_3$**, respectively.

Both **$P_2$** and **$P_3$** revealed significant aggregation in dilute solutions when dissolved in THF, chloroform or toluene, as evidenced by the temperature dependant photophysical and GPC studies. Additionaly, the successful extension of the π-conjugation *via* the ethynylene π-spacers was reflected in their low optical energy-gaps ($E_{op}$ = 1.52 eV, thin film) of both **$P_2$** and **$P_3$**.

While the substituents attached to the TQ core (phenyl *vs.* thienyl) do not seem to play a significant role on the optical energy-gap, the cyclic voltammetry studies suggest that the polymers differ in the position of their HOMO energy level. Based on these studies it was concluded that the substituents on the TQ core have little influence on the low $E_{LUMO}$ ≈ -4.05 eV of the corresponding polymers, as it was also found in the case of their corresponding model compounds. The presence of the stronger donor thienyl moieties attached to the TQ segment, slightly elevate the $E_{HOMO}$ of **$P_3$** to -5.76 eV relative to **$P_2$** with an $E_{HOMO}$ = -5.82 eV.

All-polymer solar cells were prepared based on **$P_2$** as the acceptor and **P3HT** as the donor components, in a 1 : 1 weight ratio showing a low power conversion efficiency of $\eta$ = 0.04 %. The measured open circuit voltage was 0.60 V, value below the expected 0.95 V. The unfavorable morphology of the blend combined with a very limited charge carrier mobility of the acceptor counterpart (**$P_2$**) could be the major factors limiting the power conversion efficiency of the all-polymer photovoltaic cell.

The field effect charge carrier mobility of both polymers was also investigated. While **$P_2$** exhibited no detectable charge carrier mobility, **$P_3$** demonstrated a saturation electron mobility of $\mu_e = 1.7 \times 10^{-6}$ $cm^2V^{-1}s^{-1}$. Although this mobility might be considered a relatively modest one, its importance is augmented by the fact that: (*1*) the FET devices were not optimized; (*2*) there are no polymers incorporating TQ moiety showing electron charge carrier mobility reported up to date.

Further structural modifications of the TQ-ethynylene based polymer backbone, such as insertion of a stronger donor unit, could enable an even higher electron or even ambipolar charge transport.

## 2.4.2. Thiadiazolo[3,4-*g*]quinoxalines: Ethynylene-Thiophene Copolymers

### 2.4.2.1. Polymer Synthesis

Thiophene as a stronger donor, relative to phenyl, has been chosen to be introduced in the polymer backbone, connected *via* ethynylene π-spacers to the electron deficient TQ core. 2,5-Diethynylthiophene was required in order to keep the D-A ratio per repeating unit at 1 : 1. Additionally, dodecyl substituents were introduced at the positions 3 and 4, to ensure the solubility of the resulting polymers. Thus, the desired 3,4-didodecyl-2,5-diethynylthiophene (**42**) was synthesized based on a slightly modified literature procedure[51] as depicted in Scheme 20.

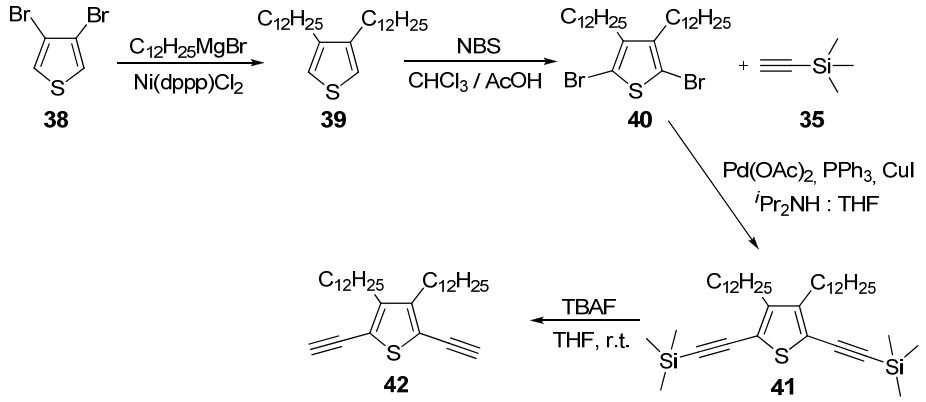


**Scheme 20.** Synthesis of alkylated 2,5-diethynylthiopehene monomer **42**.

Starting from the commercially available 3,4-dibromothiophene (**38**) the dialkylated thiophene **39** was obtained under *Kumada coupling* conditions.[4] The dibromination of **39** followed by a *Sonogashira-Hagihara*[1] cross-coupling reaction with TMS-acetylene led to the compound **41**. The desired monomer **42** was obtained by removing the TMS protecting

groups, using TBAF as deprotection agent. Note that monomer **42** needed to be stored at temperatures below $5^0$C to prevent degradation indicated by a color change from white to red-brown. Therefore, this monomer was synthesized directly prior to each polymerization reaction.

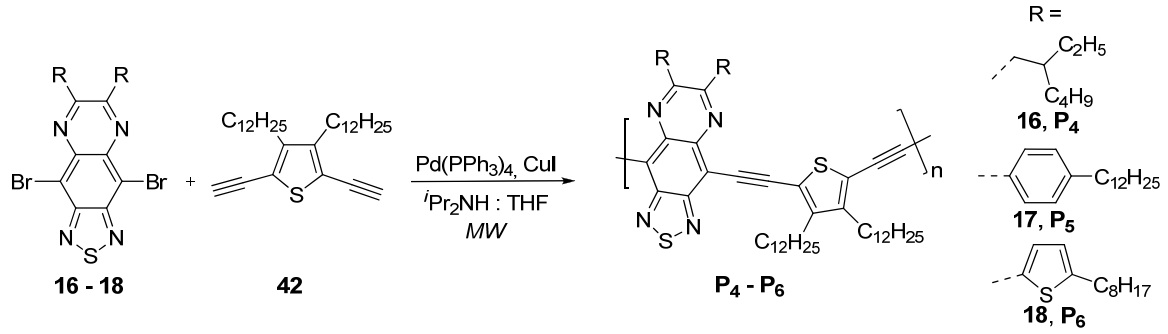


**Scheme 21.** Synthesis of TQ-based ethynylene-thiophene copolymers **$P_4$**, **$P_5$** and **$P_6$**.

**Chart 11.** Chemical structure of the synthesized TQ-based ethynylene-thiophene copolymers **$P_4$**, **$P_5$** and **$P_6$**.

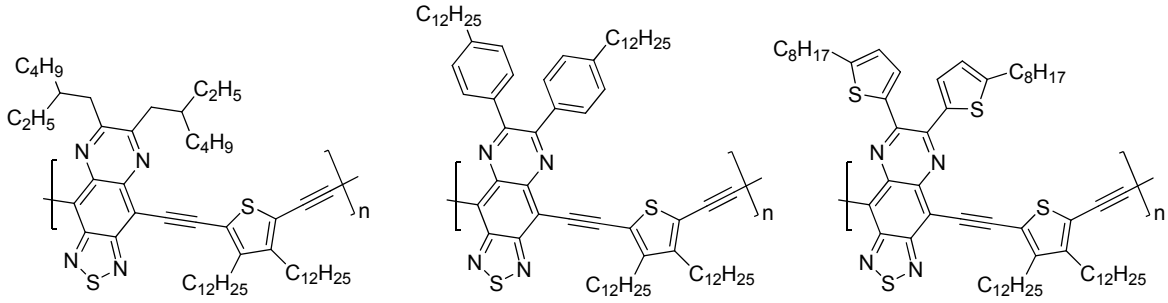


The microwave assisted polymerization procedure described for the synthesis of polymers **$P_1$**-**$P_3$** (see Subsection 2.4.1.1.) has been successfully applied for the synthesis of thiophene containing polymers (**$P_4$**-**$P_6$**) as well (Scheme 21). Hence, polymers **$P_4$**-**$P_6$** differing only in the substituents anchoring the TQ core (Chart 11), were obtained following an only 80 minutes *MW* irradiation, in the presence of $Pd(PPh_3)_4$/CuI. The corresponding polymer was then isolated after repeated precipitations in methanol. Purification by Soxhlet extraction with acetone, methanol or hexane induced an irreversible aggregation for all three polymers. As a result only low molecular weight fractions could be dissolved by any common organic solvent, such as $CHCl_3$, THF, toluene or chlorinated benzene derivatives. If the low molecular weight

fractions were not removed by Soxhlet extraction, all three polymers proved to be highly soluble in the organic solvents mentioned above. It seems that the low molecular weight fraction impede the irreversible aggregation of the high molecular weight polymer chains. Therefore, none of the below discussed materials were subjected to this purification technique. Even though not Soxhlet extracted, the solubility of polymer **$P_4$** was compromised upon prolonged storage. However, this type of irreversible aggregation is not unusual. Similar behavior was reported by the group of Bunz for poly(*p*-phenylene-ethynylene)s bearing various styryl-like side groups.[52] Nonetheless, the photophysical and electrochemical characterization of **$P_4$** was possible by avoiding complete drying.

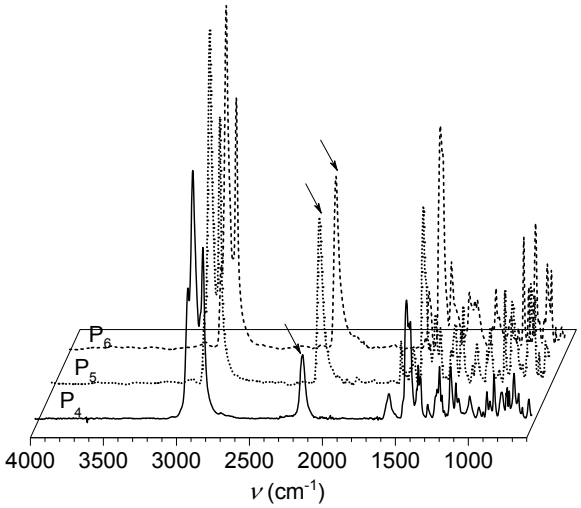


**Figure 44.** IR spectra of polymers **$P_4$**–**$P_6$**. The arrows are indicating the characteristic infrared band for the internal –*C*≡*C*– bond stretch (≈ 2135 $cm^{-1}$).

The structural proofs for **$P_4$**, **$P_5$** and **$P_6$** were obtained by NMR spectroscopy, elemental analysis and FT-IR spectroscopy (see Chapter 5). A straightforward way to prove the successful insertion of the ethynylene π-spacers in a polymer backbone is by FTIR spectroscopy. As highlighted in Figure 44, the presence of the internal –*C*≡*C*– bond gave rise to a characteristic stretching at approx. 2135 $cm^{-1}$. Additionally, the characteristic strong and narrow band between 3260 and 3330 $cm^{-1}$ corresponding to a terminal acetylene stretch was absent for all three polymers.

The molecular weights of **$P_4$**-**$P_6$** were determined by GPC measurements at two different temperatures (Figure 45*a*-*b*). In THF at $30^0$C, **$P_4$** revealed a typical bimodal molecular weight

distribution, making an accurate determination of its molecular weight problematic. As a result the PDI values were beyond 21 (Table 8). On the other hand the molecular weight distribution curve of the same polymer, taken at 135$^0$C in TCB (Table 45*b*), showed a monomodal distribution suggesting a strong aggregation of **P$_4$** in THF at 30$^0$C. Note that some aggregation was still present even at high temperature in TCB as indicated by the long tale of the distribution curve which could account for the increased PDI of 5.0. The number average molecular weight ($M_n$) of **P$_4$** as determined in reference to polystyrene at high temperature was 11700 g mol$^{-1}$ (Table 8).

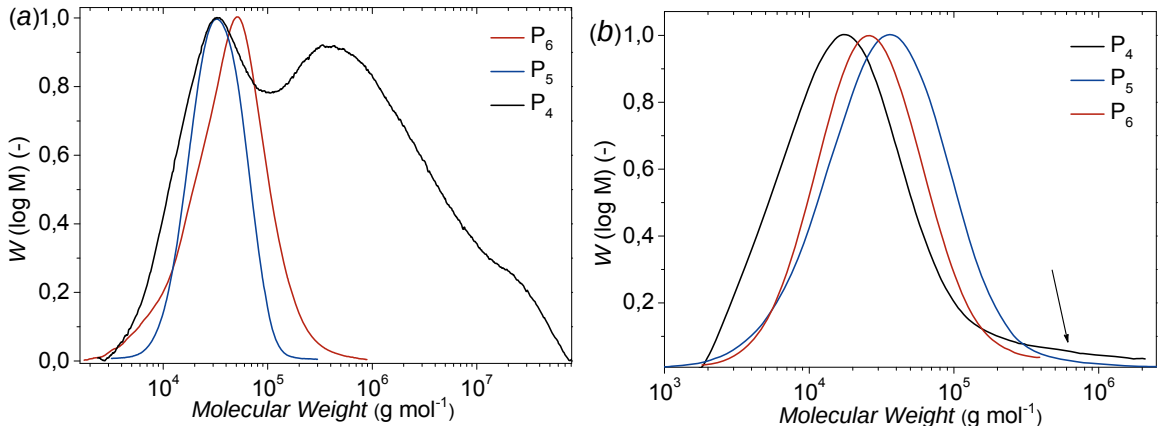


**Figure 44.** Molecular weight distribution of **P$_4$**, **P$_6$** and **P$_6$** as measured by GPC in THF at 30$^0$C (*a*) and in TCB at 135$^0$C (*b*).

**Table 8.** Summary of molecular weights as determined by GPC measurements of **P$_4$**, **P$_6$** and **P$_6$**.

| Compd. | THF, 30$^0$C *vs. PPP* | | | THF, 30$^0$C *vs. PS* | | | TCB, 135$^0$C *vs. PS* | | | |
|---|---|---|---|---|---|---|---|---|---|---|
| | $M_n$ x 10$^3$ (g mol$^{-1}$) | $M_w$ x 10$^3$ (g mol$^{-1}$) | *PDI* | $M_n$ x 10$^3$ (g mol$^{-1}$) | $M_w$ x 10$^3$ (g mol$^{-1}$) | *PDI* | $M_n$ x 10$^3$ (g mol$^{-1}$) | $M_w$ x 10$^3$ (g mol$^{-1}$) | *PDI* | *PD* |
| **P$_4$** | 32.6 | 710.8 | 21.7 | 49.6 | 2437 | 49.1 | *11.7* | *59.1* | *5.0* | 13-65 |
| **P$_5$** | 18.4 | 32.4 | 1.76 | 27.8 | 58.3 | 2.1 | *18.4* | *65.3* | *3.5* | 16-55 |
| **P$_6$** | 17.5 | 22.8 | 1.3 | 27.0 | 38.2 | 1.4 | *17.8* | *39.2* | *2.2* | 16-36 |

The molecular weight distribution curves for polymers **P$_5$** and **P$_6$** obtained in THF were much sharper compared to **P$_4$**. Furthermore, the corresponding *PDI* values relative to *PPP* were surprisingly low considering that none of these polymers was purified by Soxhlet fractionation. The $M_n$ for, both **P$_5$** and **P$_6$** was around 18000 g mol$^{-1}$, as measured at 135$^0$C in

TCB *vs. PS*. The very similar polymerization degree (*PD*) of all three polymers is highlighting the high reproducibility of the developed *MW* assisted polymerization procedure.

As one of the requirements for most of the applications involving organic materials is their high thermal stability, all three polymers (**$P_4$**-**$P_6$**) were subjected to thermogravimetric analysis (Figure 46). The temperature of 5 % weight loss based on the initial weight was over $380^0$C for all three materials. Additionally, no obvious transitions were observed at repeated heating and cooling cycles between $20^0$C and $300^0$C during the differential scanning calorimetry (DSC) measurements.

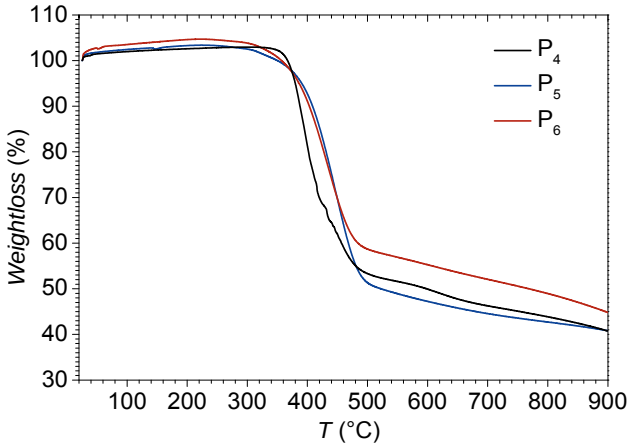


**Figure 46.** Thermogravimetric analysis ofpolymers **$P_4$**, **$P_6$** and **$P_6$** at a heating rate of 10 K $min^{-1}$ under $N_2$ atmosphere.

## 2.4.2.2. Optical and Electrochemical Characterization of $P_4$, $P_5$ and $P_6$

As previously mentioned (see Section 2.2.2.), UV-Vis spectroscopy constitutes a valuable tool in the investigation of the electronic differences that may arise between structurally close related materials. Firstly, the impact of the nature of the donor (phenyl *vs.* thienyl) incorporated in the polymer backbone could be evaluated by comparing the absorption profiles of **$P_2$** *vs.* **$P_5$** or **$P_3$** *vs.* **$P_6$**. Secondly, the influence of substituents (alkyl *vs.* phenyl *vs.* thienyl) grafted on the TQ segment can be assessed when comparing the optical and

electrochemical properties of the polymer series **$P_4$**-**$P_6$**. Therefore, the absorption spectra of the polymers **$P_4$**, **$P_5$** and **$P_6$** were registered in dilute solutions as well as in the solid state, as depicted in Figure 47*a*-*b*.

In solution all three polymers showed absorptions extending up to 875 nm, showing two main absorption bands (Figure 47*a*). The first band was located between 350 and 500 nm originating from the π-π* transitions, characteristic to the polymer backbone and a second long wavelength absorption band between 500 and 900 nm. The second absorption band arose from the successful extension of the π-conjugation in **$P_4$**-**$P_6$** as a result of an effective D-A interaction through the ethynylene π-spacer. Certainly, the substituents connected at the TQ core left their fingerprints on the absorption of their corresponding polymers. While the long wavelength absorption maximum of **$P_4$** was located at $\lambda_{max}$ = 723 nm, in case of **$P_5$** and **$P_6$** $\lambda_{max}$ was 64 nm bathochromically shifted. As all three polymers have identical backbones, the bathochromic shifts originates from the different substituents attached to the TQ core. While in the case of **$P_4$** the TQ core is bearing alkyl side chains, for both **$P_5$** and **$P_6$** the substituents are aromatic systems that are increasing the π-conjugation (see Section 2.2.2.). Hence, the absorption could not only be tuned through the donor incorporated in the polymer backbone but also *via* the substituents attached to the TQ core. Any further interpretation of the UV-Vis data obtained in solution would be speculative in the view of the presence of aggregates as suggested by the shoulder around 900 nm of the long wavelength absorption band of **$P_5$**.

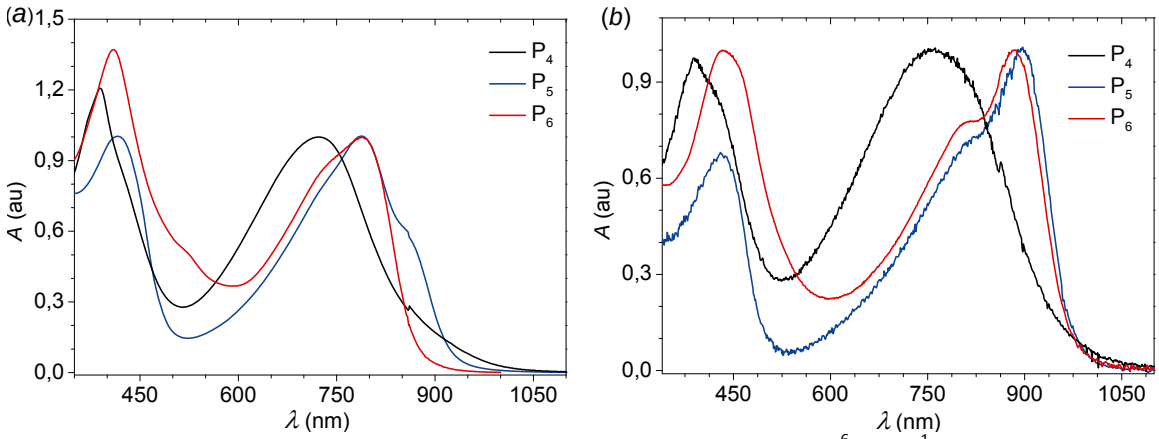


**Figure 47.** UV-Vis absorption profiles of **$P_4$**, **$P_5$** and **$P_6$** in toluene solution ($c = 10^{-6}$ mol $L^{-1}$) (*a*) and of the thin films prepared by spin-coating on a glass substrate a 5 mg $mL^{-1}$ toluene solution (*b*).

In the solid state (Figure 47*b*), **$P_4$**-**$P_6$** exhibited considerable red shifts of their absorption maxima relative to those in solution, which in case of **$P_5$** and **$P_6$** exceeds 100 nm. Additionally, the long wavelength absorption band was increased in intensity in relation to the band at higher energies. This is an indication of a greater structural organization in the solid state possibly assisted by planarization and an increase of the π-conjugation.[53] As expected, the optical energy-gap, calculated from the onset of the long wavelength absorption band of **$P_4$** was 0.03 eV higher than $E_{op}$ = 1.27 eV determined for both **$P_5$** and **$P_6$** (Table 9). Although the long wavelength absorption maximum of **$P_5$** was over 10 nm bathochromically shifted relative to **$P_6$**, their $E_{op}$ were equally low and showed similar behavior. When **$P_5$** and **$P_6$** are compared with their structurally similar **$P_2$** and **$P_3$** (see Subsection 2.4.1.2.), the fine tuning of the absorption through the replacement of phenyl with thienyl in the polymer backbone is apparent. The stronger electron donating thiophene in conjugation *via* ethynylene π-spacers with the TQ efficiently lowered the optical energy-gap by approx. 0.25 eV. These findings are in good agreement with those concluded from the studies of their corresponding model compounds (see Section 2.3.1.).

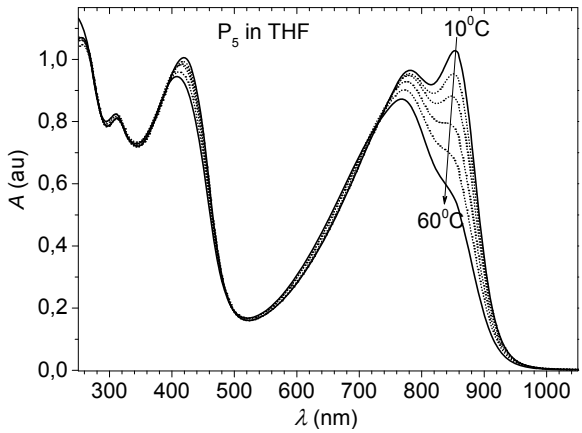


**Figure 48.** Temperature dependent UV-Vis absorption profile of **$P_5$** in THF ($c$ = $10^{-6}$ mol $L^{-1}$).

Temperature dependent UV-Vis absorption spectra were registered in THF solution for both **$P_5$** and **$P_6$**. While **$P_6$** did not show any thermally induced spectral change, **$P_5$** revealed a pronounced thermochromic effect, as shown in Figure 48. The long wavelength absorption band with a $\lambda_{max}$ located at 856 nm was reduced to a small shoulder at 60$^0$C suggesting that at temperatures close to 20$^0$C in THF this polymer tends to aggregate. Additionally, based on the

red shifted position of this band it is reasonable to assume that the polymer forms J-aggregates, similarly to the polymers **$P_2$** and **$P_3$**, presented in the previous chapter (see Subsection 2.4.1.2.). This effect was completely reversible, suggesting no permanent structural change, hence supporting the existence of aggregates.

As previously mentioned, the tendency of PPEs to form aggregates is well documented.[54] Usually, for these systems aggregation can be induced in a "good" solvent at higher concentrations or at lower temperatures or in a "poor" (non-)solvents. Moreover, aggregation can be induced at room temperature in a "good" solvent, upon addition of a non-solvent, for example methanol.[55] Therefore, the spectral changes of **$P_5$** (Figure 49*a*) and **$P_6$** (Figure 49*b*) were monitored in toluene as the "good" solvent with increasing volume concentrations of methanol as the non-solvent. For both samples the bulk solution maintained homogeneity up to 50 vol.% of methanol.

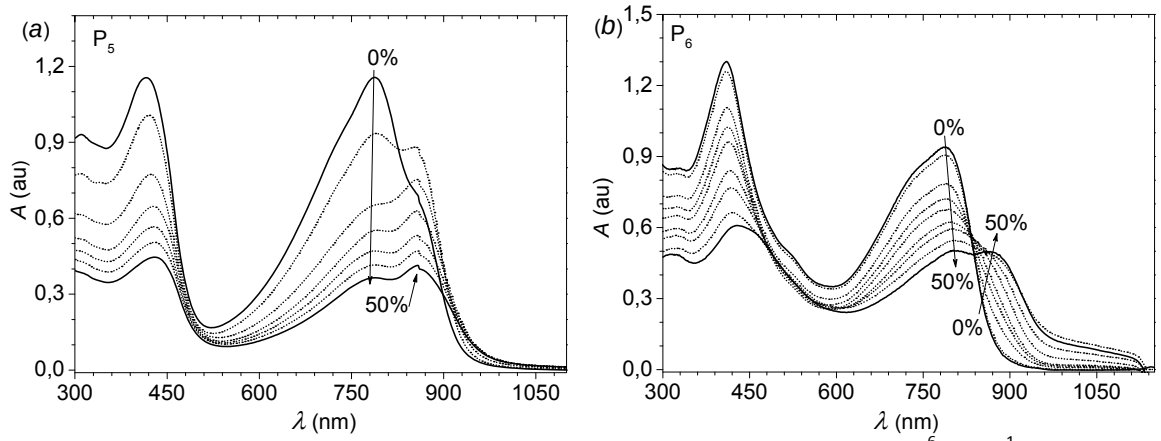


**Figure 49.** UV-Vis absorption profiles of **$P_5$** (*a*) and **$P_6$** (*b*) in toluene solution ($c = 10^{-6}$ mol $L^{-1}$) with increasing volume concentration of methanol.

With an increase of methanol, a red shifted long wavelength transition arose, for both **$P_5$** and **$P_6$**. At 50 vol.% methanol, the local $\lambda_{max} = 856$ nm of the newly formed band for **$P_5$** was identical to the band registered in THF at room temperature (Figure 49*a* and Figure 48). **$P_6$** exhibited very similar behavior demonstrating its tendency to form aggregates. This can be seen by the presence of the bathochromically shifted absorption band with $\lambda_{max} = 870$ nm at 50 vol.% non-solvent content (Figure 49*a*). Note that for both **$P_5$** and **$P_6$** the $\lambda_{max}$ of the thin films were bathochromically shifted relative to the $\lambda_{max}$ of the band due to aggregation. The lack of aggregation of **$P_6$** at room temperature, under the same conditions that the

structurally close related **$P_5$** revealed aggregation, could possibly be due to the differences in their molecular weight or the presence of the low molecular weight fractions that might hinder the tendency to form aggregates.

The redox properties were investigated by cyclic voltammetry measurements performed on thin films, prepared from toluene by drop-casting (5 mg $mL^{-1}$), in acetonitrile with $^{n}Bu_4NPF_6$ as electrolyte and ferrocene as standard (Figure 50). All three polymers showed the characteristic reversible reduction waves of the TQ segment.

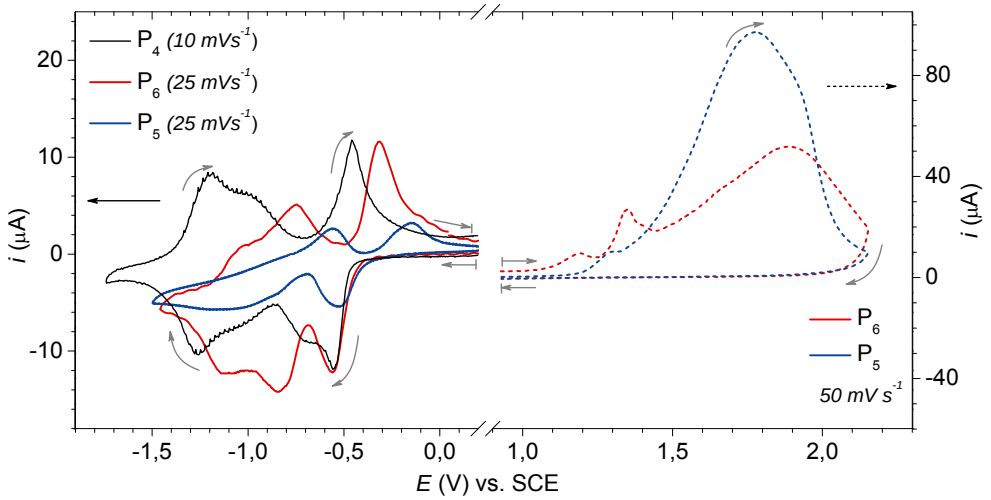


**Figure 50.** Cyclic voltammograms of **$P_4$**, **$P_5$** and **$P_6$** as thin films deposited on a Pt electrode, in acetonitrile.

**Table 9.** Summary of optical and electrochemical properties of **$P_4$**, **$P_5$** and **$P_6$**.

| Compd. | $\lambda_{max}$ (nm)[a] | $\lambda_{max}$ (nm) film[b] | $E_{op}$ (eV)[b] | $E_{LUMO}$ (eV)[c] | $E_{HOMO}$ (eV)[c] | $E_{CV}$ (eV)[d] |
|---|---|---|---|---|---|---|
| **$P_4$** | 723 | 761 | 1.30 | -3.87 | - | - |
| **$P_5$** | 767[#] | 895 | 1.27 | -3.96 | -5.50 | 1.54 |
| **$P_6$** | 787[#] | 882 | 1.27 | -3.91 | -5.40 | 1.49 |

[a]in toluene ([#]in THF @ 60$^0$C); [b]spin – coated on a glass substrate from a 5 mg $mL^{-1}$ solution; [c]calculated $E_{LUMO} = -(E_{Red}^{onset} - E_{Fc/Fc^+}^{1/2} + 4.8)$ eV; [d]calculated from $E_{CV} = |E_{HOMO}| - |E_{LUMO}|$

While in case of **$P_4$** the p-doping process could not be measured, **$P_5$** and **$P_6$** revealed irreversible oxidation. The $E_{HOMO}$ and $E_{LUMO}$, as estimated from the onset of the first oxidation and reduction sweeps are listed in Table 9. It becomes apparent that the donor substituents anchoring the TQ segment only slightly affect the corresponding polymer $E_{LUMO}$, while these

substituents efficiently tune the $E_{HOMO}$ following a very similar trend as their analogous **P₂** and **P₃**. The generally larger $E_{CV}$ relative to $E_{op}$ is not surprising considering the interface energy barrier for charge injection between the polymer film and the electrode surface.[56] The origin of this energy difference may lie in the "insulating (shielding) effects" of the side chains.[57] Moreover, it has been suggested that the film preparation method (spin-coating *vs.* drop-casting) might also influence the outcome of the cyclic voltammetry measurements.[58]

### 2.4.2.3. $P_5$ and $P_6$ as Active Components of Ambipolar Field Effect Transistors

Due to the applied synthetic design, both **P₅** and **P₆** fulfill the initial requirements, such as low laying $E_{LUMO}$, good solubility, of a promising active n-type material in a field effect transistor (FETs). Therefore, in collaboration with Dirk Beckmann, Max Planck Institute for Polymer Research, Mainz both polymers were tested. The semiconducting properties were evaluated in a bottom contact, bottom gate transistor configuration (Figure 51). Heavily n-doped silicon was used as the gate electrode. A 200 nm thick hexamethyldisilazane (HMDS) treated silicon dioxide layer was the choice of dielectric in order to enhance the interface morphology and to avoid trapping by protonation.[59] Finally, the semiconducting layer was drop-casted from a 10 mg $mL^{-1}$ solution of **P₅** or **P₆** onto the substrates.

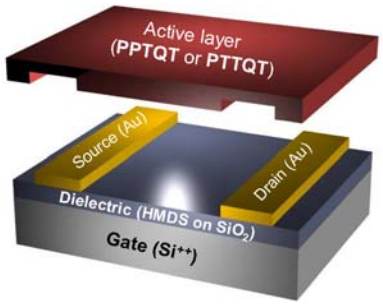


**Figure 51.** Schematic representation of a bottom contact, bottom gate field effect transistor configuration.

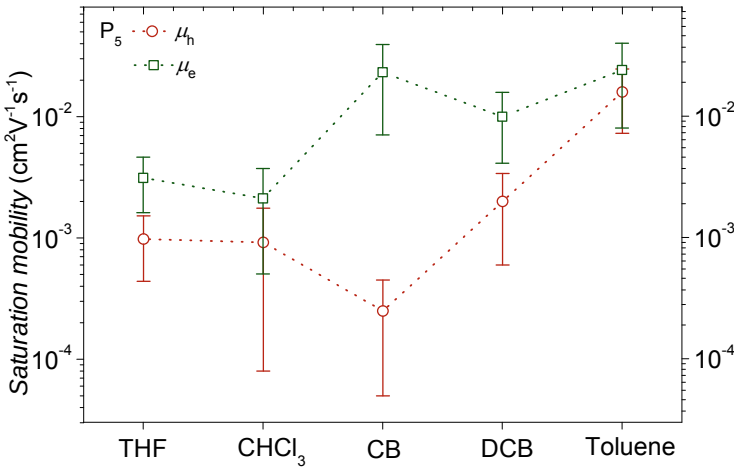


**Figure 52.** Effect of different solvents used in processing of **$P_5$** on the saturation hole and electron mobilities as measured in FETs (average mobilities of 7 measurements with the 90 % confidence interval).

Several processing solvents with different boiling points were tested for the deposition of **$P_5$** and all the prepared devices showed ambipolar transport characteristics. The dependence of the saturation hole and electron mobilities on the processing solvent is illustrated in Figure 52. This dependence of the FET performance on the boiling point of the solvent used for the deposition is not unusual. Studies performed on **P3HT** showed that deposition from different solvents and / or different deposition techniques led to distinct morphologies and consequently different charge carrier mobilities.[60] The best performance was obtained upon deposition from toluene solution. The highest hole and electron mobilities extracted for **$P_5$** are $\mu_h = 0.028$ $cm^2V^{-1}s^{-1}$ and $\mu_e = 0.042$ $cm^2V^{-1}s^{-1}$, respectively. Although the larger $E_{HOMO}$ of **$P_6$** would promote a reduced injection barrier, a one order of magnitude lower ambipolar charge transport was measured ($\mu_{e,h} = 0.002$ $cm^2V^{-1}s^{-1}$) under identical processing conditions (Table 10).

**Table 10.** Charge transport characteristics of the FET devices with **$P_5$** or **$P_6$** as active components.

| Compd. | $\mu_{sat,e}$[a] ($cm^2V^{-1}s^{-1}$) | $I_{ON}$ / $I_{OFF}$ | $\mu_{sat,h}$[a] ($cm^2V^{-1}s^{-1}$) | $I_{ON}$ / $I_{OFF}$ |
|---|---|---|---|---|
| **$P_5$** | 0.016 (±0.008) | $<10^2$ | $8.7\ (\pm6.6)\times10^{-3}$ | $<10^2$ |
| **$P_6$** | $1.1\ (\pm0.3)\times10^{-3}$ | $\sim5\times10^3$ | $1.3\ (\pm0.3)\times10^{-3}$ | $\sim4\times10^2$ |

[a]average electron and hole mobility obtained from 7 devices with the 90 % confidence interval in parentheses

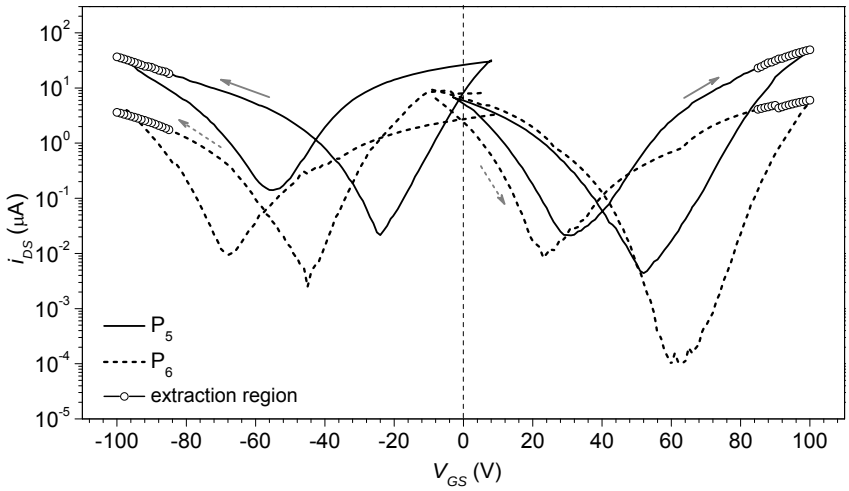


**Figure 53.** Transfer characteristics of a typical FET device based on drop-casted **P5** and **P6** from toluene solution ($L$ = 20 µm, $W$ = 1400 µm).

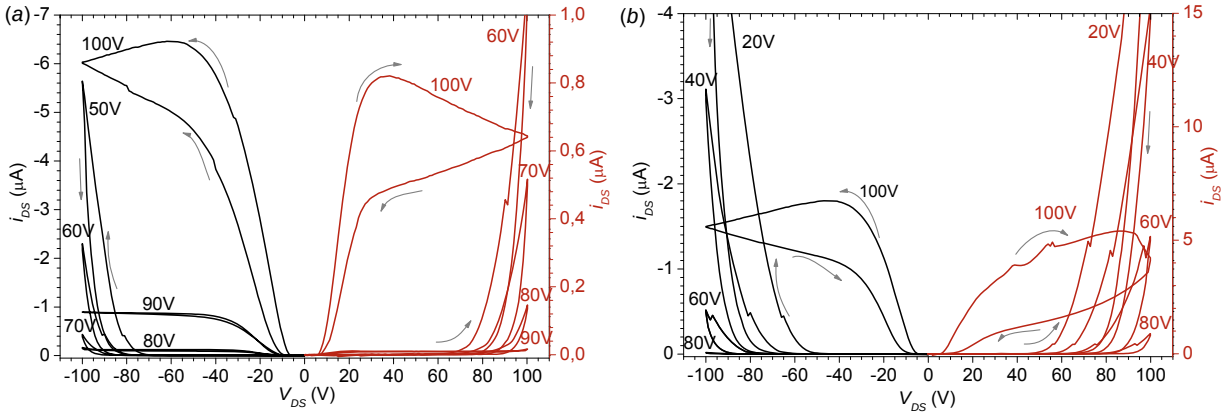


**Figure 54.** p- and n-Channel output characteristics of the ambipolar FET devices based on **P5** (*a*) and **P6** (*b*) with the transfer characteristics presented in Figure 53.

Figures 53 and 54 depict the typically observed transfer and output characteristics, respectively, for both materials. The electron transport was injection limited at low $V_{DS}$ as evidenced in the output characteristics. A possible reason could be the energy offset between the work function of gold (5.1 eV)[61] and the $E_{LUMO}$ (< -3.9 eV) of the active component. Additionally, severe trapping problems could be assumed from the hysteresis between the forward and backward swept transfer and output curves. These phenomena could be caused by supramolecular defects, for instance the presence of charge trapping impurities or defects in the polymer such as insufficient interchain packing or domain boundaries with interfacial trap distribution.[62] However, it has to be noted that these devices were not fully optimized. Increasing the molecular weight of the polymers or a further optimization of the source

and / or drain electrodes or deposition techniques may lead to a further improved device performance.[63]

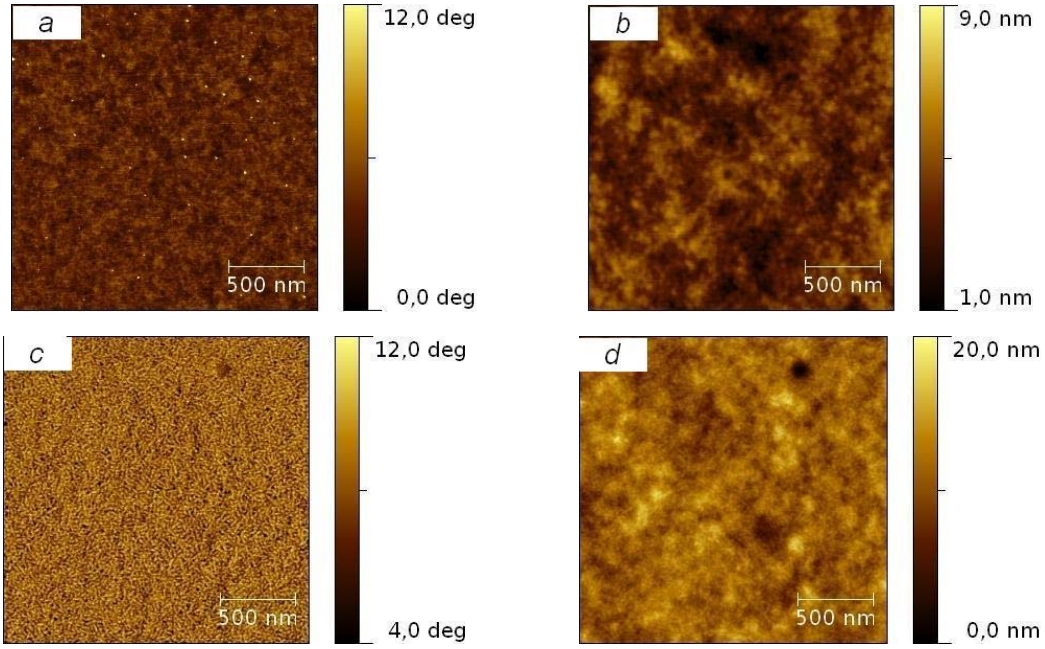


**Figure 55.** AFM images (taping mode) of the ambipolar FET devices based on **$P_5$** (*a*, *b*) and **$P_6$** (*c*, *d*) with the OFET transfer characteristics presented in Figure 53.

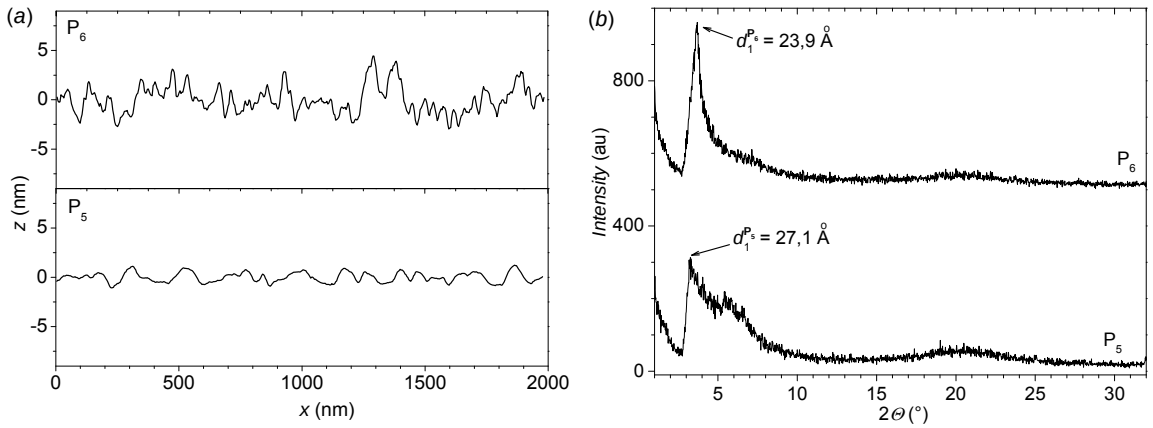


**Figure 56.** Typical cross-section profile of the AFM topographic images presented in Figure 55 (*a*). Θ–2Θ X-ray diffraction scans of the thin films with the morphological characteristics presented in Figure 55 (*b*).

As both **$P_5$** and **$P_6$** have virtually the same polymer backbone, the one order of magnitude lower performance of **$P_6$** *vs.* **$P_5$** most probably lies in microstructural and morphological differences induced by the thienyl substituents grafted on the TQ segment. The architecture of the presented devices enabled the investigation of the active layers by means

of X-ray diffraction and atomic force microscopy (AFM) in tapping mode. Both **$P_5$** and **$P_6$** revealed X-ray diffraction patterns corresponding to a highly isotropic organization (Figure 56*b*). One first order peak could be extracted suggesting a rather poor 1D lamellar packing, perpendicular to the substrate. Furthermore, no clear indication of π-π stacking was noticeable. A $d_1$ = 27.1 Å out-of-plane spacing was calculated for **$P_5$**, which is roughly equal to the size of the TQ segment functionalized with dodecylphenyl substituents. The AFM images of the same material (Figure 55*a*-*b*) showed a very smooth amorphous-like superstructure, having an rms roughness of 0.9 nm (Figure 56*a*). The extracted smaller $d_1$ = 23.9 Å spacing in case of **$P_6$** suggests either a tighter lamellar packing or a different tilt angle. As revealed by the AFM images (Figure 54*c*-*d*) of the same film, the octyl-thiophenes grafted onto the TQ core, facilitated the formation of randomly oriented worm-like morphology with an average length and width of approx. 50 and approx. 9 nm, respectively (rms roughness of 1.8 nm, Figure 56*a*). Based on the similarities of this macroscopic organization to that of **P3HT**, it is reasonable to assume that the lower charge carrier mobilities of **$P_6$** may be caused by the domain boundaries created alongside the small worm-like nanofibrills.[64]

### 2.4.2.4. Conclusion

The introduction of ethynylene π-spacers, in an alternating fashion, in a polymeric backbone between the thiadiazoloquinoxaline (A) and thiophene (D), in a 1 : 1 ratio per repeating unit, resulted in materials that revealed *ambipolar charge transport* in FET devices. The choice of substituents attached to the TQ segment plays a major role in the processability of the polymers and in defining the microstructure and surface morphology in the solid state and therefore on the FET performance. Functionalizing the TQ core with branched alkyl chains is insufficient for preventing irreversible aggregation of the corresponding high molecular weight polymer (**$P_4$**). Through the introduction of alkylated aromatic systems, such as dodecylphenyl (**$P_5$**) or octylthiophene (**$P_6$**), the solubility issues were overcome, while

extending the π-conjugation. Furthermore, by attaching substituents with different electron donating strength, the effective tuning of the HOMO and LUMO energy levels was achieved.

The one order of magnitude lower ambipolar charge transport in case of **$P_6$** *vs*. **$P_5$** could be explained through the differences at the microstructural and morphological level. While **$P_5$** forms uniform films with a rather poor 1D lamellar packing, **$P_6$** organizes in small randomly oriented worm-like nanofibrills, when processed under identical conditions. Nonetheless, both **$P_5$** and **$P_6$** were forming disordered films, showing no signal corresponding to π-π stacking in the X-ray diffraction scans. As such, the ambipolar charge transport showed by **$P_5$** ($\mu_{h,e} \approx 0.03$ $cm^2V^{-1}s^{-1}$) is just one order of magnitude lower than the unipolar charge transport exhibited by the representative polymers forming disordered films.[65]

Certainly, there is still room for improvement as the here reported mobilities were not measured on fully optimized OFET devices. Apart from the optimization of the processing conditions, it is also possible that by increasing the molecular weight of both **$P_5$** and **$P_6$** the performance of these materials in FET devices could be increased.

Among the copolymers based on TQ as the acceptor moiety, the mobilities in both hole and electrons are not only the highest values, but also show nearly equivalent hole and electron transport properties. Moreover, ***$P_5$*** *constitutes the first example of a triple bond containing polymer presenting ambipolar charge transport characteristics.* Consequently, it was shown that, incorporating ethynylene π-spacers in π-conjugated systems is an effective strategy for tuning charge transport characteristics. Hence, D-A type copolymers can function as p-type, or ambipolar semiconductor depending on the connection mode between the donor and the acceptor units.

## 2.4.2.5. References

*1*. Dieck, H. A.; Heck, R. F. *J. Organomet. Chem.* **1975**, *93*, 259.

*2*. Sauvé, J.; Javier, A. E.; Zhang, R.; Liu, J.; Sydlik, S. A.; Kowalewski, T.; McCullough, R. D. *J. Mater. Chem.* **2010**, *20*, 3195.

*3*. Francke, V.; Mangel, T.; Müllen, K. *Macromolecules* **1998**, *31*, 2447.

*4*. Tamao, K.; Sumitani, K.; Kumada, M. *J. Am. Chem. Soc.* **1972**, *94*, 4374.

*5*. (a) Rehan, M.; Schlüter, A. -D.; Feast, W. J. *Synthesis* **1988**, 386. (b) Bao, Z.; Chan, W.; Yu, L. *Chem. Mater.* **1993**, *5*, 2.

*6*. (a) Cassar, I. *J. Organomet. Chem.* **1975**, *93*, 253. (b) Sonogashira, K.; Tohda, Y.; Hagihara, N. *Tetrahedron Lett.* **1975**, *16*, 4467.

*7*. Valverde, I. E.; Delmas, A. F.; Aucagne, V. *Tetrahedron* **2009**, *65*, 7597.

*8*. Frahn, J.; Karakaya, B.; Schäfer, A.; Schlüter A. *Tetrahedron* **1997**, *53*, 15459.

*9*. (a) Young, J. K.; Moore, J. S. *„Modern Acetylene Chemistry"* Stang, P.J.; Diederich, F. Eds.; CH: Weinheim, Germany, **1995**, *p.* 415. (b) Bunz, U. H. F. *Chem. Rev.* **2000**, *100*, 1605.

*10*. (a) Swager, T. M.; Gil, C. J.; Wrighton, M. S. *J. Phys. Chem.* **1995**, *99*, 4886. (b) Ofer, D.; Swager T. M.; Wrighton. M. S. *Chem. Mater.* **1995**, *7*, 418.

*11*. Wilson, J. N.; Windscheif, P. M.; Evans, U.; Myrick, M. L.; Bunz, U. H. F. *Macromolecules* **2002**, *35*, 8681.

*12*. Pschirer, N. G.; Bunz, U. H. F. *Macromolecules* **2000**, *33,* 3961.

*13*. Lide, D. R. *"Handbook of Chemistry and Physics"*, 75$^{th}$, Boca Raton, FL: CRC Press, **1994**.

*14*. (a) Schumm, J. S.; Pearson, D. L.; Tour, J. M. *Angew. Chem.* **1994**, *33*, 1360. (b) Huang, S. L.; Tour, J. M. *J. Am. Chem. Soc.* **1999**, *121*, 4908.

*15*. Francke, V.; Mangel, T.; Müllen, K. *Macromolecules* **1998**, *31*, 2447.

*16*. (a) Cotts, P. M.; Swager, T. M.; Zhou, Q. *Macromolecules* **1996**, *29*, 7323. (b) Socci, E. P.; Farmer, B. L.; Adams, W. W. *J. Polym. Sci., Polym. Phys. Ed.* **1993**, *31*, 1975.

*17*. (a) Ashraf, R. S.; Gilot, J.; Janssen, R. A. J. *Sol. Energ. Mat. Sol. Cells*, **2010**, *94*, 1759. (b) Popere, B. C.; Della Pelle, A. M.; Thayumanavan, S. *Macromolecules* **2011**, *44*, 4767. (c) Donuru, V. R.; Vegesna, G. K.; Velayudham, S.; Green, S.; Liu, H. *Chem. Mater.* **2009**, *21*, 2130.

*18*. (a) Hotta, S.; Rughooputh, D. D. V.; Heeger, A. J.; Wudl, F. *Macromolecules* **1987**, *20*, 212. (b) Rughooputh, D. D. V.; Hotta, S.; Heeger, A. J. *J. Polym. Sci.* **1987**, *25B*, 1071. (c) Lee, D. C.; Sahoo, S. K.; Cholli, A. L.; Sandman, D. J. *Macromolecules* **2002**, *35*, 4347.

*19*. (a) Apperloo, J. J.; Janssen, R. A. J.; Malenfant, P. R. L.; Frechet, J. M. J. *Macromolecules* **2000**, *33*, 7038. (b) Miteva, T.; Palmer, L.; Kloppenburg, L.; Neher, D.; Bunz, U. H. F. *Macromolecules* **2001**, *33*, 652.

*20*. Ashraf, R. S.; Klemm, E. *J. Polym. Sci. Part A*, **2005**, *43*, 6445

*21*. (a) Kasha, M.; Rawls, H.R.; El-Bayoumi, M. A. *Pure Appl. Chem.* **1965**, *11*, 371. (b) Kuhn, H.; Kuhn, C. *"Chromophore coupling effects*" Singapore: World Scientific; **1996**, *p.* 1.

*22*. Moliton, A.; Hiorns, R. C. *Polym. Int.* **2004**, *53*, 1397.

*23*. Kaner, R. B.; Porter, S. J.; Nairns, D. P.; MacDiarmid, A. G. *J. Chem. Phys.* **1989**, *90*, 5102.

*24*. Egbe, D. A. M.; Bader, C.; Nowotny, J.; Günther, W.; Klemm, E. *Macromolecules* **2003**, *36*, 5459.

*25*. Mühlbacher, D. *"Comparative studies of electrochemical bandgap with optical bandgap of organic semiconductors"* Diploma thesis. Linz, Austria: Johann Kepler University; **2002**.

*26*. Sariciftci, N. S. *"Primary Photoexcitations in Conjugated Polymers: Molecular Excitons vs. Semiconductor Band Mode"*; World Scientific: Singapore, **1997**.

*27*. (a) Boudreault, P. L. T.; Najari, A.; Leclerc, M. *Chem. Mater.* **2011**, *23*, 456. (b) Liang, Y.; Yu, L. *Acc. Chem. Res.* **2010**, *43*, 1227. (c) Chen, J.; Cao, Y. *Acc. Chem. Res.* **2010**, *43*, 1709. (c) Cheng, Y. J.; Yang, S. H.; Hsu, C. S. *Chem. Rev.* **2009**, *109*, 5868.

*28*. (a) Yu, G.; Gao, J.; Hummelen, J. C.; Wudl, F.; Heeger, A. J. *Science* **1995**, *270*, 1789. (b) Wienk, M. M.; Kroon, J. M.; Verhees, W. J. H.; Knol, J.; Hummelen, J. C.; van Hal, P. A.; Janssen, R. A. J. *Angew. Chem., Int. Ed.* **2003**, *42*, 3371.

*29*. Mihailetchi, V. D.; van Duren, J. K. J.; Blom, P. W. M.; Hummelen, J. C.; Janssen, R. A. J.; Kroon, J. M.; Rispens, M. T.; Verhees, W. J. H.; Wienk, M. M. *Adv. Funct. Mater.* **2003**, *13*, 43.

*30*. Yang, X.; van Duren, J. K. J.; Rispens, M. T.; Hummelen, J. C.; Janssen, R. A. J.; Michels, M. A. J.; Loos, *J. Adv. Mater.* **2004**, *16*, 802.

*31*. McNeill, C. R.; Greenham, N. C. *Adv. Mater.* **2009**, *21*, 3840.

*32*. (a) Mikroyannidis, J. A.; Kabanakis, A. N.; Sharma, S. S.; Sharma, G. D. *Adv. Funct. Mater.* **2011**, *21*, 746; (b) Mikroyannidis, J. A.; Tsagkournos, D. V.; Sharma, S. S.; Sharma, G. D. *J. Phys. Chem. C* **2011**, *115*, 7806; (c) Varotto, A.; Treat, N. D.; Jo, J.; Shuttle, C. G.; Batara, N. A.; Brunetti, F. G.; Seo, J. H.; Chabinyc, M. L.; Hawker, C. J.; Heeger, A. J.; Wudl, F. *Angew. Chem., Int. Ed.* **2011**, *50*, 5166.

*33*. (a) Rajaram, S.; Armstrong, P. B.; Kim, B. J.; Frechet, J. M. *J. Chem. Mater.* **2009**, *21*, 1775; (b) Sharma, G. D.; Suresh, P.; Mikroyannidis, J. A.; Stylianakis, M. M. *J. Mater. Chem.* **2010**, *20*, 561.

*34*. (a) Schwenn, P. E.; Gui, K.; Nardes, A. M.; Krueger, K. B.; Lee, K. H.; Mutkins, K.; Rubinstein-Dunlop, H.; Shaw, P. E.; Kopidakis, N.; Burn, P. L.; Meredith, P. *Adv. Energy Mater.* **2011**, *1*, 73; (b) Zhou, Y.; Pei, J.; Dong, Q.; Sun, X.; Liu, Y.; Tian, W. *J. Phys. Chem. C* **2009**, *113*, 7882.

*35*. (a) Shin, R. Y. C.; Kietzke, T.; Sudhakar, S.; Dodabalapur, A.; Chen, Z. -K.; Sellinger, A. *Chem. Mater.* **2007**, *19*, 1892; (b) Woo, C. H.; Holcombe, T. W.; Unruh, D. A.; Sellinger, A.; Frechet, J. M. *J. Chem. Mater*. **2010**, *22*, 1673.

*36*. (a) Yu, G.; Heeger, A. J. *J. Appl. Phys.* **1995**, *78*, 4510. (b) Offermans, T.; van Hal, P. A.; Meskers, S. C. J.; Koetse, M. M.; Janssen, R. A. J. *Phys. Rev. B* **2005**, *72*, 045213. (c) Yin, C.; Kietzke, T.; Neher, D.; Hörhold, H.-H. *Appl. Phys. Lett.* **2007**, *90*, 092117.

*37*. (a) Kötse, M. M.; Sweelssen, J.; Hoekerd, K. T.; Schoo, H. F. M.; Veenstra, S. C.; Kroon, J. M.; Yang, X.; Loos, J. *Appl. Phys. Lett.* **2006**, *88*, 083504; (b) Veenstra, S. C.; Loos, J.; Kroon, J. M.; *Prog. Photovolt.: Res. Appl.* **2007**, *15*, 727; (c) McNeill, C. R.; Abrusci, A.; Zaumseil, J.; Wilson, R.; McKiernan, M. J.; Halls, J. J. M.; Greenham, N. C.; Friend, R. H. *Appl. Phys. Lett.* **2007**, *90*, 193506.

*38*. Falzon, M. -F.; Wienk, M. M.; Janssen, R. A. J. J. *Phys. Chem. C* **2011**, *115*, 3178.

*39*. Veldman, D.; Meskers, S. C. J.; Janssen, R. A. J. *Adv. Funct. Mater.* **2009**, *19*, 1939.

*40*. Gueymard, C. A. *Sol. Energy* **2004**, *76*, 423.

*41*. Mandoc, M. M.; Veurman, W.; Koster, L. J. A.; Koetse, M. M.; Sweelssen, J.; de Boer, B.; Blom, P. W. M. *J. Appl. Phys.* **2007**, *101*, No. 104512.

*42*. Lenes, M.; Morana, M.; Brabec, C. J.; Blom, P. W. M. *Adv. Funct. Mater.* **2009**, *19*, 1106.

*43*. (a) Mandoc, M. M.; Veurman, W.; Sweelssen, J.; Koetse, M. M.; Blom, P. W. M. *Appl. Phys. Lett.* **2007**, *91*, 073518. (b) McNeill, C. R.; Westenhoff, S.; Groves, C.; Friend, R. H.; Greenham, N. C. *J. Phys. Chem. C* **2007**, *111*, 19153.

*44*. Lampert, M. A.; Mark, P. *"Current Injection in Solids"* Academic Press, New York **1970**

*45*. Tiwari, S.; Greenham, N. C. *Opt. Quant. Electron* **2009**, *41*, 69.

*46*. (a) Kitamura, M.; Imada, T.; Kako, S.; Arakawa, Y. *Jpn. J. Appl. Phys.* **2004**, *43*, 2326. (b) Shirota, Y.; Okumoto, K.; Ohishi, H.; Tanaka, M.; Nakao, M.; Wayaku, K.; Nomura, S.; Kageyama, H. *Proceedings of SPIE-International Society Optical Engineering* **2005**, *5937*, 593717.

*47*. (a) Kimura, M.; Inoue, S.; Shimada, K.; Tokito, S.; Noda, K.; Taga, Y.; Sawaki, Y. *Chem. Lett.* **2000**, 192. (b) Saragi, T. P. I.; Fuhrmann-Lieker, T.; Salbeck, J. *Adv. Funct. Mater.* **2006**, *16*, 966.

*48*. Brabec, C. J.; Dyakonov, V.; Scherf, U. *"Organic Photovoltaics"* **2008** Wiley-VCH.

*49*. (a) Singh, T. B.; Marjanovic, N.; Stadler, P.; Auinger, M.; Matt, G. J.; Gunes, S.; Sariciftci, N. S. *J. Appl. Phys.* **2005**, *97*, 083714. (b) Cho, S.; Seo, J. H.; Lee, K.; Heeger, A. J. *Adv. Funct. Mater.* **2009**, *19*, 1.

*50*. Facchetti, A.; Yoon, M. H.; Marks, T. J. *Adv. Mater.* **2005**, *17*, 1705.

*51*. Bäuerle, P.; Pfau, F.; Schlupp, H.; Würthner, F.; Gaudl, K. U.; Balparda Caro, M.; Fischer, P. *J. Chem. Soc. Perkin Trans. 2* **1993**, *3*, 489.

*52*. Wilson, J. N.; Windscheif, P. M.; Evans, U.; Myrick, M. L.; Bunz, U. H. F. *Macromolecules* **2002**, *35*, 8681.

*53*. Apperloo, J. J.; Janssen, R. A. J.; Malenfant, P. R. L.; Frechet, J. M. J. *Macromolecules* **2000**, *33*, 7038.

*54*. Egbe, D. A. M.; Carbonnier, B.; Birckner, E.; Grummt, U. -W. *Prog. Polym. Sci.* **2009**, *34*, 1023.

*55*. Ding. L.; Egbe, A. A. M.; Karasz, F. E. *Macromolecules* **2004**, *37*, 6124.

*56*. (a) Yamamoto, T.; Lee, B. L. *Macromolecules* **2002**, *35*, 2993; (b) Egbe, D. A. M.; Nguyen, L.H.; Hoppe, H.; Mühlbacher, D.; Sariciftci, N. S. *Macromol. Rapid. Commun.* **2005**, *26*, 1389.

*57*. Kim, H.; Jin, S. H.; Suh, H.; Lee, K. *Proc. SPIE* **2004**, *5215*, 111.

*58*. (a) McGehee, M. D.; Heeger, A. J. *Adv. Mater.* **2000**, *12*, 1655; (b) Kumar, P.; Mehta, A.; Mahurin, S. M.; Dai, S.; Dadmun, M. D.; Sumpter, B. G. , *et al. Macromolecules* **2004**, *37*, 6132.

*59*. (a) Sirringhaus, H. *Adv. Mater.* **2005**, *17*, 2411. (b) Kline, R. J.; McGehee, M. D. *Polym. Rev.* **2006**, *46*, 27. (c) Surin, M.; Leclere, P.; Lazzaroni, R.; Yuen, J. D.; Wang, G.; Moses, D.; Heeger, A. J.; Cho, S.; Lee, K. *J. Appl. Phys.* **2006**, *100*, 33712.

*60*. (a) Chang, J.-F.; Sun, B.; Breiby, D. W.; Nielsen, M. M.; Sölling,T. I.; Giles, M.; McCulloch, I.; Sirringhaus, H. *Chem. Mater.* **2004**, *16*, 4772. (b) Yang, H.; Shin, T. J.; Yang, L.; Cho, K.; Ryu; C. Y.; Bao, Z. *Adv. Funct. Mater.* **2005**, *15*, 671.

*61*. Farral, G. A. *"Electrical Breakdown in Vacuum"* Lafferty J. M. Eds. John Wiley & Sons, New York, **1980**, *p.*28.

*62*. Verlaak, S.; Arkhipov, V.; Heremans, P. *Appl. Phys. Lett.* **2003,** *82*, 745.

*63*. Tsao, H. N.; Müllen, K. *Chem. Soc. Rev.* **2010**, *39*, 2372.

*64*. Zhang, R.; Iovu, M. C.; Jeffries-EL, M.; Sauvé, G.; Cooper, J.; Jia, S.; Tristam-Nagle, S.; Smilgies, D. M.; Lambeth, D. N.; McCullough, R. D.; Kowalewski, T. *J. Am. Chem. Soc.* **2006**, *128*, 3480.

*65*. (a) Zhang, M.; Tsao, H. N.; Pisula, W.; Yang, C.; Mishra, A. K.; K. Müllen, K. *J. Am. Chem. Soc.* **2007**, *129*, 3472. (b) Liu, J.; Zhang, R.; Sauvé, G.; Kowalewski, T.; McCullough, R. D. *J. Am. Chem. Soc.* **2008**, *130*, 13167.

# 3. Mixed-Valence Phenothiazines: Poly [(*N*-Alkyl Phenothiazine)-*alt*-(Benzo[*c*][2,1,3]thiadiazole)] and its Model Compounds

## 3.1. Introduction

Since the first report on its synthesis in 1883 by Bernthsen,[1] phenothiazine (**Ptz**) has become a major building block in fundamental as well as applied chemical research. Its derivatives have earned their place in the dye[2] and especially pharmaceutical industry[3] as neuroleptic antipsychotic drugs in the treatment of mental disorders such as Parkinson's syndrome, schizophrenia or Alzheimer's disease.[4] Furthermore, the unique electro- and optical properties that characterize **Ptz** containing small molecules and polymers are increasingly explored in the view of their potential application in organic light emitting diods (OLEDs),[5] organic photovoltaic devices (OPVs)[6] and chemiluminescence.[7]

Phenothiazines in their electronic ground state are characterized by an inherent butterfly conformation.[8] The molecule becomes planar in the optical excited state yielding considerable Stokes shifts that are tunable *via* the substitution pattern of the **Ptz**.[9] In close connection one of the most explored properties of **Ptz** derivatives is their reversible oxidation that generates stable, planar cation radicals and dications.[10] Furthermore, phenothiazine shows sizable reorganization energy, ascribed to the conformational changes that occur upon oxidation.

The pioneer work of Bard[11] on the intermolecular electron transfer (ET) process between the parent phenothiazine donor and its cation radical ($(\mathbf{PtzH})_2^{\bullet+}$, Chart 12) triggered a larger

general interest to understand these peculiar systems in more detail. Within this context, Baumgarten and co-workers[12] delivered the first experimental proof of the violation of the topology rule,[13] by finding a singlet ground state in *m*-phenylene-diphenothiazine dication (**Ptz**$^{2+}$**P**(***m***)) and a triplet ground state in *p*-phenylene-diphenothiazine dication (**Ptz**$^{2+}$**P**(***p***)). The inter- and intramolecular ET between π-bridged mixed-valence **Ptz** centers (**Ptz**$^{\bullet+}$**P**(***p***), **Ptz**$^{\bullet+}$**P**(***o***)), within the Mulliken-Hush two-state model[14] was outlined by Kochi (Chart 12).[15] The good agreement of the experimental and theoretically predicted values of the activation barrier and ET rates between the **Ptz** / **Ptz**$^{\bullet+}$ centers indicated that the Marcus-Hush theory,[16] in combination with the two state model of Mulliken-Hush, suitably describe the inter- and intramolecular ET rates, if the electronic coupling between the two redox centers is taken into account. Note that for all the π-bridged mixed-valence **Ptz** derivatives explored, a considerable dihedral angle (approx. 80-90$^0$) between the π-bridge and the plane of **Ptz** was found.

**Chart 12.** Studied mixed-valence systems for inter- and intramolecular self exchange between phenothiazine redox centers.

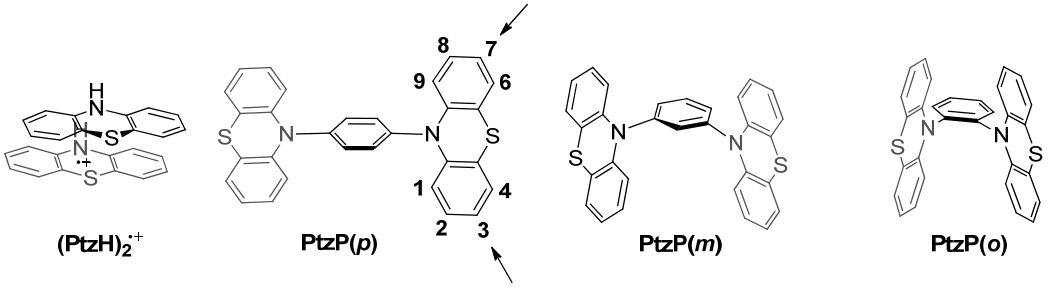


The major part of the research was directed towards the study of the mixed-valence **Ptz** centers when connected by a π-bridge *via* its aromatic nitrogen.[17] However, the availability of synthetic procedures for the introduction of one or multiple π-bridges, at positions 3 and / or 7 (Chart 12, **PtzP**(***p***)), enables the investigation of **Ptz** based mixed-valence systems with increased distance between the redox centers. Moreover, the spin interaction through the π-conjugation could be increased by reducing the steric hindrance between the redox centers and the π-bridge. By far the most scrutinized molecular π-bridge, connecting mixed-valence redox centers, is phenyl.[18] Examples of electron deficient π-bridges in a cation radical are

scarce apart from anthracene. However, the anthracene containing systems were still suffering from considerable steric interactions.

To study the intramolecular self exchange between **Ptz** redox centers over a larger distance, the π-bridge has been introduced at the position 3 of the **Ptz** core. Furthermore, the influence of an electron deficient π-bridge on the intramolecular self exchange can be evaluated by introducing benzo[*c*][2,1,3]thiadiazole (**BT**) as a π-bridge. Therefore, model compounds and their corresponding polymer were synthesized and characterized.

# 3.2. Intramolecular Self-Exchange between Phenothiazine Redox Centers Bridged by Benzo[*c*][2,1,3]thiadiazole

## 3.2.1. Synthesis

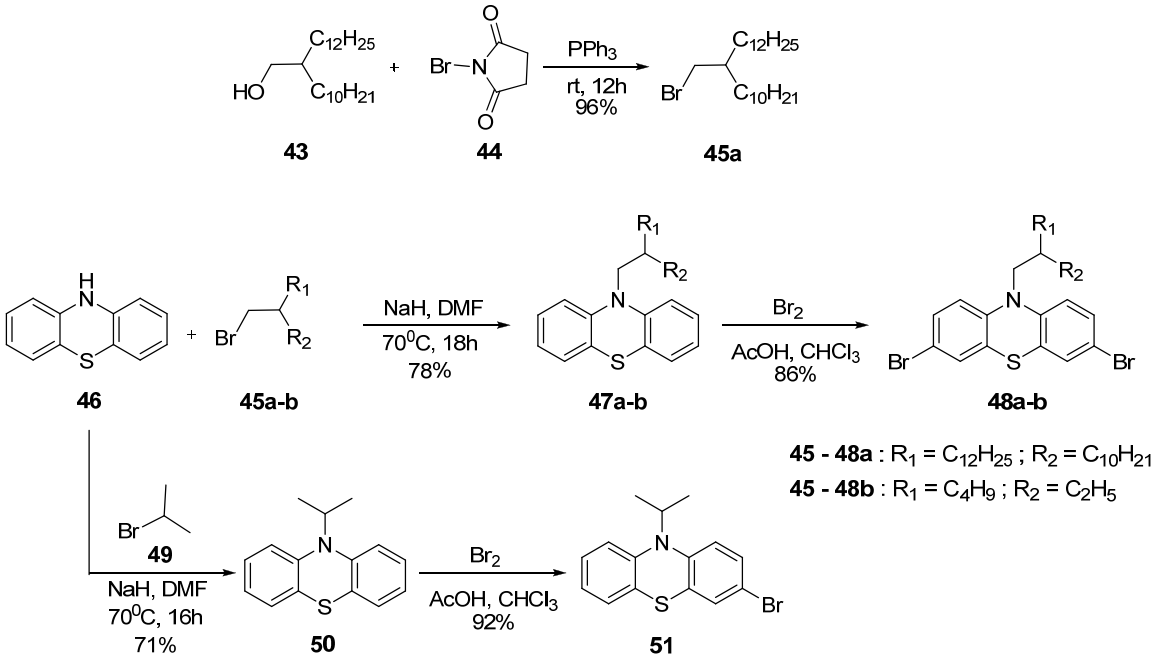


**Scheme 22.** Synthesis of 3,7-dibromo-10-(alkyl)-10*H*-phenothiazine (**48a-b**) and mono-bromo-10-(isopropyl)-10*H*-phenothiazine (**51**).

The N-alkyl phenothiazine was obtained through the reaction of unsubstituted phenothiazine (**46**) with alkyl halides in a basic medium, using sodium hydride (NaH) as base (Scheme 22).[19] Long, branched alkyl chains were attached to the phenothiazine core (**47a**) in order to ensure a good solubility as well as a high molecular weight of the corresponding polymer. Ethylhexyl (**47b**) and isopropyl (**50**) functionalized **Ptz** were synthesized to be incorporated in the model compounds. The obtained N-alkylated phenothiazines **47a-b** and **50** were subjected to di- and mono-bromination, respectively, in glacial acetic acid[20] leading to the desired precursors for the subsequent *Suzuki* cross-coupling,[21] **48a-b** and **51**. The purity of the **Ptz** precursors was probed by NMR spectroscopy as well as HRMS spectrometry.

The synthesis of the model compounds and polymers under *Suzuki* cross-coupling conditions required the synthesis of mono- and di-borylated benzothiadiazole coupling partners (**53a-b**, Scheme 23). While the dibromination of benzothiadiazole (**2b**) was carried out nearly quantitatively, in the presence of $Br_2$ and HBr, the mono-brominated derivative (**2a**) was isolated after steam distillation followed by recrystallization from ethanol in 38 % yield.[22] Next, **2a-b** were converted to the corresponding boronate esters **53a-b** via a palladium ($Pd(dppf)Cl_2$) catalyzed reaction with bis(pinacolato)diboron (**52**).[23] The pure compounds **53a-b** were isolated after column chromatography followed by recrystallization from hexane and confirmed by NMR spectroscopy and HRMS spectrometry. The high purity of the monomers is essential for an efficient *Suzuki* cross-coupling polymerization reaction[24] in combination with a their strict 1 : 1 stoichiometric ratio.

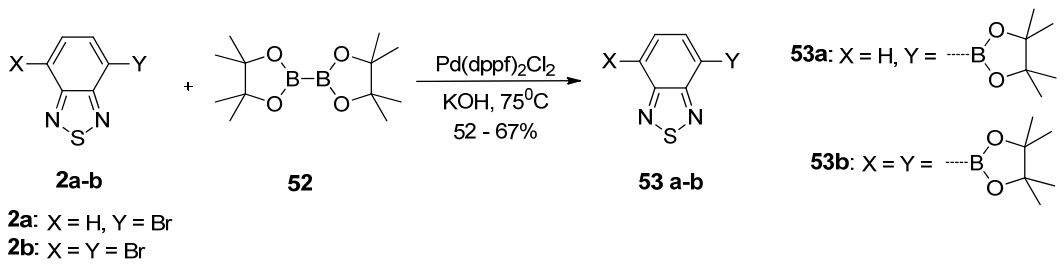


**Scheme 23.** Synthesis of 4,4,5,5-tetramethyl-1,3,2-dioxaborolan functionalized benzo[*c*][2,1,3]thiadiazole derivatives **53a-b**.

With the required reactants, halogenated phenothiazines (**48b**, **51**) and borylated benzothiadiazoles (**53a-b**), in hand, two different model compounds were synthesized. The

first triad containing only one alkylated **Ptz** anchored by two **BT** units (**M1**, Scheme 24), and the second designed to combine the **BT** segment, as a molecular π-bridge connecting two phenothiazines (**M2**, Scheme 25).

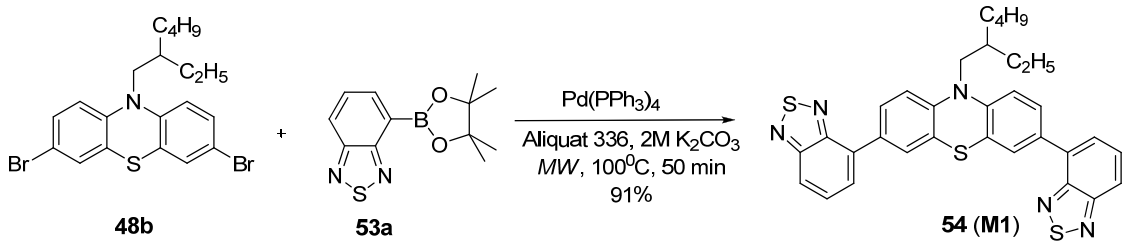


**Scheme 24.** Synthesis of 3,7-di(benzo[*c*][2,1,3]thiadiazol-4-yl)-10-(2-ethylhexyl)-10*H*-phenothiazine (**M1**).

The model compounds were obtained *via* Pd(0) catalyzed *Suzuki* cross-coupling reaction, performed under microwave irradiation (*MW*). The major benefit of the microwave irradiation is an efficient internal heating (bulk heating),[25] which translates into excellent reaction yields in short reaction times. **M1** was isolated as a yellow powder and **M2** as a red powder subsequent to a 50 min *MW* irradiation at 100$^0$C of their corresponding starting materials, as described in Schemes 24 and 25, respectively.

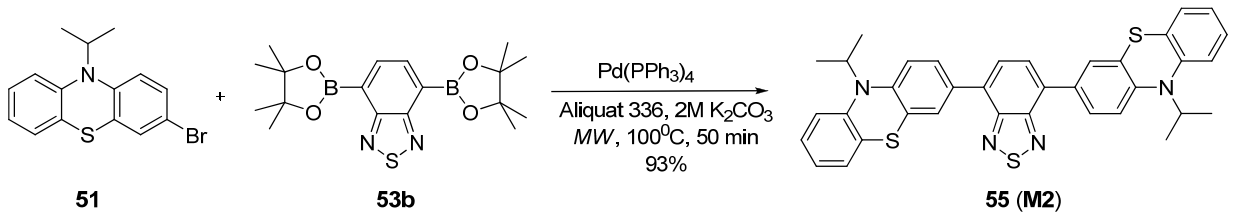


**Scheme 25.** Synthesis of 4,7-bis(10-isopropyl-10*H*-phenothiazin-3-yl)benzo[*c*][2,1,3]thiadiazole (**M2**).

Both structures were unambiguously assigned by $^1$H and $^{13}$C-NMR, IR spectroscopy and HRMS. The NMR spectra clearly support the highly symmetrical structure of both **M1** and **M2** by the appearance of a half set of aromatic resonances with respect to the actual number of nuclei. In case of **M1**, consisting of only one **Ptz** core functionalized with 2-ethylhexyl at its N atom, the signal corresponding to the alkyl proton of the tertiary *C* atom was in a 1 : 2 relation relative to the aromatic proton signals.

Having established the conditions for the *Suzuki* cross-coupling reaction mediated by *MW* irradiation, the attention turned towards the synthesis of the corresponding alternating donor-acceptor polymer (poly(**Ptz-BT**)**a**, Scheme 26) *via* the polycondensation of the monomers **48a** and **53b**. In a standard procedure, a 35 mL vial was charged with **48a** and **53b** dissolved in the smallest amount of toluene possible. To this solution, 12 equiv. of $K_2CO_3$ were added as a 2M aqueous solution and a few drops of Aliquat 336 as a phase transfer catalyst. The biphasic system was degassed with an argon stream for approx. 20 min after which a catalytic amount of $Pd(PPh_3)_4$ was added. The vial was sealed and placed in the microwave oven. The reaction mixture typically reached $100^0$C in approx. 1 min subsequent to which the polymerization was allowed to proceed for 50 min. The end-capping of the polymer was realized by adding 5 equiv. of bezene-boronic acid dissolved in toluene alongside with another 5 mol % of Pd catalyst, while constantly maintaining an argon stream. This mixture was then reacted under *MW* irradiation for 20 min at $100^0$C. In the last step, 10 equiv. of bromobenzene toluene solution were added to the polymer solution and let to react under the conditions described above.

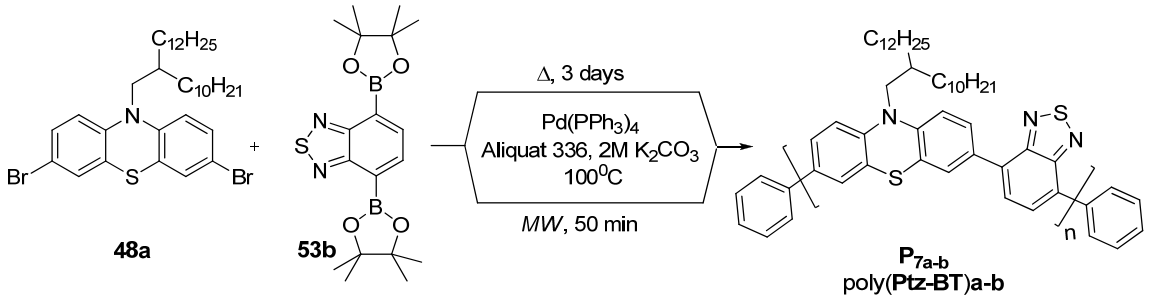


**Scheme 26.** Synthesis poly(N-alkyl-phenothiazine)-*alt*-benzo[*c*][2,1,3]thiadiazole poly(**Ptz-BT**)**a**-**b**.

A very important issue in case of polymers with an application prospect is their purity. To ensure a good performance the purity should be as high as possible, since impurities could be trapping sites and inhibit the charge carrier mobility in organic devices.[26] Small molecules have the advantage of "easy" purification by column chromatography, sublimation,[27] recrystallization, etc.[28] On the contrary, for polymeric materials the available purification techniques are somewhat limited. Repeated precipitation from different solvents[29] accompanied by treatment with different neutralizing agents, such as sodium diethyldithiocarbamate trihydrate[30] or sodium cyanide[31] is customarily employed to remove

the metal catalyst from the polymer mixture. Apart from the above mentioned procedures, metal organic frameworks (MOFs)[32] are believed to perform effectively in the purification of polymers. Nonetheless, the purification of the obtained poly(**Ptz-BT**)**a** was carried out by two fold washing of the polymer solution with 100 mL 1% NaCN aqueous solution. After drying and concentrating the organic phase, the polymer was slowly precipitated from methanol. The precipitation was repeated three times in methanol and acetone. Furthermore, the polymer was subjected to Soxhlet extraction with methanol, acetone and chloroform in order to remove the low molecular weight fractions.

During the course of these investigations the synthesis of a similar **Ptz** containing polymer, functionalized with octyl alkyl chains, has been reported with a quite low number average molecular weight of 3600 g $mol^{-1}$ (*PDI* = 1.62) relative to *PS*.[33] The authors chose to introduce the boronic acid functionalities at the phenothiazine core. The electron rich coupling partner bearing the boronic acid functionalities is typically expected to result in an efficient coupling of a donor with an acceptor *via* a *Suzuki* polycondensation. The author's approach is supposed to have mechanistic advantages since the polymerization involves a base that causes the cleavage of the boronate and subsequent nucleophilic attack to the aryl palladium species. Hence, it is comprehensible that an electron rich coupling partner forming the anion would lead to a more efficient reaction. However, in case of strong donors, such as thiophene derivatives, hydrolytic deboronation may limit the formation of high molecular weight polymers.[34] Furthermore, a stoichiometric imbalance could also result in reduced molecular weight polymers.[24]

An identical polymer was synthesized by conventional conductive heating (poly(**Ptz-BT**)**b**, Scheme 26), following a synthetic procedure recently described by Don Cho.[35] The monomer batches used for the previous method were employed here as well, so as to be able to evaluate the benefits and / or drawbacks of the *MW* mediated *vs.* conventional conductive heating promoted polymerization reaction. The polycondensation reaction was allowed to proceed for 3 days, in order to ensure the consumption of the starting materials and a high molecular weight of the desired product. The end-capping was carried out using the same bezene derivatives adding 12 h for each end-capping step to the reaction time.

Finally, the isolation of the polymer poly(**Ptz-BT**)**b** was achieved subsequent to the work up and purification procedure described above.

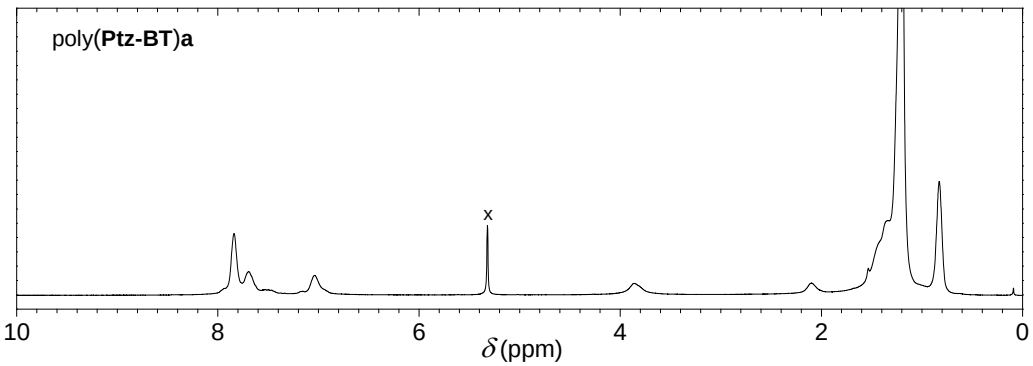


**Figure 57.** $^{1}$H-NMR registered in $CD_2Cl_2$ at r.t., at 300 MHz of poly(**Ptz-BT**)**a**.

The two polymers obtained *via* the two different synthetic procedures were characterized independently. Their structure was validated by $^{1}$H-NMR and $^{13}$C-NMR spectroscopy. The good solubility of both polymer batches in common organic solvents such as THF, $CHCl_3$, DCM or toluene allowed the registration of the $^{1}$H and $^{13}$C-NMR in $CD_2Cl_2$ at room temperature. Both poly(**Ptz-BT**)**a** and poly(**Ptz-BT**)**b** revealed the same number of proton and carbon signals, confirming their identical structure. As expected, the aromatic region (between 7 and 8.2 ppm) of the $^{1}$H-NMR (Figure 57) consisted of three signals being in a 1 : 1 : 2 ratio, corresponding to the 3 times 2 equivalent protons of the phenothiazine core and the 2 equivalent protons of the benzothiadiazole. The alkyl region exhibited a signal at 3.9 ppm related to the protons in α-position to the methyl bridge of the **Ptz** unit, a second signal of the proton in β-position to the same bridge at 2.1 ppm, a third broad signal between 1 ppm and 1.6 ppm arising from the inner protons of the branched alkyl chain, and finally one last signal of the terminal methyl protons.

The difference between poly(**Ptz-BT**)**a** and poly(**Ptz-BT**)**b**, if any, must lay in their molecular weight distribution. Therefore, the relative molecular weights were calculated based on GPC measurements (Figure 58). The attainable number average molecular weight ($M_n$) achieved under *MW* promoted polycondensation for poly(**Ptz-BT**)**a** was 12700 g mol$^{-1}$ (in THF, at 30$^{0}$C) relative to *PPP* with a *PDI* of 1.20. Under identical measurement conditions,

poly(**Ptz-BT**)**b** displayed a somewhat lower $M_n$ = 8000 g mol$^{-1}$ *vs. PPP* and a slightly higher *PDI* = 1.37. It is evident that apart from the significantly shorter reaction times, the *MW* assisted polycondensation offered higher molecular weights and a narrower molecular weight distribution.

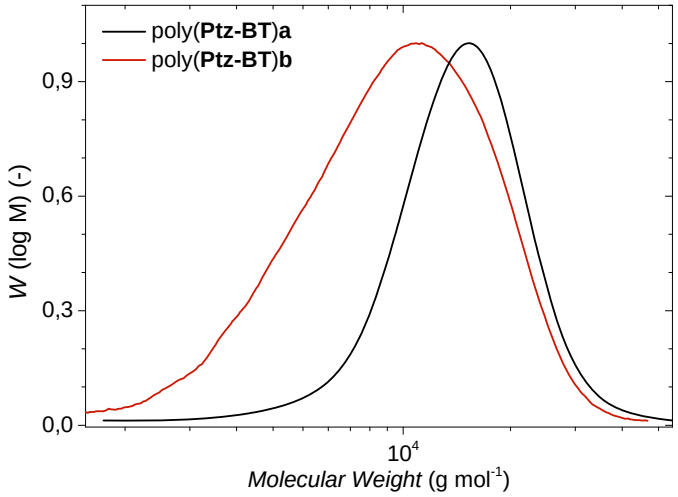


**Figure 58.** GPC curves of poly(**Ptz-BT**)**a-b** as registered in THF at 30$^0$C.

## 3.2.2. Electronic Properties: UV-Vis absorption, Steady State Fluorescence and Cyclic Voltammetry

Phenothiazine derivatives with extended π-conjugation are in general redox-active as well as highly emissive functional π-electron systems.[36] Hence, it is important to investigate the electronic properties of the neutral synthesized model compounds **M1** and **M2** and elucidate the differences between an A-D-A (**M1**) and a D-A-D (**M2**) architecture. Furthermore, the obtained data could be correlated with the properties of their corresponding polymer poly(**Ptz-BT**). The electronic properties could be scrutinized experimentally by studying the ground state properties *via* UV-Vis absorption spectroscopy

and cyclic voltammetry. Information about the excited state could be collected by means of steady state fluorescence spectroscopy.

Both model compounds were subjected to optical spectroscopic studies including UV-Vis absorption and fluorescence spectroscopy. These measurements were recorded in solvents with different polarities and the results are illustrated in Figure 59 (**M1**) and Figure 60 (**M2**), respectively. The absorption of **M1**, in which the **Ptz** unit is flanked by two **BT** acceptor cores, was composed of two main absorption bands. The successful extension of the π-conjugation translated in extended absorption up to approx. 500 nm peaking at 430 nm in toluene. When going from hexane to toluene, a small 5 nm bathochromic shift of the long wavelength absorption maximum ($\lambda_{max}$) could be observed. Furthermore, this band was slightly broadened by a polar protic medium such as $^{i}$PrOH, without affecting its $\lambda_{max}$ = 425 nm relative to the non-polar hexane. The optical energy-gap ($E_{op}$), as extracted from the onset of the long wavelength absorption band, varied between 2.54 eV in case of hexane and 2.46 eV for chloroform (Table 11).

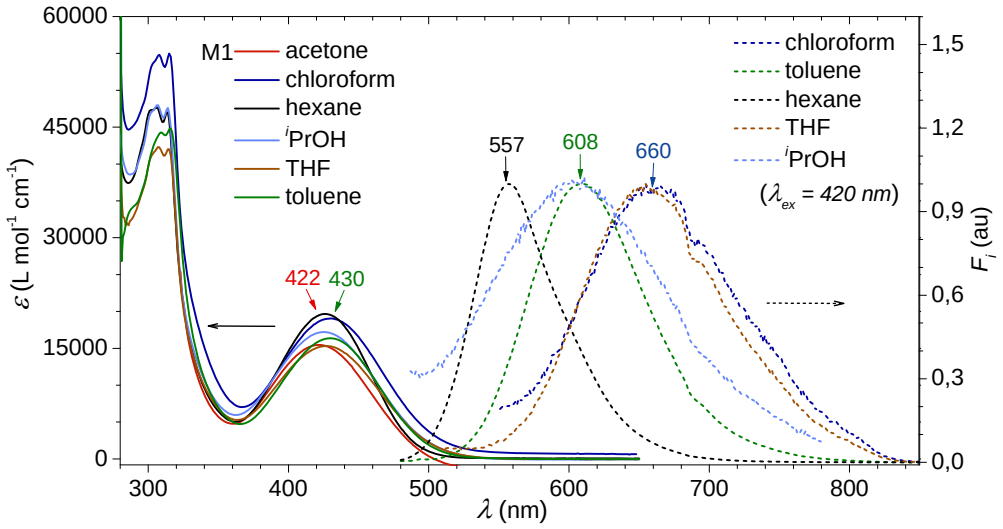


**Figure 59.** Solvent dependent UV-Vis absorption and steady state fluorescence of **M1** ($c$ = $10^{-5}$ mol $L^{-1}$).

While the solvent polarity seemed to have little effect on the absorption of **M1**, the situation was quite the opposite concerning the emission of this compound. An over 100 nm red shift of the emission maximum ($\lambda_{em}$) could be observed between the non-polar hexane ($\lambda_{em}$ = 557 nm) and chloroform ($\lambda_{em}$ = 660 nm). Placing **M1** in a polar media, such as acetone

or $^{i}$PrOH, resulted in decreased emission. The large bathochromic shifts are indicating that the molecule undergoes an intramolecular charge transfer upon photoexcitation.[37] Additionally, the large and increasing (from 5600 cm$^{-1}$ to 8400 cm$^{-1}$) *Stokes* shifts observed with increasing polarity is suggesting a higher dipole moment of **M1** in the excited state than in the ground state.[37] The solvent dependency of the emission maximum and *Stokes* shift is not unusual for **Ptz** with extended π-conjugated substitution patterns.[36, 38] These phenomena have been ascribed to conformational changes that occur upon excitation of the folded butterfly shaped phenothiazine,[8] resulting in a peculiar electronic structure of the excited state.

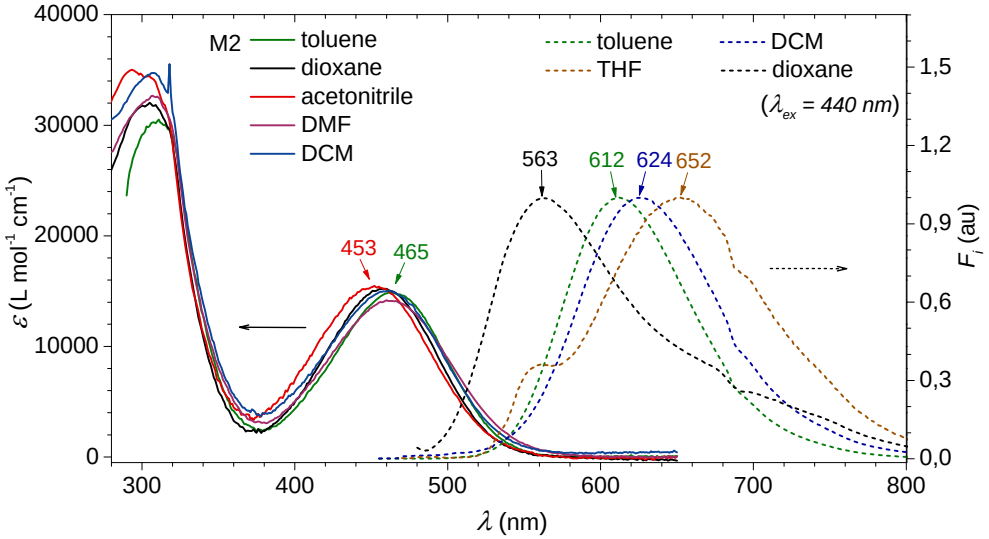


**Figure 60.** Solvent dependent UV-Vis absorption and steady state fluorescence of **M2** ($c$ = 10$^{-5}$ mol L$^{-1}$).

The evaluation of the photophysical properties of **M2** has been performed as well (Figure 60, Table 11). Unlike **M1**, **M2** was designed to have the **BT** core serving as a π-bridge between two **Ptz** units. In toluene, the long wavelength absorption maximum of this compound was 25 nm bathochromically shifted relative to **M1** implying an improved π-electron delocalization in **M2** *vs*. **M1**. This also reflected in the lower $E_{op}$ calculated to be in the range of 2.35-2.30 eV going from hexane to THF. Another fingerprint of the enhanced π-electron delocalization in **M2**, is the higher relative intensity of the long *vs.* the short wavelength absorption band ($\varepsilon_{\lambda max}^{s} / \varepsilon_{\lambda max}^{l} = 2$) in relation to **M1** ($\varepsilon_{\lambda max}^{s} / \varepsilon_{\lambda max}^{l} = 2.7$). However, **M2** presented similarly weak solvatochromism ($\Delta\lambda_{max}$ = 8 nm), as a result of a very weak charge transfer interaction between the **Ftz** and **BT** segments, in the ground state. The

situation was reversed in the excited state, as it is entailed by the strong solvent dependency of the emission. An almost 90 nm red shift was observed going from hexane to THF, accompanied by an increased *Stokes* shifts from 4000 $cm^{-1}$ to 6300 $cm^{-1}$. Placing **M2** in a highly polar medium, such as acetonitrile or DMF, led to the quenching of the fluorescence. All these solvent induced changes in the fluorescence imply a more planar excited state, characterized by an efficient charge transfer.

It has to be mentioned that similar diphenothiazine dumbbells expanded by π-conjugated arenes and heteroarenes have been recently reported by the group of Thomas J. J. Müller.[39] Apart from using donors, such as thiophene or fluorene, acceptors such as anthracene or perylene were also employed as π-bridges. As perylene is a stronger electron acceptor system than **BT**, one would expect that by incorporating it as a π-bridge between two **Ptz** units, would lead to a compound with lower energie-gap. However, due to steric hindrance disrupting the orbital overlap and the electronic transmission between the adjacent π-systems,[40] $\lambda_{max}$ was reported to be 468 nm as the highest value in the series. Nonetheless, all these compounds revealed similar excited state characteristics, as also observed in case of **M1** and **M2**. A considerable excited state electronic coupling was observed, as a consequence of the large structural and electronic distributional changes upon photoexcitation.[39]

The UV-Vis absorption and fluorescence of the poly(**Ptz-BT**)**a-b** polymer batches were evaluated in solution as well as in the solid state (Figure 61, Table 11). Poly(**Ptz-BT**)**a** and poly(**Ptz-BT**)**b**, which differ only in the number of their repeating units, presented virtually identical absorption and emission, both in solution and solid state. Therefore, it is reasonable to assume that at a molecular weight of $M_n \approx 8000$ g $mol^{-1}$, poly(**Ptz-BT**) reached the number of repeating units beyond which the photophysical properties are very little, if at all, affected. Hence, the following characterizations and the discussions related to the polymers are based on measurements performed on the batch with the higher number average molecular weight, poly(**Ptz-BT**)**a**, henceforth referred to as poly(**Ptz-BT**).

The absorption cross section of poly(**Ptz-BT**) was composed of two main bands, similar to its model compounds. The long wavelength absorption band, originating from the efficient D-A interaction was extended up to 560 nm with a $\lambda_{max} = 482$ nm, less than 20 nm bathochromically shifted relative to **M2** in dilute toluene solution. Furthermore, poly(**Ptz-BT**) revealed 2.23 eV energy-gap. The reduced red shift of $\lambda_{max}$ is somewhat surprising. For

example, bathochromic shifts extending 150 nm were reported for polythiophenes with respect to their corresponding oligomers.[41]

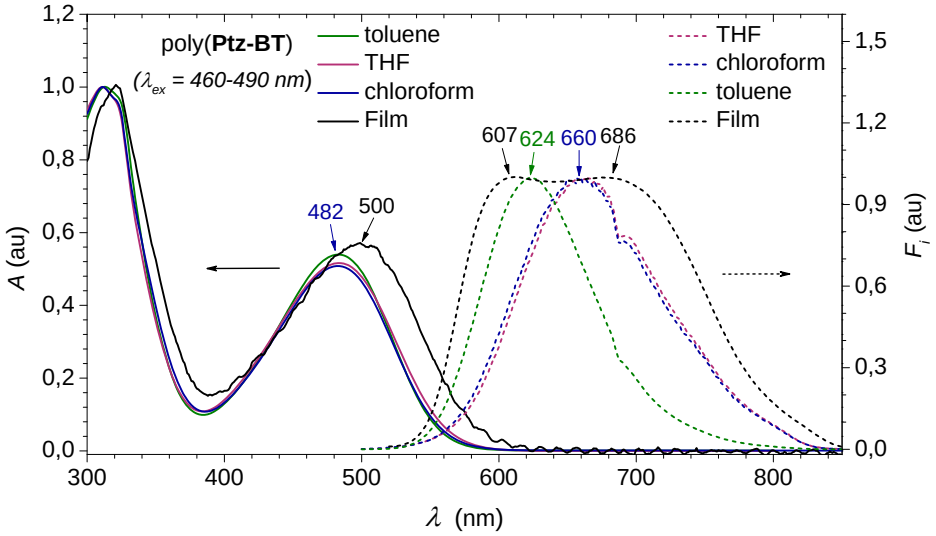


**Figure 61.** UV-Vis absorption and steady state fluorescence ($c = 10^{-5}$ mol $L^{-1}$) and thin film as spin-coated on a glass substrate from a 5 mg $mL^{-1}$ toluene solution of poly(**Ptz-BT**).

**Table 11.** Summary of optical and electrochemical properties of monomers **M1**, **M2** and poly(**Ptz-BT**).

| Compd. | $\lambda_{max}$ (nm)[a] | $\lambda_{max}$ (nm)[b] | $\lambda_{em}$ (nm)[a] | $\lambda_{em}$ (nm)[b] | $\Phi_F$ (%)[a] | $E_{op}$ (eV)[a] | $E_{op}$ (eV)[b] |
|---|---|---|---|---|---|---|---|
| **M1** | 422 | - | 608 | - | 22 | 2.50 | - |
| **M2** | 465 | - | 612 | - | 20 | 2.30 | - |
| poly(**Ptz-BT**) | 482 | 500 | 624 | 607-686 | 13 | 2.23 | 2.13 |

[a]in toluene ($c = 10^{-5}$ mol $L^{-1}$); [b]spin-coated on a glass substrate from a 5 mg $mL^{-1}$ toluene solution.

The intramolecular conformation of a single conjugated polymer is decisive to its absorption and emission by affecting the effective conjugation length through altering the degree of p-orbital overlap along the conjugated polymer backbone.[42] In the absence of crystal structures of **M1** or **M2**, theoretical calculations could provide additional information about the steric interaction between the **Ptz** and **BT** moieties. Poly(**Ptz-BT**) showed a 20 nm bathochromic shift of $\lambda_{max}$ and a 0.1 eV decrease in $E_{op}$ (2.13 eV) when going from solution to solid state, ascribed to the improved π-π interactions in the later.

The emission of poly(**Ptz-BT**) disclosed solvatochromic effects. The emission maximum of the polymer in toluene appeared at $\lambda_{em}$ = 624 nm while in the more polar THF and chloroform at $\lambda_{em}$ = 660 nm. Furthermore, the emission in the solid state revealed an interesting feature

of this polymer. Poly(**Ptz-BT**) showed a very broad emission with two local maxima, peaking at 607 and 686 nm. Further measurements would be required to elucidate the origin of this broad emission in the solid state.

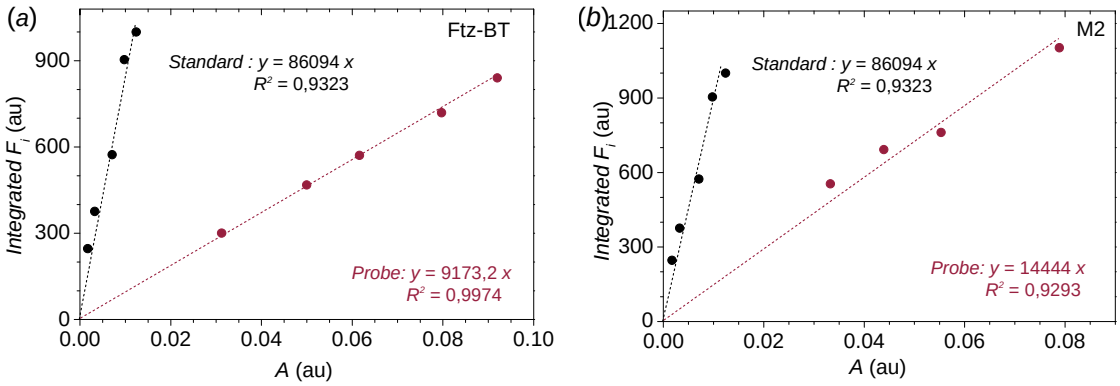


**Figure 62.** Linear plots of the standard and poly(**Ptz-BT**) (*a*) and **M2** (*b*). The data illustrated in these representations were converted into the specific $\Phi_F$.

Apart from their redox-active nature phenothiazinyl π-extended systems are known for their substantial emission efficiency.[39] Consequently, **M1** and **M2** as well as poly(**Ptz-BT**) were subjected to fluorescence quantum efficiency measurements based on the comparative method[43] (Figure 62, Table 11). Poly(**Ptz-BT**) showed the lowest fluorescence quantum yield ($\Phi_F$) of 13 %, while **M1** and **M2** a 28 % and 22 %, respectively. Although moderate, the emission efficiencies of both model compounds and polymer are among the highest reported values for the structurally similar phenothiazine derivatives.[36, 39]

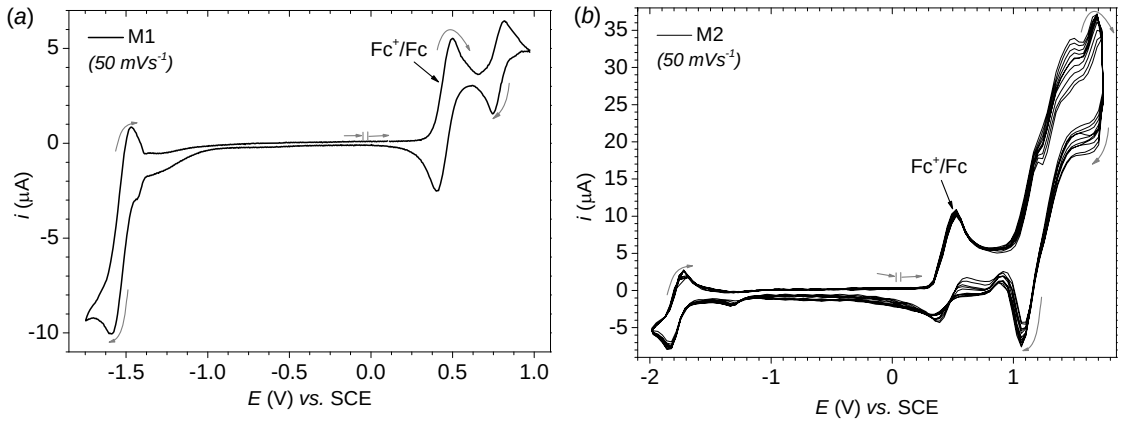


**Figure 63.** Cyclic voltammograms of **M1** (*a*) and **M2** (*b*) as measured in DCM with ferrocene as internal standard.

Upon performing cyclic voltammetry measurements on the model compounds, it was found that for **M1** (Figure 63*a*) the first anodic oxidation potential ($E_0^{0/+1}$ = 810 mV) could be readily assigned to a phenothiazine centered oxidations. In case of **M2** (Figure 63*b*), it was difficult to exclude a first anodic oxidation taking place at a lower potential than 1 V, due to the presence of ferrocene used as internal standard.

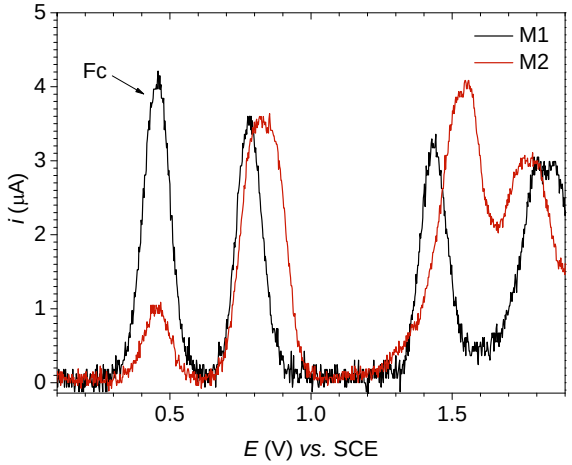


**Figure 64.** Differential pulse voltamograms of **M1** and **M2** measured in DCM with ferrocene as internal standard.

However, the differential pulse voltammetry measurements revealed similar first oxidation characteristic of the phenothiazine units for both **M1** and **M2** (Figure 64). The first and second reversible oxidations could be attributed to the formation of phenothiazinyl cation radical and dication. The much broader first oxidation peak of **M2** suggests a two electron process occurring almost instantaneously. Once the radical cation is formed, **M2** became more difficult to oxidize relative to **M1**, probably due to the stabilization of the first *via* π-conjugation through the **BT** spacer. Unfortunately, no utilizable cyclic or differential pulse voltammograms could be obtained for poly(**Ptz-BT**).

The electronic structure of both **M1** and **M2,** was further scrutinized by computations on DFT level of theory applying the B3LYP functional[44] together with Pople's 6-311G(d,p) basis set[45] as implemented in the program Gaussian03.[46] The branched alkyl substituents on the phenothiazine were truncated to methyl for the computations in order to reduce computational time. Concerning the intramolecular electronic communication between the terminal phenothiazine units (**M2**) in the ground state it is of fundamental importance to

evaluate the degree of conjugation within the system. The delocalization and transmission of electron density between two adjacent π-systems is dictated by the orbital overlap of the constituting systems. This, in turn is related to cos $\vartheta$, where $\vartheta$ is the dihedral angle between the two moieties, while the electron transmission correlates with $\cos^2 \vartheta$.[47] Therefore, steric biases of the π-bridges may considerably reduce the orbital overlap and electronic transmission in a given system.

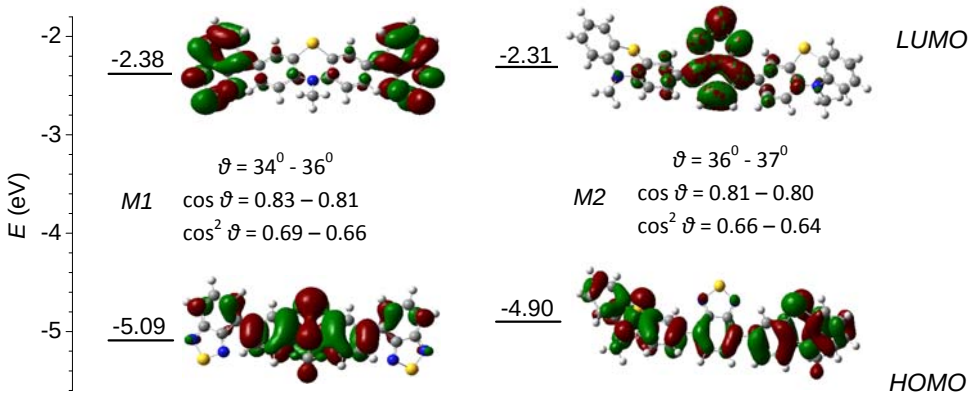


**Figure 65.** Orbital energies and corresponding frontier molecular orbital electronic density contours based on theoretical calculations of **M1** and **M2**.

Both **M1** and **M2** remained essentially conjugated, showing similarly low dihedral angles between the π-bridge and the termini (Figure 65). Furthermore, looking into the electronic ground state it is clear that the electron density distribution in the HOMOs is equally and largely located on the phenothiazine units. Similarly, the LUMO in both cases resides on the electron deficient unit(s). Note that in case of **M2** the HOMO coefficient is distributed over the entire π-system, implying a significant electronic interaction of the terminal phenothiazine units and the bridge. Such electronic ground state features have been previously reported for diphenothiazine dumbbells connected via different electron rich π-bridges, such as phenyl, thienyl or fluorenyl.[39]

## 3.2.3. UV-Vis-NIR Absorption of the Phenothiazinyl Cation Radicals and Dications

The intramolecular electron exchange between phenothiazinyl redox centers in mixed-valence cation radicals interconnected by molecular bridges was investigated by chemical oxidation processes of **M1**, **M2** and the polymer poly(**Ptz-BT**). These processes were evaluated by UV-Vis-NIR absorption, with particular attention to the transient appearance of the diagnostic intervalence (charge resonance, CR) absorption bands. The selective oxidation of the phenothiazine derivatives was readily carried out in dichloromethane by a stepwise addition of 1 equiv. of the (one-electron) oxidant antimony perchloride ($SbCl_5$).[48] Hence, the gradual formation of the corresponding **PtzR**$^{\bullet+}$$SbCl_6^-$ salt could be examined. The choice of counterion was made based on the rather large and relatively noncoordinating nature of $SbCl_6^-$ which will minimize the electrostatic effects on the phenothiazinyl cation radicals in the existent electron transfer (ET), if any, and self association processes.[15]

The oxidative titration of the N-alkyl phenothiazine **48a** (Figure 66 Table 12) served as a reference to illustrate the typical electronic transitions of **48a**$^{\bullet+}$ and **48a**$^{2+}$. The absorption spectrum of **48a**$^{2+}$ is characterized by three groups of bands: (a) local (UV) absorption at 277 that is related to one at 257 nm in the parent compound, (b) prominent (Vis) band at 518 nm (48000 L mol$^{-1}$ cm$^{-1}$) with a shoulder at 445 nm (18200 L mol$^{-1}$ cm$^{-1}$) that is absent in the parent donor, and (c) weak (NIR bands) at 771 nm (7900 L mol$^{-1}$ cm$^{-1}$) and 875 nm (8700 L mol$^{-1}$ cm$^{-1}$). The absorption spectrum of N-alkylated phenothiazine was completely transparent in the NIR region (1000-2200 nm) through the stepwise addition of the 2 equiv. of $SbCl_5$. Hence, no spectroscopic evidence of facile association of the cation radical **48a**$^{\bullet+}$ with its diamagnetic parent compound (**48a**), usually referred to as transient complex or pimer, could be found. This is in line with the observations originally delineated by Bard and co-workers[11] and later on reexamined by Kochi's group[49] for N-methyl and N-isopropyl

phenothiazine, respectively. Their research shows that the presence of alkyl substituents connected to the N atom of the **Ptz** impedes the formation of such pimer.[15]

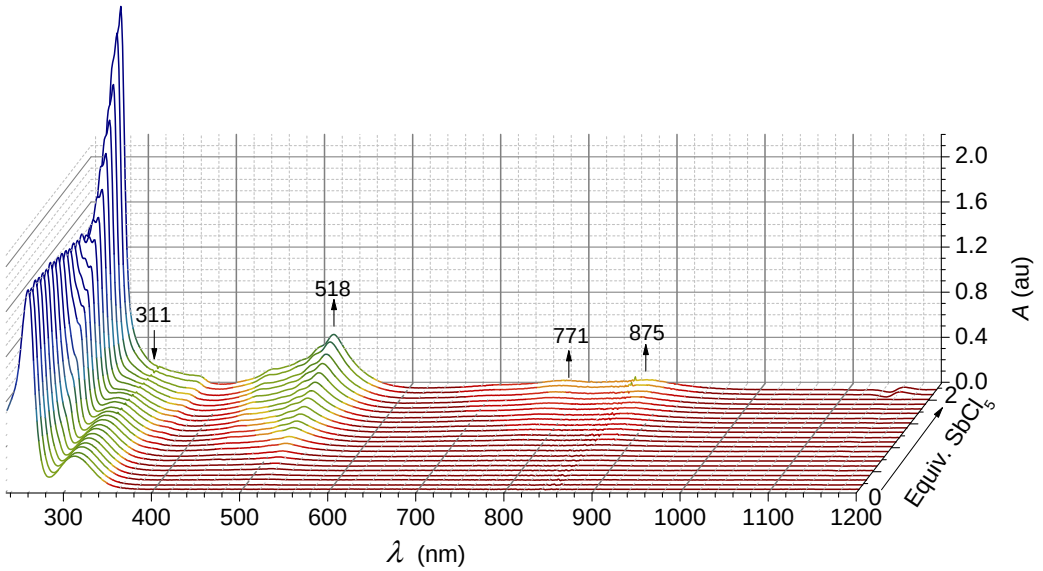


**Figure 66.** Oxidative titration of monomer **48a** (DCM, $c = 10^{-5}$ mol $L^{-1}$) with $SbCl_5$ (2 equiv.) monitored by UV-Vis-NIR spectroscopy.

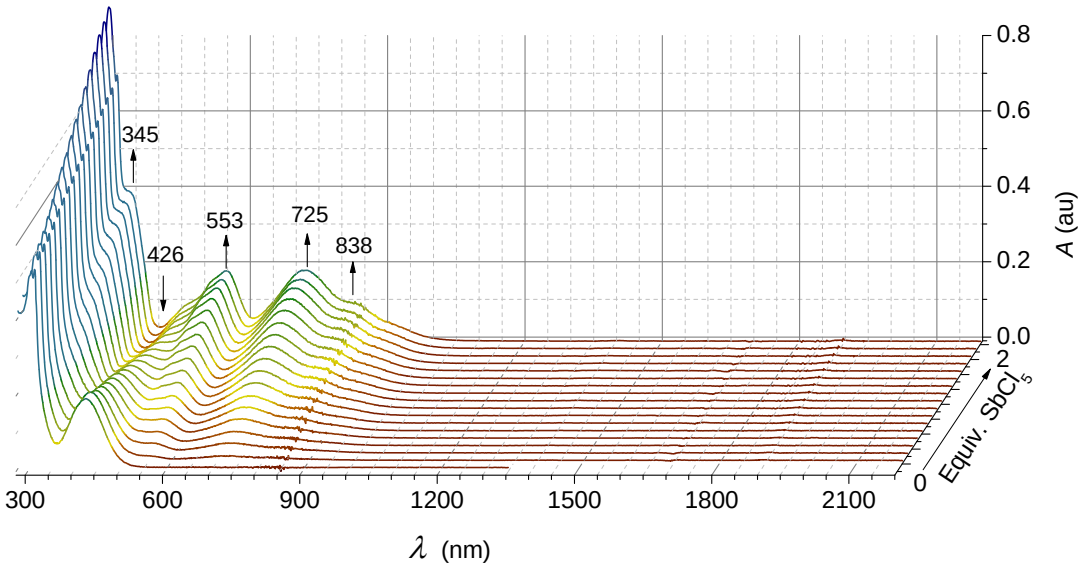


**Figure 67.** Oxidative titration of **M1** (DCM, $c = 10^{-5}$ mol $L^{-1}$) with $SbCl_5$ (2 equiv.) monitored by UV-Vis-NIR spectroscopy.

Similar absorption spectrum patterns were expected for the oxidative titration of **M1**, a model compound in which there is only one N-alkylated phenothiazine center and the formation of the paramagnetic pimer **M1** / **M1**$^{\bullet+}$ is not possible. As illustrated in Figure 67 (Table 12) no absorption could be detected in the characteristic region (between 1000 and 2200 nm) for an intervalence charge resonance. Although **M1**$^{2+}$ shows the three groups of absorption bands seen for **48a**$^{2+}$, there are a few differences. The absorption in the visible range was slightly bathochromically shifted to 553 nm (18400 L mol$^{-1}$ cm$^{-1}$) and the local maximum of the more intense NIR band was located at 725 nm (18700 L mol$^{-1}$ cm$^{-1}$) with a shoulder at 838 nm (9800 L mol$^{-1}$ cm$^{-1}$). The increase in the molar extinction coefficient ($\varepsilon$) and the slight hypsochromic shift of this band could be attributed to the charge delocalization over the electron deficient **BT** units which are in π-conjugation with the N-alkylated phenothiazine center.

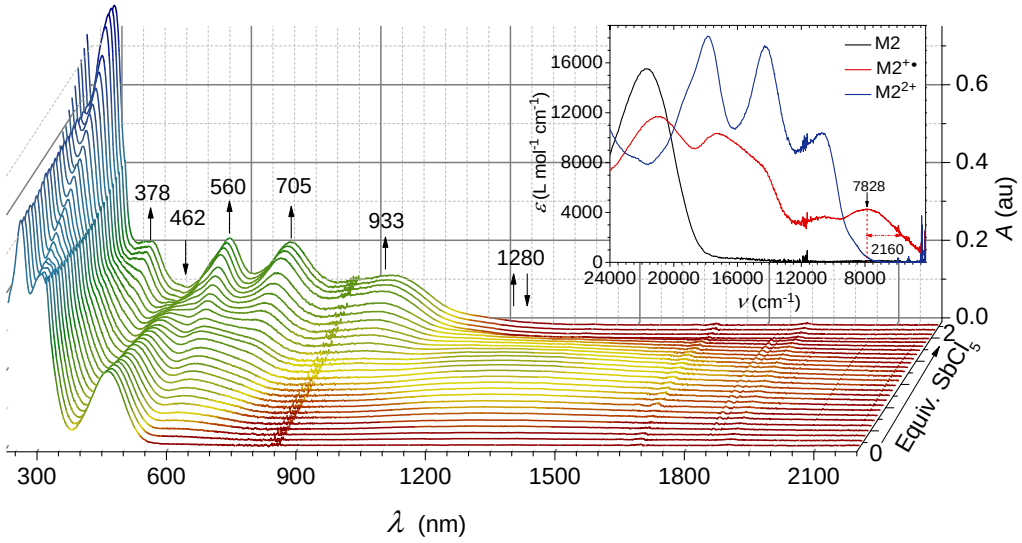


**Figure 68.** Oxidative titration of **M2** (DCM, $c = 10^{-5}$ mol L$^{-1}$) with $SbCl_5$ (2 equiv.) monitored by UV-Vis-NIR spectroscopy.

The oxidative titration of **M2**, in which two phenothiazine redox centers are connected through a molecular π-bridge, revealed different UV-Vis-NIR absorption blueprint, as shown in Figure 68 (Table 12). The addition of 1 equiv. of $SbCl_5$ (**M2**$^{\bullet+}$) resulted in the appearance of a new and unique absorption band in the NIR region, at 1280 nm ($\nu = 7828$ cm$^{-1}$), a region in which neither **M2** nor the structurally close related **48a**$^{\bullet+}$ or **M1**$^{\bullet+}$ showed any electronic

transitions. Such extremely red-shifted NIR band with a broad and weak ($\varepsilon$ = 4250 mol $L^{-1}$ $cm^{-1}$) absorbance is indicative of an intervalence charge resonance (IV-CR) transition in the π-bridged mixed-valence cation radical **M2$^{\bullet+}$** (Scheme 27).

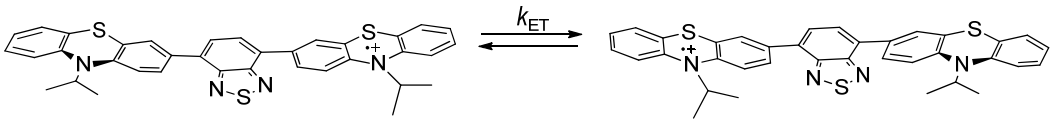


**Scheme 27.** Reversible equilibrium of the intramolecular electron transfer process in **M2$^{\bullet+}$**.

Further additions of the oxidant led to the gradual disappearance of the band at 1280 nm, while the absorption intensity in the 700-1100 nm range continued to increase. The absorption in this range was reminiscent of the spectral shape of **M1$^{2+}$**, apart from the shoulder at 838 nm that evolved into a bathochromically shifted band peaking at 933 nm. Finally, upon addition of 2 equiv. of $SbCl_5$ the low energy band at 1280 nm disappeared and a very intense band (with three local maxima) was observed in the spectral range 460-1100 nm. The intense absorption around 700 nm of the **M2$^{2+}$** resembles the unsubstituted phenothiazine dimer studied by Kochi and co-workers[15] and it was ascribed to the strong interaction of the phenothiazine cation radical centers in the formation of a diamagnetic dication.[50]

**Table 12.** Electronic spectra (relevant maxima) of cation radicals and dications of phenothiazine based mixed-valence donor-acceptors (**M2** and poly(**Ptz-BT**)) their mononuclear models (**48a** and **M1**).

| Compd. | $\lambda_{max}$ (nm) [a] [$\varepsilon$ (mol $L^{-1}$ $cm^{-1}$)[a]] | $\lambda_{IV\text{-}CR}$ (nm)[a,b] | $\nu_{IV\text{-}CR}$ ($cm^{-1}$)[a,b] | $\varepsilon$ (mol $L^{-1}$ $cm^{-1}$)[a] |
|---|---|---|---|---|
| **48a$^{\bullet+}$** | 309 (27700), 515 (8700), 780 (1300), 873 (1500) | - | | |
| **48a$^{2+}$** | 518 (48300), 778 (8000), 875 (8600) | - | | |
| **M1$^{\bullet+}$** | 440 (10000),556 (10900), 718 (11300) | - | | |
| **M1$^{2+}$** | 553 (18500), 725 (18700), 838sh (10000) | - | | |
| **M2$^{\bullet+}$** | 472 (11700), 580 (10300), 680 (8000) | 1280 | 7828 | 4250 |
| **M2$^{2+}$** | 553 (18000), 705 (17300), 933 (10300) | - | | |
| poly(**Ptz$^{\bullet+}$-BT**) | 531 (34300), 863 (13900) | 1410 | 7090 | 10000 |
| poly(**Ptz$^{2+}$-BT**) | 569 (45000), 8520 (42800) | - | | |

[a]in DCM ($c \approx 10^{-5}$ mol $L^{-1}$); [b]intervalence charge resonance band.

The electron spin resonance (ESR) spectrum of benzothiadiazole bridged cation radical **M2**$^{\bullet+}$ consisted of five major lines (Figure 69) corresponding to a hyperfine splitting of 2 equiv. nitrogen nuclei, but otherwise with no resolved proton splittings. Similar increased number and decreased splittings of hyperfine lines was previously observed in case of some dimer cation radicals.[15, 51]

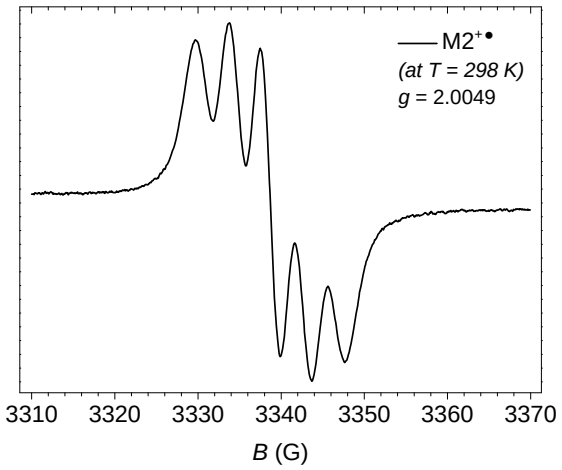


**Figure 69.** ESR spectrum of **M2**$^{\bullet+}$ in dilute oxygen-free DCM solution, at 298 K. Experimental parameters: 9.4 (9.38433) GHz, 100 kHz modulation frequency, 1.6 mW power, 82 msec time constant, 42 sec sweep time, $10^5$ gain, 0.13 mT modulation amplitude.

Two possible reasons could be the origin of this phenomenon: first, the unpaired electron is completely delocalized over the two redox centers, or second, the electron exchange in Scheme 27 is too fast to be resolved on the ESR time scale (half life $\tau_{ESR} < 10^{-9}$ s$^{-1}$). Furthermore, the dication **M2**$^{2+}$ was ESR silent suggesting that **M2**$^{2+}$ is a diamagnetic dication with strongly spin-coupled (**Ptz**$^{\bullet+}$ / **Ptz**$^{\bullet+}$) centers. This is in agreement with the strong electronic interaction between **Ptz** / **Ptz**$^{\bullet+}$ centers in **M2**$^{\bullet+}$ that is necessary to describe ultrafast electron exchange in **M2**$^{\bullet+}$.

Hush[14] and Sutin[16] showed that the characteristic intervalence absorption band of a mixed-valence complex such as **M2**$^{\bullet+}$ can serve for the estimation of the critical electronic coupling element ($H_{DA}$) for an intramolecular electron transfer. According to Hush, $H_{AD}$ can be directly estimated from the intervalence absorption band as:[52]

$$H_{DA} = 0.0206 \, (\nu_{IV} \, \Delta\nu_{IV} \, \varepsilon)^{1/2} / \, r_{DA} \qquad (7)$$

where:

$\nu_{IV}$ and $\Delta\nu_{IV}$ are the maximum and full-width at half heights, respectively (in $cm^{-1}$) of the intervalence absorption band;

$\varepsilon$ is the molar extinction coefficient of the intervalence absorption maximum (in mol $L^{-1}$ $cm^{-1}$);

$r_{DA}$ is the effective electron transfer distance (in Å).

However, an important point in such an analysis is the proper choice of the separation parameter $r_{DA}$. X-Ray crystallography is of limited use in determining the distance between the two redox active centers of organic mixed-valence compounds, as electron-transfer distances are not necessarily directly related to interatomic distances. Furthermore, the degree of electron delocalization in solution may be affected by time and density fluctuation of the solvent.[18] Therefore, the precise evaluation of this parameter is very difficult in extended organic redox systems, for two reasons: (a) it refers to the separation between two hypothetical (diabatic) states[53] and (b) the "charge" is highly delocalized.[54] As the bridge is in conjugation with the phenothiazine redox centers, delocalization of the charge away from the charge bearing center towards the bridge (for diabatic states) will result in reduced $r_{DA}$ values.[55] Nonetheless, a lower limit of the $H_{AD}$ can be assessed when using the N–N distance ($r_{DA}$ = 13 Å) to define the separation parameter. With a $\Delta\nu_{IV}$ = 4320 $cm^{-1}$ an electronic coupling of $H_{DA}$ = 560 $cm^{-1}$ (1.6 kcal $mol^{-1}$) is calculated. This result suggests a stronger electronic coupling between the two phenothiazine units over the benzothiadiazole bridge than for other reported mixed-valence system in which the phenothiazine cation radicals (**Ptz** and **Ptz**$^{\bullet+}$) are interconnected by *para*-phenylene (**Ptz**$^{\bullet+}$**P**(***p***), $H_{DA}$ = 400 $cm^{-1}$, Chart 12).[15] However, in the aforementioned case, the backbone of the radical cation is not planar, but with a dihedral angle of $90^0$ between the planes of the phenothiazine and the bridging phenyl ring. For **M2**$^{\bullet+}$, the initial dihedral angle of approx. $33^0$ between the bridge and the phenothiazine units is most likely decreased upon oxidation accompanied by planarization of the phenothiazine, creating effective π-delocalization pathways that are usually most favorable for charge transfer.[56] Furthermore, electronic coupling of 548 $cm^{-1}$ was calculated for a diarylamine cation connected via a ladder-type pentaphenylene bridge, with an N–N distance of 22 Å[57], underlining the importance of π-delocalization pathways. Both the above mentioned mixed-valence cation radicals were assigned to the Robin-Day Class II category[58]

and as **M2**$^{\bullet+}$ presented similar spectral characteristics (the Gaussian shaped, structureless and broad intervalence charge transfer band) justifies the inclusion of **M2**$^{\bullet+}$ into the Robin-Day Class II mixed-valence systems, as suggested already from equation (*2*) (see Subchapter 1.1.). This class includes redox centers that are weakly coupled, in other words "quasi" localized systems. This classification also allows the direct evaluation of the reorganization energy ($\lambda_{reorg}$) from the intervalence absorption band as $\lambda_{reorg} = \nu_{IV\text{-}CR} = 7828\ cm^{-1}$ (22.38 kcal mol$^{-1}$). The calculation of the activation barrier can now be performed based on the Marcus-Hush equation (*3*):[16, 59]

$$\Delta G^{\#} = (\lambda_{reorg} - 2H_{DA})^2 / 4\,\lambda_{reorg} \qquad (3)$$

Hence, a theoretical activation barrier $\Delta G^{\#} = 4.1$ kcal mol$^{-1}$ is derived for the intramolecular electron exchange between the phenothiazynyl redox centers bridged by a benzothiadiazole unit. Going one step further following the two-state model for the intramolecular ET, the rate constant ($k_{ET}$) can be evaluated within the Markus-Hush formalism as:[16]

$$k_{ET} = \kappa\, \nu_n \exp(-\Delta G^{\#} / R\,T) \qquad (8)$$

where:

$\kappa$ is the electronic transmission coefficient;

$\nu_n$ is the nuclear vibration frequency related to the electron transfer;

$\Delta G^{\#}$ is the activation free energy for the same process.

For a sufficiently strong electronic coupling, as in this case, $\kappa$ can be taken as unity. The nuclear vibration frequency was taken as $\nu_n = 10^{12}\ s^{-1}$, a value that was repeatedly used for the description of ET in phenylene bridged organic mixed-valence cation radicals.[55b, 60] Hence, $k_{ET} = 1 \times 10^9\ s^{-1}$ was calculated as the first order rate constant for the intramolecular ET (at 25$^0$C) for the mixed-valence cation radical **M2**$^{\bullet+}$. The theoretically derived rate constant is in good agreement with the observations made based on the ESR measurements, suggesting an ultrafast electron transfer for **M2**$^{\bullet+}$.

The reorganization energy, activation barrier and rate constant calculated for **M2**$^{\bullet+}$ correlate quite well with the parameters of the structurally similar mixed-valence cation

radicals: $(\mathbf{PtzH})_2^{\bullet+}$ dimer cation radical of unsubstituted phenothiazine, or $\mathbf{Ptz}^{\bullet+}\mathbf{P}$ (Table 13, Chart 12). The electronic coupling element calculated from the Mulliken–Hush formalism, for $\mathbf{Ptz}^{\bullet+}\mathbf{P}$, is comparable to that of the intermolecular pimer $(\mathbf{PtzH})_2^{\bullet+}$, but the electron transfer reorganization energy ($\lambda_{reorg}$) is considerably lower. The authors have explained the difference in $\lambda_{reorg}$ through the different arrangement of the phenothiazine redox centers.

**Table 13.** Comparison of calculated intramolecular electron transfer reorganization energy, activation barrier and rate constant in mixed-valence cation radicals and intermolecular self-exchange.

| Compd. | $H_{DA}$ ($cm^{-1}$) | $\lambda_{reorg}$ (kcal $mol^{-1}$) | $\Delta G^{\#}$ (kcal $mol^{-1}$) | $k_{ET}$ ($s^{-1}$) |
|---|---|---|---|---|
| $\mathbf{M2}^{\bullet+}$ | 560 | 22.38 | 4.1 | $1 \times 10^9$ |
| $\mathbf{Ptz}^{\bullet+}\mathbf{P}$[15] | 400 | 30 | 6.4 | $3 \times 10^7$ |
| $(\mathbf{PtzH})_2^{\bullet+}$[15] | 660 | 17 | 2.5 | $1.2 \times 10^{10}$ |

For $(\mathbf{PtzH})_2^{\bullet+}$, the strong electronic coupling of the cofacial $\mathbf{Ptz}^{\bullet+}$ / **Ptz** redox centers possibly originates in an incomplete solvation and an implicit decrease in outer-sphere reorganization energy.[15] Conversely, in case of $\mathbf{Ptz}^{\bullet+}\mathbf{P}$ such a solvent restriction is more favorable and the interplanar separation could result in an increased solvation of the mixed-valence cation radical. The same explanation might apply for $\mathbf{M2}^{\bullet+}$ as well. The enhanced π-conjugation in $\mathbf{M2}^{\bullet+}$ relative to $\mathbf{Ptz}^{\bullet+}\mathbf{P}$ yielded a stronger electronic coupling between the two phenothiazinyl redox centers, in spite of the longer distance between them. The electron deficient nature of the bridging benzothiadiazole may also play a positive role in promoting the electronic coupling between the two redox centers.

The reversibility of the oxidation process was probed by UV-Vis-NIR spectroscopy. The oxidative titration of **M2** with 1 equiv. of $SbCl_5$ yielding $\mathbf{M2}^{\bullet+}$ (Figure 70*a*) was followed by the stepwise addition of hydrazine hydrate (Figure 70*b*). The $\mathbf{M2}^{\bullet+}$ characteristic intervalence charge resonance band at 1280 nm and the band peaking at 580 nm continuously decreased in intensity upon hydrazine hydrate addition until spectral characteristics identical to **M2** were reached. Hence, the reversible chemical oxidation of **M2** to $\mathbf{M2}^{\bullet+}$ was proven by spectroscopic techniques.

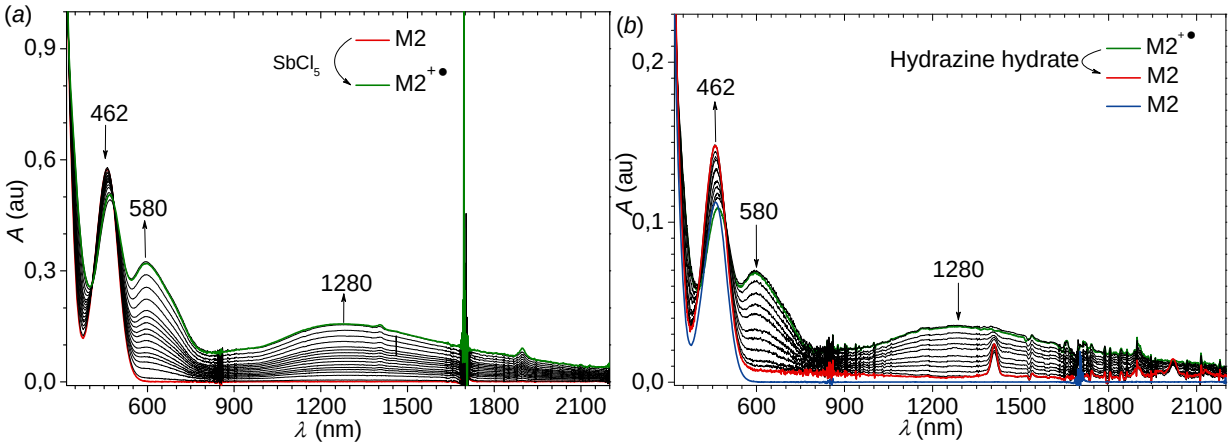


**Figure 70.** Oxidative titration of **M2** (DCM, $c = 10^{-5}$ mol $L^{-1}$) with 1 equiv. of $SbCl_5$ (a) and reductive titration of **M2$^{\bullet+}$** (DCM, $c = 10^{-5}$ mol $L^{-1}$) with 1 equiv. of hydrazine hydrate (b) monitored by UV-Vis-NIR spectroscopy.

Not surprisingly, the absorption spectra corresponding to the oxidative titration of poly(**Ptz-BT**) followed similar patterns to its model compound **M2**. The formation of the bridged cation radicals within the polymeric backbone was accompanied by the appearance of a distinctive low energy band at 1410 nm (Figure 71).

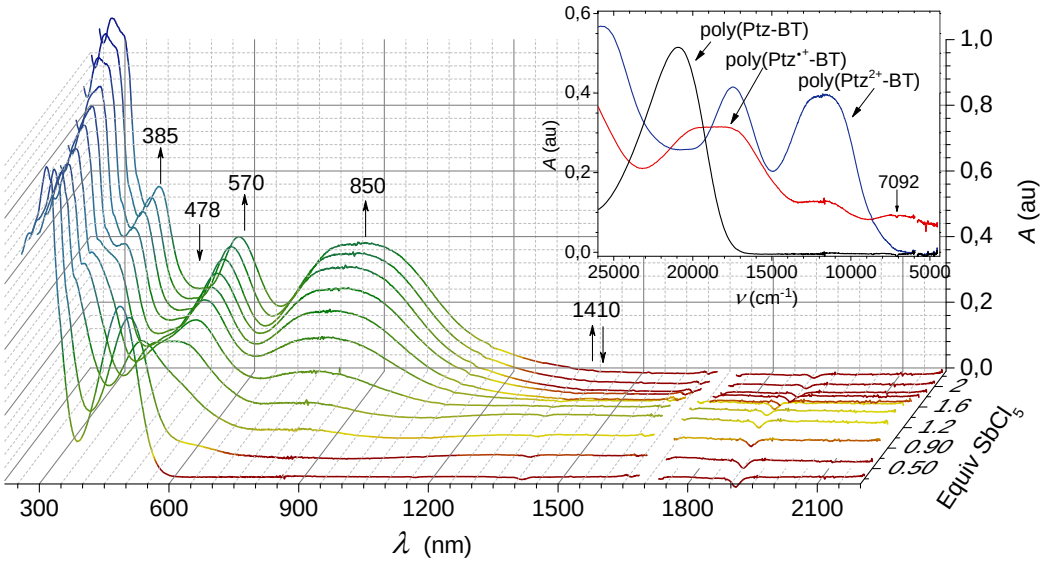


**Figure 71.** Oxidative titration of poly(**Ptz-BT**) (DCM, $c = 10^{-5}$ mol $L^{-1}$) with $SbCl_5$ (2 equiv.) monitored by UV-Vis-NIR spectroscopy.

The addition of 1 equiv. of $SbCl_5$ yielded poly(**Ptz$^{\bullet+}$-BT**) with an intervalence transition band quasi separated from the local bands and red shifted to the NIR region (1000-2200 nm).

This band peaking at $\lambda_{IV\text{-}CR}$ = 1410 nm (Table 12) can be associated with an intramolecular electron transfer from the neutral **Ptz** moiety to the oxidized **Ptz**$^{\bullet+}$ partner over the **BT** bridge. The 130 nm bathochromic shift of the $\lambda_{IV\text{-}CR}$ relative to **M2**$^{\bullet+}$ can be attributed to the presence of multiple phenothiazinyl redox centers interconnected *via* the benzothiadiazole π-bridge of a polydisperse material.[61] The further treatment with the oxidant resulted in a linear decrease of the intervalence charge resonance band intensity. Simultaneously, the absorption intensity in the 700-1150 nm range continued to grow, although the spectral shape changed significantly relative to that of model cation radical **M2**$^{\bullet+}$ (Figure 68 or Figure 70*a*). Finally, when the concentration of the oxidant reached twice the one of the initial concentration of poly(**Ptz-BT**), the low energy band at ~1410 nm disappeared and a single intense broad band with maximum at 850 nm was observed.

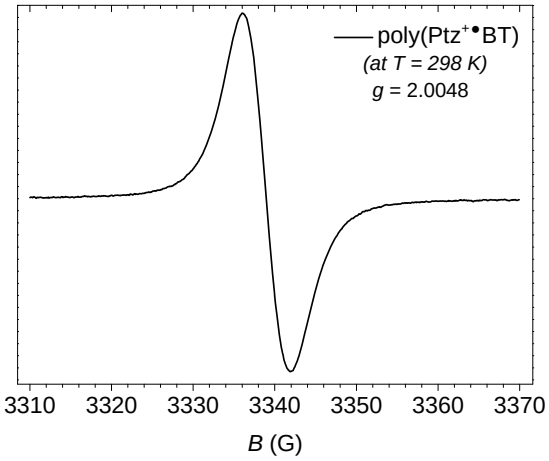


**Figure 72.** ESR spectrum of poly(**Ptz**$^{\bullet+}$**-BT**) in dilute oxygen-free DCM solution, at 298 K . Experimental parameters: 9.4 (9.38500) GHz, 100 kHz modulation frequency, 2.5 mW power, 82 msec time constant, 42 sec sweep time, $4 \times 10^4$ gain, 0.23 mT modulation amplitude.

Any interpretation based on the intervalence charge transfer band within the Marcus-Hush theory is restricted in this case, due to the inability to accurately determine the molar extinction coefficient. However, a similar coupling magnitude as for its model compound **M2**$^{\bullet+}$ could be expected, between the phenothiazinyl redox centers, unless a dramatic decrease of the molar extinction coefficient occurred upon polymerization. A strong coupling in poly(**Ptz**$^{\bullet+}$**-BT**) is also supported by the ESR investigation (Figure 72). The corresponding

spectrum of poly(**Ptz$^{\bullet+}$-BT**) appeared as a broad single line at $g$ = 2.0048, similarly to **M2$^{\bullet+}$**. The ability to observe an intramolecular spin interaction would require the registration of the ESR spectrum of the polyradical cation with a matrix, such as poly(methyl-methacrylate) (PMMA).[62] However, such an elaborate analysis of the spin state was beyond the scope of this investigation.

It would be intriguing to see whether poly(**Ptz-BT**) is electrically conducting in the doped state or not. Yet it is difficult to answer this question without conductivity measurement of the films or of the bulk material. Nonetheless, the hole transport properties of the neutral poly(**Ptz-BT**) polymer were tested when applied in field effect transistors in a top contact[63] architecture. Processed from chloroform solution by spin coating, the polymer showed a saturation hole mobility of $\mu_{h,sat}$ = 3 x $10^{-6}$ $cm^2V^{-1}s^{-1}$ with $I_{ON}$ / $I_{OFF}$ < 100. Note that this hole mobility was not measured on an optimized device, but being a single trial, with the active component processed from a low boiling point solvent.

## 3.3. Conclusion

Alternating D-A type poly(**Ptz-BT**) and its corresponding model compounds (**M1** and **M2**) were efficiently synthesized in order to investigate intramolecular ET self-exchange phenomena. The microwave mediated synthetic procedure of poly(**Ptz-BT**) enabled the isolation of a polymer with a higher molecular weight relative to the polycondensation promoted by conventional conductive heating.

The assessment of the electronic properties of poly(**Ptz-BT**) relative to **M1** and **M2** supported the presence of extended π-electron conjugation with considerable excited state electronic coupling due to the large structural and electronic distributional changes upon photoexcitation. Additionally, the cyclic and differential pulse voltammetry investigations confirmed the potential of these materials to form reversibly stable cation radicals.

Analysis of the UV-Vis-NIR and ESR spectral data of the phenothiazine mixed-valence cation radical **M2**$^{\bullet+}$ yielded considerable insight into the mechanism of intramolecular ET self-exchange. The Mulliken-Hush two state model enables the evaluation of the critical electronic coupling element $H_{DA}$ and the Marcus reorganization energy $\lambda_{reorg}$ *via* the intervalence absorption band. Additionally, the application of the Marcus-Hush theory (equation 4) allows the theoretical prediction of the ET rate constant, value that is in good agreement with the experimental (ESR) observations. The electronic coupling element with $H_{DA}$ = 560 cm$^{-1}$ in **M2**$^{\bullet+}$ ($r_{DA}$ = 13 Å) is stronger than in case of the previously reported **Ptz**$^{\bullet+}$**P**(***p***) ($r_{DA}$ = 8.6 Å) $H_{DA}$ = 400 cm$^{-1}$ mixed-valence system, despite the larger distance between the phenothiazinyl redox centers ($r_{DA}$ = 13 Å). The strong electronic coupling resulted in a lower activation barrier ($\Delta G^{\#}$ = 4.1 kcal mol$^{-1}$) and ET rates at the diffusion-control limit in **M2**$^{\bullet+}$. The reduced steric interaction in **M2**$^{\bullet+}$ could promote a stronger electronic coupling, due to favored spin interaction through π-conjugation. Moreover, as the magnitude of electronic coupling is dictated by a delicate interplay of energetic and geometric factors,[18, 64] the gain in electronic coupling might be also attributed to the decreased energy-gap between the phenothiazines and the bridge.

Although such a thorough analysis of the polycation radical poly(**Ptz**$^{\bullet+}$**-BT**) was hindered by the inability to accurately determine the molar extinction coefficient, the preliminary investigations suggest the presence of similar interactions between the redox centers in polycation radical poly(**Ptz**$^{\bullet+}$**-BT**).

# 3.4. References

*1.* A. Bernthsen *Chem. Ber.* **1883**, *16*, 2896.

*2.* (a) Lauth C. *Ber. deutsch. chem. Ges.* **1883,** *16*, 2896. (b) Zolfaghari, P. S.; Packer, S.; Singer, M.; Nair, S. P.; Bennett, J.; Street, C.; Wilson, M. *BMC Microbiol.* **2009**, *9*, 27. (c) Linz, A. J.; Greenham, R. K.; Fallon, L. F. *J. Occup. Environ. Med.* **2006,** *48*, 523 (d) B, Nietzki *„Chemistry of the Organic Dye-Stuffs"* **1898**, Taylor and Francis, London.

*3*. Hollister, L. E. *JAMA* **1964**, *189,* 311.

*4.* (a) Longo, V. G.; Bovet, D. *Farm. Sci. Techn*. **1940**, *4*, 515. (b) Mahaux, J.; Kowalewski, K. K. *Arch. Intern. Pharmacodynamie* **1949**, *80*, 464. (c) Atamna, H.; Nguyen, A.; Schultz, C.; Boyle, K.; Newberry, J.; Kato, H.; Ames, B. N. *FASEB J.* **2008**, *22*, 703.

*5*. (a) Higuchi, A.; Inada, H.; Kobata T.; Shiraota, Y. *Adv. Mater.* **1991**, *3*, 549. (b) Kong, X.; Kulkarni, A. P.; Jenekhe, S. A. *Macromolecules* **2003**, *36,* 8992. (c) Park, M. J.; Lee, J.; Park, J. H.; Lee, S. K.; Lee, J. I.; Chu, H. Y.; Hwang, D. H.; Shim, H. K. *Macromolecules* **2008**, *41*, 3063.

*6*. (a) Wu, W.; Yang, J.; Hua, J.; Tang, J.; Zhang, L.; Long Y.; Tian, H. *J. Mater. Chem.* **2010**, *20*, 1772. (b) Cho, N. S.; Park, J. H.; Lee, S. K.; Lee, J.; Shim, H. K.; Park, M. J.; Hwang D. H.; Jung, B. J. *Macromolecules* **2006**, *39*, 177.

*7*. Lai, R. Y.; Kong, X.; Jenekhe S. A.; Bard, A. J. *J. Am. Chem. Soc.* **2003**, *125*, 12631.

*8.* McDowell, J. J. H. *Acta. Crystallogr., Sect. B: Found. Crystallogr*. **1976**, *B32*, 5.

*9*. (a) Krämer, C. S.;Müller, T. J. J. *Eur. J. Org. Chem.* **2003**, 3534. (b) Sailer, M.; Nonnenmacher, M.; Oeser, T.; Müller, T. J. J. *Eur. J. Org. Chem.* **2006**, 423. (c) Franz, A. W.; F. Rominger, F.; Müller, T. J. J. *J. Org. Chem.* **2008**, *73*, 1795. (d) Sailer, M.; Franz, A. W.; Müller, T. J. J. *Chem. -Eur. J.* **2008**, *14*, 2602. (e) Franz, A. W.; Popa, L. N.; Müller, T. J. J. *Tetrahedron Lett.* **2008**, *49*, 3300. (f) Franz, A. W.; Popa, L. N.; Rominger, F.; Müller, T. J. J. *Org. Biomol. Chem.* **2009***, 7, 469.*

*10.* Uchida, T.; Ito, M.; Kozawa, K. *Bull. Chem. Soc. Jpn.* **1983**, *56*, 577.

*11*. Kowert, B. A.; Marcoux, B. A.; Bard, A. J. *J. Am. Chem. Soc.* **1972**, *94*, 5538.

*12*. (a) Okada, K.; Imakura, T.; Oda, M.; Murai, H.; Baumgarten, M. *J. Am. Chem. Soc*. **1996**, *118*, 3047. (b) Okada, K.; Imakura, T.; Oda, M.; Kajiwara, A.; Kamachi, M.; Sato, K.; Shiomi, D.; Takui, T.; Itoh, K.; Gherghel, L.; Baumgarten, M. *J. Chem. Soc., Perkin Trans. 2* **1997**, 1059.

*13*. (a) Patai, S., Rappaport, Z. *„The Chemistry of Quinonoid Compounds*“, Eds; Wiley: New York, **1988**. (b) Longuet-Higgins, H. C. *J. Chem. Phys.* **1950**, *18*, 265. (c) Ovchinnikov, A. A. *Theor. Chim. Acta (Berlin)* **1978**, *47*, 279. (d) Klein, D. J.; Nelin, C. J.; Alexander, S.; Matsen, F. A. *J. Chem. Phys.* **1982**, *77*, 3101.

*14*. Hush, N. S. *Prog. Inorg. Chem*. **1967**, *8*, 391.

*15.* Sun, D.; Rosokha, S. V.; Kochi, J. K. *J. Am. Chem. Soc.* **2004**, *129*, 1388.

*16*. (a) Sutin, N. *Prog. Inorg. Chem.* **1983**, *30*, 441. (b) Nelsen, S. *“Electron Transfer in Chemistry”* Balzani, V., Ed.; Wiley-VCH: New York, **2001**, *pp.* 342.

*17*. (a) Okamato, T.; Kuratsu, M.; Kozaki, M.; Hirotsu, K.; Ichimura, A.; Matsushita, T.; Okada, K. *Org. Lett.* **2004**, *6*, 3493. (b) Yen, H-. J.; Liou, G-. S. *J. Mater. Chem*. **2010**, *20*, 9886.

*18.* Hankache, J.; Wenger, O. S. *Chem. Rev.* **2011**, *111*, 5138.

*19*. (a) Gilman, H.; Nelson, R. D.; Champaigne, J. F. *J. Am. Chem. Soc.* **1952**, *74*, 4205. (b) Gilman, H.; Shirley, D. A.; Van Ess, P. R. *J. Am. Chem. Soc.* **1944**, *66*, 625.

*20*. (a) Chiou, H.; Reeves, P.; Biehl E. R. *J. Het. Chem.* **1976**, *13*, 77. (b) Sailer, M., Franz, A. W.; Müller, J. J. T. *Chem. – Eur. J.* **2008**, *14*, 2602.

*21*. (a) Miyaura, N.; Suzuki, A. *Chem. Rev*. **1995**, *95*, 2457. (b) Suzuki, A. “*Metal Catalyzed Cross Coupling Reactions*” Stang, P. J.; Diederich, F.; Eds.; Wiley-VCH: Weinheim, **1998**, *pp.* 49. (c) Suzuki, A. *J. Organomet. Chem*. **1999**, *576*, 147.

*22*. Pilgram, K.; Zupan, M.; Skils, R. *J. Heterocycl. Chem.* **1970**, *7*, 629.

*23*. Zhang, M.; Tsao, H. N.; Pisula, W.; Yang, C.; Mishra, A. K.; Müllen, K. *J. Am. Chem. Soc.* **2007,** *129*, 3472. (b) Anant, P.; Lucas, N. T.; Jacob, J. *Org. Lett.* **2008**, *10*, 5533.

*24.* Sakamoto, J.; Rehahn, M.; Wegner, G.; Schlüter, A. D. *Macromol. Rapid Commun.* **2009**, *30*, 653.

*25*. Kappe, C. O.; Dallinger, D.; Murphree, S. S. *„Practical Microwave Synthesis for Organic Chemists“* Wiley-VCH: Weinheim, **2009**, *p.* 19.

*26*. (a) Bjoerklund, N.; Lill, J. -O.; Rajander, J.; Oesterbacka, R.; Tierney, S.; Heeney, M.; McCulloch, I.; Coelle, M. *Org. Electron.* **2009**, *10*, 215. (b) Cowan, S. R.; Leong, W. L.; Banerji, N.; Dennler, G.; Heeger A. J. *Adv. Funct. Mater.* **2011**, *21*, 3083. (c) Meyer, H.; Haarer, D.; Naarmann, H.; Horhold, H. H. *Phys. Rev. B* **1995**, *52*, 2587.(d) Chiguvare, Z.; Dyakonov, V. *Phys. Rev. B* **2004** , *70*.

*27*. Haas, S.; Takahashi, Y.; Takimiya, K.; Hasegawa, T. *App. Phys. Lett.* **2009**, *95*, 022111/1.

*28*. Sundar V. C.; Zaumseil, J.; Podzorov, V.; Menard, E.; Willett R. L.; Someya, T.; Gershenson M, E.; Rogers J. A. *Science (New York, N.Y.)* **2004**, *303*, 1644.

*29.* McCullough, R. D.; Iovu, M. C. *"Method for purification of polymer and purified polymers."*2007-US77456 2008063731, **2008**, 20070831.

*30*. Wang, E.; Hou, L.; Wang, Z.; Hellström, S.; Mammo, W.; Zhang, F.; Inganäs, O.; Andersson, M. R. *Org. Lett.* **2010**, *12*, 4470.

*31*. Saleh, M.; Baumgarten, M.; Mavrinskiy, A.; Schäfer, T.; Müllen, K. *Macromolecules* **2010**, *43*, 137.

*32*. James, S. L. *Chem. Soc. Rev.* **2003**, *32*, 276.

*33.* Nowakowska-Oleksy, A.; Cabaj, J.; Olech, K.; Soloducho, J.; Roszak, S. *J. Fluoresc.* **2011**, *21*, 1625.

*34*. Jayakannan, M.; van Dongen, J. L. J.; Janssen, R. A. J. *Macromolecules* **2001**, *34*, 5386.

*35*. Cho, D. "*Donor-Acceptor Materials for Organic Field Effect Transistors"*, PhD Thesis, Mainz, **2010**, *p.* 63.

*36*. (a) Krämer, C. S.; Müller, T. J. J. *Eur. J. Org. Chem.* **2003**, 3534. (b) Franz, A. W.; Rominger, F.; Müller, T. J. J. *J. Org. Chem.* **2008**, *73*, 1795. (c) Franz, A. W.; Popa, L. N.; Rominger, F.; Müller, T. J. J. *Org. Biomol. Chem.* **2009**, *7*, 469.

*37*. Valeur, B. *"Molecular Fluorescence: Principles and Applications"* Wiley-VCH Verlag GmbH, **2001**.

*38*. (a) Sailer, M.; Nonnenmacher, M.; Öser, T.; Müller, T. J. J. *Eur. J. Org. Chem.* **2006**, 423. (b) Sailer, M.; Franz, A. W.; Müller, T. J. J. *Chem. -Eur. J.* **2008**, *18*, 2602. (c) Franz, A. W.; Popa, L. N.; Müller, T. J. J. *Tetrahedron Lett.* **2008**, *49*, 3300.

*39.* Hauck, M.; Turdean, R.; Memminger, K.; Schönhaber, J.; Rominger, F.; Müller, T. J. J. *J. Org. Chem.* **2010**, *75*, 8591.

*40*. Woitellier, S.; Launay, J P.; Joachim, C. *Chem. Phys*. **1989**, *131*, 481.

*41*. (a) Choi, Y.; Tepavcevic, S.; Xu, Z.; Hanley, L. *Chem. Mat.* **2004**, *16*, 1924. (b) Zen, A.; Pflaum, J.; Hirschmann, S.; Zhuang, W.; Jaiser, F.; Asawapirom, U.; Rabe, J. P.; Scherf, U.; Neher, D. *Adv. Funct. Mater.* **2004**, *14*, 757.

*42*. Kim, J. *Pure Appl. Chem.* **2002**, *74*, 2031

*43.* (a) Williams, A. T. R.; Winefield, S. A.; Miller, J. N. *Analyst* **1983**, *108*, 1067. (b) Birks, J. B. *"Photophysics of Aromatic Molecules"* Wiley VCH: Weinheim, **1970**.

*44*. (a) Becke, A. D. *J. Chem. Phys.* **1993**, *98*, 5648. (b) Becke, A. D. *J. Chem. Phys.* **1993**, *98*, 1372. (c) Parr, R. G.; Yang, W. *"Density-Functional Theory of Atoms and Molecules";* Oxford University Press: Oxford, **1989**.

*45*. Ditchfield, R.; Hehre, W. J.; Pople, J. A. *J. Chem. Phys.* **1971**, *54*, 724.

*46*. Frisch, M. J. *et al. Gaussian 03, Revision B.03*; Gaussian, Inc.:Wallingford, CT, **2004**.

*47*. Woitellier, S.; Launay, J. P.; Joachim,C. *Chem. Phys*. **1989**, *131*, 481.

*48.* (a) Bell, F. A.; Ledwith, A.; Sherrington, D. C. *J. Chem. Soc. C* **1969**, 2719. (b) Connelly, N. G.; Geiger, W. E. *Chem. Rev.* **1996**, *96*, 877.

*49.* Rosokha, S. V.; Kochi, J. K. *J. Am. Chem. Soc.* **2007**, *129*, 3683.

*50*. Lü, J. -M.; Rosokha, S. V.; Kochi, J. K. *J. Am. Chem. Soc.* **2003**, *125*, 12161.

*51.* (a) Gerson, F.; Kaupp, G.; Ohya-Nishiguchi, H. *Angew. Chem., Int. Ed.* **1977**, 16, 657. (b) Wartin, A. R.; Valenzuela, J.; Staab, H. A.; Neugebauer, F. A. *Eur. J. Org. Chem.* **1998**, *139*, 9. (c) Lau, W.; Kochi, J. K. *J. Org. Chem.* **1986**, *51*, 1801.

*52.* (a) Hush, N. S. *Electrochem.* **1957**, *61*, 734. (b) Hush, N. S.; *Trans. Faraday Soc.* **1961**, *57*, 557. (c) Hush, N. S. *Electrochem. Acta* **1968**, *13*, 1005.

*53.* (a) Nelsen, S. F.; Newton, M. D. *J. Phys. Chem.* **2000**, *104*, 10023. (b). Newton, M. D. *"Electron Transfer in Chemistry"* Balzani, V., Ed.; Wiley-VCH: New York, **2001**, *p.*3.

*54*. (a) Hanson, A. W. *Acta Crystallog*. **1968**, *B24*, 773. (b) Fritchie, C. J.; Arthur, P., Jr. *Acta Crystallog*. **1966**, *21*, 139.

*55.* (a) Barlow, S.; Risko, C.; Chung, S. -J.; Tucker, N. M.; Coropceanu, V.; Jones, S. C.; Levi, Z.; Brédas, J. -L.; Marder, S. R. *J. Am. Chem. Soc.* **2005***, 127,* 16900. (b) Rosokha, S. V.; Sun, D. -L.; Kochi, J. K. *J. Phys. Chem. A* **2002***, 106,* 2283.

*56.* (a) Benniston, A. C.; Harriman, A. *Chem. Soc. Rev.* **2006**, *35*, 169. (b) Hanss, D.; Wenger, O. S. *Eur. J. Inorg. Chem.* **2009**, 3778.

*57.* Zhou, G.; Baumgarten, M.; Müllen, K. *J. Am. Chem. Soc.* **2007**, *129*, 12211.

*58.* Robin, M. D.; Day, P. *Adv. Inorg. Chem. Radiochem.* **1967**, *10*, 247.

*59.* (a) Brunschwig, B. S.; Sutin, N. *"Electron Transfer in Chemistry"*, Balzani, V., *Ed*.; Wiley-VCH: New York, **2001**; Vol. 1, *pp.* 583. (b) Brunschwig, B. S.; Sutin, N. *Coord. Chem. Rev.* **1999**, *187*, 233. (c) Sutin, N. *Adv. Chem. Phys.* **1999**, *106*, 7. (d) Creutz, C.; Newton, M. D.; Sutin, N. J. *Photochem. Photobiol. A* **1994**, *82*, 47.

*60.* Ganesan, V.; Rosokha, S. V.; Kochi, J. K. *J. Am. Chem. Soc.* **2003**, *125*, 2559.

*61.* Lambert, C.; Nöll, G. *Synth. Met.* **2003**, *139*, 57.

*62*. Oka, H. *J. Mater. Chem.* **2008**, *18*, 1927.

*63.* Roichman Y.; Tessler N. *Appl. Phys. Lett.* **2002**, *80*, 151.

*64*. McConnell, H. M. *J. Chem. Phys*. **1961**, *35*, 508.

# 4. Summary and Outlook

The aim of this research was the development, synthesis and characterization of donor-acceptor type copolymers with tuned optoelectronic properties, meant to be scrutinized with respect to their possible applications in organic electronics and as model systems in the study of the basic aspects concerning ET theories.

The first part of this work (Chapter 2.) was focused on thiadiazolo[3,4-*g*]quinoxaline (TQ), a planar, electron deficient *o*-quinoid heterocycle, as an ideal acceptor building block for the construction of donor-acceptor type semiconductors for ambipolar charge transport.
Within this frame of work several issues were addressed as follows:

*1. Tuning the optoelectronic properties of the TQ monomers (Subchapter 2.2.).*

The photophysical and electrochemical studies, supported by theoretical calculations, revealed that electron donating aromatic substituents attached to the TQ core, at positions 6 and 7, are an efficient tool in realizing TQ based electron deficient monomers with enhanced π-conjugation. This translates into compounds with extended absorption (**TTQ**, $\lambda_{max}$ = 497 nm, $E_{op}$ = 2.17 eV) and low LUMO energy levels (-3.80 eV ≤ $E_{LUMO}$ ≤ -3.63 eV). Hence, the HOMO energy levels could be effectively tuned, while preserving a low LUMO energy level (see series **RTQ**, **PTQ** and **TTQ**, Subchapter 2.2.). Furthermore, the direct comparison of the photophysical and electrochemical properties of **TTQ** with its pyrazino[2,3-*g*]quinoxaline analogue **TPQ** confirms the choice of TQ as a strong acceptor. Although **TTQ** and **TPQ** have almost identical optical energy-gaps, they differ significantly in the position of their energy levels. The 0.2 eV lower $E_{LUMO}$ of **TTQ**, relative to **TPQ**, shows the great potential of the former as an electron deficient unit.

Using the synthetic route established in this work, a great variety of functionalized TQ monomers became accessible. Further tuning of the acceptor strength could be possible through the modification of the TQ core. Within this context, the attachment of electron deficient substituents (**PyTQ**) or even fused aromatic π-systems should be viable options (Chart 13).

**Chart 13.** Proposed structure for further investigations.

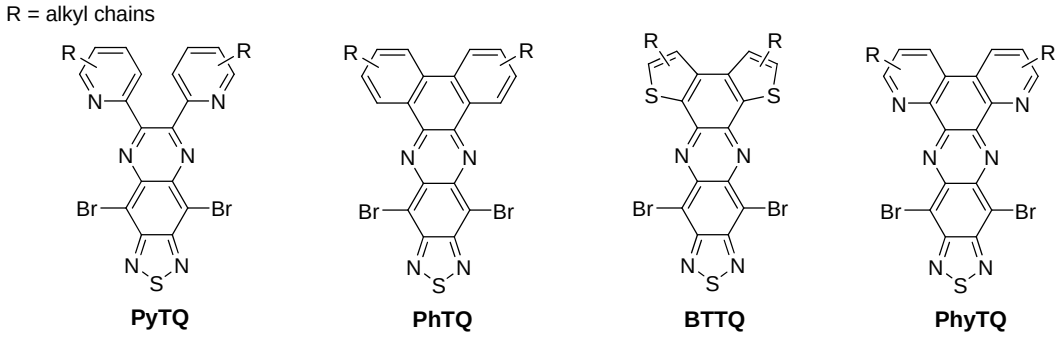


*2. TQ model compounds (Subchapter 2.3.).*

The synthesis and characterization of TQ model compounds containing different π-spacers had two main advantages.

Firstly, TQ model compounds with ethynylene and / or ethylene π-spacers were synthesized under *Sonogashira-Hagihara* coupling reaction conditions by only varying the molar ratio of the terminal acetylene derivative employed. The *in situ* reduction of the ethynylene bond was triggered by the electron deficient nature of the TQ segment in combination with the presence of excess terminal acetylene derivative. The successful isolation of the double-bond containing TQ model compounds, following the *in situ* reduction procedure, gains importance in the view of the fact that the synthesis of these materials was not possible *via Heck* coupling reaction.

Secondly, the comprehensive comparative study of the photophysical and electrochemical properties of the model systems (**PTQET**, **PTQVT** and **PTQV2T**) revealed the beneficial effect of the ethynylene *vs.* ethylene π-spacer by promoting a low laying LUMO energy level.

The study of the synthesis and properties of these model compounds served multiple purposes. It was possible to identify the exact conditions for the preparation of triple bond

containing TQ derivatives, while overcoming undesired side reactions. Furthermore, the meticulous examination of the optoelectronic properties of these model systems was of aid in the identification of the most suitable π-spacer that would favor the electron transport in TQ based polymers (see series **PTQEP**, **PTQET** and **TTQET**).

*3. Thiadiazolo[3,4-g]quinoxalines: Ethynylene-Phenylene Copolymers (Section 2.4.1.).*

Three high molecular weight PAE type polymers (**$P_1$**, **$P_2$** and **$P_3$**) were synthesized, bearing functionalized TQ and phenylene moieties connected *via* ethynylene π-spacers. The developed microwave mediated *Sonogashira-Hagihara* polymerization procedure enabled the reproducible synthesis of high molecular weight ($M_n$ = 14000 - 17500 g mol$^{-1}$) polymers. Having identical polymer backbone, **$P_1$**, **$P_2$** and **$P_3$** differ only in the nature of the substituents attached to the TQ core. Ethyl-hexyl side chains attached to the TQ were insufficient for securing the solubility of the corresponding high molecular weight polymer **$P_1$**. The presence of alkylated phenyl (**$P_2$**) or thienyl (**$P_3$**) functionalities on the TQ core resulted in high molecular weight polymers with good solubility.

The electrochemical study of both **$P_2$** and **$P_3$** showed the influence of the substituents grafted on the TQ core on the HOMO energy levels. The presence of the stronger electron donating thienyl moieties attached to the TQ segment increased the $E_{HOMO}$ of **$P_3$** to -5.76 eV relative to **$P_2$** with a $E_{HOMO}$ = -5.82 eV, while conserving an equally low $E_{LUMO}$ = -4.05 eV.

The potential application of **$P_2$** as the acceptor component in all-polymer BHJ OPV was investigated in combination with **P3HT**. Due to the unfavorable morphology of the blend combined with a very limited charge carrier mobility of the acceptor counterpart (**$P_2$**) yielded only modest power conversion efficiency. While **$P_2$** exhibited no detectable charge carrier mobility, **$P_3$** demonstrated a saturation electron mobility of $\mu_e$ = 1.7 x 10$^{-6}$ cm$^2$V$^{-1}$s$^{-1}$ when applied in OFETs. Hence, **$P_3$** constitutes the first example of the TQ containing polymer showing electron charge transport in OFET devices.

*4. Thiadiazolo[3,4-g]quinoxalines: Ethynylene-Thiophene Copolymers (Section 2.4.2.).*

The introduction of ethynylene π-spacers, in an alternating fashion, in a polymer backbone, between the thiadiazoloquinoxaline (A) and thiophene (D), in a 1 : 1 ratio per repeating unit, resulted in materials showing *ambipolar charge transport*, as active components in OFET devices. It has been demonstrated that the substituents attached to the

TQ core play a major role in the fine tuning of the energy levels as well as in the microstructure and surface morphology of the thin films and therefore have a considerable influence on the OFET performance. The one order of magnitude difference in charge carrier mobility between **$P_5$** ($\mu_{h,e} \approx 0.03$ $cm^2V^{-1}s^{-1}$) and **$P_6$** ($\mu_{h,e} \approx 0.002$ $cm^2V^{-1}s^{-1}$) was attributed to differences on the morphological and microstructural level. While **$P_5$** formed uniform films with a rather poor 1D lamellar packing, **$P_6$** organized in small randomly oriented worm-like nanofibrills. Furthermore, both **$P_5$** and **$P_6$** formed disordered films, showing no signal corresponding to π-π stacking in the X-ray diffraction scans.

Higher charge carrier mobilities of either **$P_5$** or **$P_6$** could probably be achieved by a systematic optimization of the OFET devices, including processing conditions, device architecture, the electrode materials, dielectrics or increasing the molecular weight of the polymers.

Among the copolymers based on TQ as the acceptor moiety, the presented mobilities, in both hole and electrons, are not only the highest values so far, but also show "nearly equivalent" hole and electron transport properties. Moreover, ***$P_5$*** *is the first example of a triple bond containing polymer presenting ambipolar charge transport characteristics.* Consequently, it was shown that, incorporating ethynylene π-spacers in π-conjugated polymer systems is an effective strategy for tuning charge transport characteristics. Hence, D-A type copolymers can function as p-type or ambipolar semiconductor depending on the connection mode between the donor and the acceptor units.

In the last part of this research work (Chapter 3.), the intramolecular self-exchange between phenothiazine redox centers bridged by benzo[*c*][2,1,3]thiadiazole was examined. The chemical oxidative titration of the model compounds (**M1** and **M2**), as well as their corresponding polymer (poly(**Ptz-BT**)) was monitored by UV-Vis-NIR spectroscopy with special attention to the transient appearance of the diagnostic intervalence absorption bands. In case of the phenothiazine mixed-valence cation radical **$M2^{\bullet+}$** it was possible to determine the electronic coupling element $H_{DA}$ and the Marcus reorganization energy $\lambda_{reorg}$ *via* the intervalence absorption band, within the Mulliken-Hush two state model. The ET rate constant as calculated from the Marcus-Hush theory was in very good agreement with the experimental (ESR) observations. Due to the reduced steric interaction between the

phenothiazine redox centers and the benzo[*c*][2,1,3]thiadiazole π-bridge (**M2**$^{\bullet+}$) spin interactions through π-conjugation are favored, resulting in a stronger electronic coupling. Hence, despite its electron deficient π-bridge, the phenothiazinyl redox centers in **M2**$^{\bullet+}$ revealed a strong electronic coupling ($H_{AD}$ = 560 cm$^{-1}$) over a large distance ($r_{DA}$ = 13 Å), with low activation barrier ($\Delta G^{\#}$ = 4.1 kcal mol$^{-1}$) and ET rates that are at the diffusion-control limit.

Such a thorough analysis of the polycation radical poly(**Ptz**$^{\bullet+}$**-BT**) was hindered by the inability to accurately determine the molar extinction coefficient. However, the preliminary investigations suggest the presence of similar interactions between the phenothiazinyl redox centers.

Overall, it is strongly believed that the herein presented extensive study could well lead to advances in the design and development of new organic semiconductors for efficient OPV and OFET applications.

# 5. Experimental Part

## 5.1. General Methods

### 5.1.1. Chemicals and solvents

All chemicals and reagents were used as received from commercial sources (Acros Organics, Aldrich, Fluka, Lancaster, Merck and Strem) without further purification. Solvents for chemical synthesis were used as received, unless otherwise mentioned.

### 5.1.2. Chromatography

Preparative column chromatography was performed on silica gel from Merck with a grain size of 0.063-0.200 mm (silica gel) or 0.04-0.063 mm (flash silica gel, Geduran Si 60). For analytical thin layer chromatography (TLC), silica gel coated substrates “60 F254” from Merck were used. Compounds were detected by fluorescence quenching at 254 nm, self-fluorescence at 366 nm or staining in an iodine vapour chamber. For eluents, analytically pure solvents (p.a. or technical grade) were distilled prior to the use.

### 5.1.3. Inert atmosphere

Oxygen or moisture sensitive reactions were carried out using standard Schlenck technique. The reactions carried out under microwave irradiation were degassed using a stream of argon.

## 5.1.4. Microwave Assisted Synthesis

The microwave assisted synthesis were carried out in a CEM Discover™ system, in a closed vials (35 mL or 10 mL, respectively), equipped with temperature and pressure sensor and magnetic stirring.

## 5.1.5. Analytical Techniques

### 5.1.5.1. NMR Spectroscopy

$^{1}$H-NMR, $^{13}$C-NMR experiments were recorded in the listed deuterated solvents on a Bruker DPX 250, Bruker DMX 300, Bruker DRX 500 or a Bruker DRX 700 spectrometer. Chemical shifts ($\delta$) are given in parts per million (ppm) with tetramethylsilane (TMS) as internal standard. The measurements were recorded at room temperature (T = 293 K), unless stated otherwise.

### 5.1.5.2. Mass Spectrometry

Field-desorption mass spectra were recorded on a VG Instruments ZAB 2-SE-FPD spectrometer (range 100-3300). MALDI-TOF spectrometry was obtained on a Brucker Reflex IITOF spectrometer, using a 337 nm nitrogen laser. Tetracyanoquinodimethane (TCNQ) was employed as the matrix substance for solid state prepared samples, when not mentioned otherwise.

### 5.1.5.3. Melting Points

The listed melting points were registered on a Büchi B-545 device.

### 5.1.5.4. UV-Vis and Steady Sate Fluorescence Spectroscopy

Solution and solid state UV-vis spectra were recorded on a Perkin Elmer Lambda 15 spectrophotometer. Unless otherwise noted, a concentration of $10^{-5}$ mol $L^{-1}$ was used in solvents of spectroscopic grade at room temperature. The quantum corrected steady state fluorescence spectra were registered on a SPEX-Fluorolog II (212) spectrometer. Fluorescence quantum yields were determined by the comparative method[1] ($10^{-5}$ mol $L^{-1}$ solution of cresyl violet in methanol as reference) and corrected for the refractive index of the solvent of the probe. The solutions were prepared with an absorbance between 0 and 0.1 at the wavelength region of experimental interest. The calculation of the $\Phi_F$ from the collected data is based on the linear plots for the standard and the fluorescent probe of the integrated fluorescence intensity as a function of absorbance at the excitation wavelength. The gradient for each sample is proportional to its $\Phi_F$. Conversion into an absolute quantum yield is obtained by solving the following equation:

$$\Phi_X = \Phi_{ST}\left(\frac{Grad_X}{Grad_{ST}}\right)\left(\frac{\eta_X^2}{\eta_{ST}^2}\right)$$

where:

subscript ST and X denote standard and test;

$\Phi$ – fluorescence quantum yield;

*Grad* – the gradient from the plot of integrated fluorescence intensity *vs* absorbance;

$\eta$ – refractive index of the solvent.

### 5.1.5.5. Cyclic Voltammetry (CV)

Cyclic voltammetry experiments were performed in 0.1 mol $L^{-1}$ tetrabutylammonium hexafluorophosphate (*n*-$Bu_4NPF_6$) solution in dry, oxygen free solvents. The conventional

three-electrode cell employed consisted of a platinum electrode, with a diameter of 2 mm, platinum wire counter electrode, and $Ag/Ag^+$ reference electrode. The cyclic voltammograms were recorded on a computer controlled PGSTAT12 potentiostat / galvanostat model, at room temperature. Unless otherwise mentioned, with ferrocene (Fc) as an internal standard, the lowest unoccupied molecular orbital (LUMO) and the highest occupied molecular orbital (HOMO) energy levels were determined from the onset reduction and oxidation potentials, respectively.

#### 5.1.5.6. Thermogravimetry (TGA)

The thermogravimetric analysis was performed on a Mettler TGA-851 Analyzer at a heating rate of 10 K $min^{-1}$ under nitrogen atmosphere from 298 K to 873 K.

#### 5.1.5.7. Gel Permeation Chromatography (GPC)

All GPC measurements were performed using MZ-Gel SDplus 10E6, 10E4, and 500 columns. The detection was performed either by RI or UV detectors of Waters, ERC, Rheodyne and Soma. Prior to the measurements all samples were filtered through 0.2 µm teflon filters purchased from Milipore.

#### 5.1.5.8. Infrared Spectroscopy (FT-IR)

Infrared spectroscopy was measured on a Nicolet 730 FT-IR spectrometer equipped with a single-reflection ATR-crystal purchased from Thermo-Spectra-Tech.

#### 5.1.5.9. Elemental Analysis

Elemental analysis of solid samples was carried out on a Foss Heraeus Vario EL as a service of the Institute for Organic Chemistry, Johannes Gutenberg University of Mainz.

### 5.1.5.10. X-ray Scattering

Film X-ray diffraction was performed on a theta-theta Philips PW 1820 Kristalloflex diffractometer with a graphite-monochromized Cu-Kα X-ray beam hitting the thin film deposited as described in each case. The diffraction patterns were recorded in the 2 θ range from $1^0$ to $32^0$.

### 5.1.5.11. Atomic Force Microscopy (AFM)

Atomic force microscopy was performed by using a Nanoscope IIIa MultiMode scanning probe microscope; Digital Instruments, Santa Barbara, CA.

### 5.1.5.12. Scanning Electron Microscopy (SEM)

Scanning electron microscopy was performed on a Zeiss Gemini-1530 microscope.

## 5.1.6. Computational Methods

The geometry optimizations were performed using Gaussian 03,[2] Revision B.04 quantum chemistry program at the B3LYP[3] level of theory. All calculations were carried out using the 6-31G* basis set. For all compounds the lowest energy conformers, found by conformational search, were subjected to full geometry optimization (Gaussian, Inc., Pittsburgh PA, 2003).

## 5.1.7. Organic Field Effect Transistor (OFET)

*Standard procedure for the preparation of the transistors:* Heavily doped silicon wafers with a 200 nm thick, thermally grown silicon dioxide layer were used as substrates. The gold source and drain bottom electrodes were patterned by photolithography (≈ 50 nm thick).

Hexamethyldisilazane (HMDS) was deposited out of the gas phase at 120 °C. The active layer was deposited by drop-casting from toluene (10 mg $mL^{-1}$) solutions. The obtained devices had typically a channel length of L = 20 μm and a channel width of W = 1400 μm. For annealed OFETs, the samples were placed on a preheated hot plate (120 °C, 30 min). All procedures and measurements (using a Keithley 4200 semiconductor parameter analyzer) were carried out inside a dry nitrogen glovebox.

The charge carrier mobility was calculated in saturation (from the slope of the $I_{SD}^{½}$ / ($V_{SG}$)-curve at $|V_{SG}|$ = 90 – 100 V) from the equation:[4]

$$I_{SD} = (W C_i \mu_{sat} / 2 L) (V_{SG} - V_T)^2$$

where:

$\mu_{sat}$ – the saturation charge carrier mobility;

$V_{SD}$ – the drain voltage when the source electrode is grounded;

$W$ and $L$ – the channel width and length, respectively;

$C_i$ – the capacitance of the dielectric layer per unit area;

$V_T$ – the threshold voltage.

## 5.1.8. Organic Photovoltaic (OPV) Cells

The photovoltaic devices were prepared using the common fabrication process. The active layer was deposited by spin-coating a solution of the donor-acceptor mixture onto indium thin oxide (ITO) glass substrates, which were precoated with poly(ethylene dioxythiophene) doped with polystyrene sulfonic acid (PEDOT:PSS, a conducting polymer); then a typically 100 nm thick Al layer was vapor deposited onto the active layer. The photovoltaic response of the device was determined using an AM 1.5G standard, operating with an illumination intensity of 100 mW $cm^2$.

## 5.2. Synthetic Procedures

**4,7-Dibromobenzo[*c*][2,1,3]thiadiazole** (**2**)

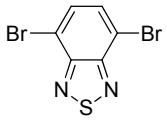

**2**

4,7-Dibromobenzo[*c*][2,1,3]thiadiazole (**2**) was prepared in analogy to the literature[5] in 68 % yield.

*$^{1}$H-NMR (250 MHz, THF-$d_8$). δ* (ppm): 7.82 (s, 2H).

*$^{13}$C-NMR (62.5 MHz, THF-$d_8$). δ* (ppm): 114.39; 133.17; 153.72.

*MS (FD, 8 kV): m/z* = 293.11, calcd. for $C_6H_2Br_2N_2S$: 293.96.

**4-Bromobenzo[*c*][2,1,3]thiadiazole** (**2a**)

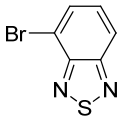

**2a**

4,7-Dibromobenzo[*c*][2,1,3]thiadiazole (**2**) was prepared in analogy to the literature[5] in 76 % yield.

*$^{1}$H-NMR (250 MHz, $CD_2Cl_2$). δ* (ppm): 8.00-8.05 (m, 2H); 7.49-7.55(m, 1H).

*$^{13}$C-NMR (62.5 MHz, $CD_2Cl_2$). δ* (ppm): 160.68, 158.47, 134.42, 132.26, 120.92, 116.23.

*MS (FD, 8 kV): m/z* = 213.82, calcd. for $C_6H_3BrN_2S$: 215.07.

**4,7-Dibromo-5,6-dinitrobenzo[*c*][2,1,3]thiadiazole** (**3**)

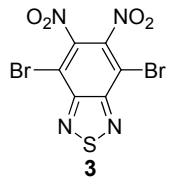


**3**

4,7-Dibromo-5,6-dinitrobenzo[*c*][2,1,3]thiadiazole (**3**) was prepared in analogy to the literature,[5] in 72 % yield.

*$^{1}$H-NMR (250 MHz, DMSO-d6): -*

*$^{13}$C-NMR (62.5 MHz, DMSO-d6). δ* (ppm): 112.71, 144.63; 152.12.

*MS (FD, 8 kV): m/z* = 383.73, calcd. for $C_6Br_2N_4O_4S$: 383.96.

**4,7-Dibromobenzo[*c*][2,1,3]thiadiazolo-5,6-diamine** (**4**)

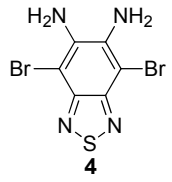


**4**

4,7-Dibromobenzo[*c*][2,1,3]thiadiazole-5,6-diamine(**4**) was prepared in analogy to the literature,[5] in 87 % yield.

*$^{1}$H-NMR (250 MHz, THF-$d_8$). δ* (ppm): 5.6 (s, 4H).

*$^{13}$C-NMR (62.5 MHz, THF-$d_8$). δ* (ppm): 91.82; 140.95; 149.55.

*MS (FD, 8 kV): m/z* = 324.31, calcd. for $C_6H_4Br_2N_4S$: 324.00.

**5,10-Diethyltetradecane-7,8-dione** (**8**)

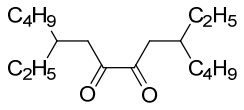


**8**

To a suspension of activated Mg (675.00 mg, 27.86 mmol, 2.74 equiv.) in 25 mL THF 2.49 equiv. of 2-ethyl-hexylbromide (**5**, 4.89 g, 25.33 mmol) was added dropwise. The reaction mixture was left to stir for 3 h at r.t. In a separate three necked flask LiBr (4.25 g, 48.83 mmol, 4.80 equiv.) in 30 mL THF was added to a stirring solution of CuBr(I) (3.52 g, 24.33 mmol, 2.39 equiv.) in 25 mL THF to form a pale green solution. The reaction mixture is cooled down to -90$^0$C using n-pentane / liquid nitrogen cooling mixture. The Grignard reagent (**6**) was added slowly to the cooled LiBr/CuBr mixture such that its temperature did not exceed -75$^0$C. Subsequently, oxalyl chloride (**7**, 1.295 g, 10.17 mmol, 1 equiv.) is added very slowly in order to prevent the temperature from rising higher than -75$^0$C. The mixture was further stirred at -80$^0$C for 2 h and subsequently allowed to warm up to r.t. and quenched with saturated $NH_4Cl$ aqueous solution. The organic layer was separated and the aqueous layer was repeatedly extracted with EtOAc. The combined organic layers were dried over $Na_2SO_4$ and the solvent was removed under reduced pressure. Purification by column chromatography (eluent: heptane) yielded α-diketone **8** as a yellow oil (1.38 g, 48 %).

*$^1$H-NMR (250 MHz, $CDCl_3$). δ* (ppm): 0.90-0.81 (m, 12H); 1.40-1.22 (m, 10H); 1.85 (q, *J* = 5.00, 7.50 Hz, 2H); 2.64 (d, *J* = 7.50 Hz, 4H).

*$^{13}$C-NMR (62.5 MHz, $CDCl_3$)*. *δ* (ppm): 10.55; 13.56; 22.60; 26.20; 28.56; 32.97; 34.96; 39.98; 200.33.

*MS (FD, 8 kV): m/z* = 141.12 (100%), 281.24 (46%) calcd. for $C_{18}H_{34}O_2$: 282.47.

**1,2-Bis(4-dodecylphenyl)ethane-1,2-dione** (**12**)

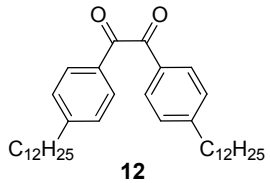


**12**

To a solution of aluminum chloride (12.00 g, 90 mmol, 4.50 equiv.) in 1,2-DCE (60 mL) cooled down to -20$^0$C was added drop wise, in succession, a solution of oxalyl chloride (**7**, 2.54 g, 20.00 mmol, 1.00 equiv.) in 1,2-DCE (10 mL), a solution of dodecylbenzene (9.86 g, 40.00 mmol, 2.00 equiv.) in 1,2-DCE (10 mL) and pyridine (3.10 g, 39.20 mmol) in 1,2-DCE (10 mL). After keeping the mixture for 20 min between -20$^0$C and -15$^0$C, the temperature was raised to 0$^0$C and the mixture was poured over ice and extracted with $CH_2Cl_2$. The extract was washed to neutral reaction with water and dried over magnesium sulfate. After removing the solvent under reduced pressure the residue was purified by column chromatography (eluent: hexane:toluene = 3:1) to give the desired compound **12** as a yellow solid (6.13 g, 56 %). m.p. = 45.6-46.4 $^0$C (reported in the literature[6] m.p. = 47$^0$C).

*$^1$H-NMR (250 MHz, $CDCl_3$). δ* (ppm): 0.88 (t, *J* = 6.75 Hz, 6H); 1.25-1.30 (m, 36H); 1.59-1.65 (m, 4H); 2.67 (t, *J* = 7.50, 7.50 Hz, 4H); 7.28 (d, *J* = 8.25 Hz, 4H); 7.88 (d, *J* = 8.25 Hz, 4H).

*$^{13}$C-NMR (62.5 MHz, $CDCl_3$). δ* (ppm): 13.87; 22.43; 28.98; 29.09; 29.18; 29.28; 29.37; 30.76; 31.66; 35.97; 128.79; 129.80; 130.58; 150.74; 194.28.

*MS (FD, 8 kV): m/z* = 546.42, calcd. for $C_{38}H_{58}O_2$: 546.87.

**1,2-Bis(5-octylthiophene-2-yl)ethane-1,2-dione** (**15**)

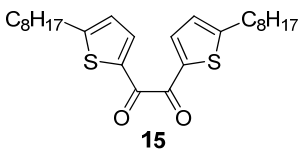


**15**

To a solution of aluminium chloride (4.46 g, 33.31 mmol, 4.45 equiv.) in 1,2-DCE (15 mL) cooled down to -20$^0$C was added dropwise, in succession, a solution of oxalyl chloride (0.95 g, 7.49 mmol, 1.00 equiv.) in 1,2-DCE (3 mL), a solution of 2-octylthiophene (3.19 g, 16.25 mmol, 2.17 equiv.) and pyridine (1.16 g, 14.71 mmol, 1.96 equiv.) in 1,2-DCE (5 mL). After keeping the mixture for 20 min between -20$^0$C and -15$^0$C, the temperature was raised to 0$^0$C and the mixture was poured over ice and extracted with methylene chloride. The extract was washed to neutral reaction with water and dried over magnesium sulfate. After removing the solvent under reduced pressure, the residue was purified by column chromatography (eluent: hexane:toluene = 3:1) to give the desired compound **15** as a yellow solid (2.17 g, 65 %), m.p. = 58.7-59.8$^0$C.

*$^1$H-NMR (250 MHz, $CDCl_3$). δ* (ppm): 0.88 (t, *J* = 6.5 Hz, 6H); 1.27-1.39 (m, 20H); 1.71 (q, *J* = 7.49 Hz, 4H); 2.87 (t, *J* = 7.56 Hz, 4H); 6.88 (d, *J* = 4.90 Hz, 2H); 7.86 (d, *J* = 3.75 Hz, 2H).

*$^{13}$C-NMR (62.5 MHz, $CDCl_3$). δ* (ppm): 14.07; 22.62; 29.00; 29.13; 29.21; 30.81; 31.26; 31.79; 126.39; 136.47; 137.72; 160.03; 182.57.

*MS (FD, 8 kV): m/z* = 446.23, calcd. for $C_{26}H_{38}O_2S_2$: 446.71.

**4,9-Dibromo-6,7-bis(2-ehtylhexyl)-[2,1,3]thiadiazolo[3,4-*g*]quinoxaline** (**16**, **RTQ**)

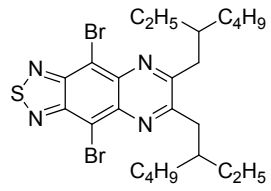


**16**
**(RTQ)**

To a solution of 4,7-dibromobenzo[*c*][2,1,3]thiadiazolo-5,6-diamine (**4**, 478 mg, 1.47 mmol, 1.00 equiv.) in 100 mL acetic acid, 1.77 mmol of 5,10-diethyltetradecane-7,8-dione (**8**, 500 mg, 1.20 equiv.) was added under inert atmosphere and the reaction mixture was stirred over night at r.t.. After removing the solvent under reduced pressure, the desired product **16** was isolated subsequent to column chromatography (eluent: hexane : $CH_2Cl_2$ = 4:1) as an orange oil (603.50 mg, 72 %).

*$^{1}$H-NMR (250 MHz, $CD_2Cl_2$). δ* (ppm): 0.86-1.25 (m, 12H); 1.35-1.57 (m, 10H); 2.28 (q, *J* = 5.00, 7.50 Hz, 2H); 3.03 (d, *J* = 7.50 Hz, 4H).

*$^{13}$C-NMR (62.5 MHz, $CD_2Cl_2$). δ* (ppm): 11.40 ($CH_3$); 14.52 ($CH_3$); 23.66 ($CH_2$); 26.73 ($CH_2$); 26.52 ($CH_2$); 33.46 ($CH_2$); 38.14 (CH); 39.97 ($CH_2$); 113.76 (C); 138.48 (C); 152.23 (C); 161.05 (C).

*MS (FD, 8 kV): m/z* = 570.20, calcd. for $C_{24}H_{34}Br_2N_4S$: 570.44.

### *General procedure for the preparation of 4,9-dibromo-6,7-bis(aryl)-[2,1,3]thiadiazolo[3,4-g]quinoxalines (17, and 18)*

A suspension of 4,7-dibromobenzo[*c*][2,1,3]thiadiazole-5,6-diamine (**4**, 1.00 mmol, 1.00 equiv.) and 1.20 equiv. of diaryl α-diketone (**12** for compound **17** and **15** for compound **18**, respectively) in 15 mL acetic acid, in a 35 mL vial was irradiated for 1 h and 45 min (**17**) and 2 h and 10 min (**18**) at 140$^0$C. After cooling the mixture to r.t., the product was filtrated and purified by washing in hexane (**17**), or column chromatography (eluent: hexane : $CH_2Cl_2$ = 3:1) in case of **18**.

**4,9-Dibromo-6,7(4-dodecylphenyl)-[2,1,3]thiadiazolo[3,4-*g*]quinoxaline (17, PTQ)**

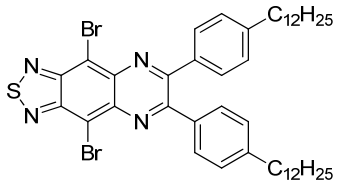


**17 (PTQ)**

Application of the general procedure to **12** yielded compound **17** as a red-orange solid (601.00 mg, 72 %), m.p. = 99.2-100.3$^0$C.

*$^{1}$H-NMR (250 MHz, $CDCl_3$). δ* (ppm): 0.88 (t, *J* = 6.50 Hz, 6H); 1.26-1.33 (m, 36H); 1.64 (q, *J* = 7.20 Hz, 4H); 2.66 (t, *J* = 7.50 Hz, 4H); 7.20 (d, *J* = 8.25 Hz, 4H); 7.67 (d, *J* = 8.25 Hz, 4H).

*$^{13}$C-NMR (62.5 MHz, $CDCl_3$). δ* (ppm): 14.12, 22.69, 29.29, 29.36, 29.50, 29.63, 29.65, 29.67, 29.68, 31.16, 31.92, 35.89, 113.77, 128.47, 130.23, 135.05, 138.09, 145.86, 152.25, 156.12.

*MS (ESI+)*: $[M]^+$ = 833.2808 calcd. for $C_{44}H_{59}N_4SBr_2$: 833.2827.

*FT-IR (neat). 1/λ* ($cm^{-1}$): 720; 823; 843; 850; 857; 908; 982; 1187; 1252; 1285; 1363; 1468; 1536; 1606; 2848; 2918; 2956.

**4,9-Dibromo-6,7-bis(5-octylthiophen-2-yl)-[2,1,3]thiadiazolo[3,4-*g*]quinoxaline** (**18**, **TTQ**)

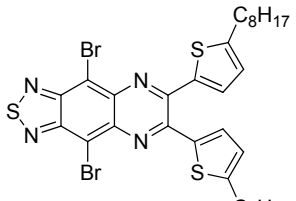


**18** (**TTQ**)

Application of the general procedure to **15** yielded compound **18** as a red solid (338.00 mg, 46 %), m.p. = 115.8-117.2 $^0$C.

*$^1$H-NMR (300 MHz, $CDCl_3$). δ* (ppm): 0.89 (t, *J* = 6.50 Hz, 6H); 1.25-1.46 (m, 20H); 1.78 (dt, *J* = 7.50 Hz, 4H); 2.90 (t, *J* = 7.50 Hz, 4H); 6.76 (d, *J* = 3.90 Hz, 2H); 7.53 (d, *J* = 3.90 Hz, 2H).

*$^{13}$C-NMR (70 MHz, $CDCl_3$). δ* (ppm): 14.10 ($CH_3$); 22.67 ($CH_2$); 29.22 ($CH_2$); 29.30 ($CH_2$); 30.66 ($CH_2$); 31.47 ($CH_2$); 31.86 ($CH_2$); 112.46 (C); 125.30 (CH); 132.39 (CH); 137.72 (C); 138.83 (C); 148.83 (C); 152.28 (C); 154.38 (C).

*MS (ESI+)*: $[M]^+$ = 733.0707 calcd. for $C_{32}H_{39}N_4S_3Br_2$: 733.0704.

*FT-IR (neat). 1/λ* ($cm^{-1}$): 722; 783; 808; 852; 890; 936; 1053; 1111; 1196; 1249; 1368; 1433; 1439; 1455; 1467; 1536; 2850; 2925; 2953.

**5,10-Dibromo-2,3,7,8-tetrakis(5-octylthiophene-2-yl)pyrazine[2,3-*g*]quinoxaline** (**19**, **TPQ**).

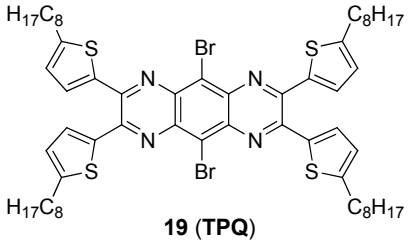


**19** (**TPQ**)

A suspension of 4,7-dibromobenzo[*c*][2,1,3]thiadiazole-5,6-diamine (**4**, 770.00 mg, 2.00 mmol, 1.00 equiv.) and zinc powder (2.60 g, 40.00 mmol, 20.00 equiv.) was stirred at $60^0$C for 4 h after which the reaction mixture was filtered, in order to remove the zinc, and the solute was reheated to $50^0$C after adding 4.00 mmol of 1,2-bis(5-octylthiophene-2-yl)ethane-1,2-dione (**15**, 446.87 mg, 2.00 equiv.). After 2 h the reaction mixture was cooled to r.t. and filtered. Column chromatography (eluent: hexane : $CH_2Cl_2$ = 4:1) of the filtrate yielded compound **19** (**TPQ**) as a brite red solid (1.70 g, 76 %).

*$^1$H-NMR (250 MHz, $CD_2Cl_2$).* $\delta$ (ppm): 0.87-0.92 (m, 12H); 1.30-1.47 (m, 40H); 1.79 (q, *J* = 7.50, 7.50 Hz, 8H); 2.91 (t, *J* = 7.50, 7.50 Hz, 8H); 6.78 (d, *J* = 5.00 Hz, 4H); 7.45 (d, *J* = 5.00 Hz, 4H).

*MS (ESI+)*: $[M]^+$ = 1115.3389, calcd. for $C_{58}H_{77}N_4S_4Br_2$: 1115.3398.

***General procedure for the synthesis of 2,3,7,8-tetrakis(5-octylthiophene-2-yl)pyrazine[2,3-g]quinoxaline (21, TPQ1) and its brominated derivative (20, TPQ2)***

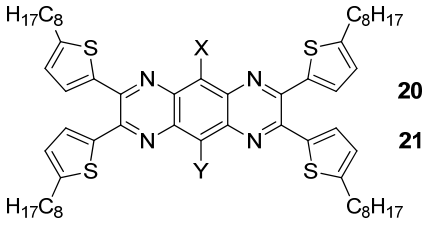


**20** (**TPQ1**) : X = Br, Y = H

**21** (**TPQ2**) : X = H, Y = H

**20-21** (**TPQx**)

A suspension of 4,7-dibromobenzo[*c*][2,1,3]thiadiazole-5,6-diamine (**4**, 770.00 mg, 2.00 mmol, 1.00 equiv.) and zinc powder (2.60 g, 40.00 mmol, 20.00 equiv.) was stirred at $80^0$C for 4 h after which the reaction mixture was filtered, in order to remove the zinc, and the solute was reheated to $80^0$C after adding 4.00 mmol of 1,2-bis(5-octylthiophene-2-yl)ethane-1,2-dione (**15**, 446.87 mg, 2.00 equiv.). After 2 h the reaction mixture was cooled to r.t. and filtered. Column chromatography (eluent: hexane : $CH_2Cl_2$ = 2:1) of the filtrate resulted in the isolation of the desired compounds **20** (**TPQ1**) and **21** (**TPQ2**).

**5-Bromo-2,3,7,8-tetrakis(5-octylthiophene-2-yl)pyrazine[2,3-*g*]quinoxaline** (**20**, **TPQ1**)

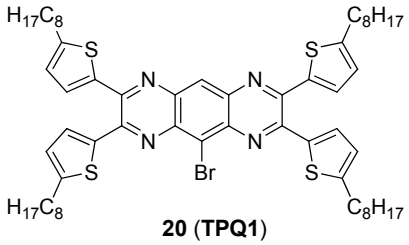


**20** (**TPQ1**)

Red-orange solid (477.60 mg, 23 %).

*$^1$H-NMR (300 MHz, $CD_2Cl_2$). δ* (ppm): 0.89 (t, *J* = 6.00 Hz, 12H); 1.30-1.42 (m, 40H); 1.77 (q, *J* = 6.00, 9.00 Hz, 8H); 2.90 (t, *J* = 6.00 Hz, 8H); 6.76 (dd, *J* = 3.25, 3.50 Hz, 4H); 7.35 (dd, *J* = 3.25, 3.50 Hz, 8H); 8.46 (s, 1H).

*$^{13}$C-NMR (62.5 MHz, $CD_2Cl_2$). δ* (ppm): 14.34 ($CH_3$); 23.15 ($CH_2$); 29.62 ($CH_2$); 29.67 ($CH_2$); 29.70 ($CH_2$); 29.79 ($CH_2$); 30.84 ($CH_2$); 30.93 ($CH_2$); 32.05 ($CH_2$); 32.08 ($CH_2$); 32.35; ($CH_2$) 116.44(CH); 122.71 (CH); 123.62 (C); 125.51 (CH); 125.69 (CH); 126.39 (CH); 127.53 (CH); 127.78 (CH); 131.33 (CH); 131.62 (CH); 138.50 (C); 139.02 (C); 139.84 (C); 140,27 (C); 148.66 (C); 148.53 (C); 148.56 (C); 152.48 (C); 153.27 (C).

*MS (ESI+)*: $[M]^+$ = 1037.4280, calcd. for $C_{58}H_{78}N_4S_4Br$: 1037.4293.

**2,3,7,8-Tetrakis(5-octylthiophene-2-yl)pyrazine[2,3-*g*]quinoxaline** (**21**, **TPQ2**)

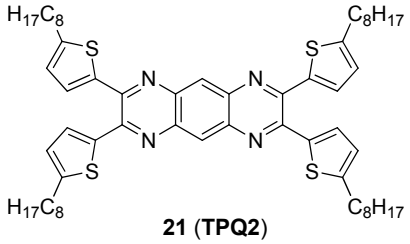


**21** (**TPQ2**)

Red-orange solid (786.80 mg, 41 %).

*$^{1}$H-NMR (250 MHz, $CD_2Cl_2$). δ* (ppm): 0.90 (t, *J* = 7.50 Hz, 12H); 1.30-1.42 (m, 40H); 1.77 (q, *J* = 7.50, 5.00 Hz, 8H); 2.90 (t, *J* = 7.50 Hz, 8H); 6.75 (d, *J* = 5.00 Hz, 4H); 7.25 (d, *J* = 5.00 Hz, 8H); 8.50 (s, 2H).

*$^{13}$C-NMR (62.5 MHz, $CD_2Cl_2$). δ* (ppm): 14.25 ($CH_3$); 23.06 ($CH_2$); 29.52 ($CH_2$); 29.61 ($CH_2$); 29.70 ($CH_2$); 30.72 ($CH_2$); 31.99 ($CH_2$); 32.25 ($CH_2$); 125.23 (CH); 126.88 (CH); 130.80 (CH); 139.41 (C); 140.10 (C); 148.47 (C); 151.83 (C).

*MS (ESI+)*: $[M]^+$ = 959.5210, calcd. for $C_{58}H_{79}N_4S_4$: 959.5232.

***General procedure for the preparation of vinyl containing 6,7(4-dodecylphenyl)-[2,1,3]thiadiazolo[3,4-g]quinoxaline derivatives 23 (PTQV2P), 24 (PTQVP), 28 (PTQV2T) and 29 (PTQVT)***

To a solution of **17** (200.36 mg, 0.240 mmol, 1.00 equiv.) under inert atmosphere, in a degassed tetrahydrofuran (THF) and diisopropylamine ($^{i}Pr_2NH$) (5 mL : 5 mL) solvent mixture, tetrakis(triphenylphosphine)palladium(0) (0.014 g, 5 mol%), copper(I) iodide (0.023 g, 5 mol%) and 3.00 equiv. of terminal acetylene (0.720 mmol) were added. After being stirred for 12 h at r.t. the mixture was filtered through Celite 545 and the solvents were removed under reduced pressure. The residue was purified by column chromatography (eluent: hexane:$CH_2Cl_2$ = 4:1).

**6,7-Bis(4-dodecylphenyl)-4,9-di((*E*)-styryl)-[2,1,3]thiadiazolo[3,4-*g*]quinoxaline (23, PTQV2P)**

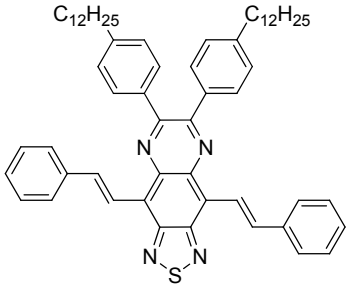


**23** (**PTQV2P**)

Application of the general procedure to ethynylbenzene (**22**) (71.70 mg, 0.72 mmol) yielded compound **23** as a green solid (23.26 mg, 11 %).

*$^{1}$H-NMR (300 MHz, $CD_2Cl_2$). δ* (ppm): 0.84-0.90 (m, 6H); 1.26-1.36 (m, 36H); 1.65-1.70 (m, 4H); 2.69 (t, *J* = 6.00, 6.00 Hz, 4H); 7.24 (d, *J* = 9.00 Hz, 4H); 7.35 (t, *J* = 6.00, 9.00 Hz, 2H); 7.5 (t, *J* = 6.00, 9.00 Hz, 4H); 7.64 (d, *J* = 6.00 Hz, 4H); 7.79 (d, *J* = 6.00 Hz, 4H); 8.85 (d, *J* = 18.00 Hz, 2H); 8.94 (d, *J* = 18.00 Hz, 2H)

*$^{13}$C-NMR (75 MHz, $CD_2Cl_2$). δ* (ppm): 14.46 ($CH_3$); 23.27 ($CH_2$); 29.89 ($CH_2$); 29.95 ($CH_2$); 30.11 ($CH_2$); 30.24 ($CH_2$); 30.27 ($CH_2$); 30.28 ($CH_2$); 31.88 ($CH_2$); 32.51 ($CH_2$); 36.37 ($CH_2$); 122.30 (CH); 124.95 (C); 127.74 (CH); 128.81 (CH); 128.86 (CH); 129.36 (CH); 130.44 (CH); 136.92 (C); 137.33 (C); 137.89 (CH); 139.26 (C); 145.48 (C); 153.07 (C); 153.81 (C).

*MALDI-TOF* found 881.653, calcd. for $C_{60}H_{72}N_4S$: 881.305.

*MS (ESI+)*: $[M]^+$ = 882.4283, calcd. for $C_{60}H_{73}N_4S$: 882.3112.

**(*E*)-6,7-Bis(4-dodecylphenyl)-4-(phenylethynyl)-9-styryl-[2,1,3]thiadiazolo[3,4-*g*]quinoxaline (24, PTQVP)**

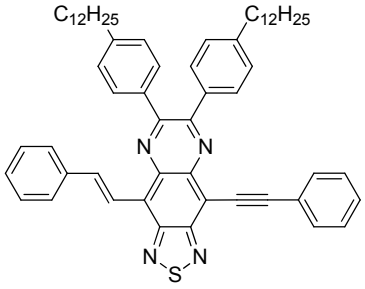


**24** (**PTQVP**)

Application of the general procedure to ethynylbenzene (**22**) (71.70 mg, 0.72 mmol) yielded compound **24** as a dark blue solid (12.66 mg, 6 %).

*$^{1}$H-NMR (300 MHz, $CD_2Cl_2$). δ* (ppm): 0.85-0.89 (m, 6H); 1.27-1.34 (m, 36H); 1.63-1.70 (m, 4H); 2.65-2.71 (m, 4H); 7.24 (t, *J* = 6.00, 6.00 Hz, 4H); 7.36 (t, *J* = 6.00, 9.00 Hz, 1H); 7.44-7.49 (m, 5H); 7.67 (t, *J* = 6.00, 9.00 Hz, 4H); 7.76-7.83 (m, 4H); 8.90 (d, *J* = 15.00 Hz, 1H); 8.96 (d, *J* = 15.00 Hz, 1H).

*$^{13}$C-NMR (75 MHz, $CD_2Cl_2$). δ* (ppm): 14.45 ($CH_3$); 23.27 ($CH_2$); 29.86 ($CH_2$); 29.87 ($CH_2$); 29.95 ($CH_2$); 30.10 ($CH_2$); 30.23 ($CH_2$); 30.26 ($CH_2$); 31.83 ($CH_2$); 31.87 ($CH_2$); 32.50 ($CH_2$); 36.37 ($CH_2$); 88.72 (C); 95.56 (C); 112.33 (C); 121.96 (CH); 127.01 (C); 127.92 (CH); 128.84 (CH); 128.91 (CH); 129.14 (CH); 129.20 (CH); 129.41 (CH); 128.57 (CH); 130.44 (CH); 130.58 (CH); 132.49 (CH); 136.52 (C); 136.84 (C); 138.96 (C); 139.31 (CH); 145.68 (C); 145.88 (C).

*MALDI-TOF* found 879.140, calcd. for $C_{60}H_{70}N_4S$: 879.290

*MS (ESI+)*: $[M]^+$ = 880.0361, calcd. for $C_{60}H_{71}N_4S$: 880.1921.

**6,7-Bis(4-dodecylphenyl)-4,9-di((*E*)-2-(thiophene-2-yl)vinyl)-[2,1,3]thiadiazolo[3,4-*g*]quinoxaline (27, PTQV2T)**

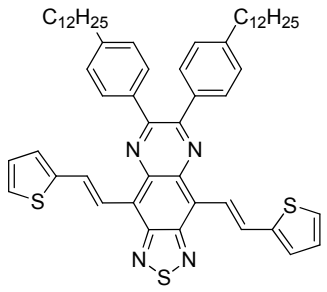


**27** (**PTQV2T**)

Application of the general procedure to 2-ethynylthiophene (**26**, 77.87 mg, 0.72 mmol) furnished compound **27** as a dark green solid (25.73 mg, 12 %), m.p. = 119.5-121.1$^0$C.

*$^1$H-NMR (300 MHz, $CD_2Cl_2$). δ* (ppm): 0.85-0.90 (m, 6H); 1.26-1.34 (m, 36H); 1.65-1.69 (m, 4H); 2.69 (t, *J* = 6.50 Hz, 4H); 7.12 (dd, *J* = 3.60, 5.10 Hz, 2H); 7.24 (d, *J* = 8.10 Hz, 4H); 7.35 (t, *J* = 5.40, 4.1 Hz, 4H); 7.65 (d, *J* = 8.10 Hz, 4H); 8.71 (d, *J* = 16.20 Hz, 2H); 9.98 (d, *J* = 16.20 Hz, 2H).

*$^{13}$C-NMR (70 MHz, $CD_2Cl_2$). δ* (ppm): 14.46 ($CH_3$); 23.29 ($CH_2$); 29.92 ($CH_2$); 29.96 ($CH_2$); 30.13 ($CH_2$); 30.27 ($CH_2$); 30.28 ($CH_2$); 31.88 ($CH_2$); 32.53 ($CH_2$); 36.40 ($CH_2$); 122.08 (CH); 124.42 (C); 126.35 (CH); 128.21 (CH); 128.67 (CH); 128.86 (CH); 130.44 (CH); 130.70 (CH); 136.91 (C); 137.18 (C); 145.57 (C); 145.59 (C); 152.96 (C); 153.69 (C).

*MALDI-TOF:* found 894.087, calcd. for $C_{56}H_{68}N_4S_3$: 892.465.

*MS (ESI+)*: $[M]^+$ = 893.4674, calcd. for $C_{56}H_{69}N_4S_3$: 893.4684.

*FT-IR (neat). 1/λ* ($cm^{-1}$): 689; 812; 855; 957; 1040; 1184; 1289; 1415; 1596; 2850; 2916.

**(*E*)-6,7-Bis(4-dodecylphenyl)-4-(2-(thiophen-2-yl)vinyl)-9-(thiophen-2-ylethynyl)-[2,1,3]thiadiazolo[3,4-*g*]quinoxaline (28, PTQVT)**

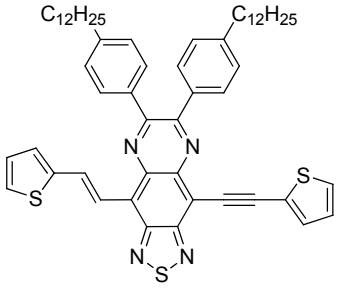


**28** (**PTQVT**)

Application of the general procedure to 2-ethynylthiophene (**26**, 77.87 mg, 0.72 mmol) furnished compound **28** as a dark blue solid (34.23 mg, 16 %), m.p. = 122.7-124.0$^0$C.

*$^1$H-NMR (250 MHz, $CD_2Cl_2$). δ* (ppm): 0.88 (t, *J* = 6.50 Hz, 6H); 1.27-1.34 (m, 36H); 1.63-1.70 (m, 4H); 2.65-2.71 (m, 4H); 7.11-7.16 (m, 2H); 7.21-7.26 (m, 4H); 7.39-7.41 (m, 2H); 7.48-7.54 (m, 2H); 7.65-7.70 (m, 4H); 8.75 (d, *J* = 16.5 Hz, 1H); 9.06 (d, *J* = 16.2 Hz, 1H).

*$^{13}$C-NMR (62.5 MHz, $CD_2Cl_2$). δ* (ppm): 14.47 ($CH_3$); 23.29 ($CH_2$); 29.90 ($CH_2$); 29.92 ($CH_2$); 29.97 ($CH_2$); 30.12 ($CH_2$); 30.25 ($CH_2$); 30.29 ($CH_2$); 31.84 ($CH_2$); 31.88 ($CH_2$); 32.53 ($CH_2$); 36.41 ($CH_2$); 90.60 (C); 97.60 (C); 111.23 (C); 121.65 (CH); 123.99 (C); 126.76 (C); 127.03 (CH); 128.20 (CH); 128.78 (CH); 128.86 (CH); 128.92 (CH); 129.33 (CH); 130.45 (CH); 130.63 (CH); 132.21 (CH); 133.40 (CH); 136.47 (C); 136.83 (C); 141.45 (C); 145.24 (C); 145.76 (C); 145.96 (C); 152.04 (C); 153.97 (C); 155.13 (C); 155.52 (C).

*MALDI-TOF:* found 892.223, calcd. for $C_{56}H_{66}N_4S_3$: 890.45.

*MS (ESI$^+$):* $[M]^+$ = 891.4495; calcd. for $C_{56}H_{67}N_4S_3$: 891.4528.

*FT-IR (neat). 1/λ* (cm$^{-1}$): 690; 850; 1183; 1459; 1590; *2180*; 2850; 2917.

***General procedure for the preparation of vinyl containing 6,7-bis(aryl)-4,9-bis(arylethynyl)-[2,1,3]thiadiazolo[3,4-g]quinoxaline derivatives 25 (PTQEP), 29 (PTQET) and 31 (TTQET)***

To a solution of 4,9-dibromo-6,7-bis(aryl)-[2,1,3]thiadiazolo[3,4-*g*]quinoxalines (**17** or **18**, 0.24 mmol, 1.00 equiv.), under inert atmosphere in degassed THF and $^{i}Pr_2NH$ (5 mL : 5 mL) solvent mixture, tetrakis(triphenylphosphine)palladium(0) (0.014 g, 5 mol%), copper(I) iodide (0.023 g, 5 mol%) and 2 equiv. of the corresponding terminal alkyne (**22** or **26**, 0.480 mmol) were added. After being stirred for 15 min at r.t. the mixture was filtered through Celite 545 and the solvents were evaporated under reduced pressure. The residues were purified by column chromatography (eluent: hexane:$CH_2Cl_2$ = 2:1).

**6,7-Bis(4-dodecylphenyl)-4,9-bis(phenylethynyl)-[2,1,3]thiadiazolo[3,4-*g*]quinoxalines (25, PTQEP)**

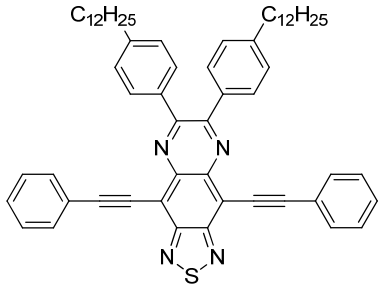


**25** (**PTQEP**)

Application of the general procedure to ethynylbenzene (**22**, 49.00 mg, 0.48 mmol) and **17** (200.36 mg, 0.24 mmol) furnushed the desired product **25** (**PTQEP**) as a dark red solid (162.12 mg, 77 %), m.p. = 116.4117.6$^{0}$C.

*$^{1}$H-NMR (300 MHz, $CD_2Cl_2$). δ* (ppm): 0.87 (t, *J* = 6.50 Hz, 6H); 1.27-1.34 (m, 36H); 1.61-1.68 (m, 4H); 2.68 (t, *J* = 7.50 Hz, 4H); 7.24 (d, *J* = 8.32 Hz, 2H); 7.47-7.49 (m, 6H); 7.70 (d, *J* = 8.30 Hz, 2H); 7.77-7.81 (m, 4H)

*$^{13}$C-NMR (62.5 MHz, $CD_2Cl_2$). δ* (ppm): 14.46 ($CH_3$); 23.27 ($CH_2$); 29.86 ($CH_2$); 29.95 ($CH_2$); 30.10 ($CH_2$); 30.23 ($CH_2$); 30.26 ($CH_2$); 30.28 ($CH_2$); 31.82 ($CH_2$); 32.50 ($CH_2$); 36.38 ($CH_2$); 85.85 (C); 105.90 (C); 114.21 (C); 123.62 (C); 128.89 (CH); 129.18 (CH); 129.87 (CH); 130.61 (CH); 132.62 (CH); 136.44 (C); 141.38 (C); 146.06 (C); 154.66 (C); 155.81 (C).

*MALDI-TOF:* found 877.146; calcd. for $C_{60}H_{68}N_4S$: 876.516.

*MS (ESI$^+$):* $[M]^+$ = 877.5259; calcd. for $C_{60}H_{69}N_4S$: 877.5243.

*FT-IR (neat). 1/λ* ($cm^{-1}$): 689; 717; 752; 849; 1017; 1092; 1185; 1247; 1375; 1468; 1497; 1609; *2197*; 2850; 2916.

**6,7-Bis(4-dodecylphenyl)-4,9-bis(thiophen-2-ylethynyl)-[2,1,3]thiadiazolo[3,4-*g*]quinoxaline (29, PTQET)**

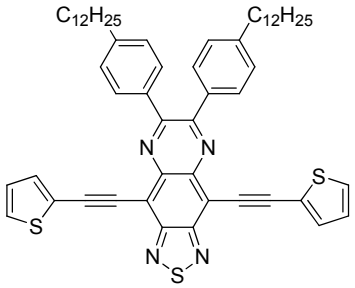


**29** (**PTQET**)

Application of the general procedure to 2-ethynylthiophene (**26**, 51.92 mg, 0.48 mmol) and compound **17** (200.36 mg, 0.24 mmol) furnished the desired product **29** (**PTQET**) as a dark violet solid (175.02 mg, 82 %), m.p. = 135.2-136.4$^0$C.

*$^1$H-NMR (300 MHz, $CD_2Cl_2$). δ* (ppm): 0.87 (t, *J* = 6.50 Hz, 6H); 1.27-1.34 (m, 36H); 1.61-1.68 (m, 4H); 2.67 (t, *J* = 7.50 Hz, 4H); 7.16 (dd, *J* = 3.68, 5.15 Hz, 2H); 7.23 (d, *J* = 8.10 Hz, 4H); 7.51 (dd, *J* = 1.10, 5.10 Hz, 2H); 7.56 (dd, *J* = 1.10, 3.60 Hz, 2H); 7.69 (d, *J* = 8.40 Hz, 2H).

*$^{13}$C-NMR (75 MHz, $CD_2Cl_2$). δ* (ppm): 14.35 ($CH_3$); 23.16 ($CH_2$); 29.75 ($CH_2$); 29.84 ($CH_2$); 29.99 ($CH_2$); 30.12 ($CH_2$); 30.15 ($CH_2$); 30.17 ($CH_2$); 31.71 ($CH_2$); 32.40 ($CH_2$); 36.28 ($CH_2$); 90.07 (C); 99.02 (C); 113.63 (C); 123.45 (C); 128.18 (CH); 128.79(CH); 129.79 (CH); 130.51 (CH); 133.81 (CH); 136.24 (C); 141.05(C); 146.05 (C); 154.15 (C); 155.67(C).

*MALDI-TOF:* found 890.374, calcd. for $C_{56}H_{64}N_4S_3$: 888.429.

*MS (ESI$^+$):* $[M]^+$ = 889.4396, calcd. for $C_{56}H_{65}N_4S_3$: 889.4371.

*FT-IR (neat). 1/λ* ($cm^{-1}$): 695; 827; 851; 901; 1006; 1090; 1183; 1247; 1336; 1377; 1466; 1524; 1608; *2184*; 2850; 2919.

**6,7-Bis(5-octylthiophen-2-yl)-4,9-bis(thiophen-2-ylethynyl)-[2,1,3]thiadiazolo[3,4-*g*]quinoxaline (31, TTQET)**

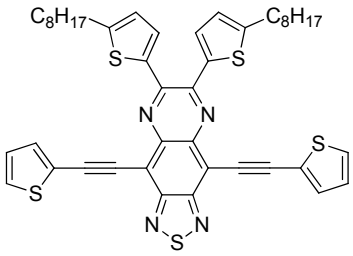


**31** (**TTQET**)

Application of the general procedure to 2-ethynylthiophene (**26**, 51.92 mg, 0.48 mmol) and compound **18** (176.16 mg, 0.24 mmol) furnished the desired compound **31** (**TTQET**) as a dark violet solid (153.42 mg, 81 %), m.p. = 164.5-165.6$^0$C.

*$^1$H-NMR (300 MHz, $CD_2Cl_2$). δ* (ppm): 0.89 (t, *J* = 6.50 Hz, 6H); 1.30-1.46 (m, 20H); 1.81 (q, *J* = 7.80 Hz 4H); 2.94 (t, *J* = 7.60 Hz, 4H); 6.80 (d, *J* = 3.60 Hz, 2H); 7.16 (dd, *J* = 3.90, 5.10 Hz, 2H); 7.50 (dd, *J* = 1.20, 5.10 Hz, 2H); 7.54 (d, *J* = 3.90 Hz, 2H); 7.58 (dd, *J* = 1.10, 3.70 Hz, 2H).

*$^{13}$C-NMR (75 MHz, $CD_2Cl_2$). δ* (ppm): 14.47 ($CH_3$); 23.28 ($CH_2$); 29.81 ($CH_2$); 29.83 ($CH_2$); 29.99 ($CH_2$); 31.18 ($CH_2$); 32.14 ($CH_2$); 32.50 ($CH_2$); 90.21 (C); 98.90 (C); 112.65 (C); 123.74 (C); 125.81 (CH); 128.26 (CH); 129.79 (CH); 132.32 (CH); 133.92 (CH); 140.20 (C); 140.83 (C); 148.65 (C); 154.14 (C); 154.24 (C).

*MALDI-TOF:* found 789.955, calcd. for $C_{44}H_{44}N_4S_5$: 788.217.

*MS (ESI$^+$):* $[M]^+$ = 789.2239, calcd. for $C_{44}H_{45}N_4S_5$: 789.2248.

*FT-IR (neat). 1/λ* ($cm^{-1}$): 692; 769; 810; 883; 1074; 1262; 1336; 1382; 1414; 1450; 1532; 2188; 2850; 2920.

**4,7-Bis(thiophen-2-ylethynyl)-benzo[*c*][2,1,3]thiadiazole (30)**

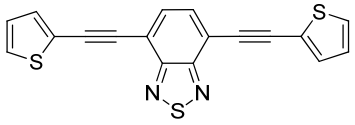

**30**

To a solution of 4,7-dibromobenzo[*c*][2,1,3]thiadiazole (**2**, 70.55 mg, 0.240 mmol, 1 equiv.), under inert atmosphere in degassed THF and $^{i}Pr_2NH$ (5 mL : 5 mL) solvent mixture, tetrakis(triphenylphosphine)palladium(0) (0.014 g, 5 mol%), copper(I) iodide (0.023 g, 5 mol%) and 4.5 equiv. of 2-ethynylthiophene (**26**, 116.80 mg, 1.080 mmol) were added. After being stirred for 48 h at r.t., the mixture was filtered and the desired product (compound **30**) was isolated after recrystallization from toluene, as bright yellow crystalls (334.52 mg, 96 %).

*$^{1}$H-NMR (300 MHz, THF-d8).* $\delta$ (ppm): 7.10 (dd, $J$ = 3.50, 5.10 Hz, 2H); 7.45 (dd, $J$ = 1.20, 3.50 Hz, 2H); 7.55 (dd, $J$ = 1.00, 5.10 Hz, 2H); 7.82 (s, 2H).

*$^{13}$C-NMR (75 MHz, THF-d8).* $\delta$ (ppm): 90.08 (C); 91.23 (C); 117.82 (C); 128.31 (CH); 129.85 (CH); 132.83 (CH); 133.99 (CH).

*MS (ESI$^{+}$):* $[M]^{+}$ = 348.9590, calcd. for $C_{18}H_9N_2S_3$: 349.1936.

***General procedure for the preparation of the aromatic dialkynes 37 and 42***

To a stirring solution containing the dihalogenated aromatic derivative (**34** or **40**, 3.00 mmol, 1.00 equiv.), copper(I) iodide (20.00 mmg, 3.3 mol%), palladium acetate (20.00 mmg, 3.3 mol%), and triphenylphosphine (60 mg, 6.6 mol%) in a THF and $^{i}Pr_2NH$ (5 mL : 5 mL) at $60^{0}$C, 7.5 mmol of trimethysilylacetylene (**35**, 736.76 mg, 2.50 equiv.) were added and stirred at the same temperature for additional 2.5 h. After the reaction mixture was cooled to r.t., it was filtered through Celite 545 and the organic layer was placed in a new flask to which 7.20 mmol of tetra-*n*-butylammonium fluoride (TBAF, 1.88 g, 2.40 equiv.) was added. Subsequent to a 10 min. stirring, the solvent was removed under reduced presure and

column chromatography (eluent: hexane) of the residue yielded the desired compound **37**, or **42**.

**1,4-Didodecyl-2,5-diethynylbenzene (37)**

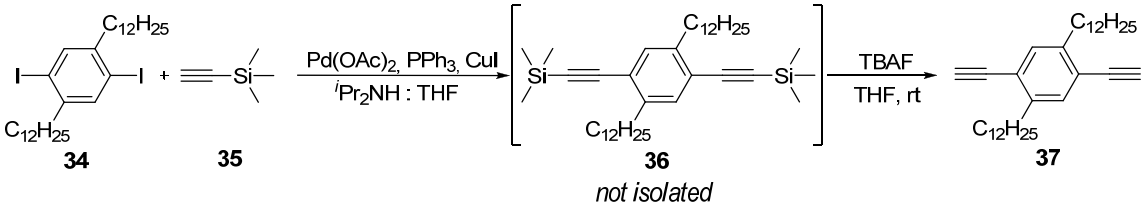


Application of the general procedure to **34** yielded compound **37** as a white solid (1.150 g, 83 % over 2 steps).

*$^{1}$H-NMR (250 MHz, $CDCl_3$). δ* (ppm): 0.88 (t, *J* = 7.00, 6.25 Hz, 6H); 1.26-1.30 (m, 36H); 1.62 (q, *J* = 7.00, 7.25 Hz, 4H); 2.71 (t, *J* = 7.5, 8.00 Hz, 4H); 3.28 (s, 2H); 7.26 (s, 2H). Data in agreement with the literature reported values.[7]

*$^{13}$C-NMR (75 MHz, $CDCl_3$). δ* (ppm): 14.49 ($CH_3$); 23.01 ($CH_2$); 29.67 ($CH_2$); 29.73 ($CH_2$); 29.76 ($CH_2$); 29.88 ($CH_2$); 29.96 ($CH_2$); 29.98 ($CH_2$); 30.00 ($CH_2$); 30.77 ($CH_2$); 32.24 ($CH_2$); 34.09 ($CH_2$); 77.32 (C); 81.81 (C); 122.23 (C); 133.25 (CH); 143.01 (C). Data in agreement with the literature reported values.[7]

**3,4-Didodecyl-2,5-diethynylthiophene (42)**

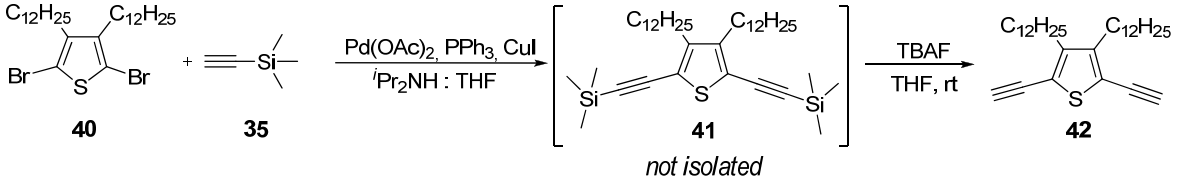


Application of the general procedure to **40** yielded compound **42** as a colourless oil (1.070 g, 76 % over 2 steps).

*$^{1}$H-NMR (250 MHz, $CDCl_3$). δ* (ppm): 0.88 (t, *J* = 6.50 Hz, 6H); 1.27-1.31 (m, 36H); 1.48-1.56 (m, 4H); 2.60 (t, *J* = 7.50 Hz, 4H); 3.42 (s, 2H). Data in agreement with the literature reported values.[8]

*$^{13}$C-NMR (62.5 MHz, $CDCl_3$). δ* (ppm): 14.13; 22.70; 28.40; 29.37; 29.54; 29.57; 29.67; 29.68; 29.71; 30.05; 31.94; 76.71; 83.52; 118.16; 147.69. Data in agreement with the literature reported values.[8]

***General Procedure for the Preparation of the Polymers under Microwave Irradiation***

In a typical reaction the TQ derivative (**16**-**18**, 0.239 mmol, 1.00 equiv.) and the corresponding aromatic dialkyne **37** or **42** (0.250 mmol, 1.04 equiv.) were placed in a 35 mL microwave vial and dissolved in a 1 : 1 solvent mixture of THF and $^{i}Pr_2NH$ (5 mL : 5 mL). The solution was degassed with a stream of argon for 15 min, following which $Pd(PPh_3)_4$ (8.20 mg, 0.007 mmol) and CuI (1.30 mg, 0.007 mmol) were added. The reaction mixture was further degassed and subsequently seald. The vial was placed in the microwave reactor and kept at $50^0$C for 80 min and at $60^0$C for 20 min.

*Work-up Procedure*

After cooling to r.t., the mixture was slowly added to a stirred acetone solution (300 mL), filtered and washed with methanol, water and acetone (2 x 100 mL each). The polymeric material was purified by dissolving it in toluene (100 mL) and vigorously stirring it at r.t. with Basolite A (MOF) for 2 h. The mixture was filtered and the solution was concentrated (to 10 mL) under reduced pressure and subsequently precipitated in acetone (300 mL), filtered and washed as indicated above. The resulting material was redissolved in a minimum amount of toluene and added dropwise to a stirred acetone (300 mL) solution. The precipitate was isolated by filtration and dried *in vacuo* to afford the desired polymer.

**Polymer $P_2$**

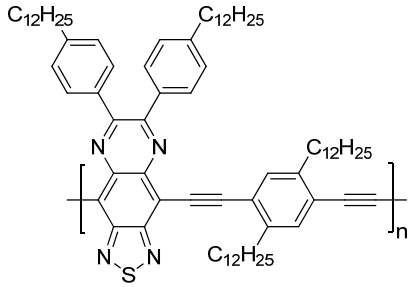


**$P_2$ (PPTQP)**

Application of the general procedure to monomers **17** and **37** yielded 241.60 mg of polymer **$P_2$** as a dark green solid (89 %).

*GPC (TCB, 135$^0$C vs. PS)*: $M_n$ = 17.4 kg mol$^{-1}$; $M_w$ = 53.6 kg mol$^{-1}$; *PDI* = 3.08

*$^1$H-NMR (500 MHz, $C_2D_2Cl_4$, 373.3K). δ* (ppm): 0.92-0.94 (m, 12H); 1.28-1.47 (m, 72H); 1.78 (s, 4H); 1.94 (s, 4H); 2.79 (s, 4H); 3.26 (s, 4H); 7.29 (broad d, *J* = 7.00 Hz, 4H); 7.81 (broad d, *J* = 7.00 Hz, 5H); (proton values with respect to the repeating unit).

*FT-IR (neat). 1/λ* (cm$^{-1}$): 720; 849; 899; 1035; 1088; 1184; 1198; 1246; 1339; 1375; 1461; 1499; 1607; *2187*; 2851; 2919; 2955.

**Polymer $P_3$**

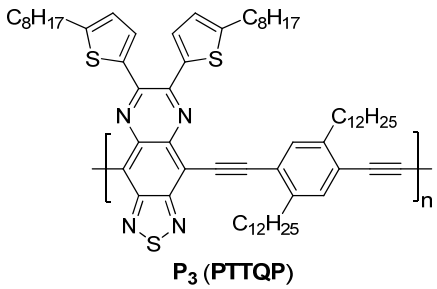


**$P_3$ (PTTQP)**

Application of the general procedure to monomers **18** and **37** yielded 193.00 mg of polymer **$P_3$** as a dark green solid (78 %).

*GPC (TCB, 135$^0$C vs. PS)*: $M_n$ = 13.8 kg mol$^{-1}$; $M_w$ = 26.9 kg mol$^{-1}$; *PDI* = 1.95

*$^1$H-NMR (500 MHz, $C_2D_2Cl_4$, 373.3K). δ* (ppm): 0.92-0.96 (m, 12H); 1.28-1.62 (m, 56H); 1.89 (s, 4H); 2.00 (s, 4H); 3.03 (s, 4H); 3.31 (s, 4H); 6.89 (broad s, 2H); 7.60 (broad s, 2H); 7.90 (broad s, 2H); (proton values with respect to the repeating unit).

*$^{13}$C-NMR (125 MHz, $C_2D_2Cl_4$, 373.3K). δ* (ppm): 13.71 ($CH_3$); 22.34 ($CH_2$); 28.96 ($CH_2$); 29.01 ($CH_2$); 29.10 ($CH_2$); 29.37 ($CH_2$); 29.44 ($CH_2$); 29.54 ($CH_2$); 30.40 ($CH_2$); 30.78 ($CH_2$); 31.18 ($CH_2$); 31.61 ($CH_2$); 34.29 ($CH_2$); 91.03 (C); 105.35 (C); 113.06 (C); 123.78 (C); 124.80 (CH); 131.51 (CH); 133.10 (CH); 139.44 (C); 140.29 (C); 143.14 (C); 147.98 (C); 152.78 (C); 154.26 (C).

*FT-IR (neat). 1/λ* (cm$^{-1}$): 690; 721; 849; 899; 997; 1088; 1185; 1199; 1237; 1338; 1375; 1456; 1522; 1608; *2168*; 2850; 2920.

**Polymer $P_4$**

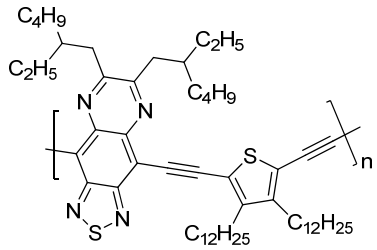


**$P_4$ (PRTQT)**

Application of the general procedure to monomers **16** and **42** yielded 190.84 mg of polymer **$P_4$** as a dark green solid (91 %).

*GPC (TCB, 135$^0$C vs. PS)*: $M_n$ = 11.7 kg mol$^{-1}$; $M_w$ = 59.1 kg mol$^{-1}$; *PDI* = 5.0

*$^1$H-NMR (500 MHz, $C_2D_2Cl_4$, 373.3K). δ* (ppm): 0.93-1.92 (broad m, 70H); 2.41 (broad s, 4H); 3.13 (broad s, 4H); (proton values with respect to the repeating unit).

*FT-IR (neat). 1/λ* (cm$^{-1}$): 721; 859; 1120; 1155; 1231; 1377; 1457; 1578; *2169*; 2852; 2922; 2955

**Polymer $P_5$**

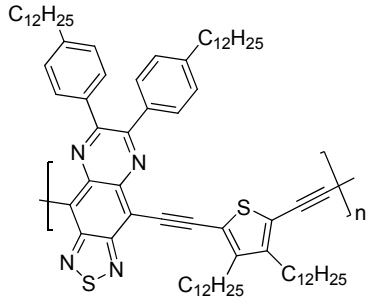

**$P_5$ (PPTQT)**

Application of the general procedure to monomers **17** and **42** yielded 227.04 mg of polymer **$P_5$** as a dark green solid (88 %).

*GPC (TCB, 135$^0$C vs. PS)*: $M_n$ = 18.4 kg mol$^{-1}$; $M_w$ = 65.3 kg mol$^{-1}$; *PDI* = 3.5

*$^1$H-NMR (300 MHz, THF-$d_8$). $\delta$* (ppm): 0.88 (s, 12H); 1.21-1.30 (broad m, 80H); 2.72 (broad s, 4H); 3.02 (broad s, 4H); 7.01-7.74 (broad m, 8H); (proton values with respect to the repeating unit).

*Elemental Anal.*: Calcd. for $(C_{76}H_{108}N_4S_2)_n$: C, 79.94; H, 9.53; N, 4.91; S, 5.62. Found: C, 78.04; H, 9.03; N, 4.70; S, 5.03.

*FT-IR (neat). 1/λ* (cm$^{-1}$): 692; 720; 848; 898; 998; 1088; 1183; 1237; 1376; 1456; 1523; 1608; *2168*; 2850; 2920.

**Polymer $P_6$**

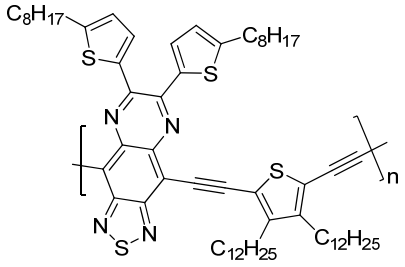

**$P_6$ (PTTQT)**

Application of the general procedure to monomers **18** and **42** yielded 217.36 mg of polymer $\mathbf{P_6}$ as a dark green solid (85 %).

*GPC (TCB, 135$^0$C vs. PS)*: $M_n$ = 17.8 kg mol$^{-1}$; $M_w$ = 39.1 kg mol$^{-1}$; *PDI* = 2.2.

*$^1$H-NMR (700 MHz, THF-$d_8$, 333.3K). $\delta$* (ppm): 0.82-0.911 (m, 12H); 1.22-1.57 (broad m, 56H); 1.87 (broad s, 8H); 2.97 (broad s, 4H); 3.14 (broad s, 4H); 6.84 (broad s, 2H); 7.54 (broad s, 2H); (proton values with respect to the repeating unit).

*FT-IR (neat). 1/λ* (cm$^{-1}$): 692; 720; 800; 881; 1071; 1253; 1377; 1453; 1503; *2168*; 2850; 2920.

**2-Decyl-1-tetradecylbromide** (**45a**)

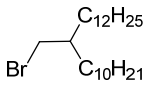


**45a**

A solution of triphenylphosphine (25.00 g, 9.50 mmol, 1.58 mol%) and 2-decyl-tetradecanol **43** (21.05 g, 0.60 mol, 1.00 equiv.) in 40 mL $CH_2Cl_2$ was cooled to 0$^0$C under inert atmosphere. N-bromsuccinimide (**44**, 16.25 g, 0.90 mol, 1.50 equiv.) was carefully added in small portions and the reaction mixture was further stirred at r.t. for 12 h. The solvent was removed under reduced pressure, the residue redissolved in hexane and filtered through a silica pad affording 23.98 g of **45a** as a colourless oil (96 %).

*$^1$H-NMR (250 MHz, $CDCl_3$). $\delta$* (ppm): 0.88 (t, *J* = 7.00, 5.5 Hz, 6H); 1.26 (broad s, 40H); 1.53-1.59 (m, 1H); 3.43 (d, *J* = 5.00 Hz, 2H). Data in agreement with the literature reported values.[9]

*$^{13}$C-NMR (62.5 MHz, $CDCl_3$). $\delta$* (ppm): 14.13; 22.86; 26.62; 29.57; 29.76; 29.82; 29.96; 29.98; 32.24; 32.92; 39.95; 40.10. Data in agreement with the literature reported values.[9]

***General Procedure for the Preparation of the N-alkylated Phenothiazine Derivatives 47a-b and 50***

In a typical reaction 4.00 g of phenothiazine **46** (20.00 mmol, 1.00 equiv.) were dissolved in 50 mL anhydrous DMF and 1.00 g (25.00 mmol, 1.25 equiv.) of NaH (60% mineral oil) were carefully added portionwise under inert atmosphere. After 30 min stirring at r.t., 23.50 mmol (1.18 equiv.) of the corresponding brominated alkyl derivative **45a-b** or **49** was added and the reaction mixture was stirred at $70^0$C for 18 h. The reaction was quenched by pouring the solution into a separatory funnel, followed by the addition of 100 mL of water and 100 mL of ethyl acetate. The organic layer was separated, and the aqueous layer was washed with ethyl acetate. The remaining organic solvent was dried over $MgSO_4$, filtered and concentrated by evaporation under reduced pressure. The resulting crude product were purifed by column chromatography (eluent: hexane).

**10-(2-Decyltetradecyl)-10*H*-phenothiazine** (**47a**)

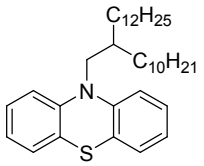


**47a**

Application of the general procedure to **46** and **45a** yielded 8.90 g of compound **47a** as a colourless oil (83 %).

*$^1$H-NMR (250 MHz, $CDCl_3$). δ* (ppm): 0.91 (t, *J* = 7.50, 7.50 Hz, 6H); 1.23-1.28 (m, 40H); 1.85-2.08 (m, 1H); 3.73 (d, *J* = 5.00 Hz, 2H); 6.86-6.94 (m, 4H); 7.12-7.18 (m, 4H).

*$^{13}$C-NMR (62.5 MHz, $CDCl_3$). δ* (ppm): 14.14; 22.71; 26.24; 29.36; 29.38; 29.48; 29.63; 29.68; 29.70; 29.96; 31.64; 31.94; 34.41; 51.47; 115.87; 122.25; 125.85; 126.99; 127.48; 145.75.

*MS (FD, 8 kV): m/z* = 535.12, calcd. for $C_{36}H_{57}NS$: 535.91.

**10-(2-Ethylhexyl)-10*H*-phenothiazine** (**47b**)

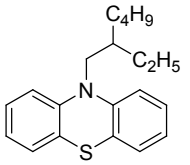


**47b**

Application of the general procedure to **46** and **45b** yielded 4.50 g of compound **47b** as a colourless oil (72 %).

*$^{1}$H-NMR (250 MHz, $CDCl_3$).* $\delta$ (ppm): 0.81-0.90 (m, 6H); 1.24-1.48 (m, 8H); 1.92 (q, *J* = 6.5, 6.25 Hz, 1H); 3.45 (d, *J* = 6.50 Hz. 2H); 6.93 (dt, *J* = 1.25, 7.5, 7.75 Hz, 2H); 7.05 (dd, *J* = 1.25, 7.75 Hz, 2H); 7.14-7.23 (m, 4H). Data in agreement with the literature reported values.[10]

*$^{13}$C-NMR (62.5 MHz, acetone-$d_6$).* $\delta$ (ppm): 11.67, 15.13; 24.56; 25.41; 30.05; 32.01; 37.54; 52.32; 117.89; 124.10; 127.16; 128.94; 129.02; 147.55. Data in agreement with the literature reported values.[10]

**10-(2-Isopropyl)-10*H*-phenothiazine** (**50**)

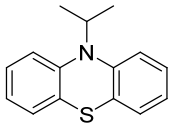


**50**

Application of the general procedure to **46** and **49** yielded 4.18 g of compound **50** as a white solid (86 %).

*$^{1}$H-NMR (300 MHz, THF-$d_8$).* $\delta$ (ppm): 1.59 (d, *J* = 6.00 Hz, 6H); 4.27 (s, *J* = 6.00, 9.00, 6.00, 6.00, 9.00, 6.00 Hz, 1H); 6.84-6.90 (m, 2H); 7.04-7.10 (m, 6H).

*$^{13}$C-NMR (75 MHz, THF-$d_8$). δ* (ppm): 22.60 ($CH_3$); 54.77 (CH); 119.23 (CH); 123.38 (CH); 127.69 (CH); 127.85 (CH); 128.05 (C); 146.37 (C).

*MS (FD, 8 kV): m/z* = 241.00, calcd. for $C_{15}H_{15}NS$: 241.35.

### *General Procedure for the Preparation of the Brominated N-alkylated Phenothiazine Derivatives 49a-b and 51*

In a typical reaction 3.73 mmol (1.00 equiv.) of N-alkyl-phenothiazine **48a-b** or **50** were dissolved in 50 mL $CH_2Cl_2$ at r.t. and to the stirring solution 7.83 mmol (1.25 g, 2.10 equiv.) bromine [for the synthesis of compound **51**, only 1.00 equiv. (3.73 mmol)] was slowly added. After stirring at room temperature for 4 h the reaction was terminated by adding a dilute NaOH aqueous solution. The reaction mixture was extracted three times using $CH_2Cl_2$ and brine, the combined organic layers was dried over $MgSO_4$, filtered and the solvent was removed under reduced pressure. The crude product was purified by column chromatography (eluent: heptane).

**3,7-Dibromo-10-(2-decyltetradecyl)-10*H*-phenothiazine** (**48a**)

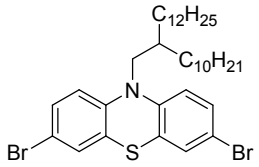


**48a**

Application of the general procedure to **47a** yielded 2.12 g of compound **48a** as a colourless oil (82 %).

*$^{1}$H-NMR (250 MHz, acetone-$d_5$). δ* (ppm): 0.86-0.91 (m, 6H); 1.23-1.73 (m, 40H); 1.92-1.99 (m, 1H); 3.83 (d, *J* = 7.50 Hz, 2H); 7.01 (d, *J* = 7.50 Hz, 2H); 7.31-7.38 (m, 4H).

*$^{13}$C-NMR (62.5 MHz, acetone-$d_6$). δ* (ppm): 14.21; 22.51; 26.28; 29.33; 29.39; 29.47; 29.61; 29.69; 29.71; 29.92; 31.65; 31.93; 34.38; 51.46; 116.71; 120.33; 129.46; 131.77; 132.73; 147.27.

*MS (ESI+)*: $[M]^+$ = 694.2007, calcd. for $C_{36}H_{56}Br_2NS$: 694.6849.

**3,7-Dibromo-10-(2-ethylhexyl)-10*H*-phenothiazine** (**48b**)

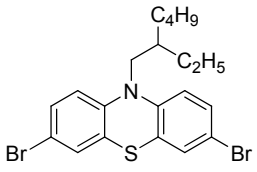


**48b**

Application of the general procedure to **47b** yielded 1.54 g of compound **48b** as a colourless oil (88 %).

*$^1$H-NMR (250 MHz, acetone-$d_5$).* $\delta$ (ppm): 0.81-0.91 (m, 6H); 1.21-1.49 (m, 8H); 1.90 (q, *J* = 5.00, 7.50 Hz, 1H); 3.82 (d, *J* = 7.50 Hz, 2H); 7.01 (d, *J* = 7.50 Hz, 2H); 7.32-7.38 (m, 4H). Data in agreement with the literature reported values.[10]

*$^{13}$C-NMR (62.5 MHz, acetone-$d_6$).* $\delta$ (ppm): 12.24; 15.74; 25.20; 25.96; 38.20; 53.25; 116.71; 120.33; 129.46; 131.77; 132.73; 147.27. Data in agreement with the literature reported values.[10]

**3-Bromo-10-(2-isopropyl)-10*H*-phenothiazine** (**51**)

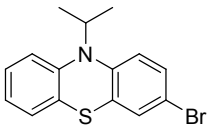


**51**

Application of the general procedure to **50** yielded 1.10 g of compound **51** as a white solid (92 %).

*$^1$H-NMR (300 MHz, THF-$d_8$).* $\delta$ (ppm): 1.58 (d, *J* = 6.00 Hz, 6H); 4.25 (s, *J* = 6.00, 9.00, 6.00, 6.00, 9.00, 6.00 Hz, 1H); 6.87-6.92 (m, 1H); 6.98 (d, *J* = 9.00 Hz, 1H); 7.03-7.12 (m, 3H); 7.22-7.25 (m, 2H).

*$^{13}$C-NMR (75 MHz, THF-$d_8$). δ* (ppm): 22.55 ($CH_3$); 55.04 (CH); 115.58 (C); 119.45 (CH); 120.55 (CH); 123.82 (CH); 127.24 (C); 128.13 (CH); 128.20 (CH); 130.20 (CH); 130.61 (CH); 130.68 (C); 145.75 (C); 146.20 (C).

*MS (FD, 8 kV): m/z* = 319.01, calcd. for $C_{15}H_{14}BrNS$: 320.25.

### *General Procedure for the Preparation of the Pinacolatoboron Functionalized Benzo[c][2,1,3]thiadiazole Derivatives 53a-b*

In a typical reaction 6.80 mmol (1.00 equiv.) of the brominated benzo[*c*][2,1,3]thiadiazole derivative **5** or **5a**, bis(pinacolato)diboron (**52**; 2.50 equiv. in case of **5** and 1.25 equiv. in case of **5a**), $PdCl_2$(dppf) (500 mg, 9 mol%), and 6.00 equiv. of potassium acetate (40.80 mmol, 4.00 g) in anhydrous 1,4-dioxane (25 mL) was stirred at $80^0$C under inert atmosphere for 15 h. The reaction was quenched by adding water. The resulting mixture was washed with ethyl acetate (3 x 100 mL) and the combined organic layers was dried over $MgSO_4$, filtered and concentrated under reduced pressure. The crude product was purified by column chromatography (eluent: hexane : ethyl acetate = 100:1 with increasing amount of ethyl acetate).

**4-(4,4,5,5-Tetramethyl-1,3,2-dioxaborolan-2-yl)benzo[*c*][2,1,3]thiadiazole** (**53a**)

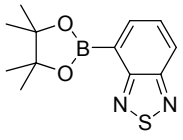


**53a**

Application of the general procedure to **5a** yielded 802.13 mg of compound **53a** as a white solid (45 %).

*$^{1}$H-NMR (250 MHz, THF-$d_8$). δ* (ppm): 1.39 (s, 12H); 7.61 (dd, *J* = 7.50 Hz, 1H); 8.05-8.11 (m, 2H).

*$^{13}$C-NMR (62.5 MHz, THF-$d_8$). δ* (ppm): 25.28; 84.89; 138.09; 157.57.

*MS (FD, 8 kV): m/z* = 261.89, calcd. for $C_{12}H_{15}BN_2O_2S$: 262.13.

**4,7-Bis(4,4,5,5-tetramethyl-1,3,2-dioxaborolan-2-yl)benzo[*c*][2,1,3]thiadiazole** (**53b**)

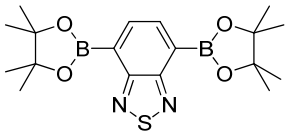

**53b**

Application of the general procedure to **5** yielded 1.48 g of compound **53b** as colourless crystalls (56 %) obtained upon repeated recrystallization from hexane.

*$^{1}$H-NMR (250 MHz, $CD_2Cl_2$). δ* (ppm): 1.45 (s, 24H); 8.08 (s, 2H).

*$^{13}$C-NMR (62.5 MHz, $CD_2Cl_2$). δ* (ppm): 25.26; 84.88; 137.98, 157.49.

*MS (FD, 8 kV): m/z* = 387.42, calcd. for $C_{18}H_{26}B_2N_2O_4S$: 388.10.

***General Procedure for the Preparation of Model Compounds M1 (54) and M2 (55)***

In a typical reaction the brominated phenothiazine derivative (**48b** or **51**) and the pinacolatoboron functionalized benzo[*c*][2,1,3]thiadiazole derivative (**53a** or **53b**) were dissolved in toluene (10 mL) in a 35 mL microwave vial under a constant stream of argon. To this solution 6.00 equiv. per coupling unit of $K_2CO_3$ (2M aqueous solution) and a few drops of Aliquat 366 were added. After 15 min of stirring under a constant stream of argon, 5 mol% of $Pd(PPh_3)_4$ were added and the vial was seald and placed in the microwave reactor. Subsequent to a 50 min microwave irradiation at $85^0$C, the reaction mixture was cooled to r.t. and extracted with ethyl acetate. The organic layer was washed with water and brine, dried over $MgSO_4$, filtered and the solvent was evaporated under reduced peassure. The crude products were purified by column chromatography (eluent: toluene : hexane = 1:1).

**3,7-Di(benzo[*c*][2,1,3]thiadiazol-4-yl)-10-(2-ethylhexyl)-10*H*-phenothiazine** (**54, M1**)

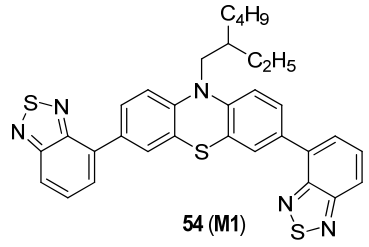


**54 (M1)**

Application of the general procedure to **48b** (500.00 mg, 1.07 mmol, 1.00 equiv.) and **53a** (698.00 mg, 2.66 mmol, 2.48 equiv.) yielded 536.62 mg of compound **54** as a yellow powder (87 %).

*$^{1}$H-NMR (300 MHz, THF-$d_8$).* $\delta$ (ppm): 0.87-0.97 (m, 6H); 1.31-1.59 (m, 8H); 2.08 (q, *J* = 6.00, 6.00 Hz, 1H); 3.96 (d, *J* = 6.00 Hz, 2H); 7.69 (dd, *J* = 6.00, 3.00 Hz, 2H); 7.78 (dd, *J* = 6.00, 3.00 Hz, 2H); 7.90-7.96 (m, 6H).

*$^{13}$C-NMR (75 MHz, THF-$d_8$).* $\delta$ (ppm): 11.05 ($CH_3$); 14.55 ($CH_3$); 24.20 ($CH_2$); 25.09 ($CH_2$); 25.52 ($CH_2$); 25.75 ($CH_2$); 29.76 ($CH_2$); 31.86 ($CH_2$); 37.40 (CH); 51.96 ($CH_2$); 116.88 (CH); 121.01 (CH); 126.48 (C); 127.64 (CH); 129.14 (CH); 129.38 (CH); 130.70 (CH); 132.97 (C); 134.14 (C); 146.77 (C); 154.42 (C); 157.04 (C).

*MS (ESI+)*: $[M]^+$ = 580.1644, calcd. for $C_{32}H_{30}N_5S_3$: 580.1663.

**4,7-Bis(10-isopropyl-10*H*-phenothiazin-3-yl)benzo[*c*][2,1,3]thiadiazole** (**55, M2**)

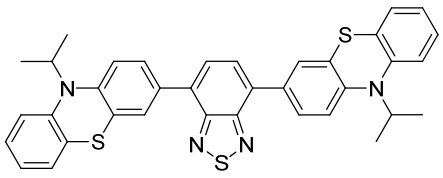


**55 (M2)**

Application of the general procedure to **51** (386.3 mg, 1.2 mmol, 2.85 equiv.) and **53b** (160 mg, 0.42 mmol, 1.00 equiv.) yielded 671.41 mg of compound **55** as a red powder (91 %).

*$^{1}$H-NMR (250 MHz, THF-$d_8$).* $\delta$ (ppm): 1.68 (d, $J$ = 7.50 Hz, 6H); 4.40 (sept, $J$ = 5.00, 7.50, 7.50, 7.50, 7.50, 5.00 Hz, 1H); 6.88-6.94 (m, 1H); 7.09-7.15 (m, 3H); 7.25 (d, $J$ = 7.50 Hz, 1H); 7.84-7.93 (m, 3H).

*$^{13}$C-NMR (62.5 MHz, THF-$d_8$).* $\delta$ (ppm): 22.57 ($CH_3$); 54.65 (CH);118.63 (CH); 118.95 (CH); 123.66 (CH); 127.49 (C); 127.71 (C); 127.99 (CH); 128.05 (CH); 128.15 (CH); 128.56 (CH); 128.98 (CH); 132.42 (C); 132.89 (C); 146.25 (C); 146.47 (C); 155.12 (C).

*MS (ESI+)*: $[M]^+$ = 615.1686, calcd. for $C_{36}H_{31}N_4S_3$: 615.1711.

***Poly[-10-(2-decyltetradecyl)-10H-phenothiazine-alt-benzo[c][2,1,3]thiadiazole] (poly(Ptz-BT)a-b)***

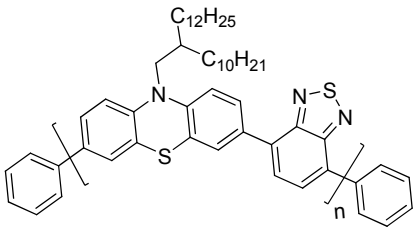


**$P_{7a-b}$**
**poly(Ptz-BT)a-b**

**Synthesis *via* Conventional Conductive Heating**

3,7-Dibromo-10-(2-decyltetradecyl)-10*H*-phenothiazine (**48a**, 0.386 mmol, 268.12 mg, 1.00 equiv.) and 4,7-bis(4,4,5,5-tetramethyl-1,3,2-dioxaborolan-2-yl) benzo[*c*][2,1,3]thiadiazole (**53b**, 0.386 mmol 150.00 mg, 1.00 equiv.) were dissolved in 3 mL anhydrous toluene under inert atmosphere. 2 mL 2M aqueous solution of $K_2CO_3$ and a few drops of Aliquat 366 were added and the resulting mixture was degassed using three times the "freeze-pump-thaw" technique. After adding 5 mol% $Pd(PPh_3)_4$ (22.33 mg), the degassing procedure was repeated and the reaction mixture was heated up to $100^0$C.

*End-capping Procedure*

Phenylboronic acid (1.930 mmol, 235.46 mg, 5.00 equiv.), dissolved in 3 mL degassed toluene, and 2 mol% (10.05 mg) $Pd(PPh_3)_4$ were added to the reaction mixture and left to stir at $100^0$C for 12 h. Brombenzene (3.860 mmol, 606.10 mg, 10.00 equiv.), dissolved in 1 mL

degassed toluene, and 2 mol% (10.05 mg) $Pd(PPh_3)_4$ is also added to the reaction mixture and left to stir at $100^0$C for additional 12 h.

*Work-up Procedure*

The resulting mixture was diluted with toluene to 100 mL and was poured in 100 mL NaCN 1 vol.% aqueous solution which was left to stir at $100^0$C for 2 h. After cooling to room temperature, the organic layer was repeatedly washed with water, dried over $MgSO_4$ and the polymer solution was concentrated under reduced pressure to 3-5 mL. The polymer was trice precipitated from methanol : acetone mixture (1 : 1) and washed with methanol, water and acetone. The solid was subjected to Soxhlet extraction with methanol, acetone, diethylether, and chloroform solution from which the polymer was precipitated from acetone to yield 211.00 mg of **poly**(**Ptz-BT**)**b** (82 %) as dark red solid.

*GPC (TCB, 135$^0$C vs. PS)*: $M_n$ = 8.0 kg mol$^{-1}$; $M_w$ = 11.0 kg mol$^{-1}$; *PDI* = 1.37.

*$^1$H-NMR (300 MHz, $CD_2Cl_2$). δ* (ppm): 0.83 (broad s, 6H); 1.20 (broad s, 40H); 2.10 (broad s, 1H); 3.86 (broad s, 2H); 7.04 (broad s, 2H); 7.70 (broad s, 2H); 7.84 (broad s, 4H) (proton values with respect to the repeating unit).

*$^{13}$C-NMR (75 MHz, $CD_2Cl_2$). δ* (ppm): 14.32 ($CH_3$); 23.11 ($CH_2$); 26.71 ($CH_2$); 29.79 ($CH_2$); 29.96 ($CH_2$); 30.09 ($CH_2$); 30.13 ($CH_2$); 30.48 ($CH_2$); 32.02 ($CH_2$); 32.35 ($CH_2$); 116.37 (CH); 125.74 (C); 127.46 (CH); 128.37 (CH); 128.62 (CH); 131.96 (C); 131.17 (C); 145.85 (C); 154.35 (C).

**Microwave Assisted Synthesis**

3,7-Dibromo-10-(2-decyltetradecyl)-10*H*-phenothiazine (**48a**, 0.386 mmol 268.12 mg, 1.00 equiv.) and 4,7-bis(4,4,5,5-tetramethyl-1,3,2-dioxaborolan-2-yl) benzo[*c*][2,1,3]thiadiazole (**53b**, 0.386 mmol, 150.00 mg, 1.00 equiv.) were dissolved in 3 mL anhydrous toluene under a constant stream of argon in a 35 mL microwave vial. 2 mL 2M aqueous solution of $K_2CO_3$ and a few drops of Aliquat 366 were added and the resulting mixture was thoroughly degassed by letting a constant stream of argon to pass through it for 25 min. Subsequent to the addition of 5 mol% $Pd(PPh_3)_4$ (22.33 mg), the vial was sealed and placed in the microwave reactor where it was kept at $100^0$C for 50 min.

*End-capping Procedure*

Phenyl boronic acid (1.93 mmol, 235.46 mg, 5.00 equiv.), dissolved in 3 mL degassed toluene, and 2 mol% (10.05 mg) $Pd(PPh_3)_4$ were added to the reaction mixture under a constant stream of argon and heated in the microwave reactor at $100^0$C for 20 min. Brombenzene (3.86 mmol, 606.10 mg, 10.00 equiv.), dissolved in 1 mL degassed toluene, and 2 mol% (10.05 mg) $Pd(PPh_3)_4$ were also added to the reaction mixture and heated in the microwave reactor at $100^0$C for additional 20 min.

*Work-up Procedure*

**Poly**(**Ptz-BT**)**a** was isolated as dark red solid (205.96 mg, $\eta$ = 80 %), subsequent to the same work-up procedure described for **poly**(**Ptz-BT**)**b**.

*GPC (THF, $60^0$C vs. PPP)*: $M_n$ = 12.7 kg mol$^{-1}$; $M_w$ = 15.2 kg mol$^{-1}$; *PDI* = 1.20.

*$^1$H-NMR (300 MHz, $CD_2Cl_2$). $\delta$* (ppm): 0.83 (broad s, 6H); 1.20 (broad s, 40H); 2.10 (broad s, 1H); 3.86 (broad s, 2H); 7.04 (broad s, 2H); 7.70 (broad s, 2H); 7.84 (broad s, 4H) (proton values with respect to the repeating unit).

*$^{13}$C-NMR (75 MHz, $CD_2Cl_2$). $\delta$* (ppm): 14.31 ($CH_3$); 23.12 ($CH_2$); 26.71 ($CH_2$); 29.80 ($CH_2$); 29.95 ($CH_2$); 30.11 ($CH_2$); 30.14 ($CH_2$); 30.46 ($CH_2$); 32.00 ($CH_2$); 32.33 ($CH_2$); 116.35 (CH); 125.72 (C); 127.49 (CH); 128.39 (CH); 128.60 (CH); 131.97 (C); 131.19 (C); 145.86 (C); 154.35 (C).

## 5.2.1. References

*1*. (a) Isak, S. J.; Eyring, E., M. *J. Phys. Chem.* **1992**, *96*, 1738. (b) Williams, A.; Winfield, S. A.; Miller, J. N. *Analyst* **1983**, *108*, 1067.

*2*. The advances presented for the first time in Gaussian 03 are the work of Frisch, M. J.; Trucks, G. W.; Schlegel, H. B.; Scuseria, G. E.; Robb, M. A.; Cheeseman, J. R.; Montgomery, Jr., J. A.;; Vreven, T.; Kudin, K. N.; Burant, J. C.; Millam, J. M.; Iyengar, S. S.; Tomasi, J.; Barone, V.; Mennucci, B.; Cossi, M.; Scalmani, G.; Rega, N.; Petersson, G. A.; Nakatsuji, H.; Hada, M.; Ehara, M.; Toyota, K.; Fukuda, R.; Hasegawa, J.; Ishida, M.; Nakajima, T.; Honda, Y.; Kitao, O.; Nakai, H.; Klene, M.; Li, X.; Knox, J. E.; Hratchian, H. P.; Cross, J. B.; Adamo, C.; Jaramillo, J.; Gomperts, R.; Stratmann, R. E.; Yazyev, O.; Austin, A. J.; Cammi, R.; Pomelli, C.; Ochterski, J. W.; Ayala, P. Y.; Morokuma, K.; Voth, G. A.; Salvador, P.; Dannenberg, J. J.; Zakrzewski, V. G.; Daniels, A. D.; Farkas, O.; Malik, D. K.; Rabuck, A. D.; Raghavachari K.; Foresman, J. B.; Ortiz, J. V.; Cui, Q.; Baboul, A.G.; Clifford, S.; Ciolowski, J.; Stefanov, B. B.; Liu, G.; Liashenko, A.; Piskorz, P.; Komaromi, I.; Martin, R. L.; Fox, D. J.; Keith, T.; Al-Laham, M. A.; Peng, C. Y.; Nanayakkara, A.; Challacombe, M.; Gill, P. M. W.; Johnson, B.; Chen, W.; Wong, M. W.; Gonzalez, C.; Pople, J. A.

*3.* (a) Becke, A. D. J. *Chem. Phys.* **1993**, *98*, 5648. (b) Lee, C.; Yang, W.; Parr, R. G. *Phys. Rev. B* **1988**, *37*, 785. (c) Vosko, S. H.; Wilk, L.; Nusair, M.; *Can. J. Phys.* **1980**, *58*, 1200. (d) Stephens, P. J.; Devlin, F. J.; Chabalowski, C. F.; Frisch, M. J. *J. Phys. Chem.* **1994**, *98*, 11623.

*4*. Katz, H. E.; Huang, J. *Annu. Rev. Mater. Res.* **2009**, *39*, 71.

*5.* Tsubata, Y.; Suzuki, T.; Yamashita, Y.; Mukai, T.; Miyashi, T. *Heterocycles* **1992**, *33*, 337.

*6*. Wehmeier, M.; Wagner, M.; Müllen, K. *Chem. Eur. J.* **2001**, *7*, 2197.

*7*. Kloppenburg, L.; Jones, D.; Bunz, U. H. F. *Macromolecules* **1999***, 32*, 4194.

*8*. Bäuerle, P.; Pfau, F.; Schlupp, H.; Würthner, F.; Gaudl, K. U.; Balparda Caro, M.; Fischer, P. *J. Chem. Soc. Perkin Trans. 2* **1993**, *3*, 489.

*9*. Pisula, W.; Kastler, M.; Wasserfallen, D.; Pakula, T.; Müllen, K. *J. Am. Chem. Soc.*, **2004**, *126*, 8074.

*10*. Hwang, D. –H; Kim, S. –K.; Park, M. –J.; Lee, J. –H.; Koo, B. –W.; Kang, I. –N.; Kim, S. –H.; Zyung, T. *Chem. Mater.* **2004**, *16*, 1298.

# 6. List of Publications

1. ***Timea Dallos***, Dirk Beckmann, Gunther Brunklaus, Martin Baumgarten: "Thiadiazoloquinoxaline-acetylene containing polymers as semiconductors in ambipolar field effect transistors" *J. Am. Chem. Soc*. **2011**, *133*, 13898–13901.

2. ***Timea Dallos***, Manuel Hamburger, Martin Baumgarten: "Thiadiazoloquinoxalines: tuning physical properties through smart synthesis" *Org. Lett.* **2011**, *13*, 1936-1939.

3. ***Timea Stelzig,*** Martin Baumgarten: "Mixed-Valence Phenothiazines: Poly [(N-Alkyl Phenothiazine)-alt-(Benzo[*c*][2,1,3]thiadiazole)] and its Model Compounds" *manuscript in preparation*.

4. Shoufa Zhou, ***Timea Stelzig,*** Bing Liao, Martin Baumgarten*:* "Low Band Gap Oligomers Based on Coplanar [1,2,5]-Thiadiazolo[3,4-*g*]quinoxaline Derivatives" *manuscript in preparation*